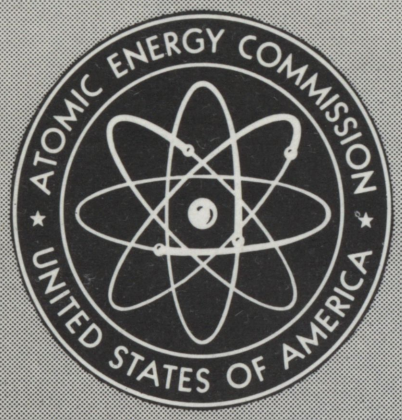

GEAP-3877

NUCLEAR SUPERHEAT PROJECT NINTH QUARTERLY PROGRESS REPORT, JULY–SEPTEMBER 1961

By
R. T. Pennington

June 1962
[DTI Issuance Date]

Atomic Power Equipment Department
General Electric Company
San Jose, California

UNITED STATES ATOMIC ENERGY COMMISSION • DIVISION OF TECHNICAL INFORMATION

LEGAL NOTICE

Printed in USA. Price $3.00. Available from the Office of Technical Services, Department of Commerce, Washington 25, D. C.

USAEC Division of Technical Information Extension, Oak Ridge, Tennessee

GEAP-3877

REACTOR TECHNOLOGY

NUCLEAR SUPERHEAT PROJECT

NINTH QUARTERLY PROGRESS REPORT

July - September, 1961

prepared for

THE U.S. ATOMIC ENERGY COMMISSION

under

CONTRACT NO. AT(04-3)-189, PROJECT AGREEMENT #13

by

R. T. Pennington

Atomic Power Equipment Department

GENERAL ELECTRIC COMPANY

San Jose, California

CONTRIBUTORS

R. T. Pennington — Project Engineer
Nuclear Superheat Project

S. F. Armour

H. N. Bass

R. F. Boyle

F. J. Brutschy

G. Brysvold

J. T. Cochran

C. O. Coffer

R. M. Cohen

F. A. Comprelli

E. L. Esch

T. F. Evans

M. D. Fitzsimmons

G. G. Gaul

V. E. Hazel

K. Hikido

R. L. Holladay

H. F. Johnston

R. Kinney

S. Levy

M. F. Lyons

J. McClaughry

I. L. Marburger

J. E. Morlock

T. B. Murdock

P. Novak

W. L. Pearl

G. T. Peterson

E. E. Polomik

W. R. Raymont

A. B. Reynolds

M. B. Reynolds

G. F. Rieger

J. I. Riesland

C. H. Robbins

J. M. Roberts

J. F. Rowe

S. G. Sawochka

R. A. Schmidt

C. M. Shields

M. Siegler

C. N. Spalaris

A. Silvester

H. E. Townsend

F. G. Warzek

B. Wolfe

TABLE OF CONTENTS

TABLE OF CONTENTS (CON'D)

TABLE OF CONTENTS (CON'D)

LIST OF ILLUSTRATIONS

LIST OF ILLUSTRATIONS (CON'D)

LIST OF ILLUSTRATIONS (CON'D)

LIST OF ILLUSTRATIONS (CON'D)

LIST OF TABLES

LIST OF TABLES (CON'D)

1.0 INTRODUCTION AND SUMMARY

1.1 Introduction

This is the ninth of a series of quarterly reports which will cover the progress and results from the conceptual design, economic evaluations and research and development work performed by the General Electric Company as part of the Nuclear Superheat Project under Contract AT(04-3)-189, Project Agreement No. 13. The followirg list of progress reports and topical reports have been published as a result of this work.

GEAP-3290, First Quarterly Progress Report, July - September, 1959

GEAP-3319, Superheat Process Tube Heat Transfer Tests

GEAP-3371, Second Quarterly Progress Report, October - December, 1959

GEAP-3387, Fabrication, Irradiation and Evaluation of Superheat Fuel Elements

GEAP-3468, Third Quarterly Progress Report, January - March, 1960

GEAP-3538, Fourth Quarterly Progress Report, April - June, 1960

GEAP-3563, Interim Report on Steam Dryer Development

GEAP-3564, Results of Air-Water Steam-Water Tests on Primary Steam Separators - October, 1960

GEAP-3581, Fifth Quarterly Progress Report, July - September, 1960

GEAP-3589, Economic Study for 300 MW(e) Separate Superheat Reactor

GEAP-3590, Economic Study of the Mixed Spectrum Superheater

GEAP-3591, Manufacture of the Adhesive Bonded AEC Superheat Critical Fuel

GEAP-3633, Economic Study for 300 MW(e) Once-Thru Superheat Reactor

GEAP-3686, Sixth Quarterly Progress Report, October - December, 1960

GEAP-3698, Erosion Experiments of Powder Compacted Uranium Dioxide Under Dynamic Steam Flow

GEAP-3703, Heat Transfer Coefficients with Annular Flow During "Once-Through" Boiling of Water to 100 Per Cent Quality at 800, 1100, and 1400 psi

GEAP-3724, Seventh Quarterly Progress Report, January - March, 1961

GEAP-3737, Flood Safety of The Mixed Spectrum Superheater

GEAP-3739, Plastic Strain in Thin Fuel Element Cladding Due to UO_2 Thermal Expansion

GEAP-3778, A Simulated Superheat Reactor Corrosion Facility

GEAP-3785, Eighth Quarterly Progress Report June - August, 1961

GEAP-3787, Results of Air-Water and Steam-Water Tests on Radial Vane Steam Separator Models

GEAP-3796, Design, Fabrication and Irradiation of Superheat Fuel Element SH-4B in VBWR

Section I of the First Quarterly Report (GEAP-3290) presented a description of the Nuclear Superheat Project including objectives, approach to the problem and expected results by individual task. The following tabulation of task titles is listed for easy reference.

TASK A - Conceptual Design and Program Evaluation

TASK B - Fuel Technology

TASK C - Materials Development

TASK D - Experimental Physics

TASK E - Coolant Chemistry

TASK F - Heat Transfer

TASK G - Mechanical Development

TASK H - SADE & E-SADE

TASK J - Mixed Spectrum Superheat Study

1.2 Summary

The following section provides a brief summary of significant results by task.

1.2.1 TASK A - Conceptual Design and Program Evaluation

Engineering physics studies were performed which indicate that significant improvements in axial fuel clad temperature profiles are realizable by the use of axial variations in enrichment and burnable poison. These improvements may be reflected in either high temperature exit steam at the same maximum cladding temperature, increase of average core power density, or reduction in maximum clad surface temperature at the same average steam exit temperature. A study was completed to review the current status of superheat development in terms of its effect on the selection of superheat fuel geometry. It was concluded that as a result of reduction in fabrication costs for rod type fuel and as a result of irradiation experience indicating possible performance limitations due to high stress level and radial thermal expansion, the rod type fuel element should be given increased emphasis in irradiation testing.

As a result of two chloride stress crack failures in stainless steel fuel elements operating in the SADE loop, the Nuclear Superheat Project is being reviewed to provide for an increased emphasis in materials development. This emphasis will include screening evaluations for other than stainless steel fuel cladding materials.

1.2.2 TASK B - Fuel Technology

During this reporting period two 0.028" thick stainless steel clad, annular fuel elements were irradiated in the SADE loop.

The SH-4 fuel element operated for 36 days at significant power level with the maximum exit steam temperature at 900°F. No loss of cladding integrity was observed during SADE testing or during post-irradiation examinations. The SH-4C fuel element was irradiated from August 26 to September 25, 1961. A fission product release of 43 μc/sec maximum was observed after an increase in activity level was detected in the SADE loop on September 19, 1961. Post-irradiation examinations indicated a circumferential cladding failure on the inside clad.

1.2.3 TASK C - Materials Development

Tensile property control tests were completed on the specimens of commercially available stainless tubing.

Control specimens for strain cycle tests were prepared to give hoop strains of a range from 0.5% to 6%. The initial control tests for a nominal hoop strain of ± 6.8% failed after 33 cycles at 1300°F.

1.2.4 TASK D - Experimental Physics

A topical report covering the experimental and analytical phases of the AEC Superheat Critical Program is being written. All of the experimental measurements for the ESADA-VESR preliminary critical program were completed during this reporting period; however, data reduction of experimental results is still in progress. Results of these measurements with a discussion of discrepancies between analytical predictions and measurements are given in Section 5.0.

1.2.5 TASK E - Coolant Chemistry

Metallographic examinations of specimens exposed isothermally for 4500 hours in 1050°F superheated steam were made. Low metal-to-system losses were measured but the data indicated the possibility of metal-to-system loss rate increasing with the increasing exposure. Chloride stress corrosion tests were started in the superheat facility on September 1, 1961. The chloride in the recirculating water is being maintained at 1.5 ± 0.5 ppm. The entrance and middle type 304 stainless steel sheaths were stressed to 1200 psi with the high temperature sheath stressed to 6000 psi. An entrance and middle sheath were examined after 400 hours exposure with no physical evidence of damage. Corrosion testing of type 304 stainless steel coupons in superheated steam environment indicated that oxidation rates of specimens under applied stresses are greater than those of unstressed specimens.

Radiochemistry measurements were made in the SADE loop during SH-4 and SH-4C irradiation. Details of these measurements are reported in Section 6.0.

1.2.6 TASK F - Heat Transfer

Three crackdown runs with Reynolds numbers up to 880,000 were completed during this reporting period. These data provide reasonable agreement with extrapolation of Argonne National Laboratory data obtained by Heineman.

1.2.7 TASK G - Mechanical Development

A modified full circle radial vane separator model has been designed and is now being fabricated for air-water and steam-water testing.

A model of the temperature actuated seal was constructed and tests were conducted up to 550°F to determine the radial expansion of the seal as a function of temperature.

1.2.8 TASK H - SADE AND E-SADE

1.2.8.1 SADE

Irradiations were performed on two .028" stainless steel clad annular fuel elements during this reporting period. Design was completed and fabrication started on SH-5 fuel element which has an 0.016" stainless steel clad. For this fuel element special precautions will be taken to minimize the amount of in-leakage of moderator water to the superheat fuel region. This will include the removal of a thermal liner in the upper section to provide for preheating the inlet steam and reworking of seal seating surface or seal welding to minimize in-leakage. Fuel pellets for the NUSU fuel element were fabricated by the General Electric Company and sent to the General Nuclear Engineering Division of the Combustion Engineering Corporation. Predicted operating conditions for the NUSU element are shown in Section 9.0.

1.2.8.2 E-SADE

Design and procurement work for the E-SADE system were continued during this reporting period. Detailed planning for the installation of external loop equipment was completed for the planned October shutdown of VBWR. Modifications were made to the ESH-2 assembly to change from 9 annular fuel elements to a new arrangement of 7 annular

fuel elements and a 0.5" diameter stainless clad rod type fuel element and a bundle cf six 1/4" diameter stainless clad rods.

1.2.9 TASK J - Mixed Spectrum Superheat Study

Design work was continued on the MSSR design study during this reporting period. Parametric studies were completed for a power range of 10 MWt to 40 MWt for a two-pass superheat flow arrangement and from 25 MWt to 65 MWt for a single-pass superheat flow arrangement. A study was initiated to determine if the ESADA-VESR facility would be suitable for testing a prototype of the MSSR.

2.0 TASK A - CONCEPTUAL DESIGN

2.1 Axial Power Shaping Study

2.1.1 Introduction

This study was undertaken to investigate the possibility of designing a one-pass separate superheat reactor with axial variations in fuel enrichment and erbium burnable poison such that the peak temperature on the fuel cladding is minimized throughout core life. If such a design is feasible, one would be able to take advantage of this optimization in one of the following ways:*

a. Produce higher temperature steam from the same fuel element for a given peak clad temperature (increase thermal efficiency).

b. Shorten the fuel channel (core and vessel height reduction) for the same steam outlet temperature and peak clad temperature, thus gaining in power density.

c. Maintain the same fuel geometry and steam conditions, but allow the fuel to run at a lower clad temperature (increased temperature margin for extra reliability).

d. Combinations of the above.

The ideal axial power shape for a one-pass fuel element would be exponential with the peak at the saturated steam inlet. This would theoretically yield a constant axial clad temperature profile. It is impractical to achieve this in a real reactor because neutron leakage at the core boundaries tends to make the flux-cosine-shaped. Partial withdrawal of control rods, non-uniform fuel burnup and non-uniform axial boiling perturb the normal cosine shape and yield axial power distributions that change drastically with core life and are often far from the ideal power distribution for a flat

* Compared with a "non-optimum" axial power shape obtained with a reference uniform fuel loading.

clad temperature profile. Fortunately, in the reference 300 MWe Separate Superheater (GEAP-3589) where steam flow is downward, the use of bottom-entry control rods helps to bring the relative axial power down near the steam outlet. This compensates in part for the relative power reduction near the steam inlet caused by the large boiling void fraction near the top of the core. However, towards the end of core life when controls approach the fully withdrawn condition, the axial power shifts towards the bottom and the peak clad temperature rises sharply in that region.

It was felt that, with the proper axial variation of fuel and burnable poison, the desired power shape can be maintained throughout core life by forcing the non-uniform burnup effect on power to compensate for the effects of control rod withdrawal and axial void distribution. The initial study assumed (for simplicity) the absence of control rod motion in order to compare the power shapes and axial clad temperature profiles throughout life for the following cases:

A. Constant Axial Fuel Loading, No Control Rod Motion

B. Variable (Five-Region) Axial Fuel Loading, No Control Rod Motion

The remainder of the study includes the effect of control rod withdrawal:

C. Constant Axial Fuel Loading, With Control Rod Motion

D. Variable Axial Fuel Loading, With Control Rod Motion

Of these two cases, only case C has been completed to date. Case D will be reported in the next quarterly.

All the above cases start out with an initial (average) fuel enrichment of 3.2% U-235 and an average erbium content of 0.0017 atoms

Er-167 per atom U. The annular fuel design of the reference 300 MWe Separate Superheater (GEAP-3589) was assumed throughout the study.

2.1.2 Analysis Results

Cases A and B are directly comparable insofar as the following assumptions were made:

a. An average power fuel element was considered, generating 0.0839 MW.

b. An average steam flow through the element of 1,027 lb/hour was assumed.

c. A saturated steam inlet temperature of 545°F was assumed.

A cosine power shape was used to obtain the axial void distribution for case A, while a skewed (peaked towards the top of the core) power shape was used to obtain the void distribution for case B. In each case the void distribution was assumed to be invariant with time. Table 2.1 gives the initial fuel concentrations and moderator void fractions in the five 18-inch axial regions.

TABLE 2.1

	Region 1 (Bottom)	Region 2	Region 3	Region 4	Region 5 (Top)
Case A					
atoms U-235/atom U	.032	.032	.032	.032	.032
atoms Er-167/atom U	.0017	.0017	.0017	.0017	.0017
mod. void fraction	-----	.090	.255	.370	.414
Case B					
atoms U-235/atom U	.025	.017	.023	.030	.065
atoms Er-167/atom U	.0010	.0010	.0015	.0020	.0030
mod. void fraction	-----	-----	.100	.280	.400

Figures 2.1 and 2.2 show the axial power and clad temperature profiles for the beginning and end of life conditions for cases A and B. It should be noted that (without the complication of control rod motion) the use of varying enrichments reduces the clad

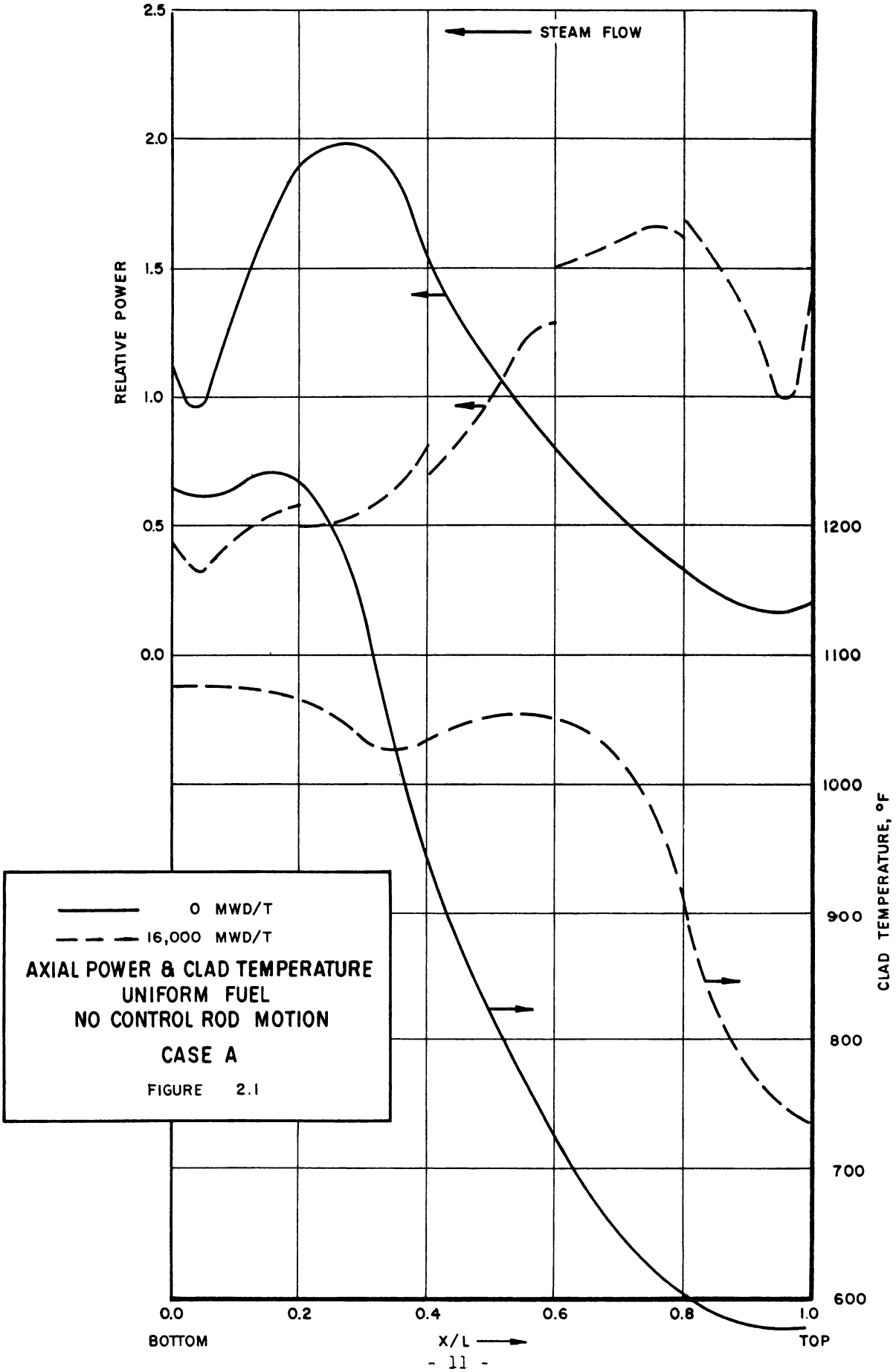
STEAM FLOW
RELATIVE POWER
2.5
2.0
1.5
1.0
0.5
0.0
1200
1100
1000
900
800
700
600
CLAD TEMPERATURE, °F
0.0
0.2
0.4
0.6
0.8
1.0
BOTTOM
X/L
TOP
0 MWD/T
16,000 MWD/T
AXIAL POWER & CLAD TEMPERATURE
UNIFORM FUEL
NO CONTROL ROD MOTION
CASE A
FIGURE 2.1

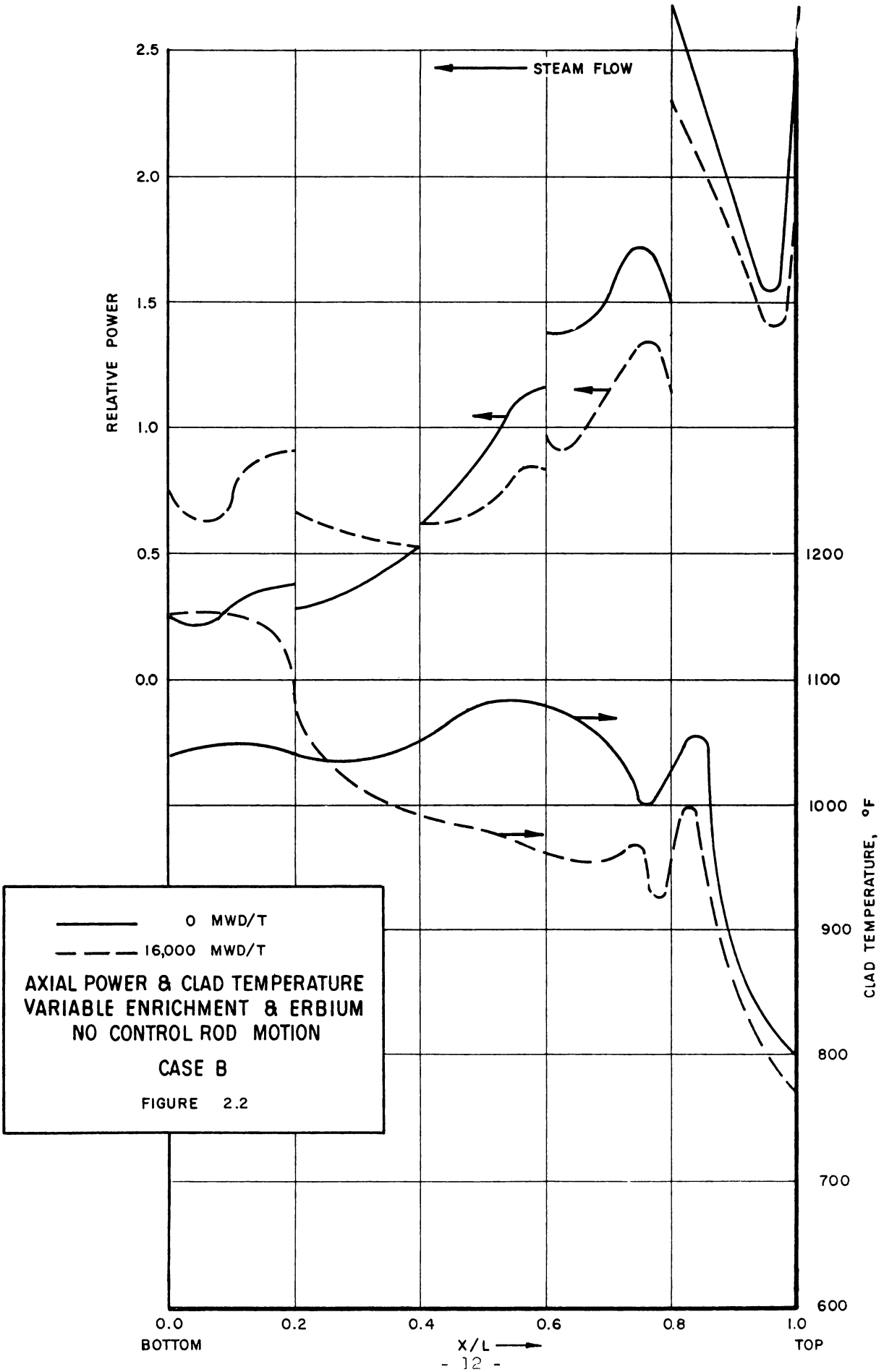

AXIAL POWER & CLAD TEMPERATURE
VARIABLE ENRICHMENT & ERBIUM
NO CONTROL ROD MOTION

CASE B

FIGURE 2.2

temperature peak at least 90°F for the same steam and conditions. Case B does not represent the best distribution of enrichments as the bottom of the core seems to be limiting at the end of life. Further refinements in loading distribution could probably make case B better than case A by about 150°F.

In the next phase of the study, a computer code was used to iterate between the axial void and power distribution at each burnup step (every 4,000 MWD/T). Case C represents such a study in which the control rods were withdrawn at each step to the "just critical" position. The total required control rod worth in the hot condition was fixed at 16% Δk because of the supplementary control with erbium. Ordinary stainless steel blades without boron would suffice in this application. A "hot" channel (1.3 times core average power) of the reference separate superheater was assumed in case C. As in case A, the fuel annulus was uniformly loaded with 3.2% U-235 and 0.0017 atoms Er-167 per atom U. Steam inlet and outlet temperatures of 545°F and 1,000°F, respectively were maintained constant with burnup. The results obtained are shown in Table 2.2.

TABLE 2.2

Average Fuel Burnup, MWD/T	Axial Peak to Average Power	Peak Clad Temperature, °F
0	1.82	1,100
4,000	1.88	1,100
8,000	2.22	1,110
12,000	2.20	1,180
16,000	2.36	1,240

The power shapes, clad temperature profiles, and control rod positions at 0, 8,000 and 16,000 MWD/T are shown in Figure 2.3. Because of the erbium burnup characteristics, initial reactivity

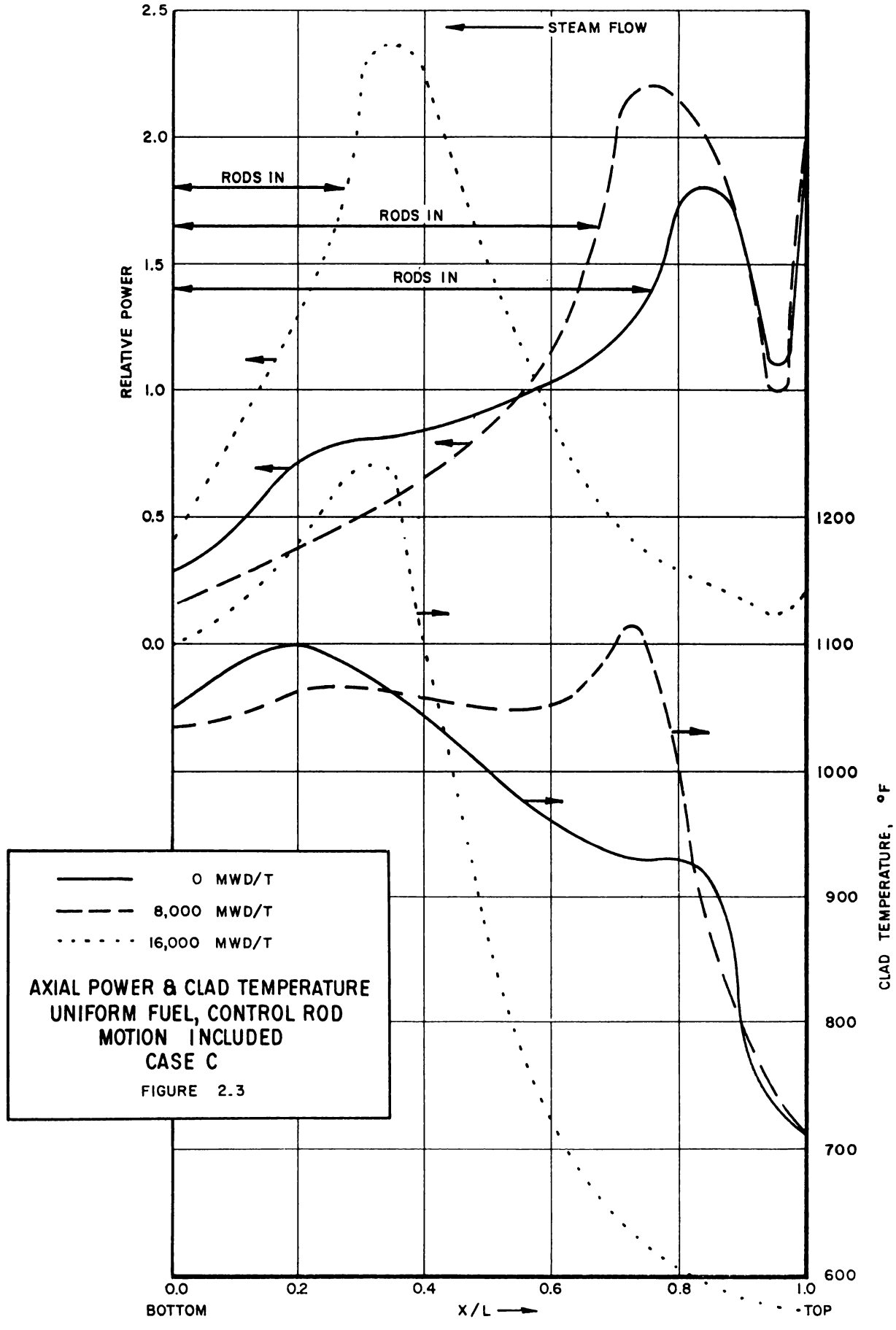
STEAM FLOW
RODS IN
RODS IN
RODS IN
RELATIVE POWER
2.5
2.0
1.5
1.0
0.5
0.0
1200
1100
1000
900
800
700
600
CLAD TEMPERATURE, °F
0.0
0.2
0.4
0.6
0.8
1.0
BOTTOM
X/L
TOP
0 MWD/T
8,000 MWD/T
16,000 MWD/T
AXIAL POWER & CLAD TEMPERATURE
UNIFORM FUEL, CONTROL ROD
MOTION INCLUDED
CASE C
FIGURE 2.3

remains fairly constant and there is little control rod motion before an exposure of 8,000 MWD/T is reached. Thus, the power shape and temperature profile exhibit little change during the first half of core life. Beyond 8,000 MWD/T, the control rods are withdrawn more rapidly and the power peak is shifted towards the bottom of the core. This causes the initial good performance to deteriorate with time as the clad temperature peaks just above the tips of the receding control blades.

A similar study (case D) has begun in which the fuel element is divided into five axial regions of varying enrichments and erbium concentrations. In case D, it is desired to "build into" the fuel element a non-uniform burnup characteristic such that the effects of control rod withdrawal on power shape (beyond 8,000 MWD/T) can be counteracted by suppressing the tendency towards bottom peaking. Case D calculations are currently in progress and will be reported in the next quarterly.

2.1.3 Conclusions

It appears that significant improvements in axial fuel clad temperature profiles are realizable by the use of axial variations in enrichment and burnable poison within a fuel element. These temperature improvements can be utilized in various ways: To make hotter steam, increase the average core power density, or improve the probable life of the fuel by running the cladding at a lower temperature. The economics of the axial temperature optimization have yet to be considered, and the final analytic proof of technical feasibility will have to await the completion of case D calculations which are currently in progress.

2.2 Comparison of Superheat Fuel Elements

2.2.1 Introduction

A study was performed to review the current status of superheat development in terms of its effect on the selection of superheat fuel element geometry. The purpose of the study is to establish the types of superheat fuel elements that should be emphasized in fuel development activities.

2.2.2 Conclusions

It was concluded that as a result of reduction in fabrication cost for rod type fuel and as a result of irradiation experience indicating possible performance limitations due to high stress level and radial cladding expansion, the rod type fuel element should be given increased emphasis in irradiation testing.

2.2.3 Two-Pass Annular Fuel Element Selection

The two-pass, bayonet-type, annular element was originally selected as the reference superheat fuel element at the beginning of the AEC Superheat Development Program. The characteristics of the bayonet element which led to its selection were:

a. It is a large fuel element (1.25 in. O.D. and 0.75 in. I.D.) with large steam path clearances (.125 - .150 inch on the outside pass). Such characteristics produce low fabrication costs.

b. It is the only type of element (besides a combination boiling water - superheat element) which does not require insulation of the process tube. The outside first pass contained steam at low temperature (545°F entrance and 700°F exit) and the hot steam flowed only in the inner second pass.

c. Due to its low fabrication cost, the two-pass annular element has lower cost than the single solid rod element in a single process tube. (GEAP-3468, Nuclear Superheat Project, Third Quarterly Report)

d. As the primary emphasis was to use a fuel element with minimum mechanical problems, more advanced elements as 7 rods in one process tube, or a combination boiling-superheat element, were not considered.

2.2.4 High Steam Volume of Two-Pass Element

Any two-pass element has inherently a larger steam volume than a single-pass element. The bayonet element has even higher steam volume than other two-pass elements. The first pass steam flow region must be opened up to heat up the first pass cladding in order to minimize temperature differential and differential expansion between the inside and outside cladding. The resulting designs had steam volume fractions of 30 - 40%. When the steam passages are flooded with water, or water is drained from the steam passages, the change in reactivity would be excessive and would pose a reactivity safety problem.

2.2.5 Single-Pass Annular Element

The reference fuel element in the AEC Steam Cooled Reactor Study (GEAP-3589) for a separate superheat reactor was changed from a two-pass annular element to a single-pass element. The primary reasons for the change were to reduce steam volume and improve reactor safety. A secondary reason was to increase the reactor and fuel power densities.

However the use of an annular element in a single-pass design raises a number of problems which are not present in a two-pass. These are:

2.2.5.1 Heat Split in Annular Elements

In an annular element the heat generated in the fuel flows out both the inside of the element and the outside of the element. This division of heat is at present a design unknown. If the heat split of the element changes during life or is different for elements in a given reactor, then the reactor must be derated to permit a change in heat split and maintain clad temperature at 1250°F.

There are several reasons why the heat division is unknown and may change during life.

a. One reason is due to the preferential build-up of plutonium on the moderator side of the fuel element. High energy fission neutrons slow down in the water moderator and must enter the element from the outside. Those neutrons which are at the resonant energy of U-238 will be captured at the outside of the fuel. This preferential neutron capture on the outside of the element and resulting plutonium build-up will produce an increase in heat flux on the outside pass.

   This effect is sufficiently large to increase the outside clad temperature by 50-75°F for an 0.716 in. O.D. element from the beginning to end of life.

b. A second reason is that the gap resistance between fuel and clad will probably not be the same for all elements.

The change in gap resistance will be due to difference in gap dimensions produced by manufacturing tolerances on pellet fuel. Even if powder fuel is used there is no assurance that gap resistance will be the same for all elements when operating at power.

c. Unknowns in UO_2 conductivity, changes in UO_2 conductivity with exposure, and cracking or subliming of UO_2 all introduce unknowns in the fuel element design and offer a possible mechanism for differences in fuel element heat flux.

2.2.5.2 High Cost of Small Process Tubes

The cost of any fuel element will increase as the size of the process tube decreases. This increase in cost is due to several items; these are:

a. The cost of the zirconium process tube, and the S.S. liner, and the labor of assembly become increasingly expensive as the diameter is reduced.

b. The stainless liner increases the stainless to fuel ratio more for a small process tube than for a large process tube.

2.2.6 7 Rod Element

The 7 solid rod element has many features which make it attractive. These are listed below:

2.2.6.1 The 7 rod element utilizes a large process tube, approximately 1.5 inch O.D., and consequently the fabrication cost of the insulated process tube portion is reduced.

Due to the high cost of small process tubes, the single rod element has very high fabrication costs.

2.2.6.2 The solid rod element will also benefit by the development of such fabrication processes as compacted powder fuel manufacturing.

2.2.6.3 It now appears that one of the limiting items in rod performance, i.e., high fuel temperature, will be alleviated by higher UO_2 conductivities.

2.2.6.4 A preliminary investigation has shown that the rod element, even though it operates at higher fuel temperatures, it superior to the annular element in its ability to retain fission product gases.

2.2.6.5 A major attraction of the rod element is that its small diameter will permit the clad thickness to be as low or lower than the annular element.

These five characteristics lead to a preliminary conclusion that the 7 rod element deserves more development activity. The 7 rod element is, of course, not without its own problem. Its major problem appears to be the spacing and support of long rod fuel elements with minimum cladding hot spots.

3.0 TASK B - FUEL TECHNOLOGY

3.1 Irradiation Tests

During the third quarter, July 1, 1961, to September 30, 1961, the following irradiation tests were performed:

Fuel Designation	Characteristics	Start Irradiation	Complete Irradiation
SH-4	Annular, 0.028" wall thickness, 3.5% U-235 enrichment pellets	June 2, 1961	August 20, 1961
SH-4C	Similar to SH-4, but with spiral spacers and no inert ZrO_2 pellets	August 26, 1961	September 25, 1961

3.1.1 SH-4 - The total number of operating days for SH-4 was 54, but only 36 days at significant power levels, with maximum exit steam temperatures of 900°F, and estimated clad temperatures of up to 1150°F. One power transient caused steam temperatures to climb to 900°F for 5 hours at a corresponding clad temperature of 1180°F. Maximum power generation for the element was 73 KW and a total accumulated peak exposure of 850 MWD/T* was achieved. No fission products were detected emanating from the fuel compartment in the SADE loop during the irradiation exposure of SH-4. The total number of power cycles (above 15 MW of reactor power) was 31. Operation history of SH-4 is shown in Figure 3.1.

3.1.2 SH-4C - The data obtained from the irradiation of SH-4C are summarized in Table 3.1. The fuel element was cycled 11 times from reactor power levels of 15 MW(t) or greater. The presence of fission products in the exit steam indicated a clad failure present during the 19th of September. Fission product release was 43 μc/sec maximum during a period of two days prior to shutdown.

* Corrected for heat losses through process tube.

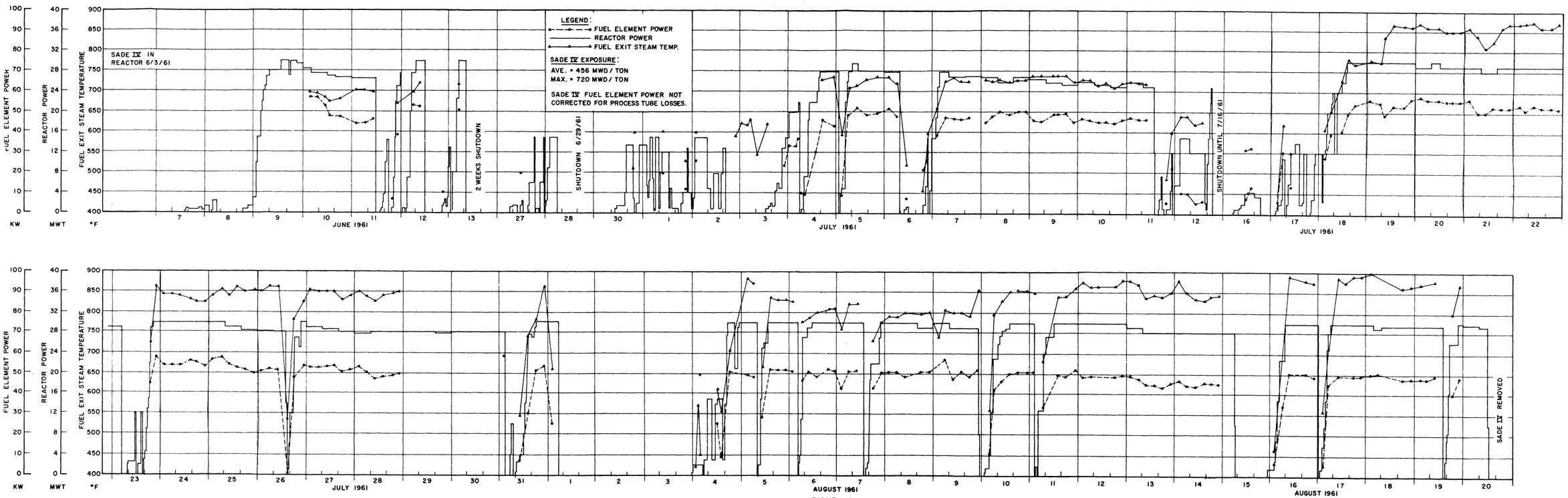

FIGURE 3.1
SADE IV OPERATIONAL HISTORY

TABLE 3.1

IRRADIATION TESTS, SADE

JULY 1, 1961, TO SEPTEMBER 30, 1961

Fuel Element	Insertion Date	Removal Date	Maximum Power	Maximum Steam Temperature	Maximum Clad Temperature	Total hrs. above 750°F Steam	Average Exposure Accumulated MWD/T	Remarks
SH-4	6/2/61	8/20/61	73 KW	900°F	1180°F	--	570	No defect experienced during exposure
SH-4C	6/26/61	9/25/61	63 KW	840°F	1050°F	492		Clad failure

This fission product release rate is within an order of magnitude of the release rate observed for purposely defected fuel elements irradiated in the boiling part of the VBWR core. The rate of water leakage into the SADE facility tube was determined on September 22 by Na-24 concentration in the effluent steam condensate. This rate was found to be a minimum of seven pounds per hour, neglecting plate-out of Na-24 on fuel and piping. Because the moisture content in the VBWR steam was less than 0.7 lbs/hr, it was concluded that the excess water entered this fuel compartment through the underwater flange. During the irradiation period of SH-4C, the chloride concentration in VBWR water was found to be above 0.5 ppm for a total of 9 hours while the reactor power was 30 MW(t). Up to September 20, the chloride level was maintained at less than 0.1 ppm at reactor powers exceeding 2 M(t), but increased to 0.12 on September 20, and 0.27 on the 21st.

Because of a small diameter opening at the top of the thermal liner the fuel element and spacer wires could not be removed intact. The wires were sheared off from the bottom of the fuel element during forced removal from the thermal tube. The spacer wires were inadvertently filed through their entire length, prior to insertion in SADE loop, to clear the obstruction at the top of the process tube flange.

The clad tensile specimens included in SH-4C instrument tube for irradiation were removed, but these were re-inserted into the next fuel element to accumulate additional neutron exposure.

Operational history for SH-4C is shown in Figures 3.2 and 3.3 Fuel assembly SH-4C was removed to RML for post-irradiation examination.

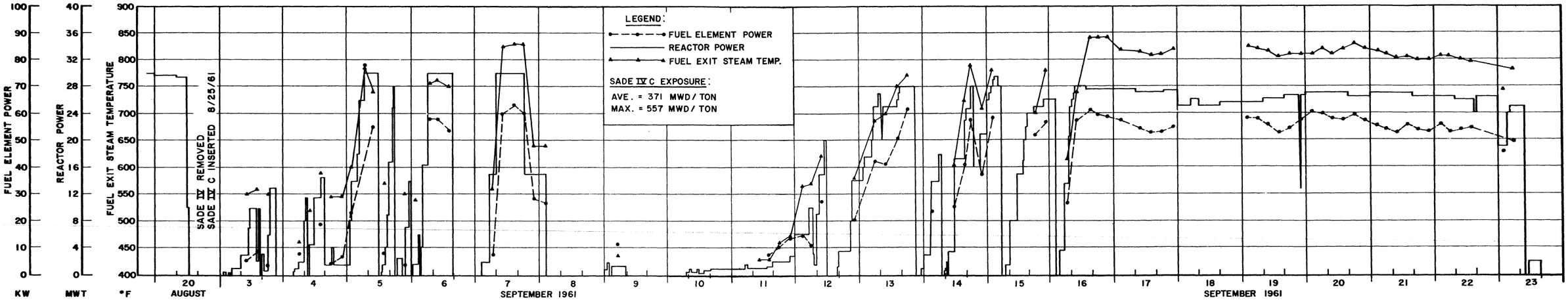

FIGURE 3.2
SADE IV C OPERATIONAL HISTORY

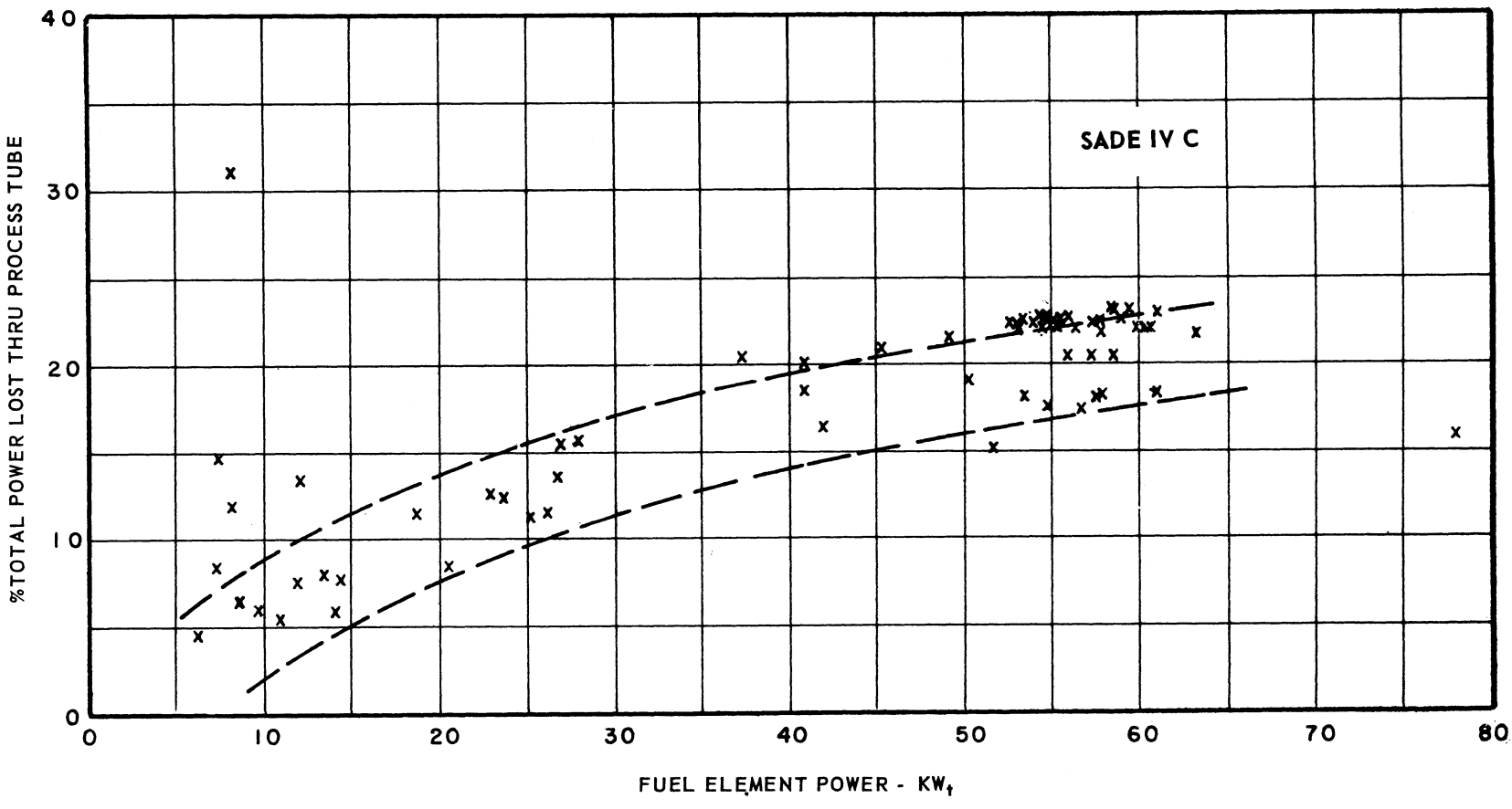

FIGURE 3.3
PROCESS TUBE LOSSES -vs- FUEL ELEMENT POWER

3.2 Post-Irradiation Examinations

3.2.1 SH-4B - The clad failures experienced during the irradiation of this fuel element were attributed to stress corrosion attack. It was concluded that the combination of high water leakage through the loop flanges, along with the concurrent increased chloride ion concentration in the VBWR water (max. 3 ppm) were responsible for the clad failures. As a result of the post-irradiation examination of SH-4B, it was recommended that 304 be retained as the reference clad in the development program, but an alternate clad experimental study be initiated immediately.

The results from the SH-4B irradiation experiment were compiled in the following report: "Design, Fabrication, and Irradiation of Superheat Fuel Element SH-4B in VBWR," GEAP-3796, C. N. Spalaris, R. F. Boyle, T. Evans, and E. L. Esch, September 1, 1961.

3.2.2 SH-4 - Post-irradiation examination for SH-4 included visual, dimensional, corrosion film, and crud analysis for the determination of chloride impurities.

The fuel section was bent in a pattern similar to that observed in SH-4B. Corrosion and crud deposition were observed in the thermal liner cup, and on the fueled section exterior cladding. The hardware above the fueled section was free from crud plate-out. Corrosion on the fueled section exterior was blue-gray in color. Reddish-brown deposits began about 8 inches down from the top weld on the fuel cladding exterior.

Four corrosion plus crud samples were taken for chloride ion analysis and a fifth sample was removed for X-ray diffraction to determine the presence of chlorides in the corrosion film. Three samples for chloride ion analysis were taken by scraping a 4-inch section of the outer cladding, first at a location 8" to 12" from the top of the fueled section, second at 0" to 4" below the center spacing fins, and third, 0" to 4" above the bottom spacing fins. A fourth sample containing crud only, was removed from the inner bore of the element using a cotton ball wrapped in gauze. The X-ray diffraction sample was scraped from a location 0" to 4" above the center spacing fins. Results from the crud and corrosion film analysis were not available as of the end of the reporting period.

Dimensional measurements along with the corresponding pre-irradiation measurements, are shown in Figures 3.4, 3.5, and 3.6. The lower half of the outer cladding collapsed uniformly upon the fuel without forming longitudinal or circumferential wrinkles. However, there was warpage evident in this collapsed section. The inner cladding exhibited a necking down of about 21 mils in diameter near the bottom seal weld. I.D. values measured 20" to 36" from the bottom in the inner bore are probably in error because the warpage did not permit aligning the gage to make reliable measurements.

When several O.D. measurements were spot checked, they were found to be about 4 mils less than the first measurements. Inspection of the area by Kollmorgen periscope showed that the first measurement included crud, and the second measurement did not. Therefore, the crud plate-out is about 1.5 to 2 mils in thickness. Gamma scans for SH-4 are shown in Figure 3.7.

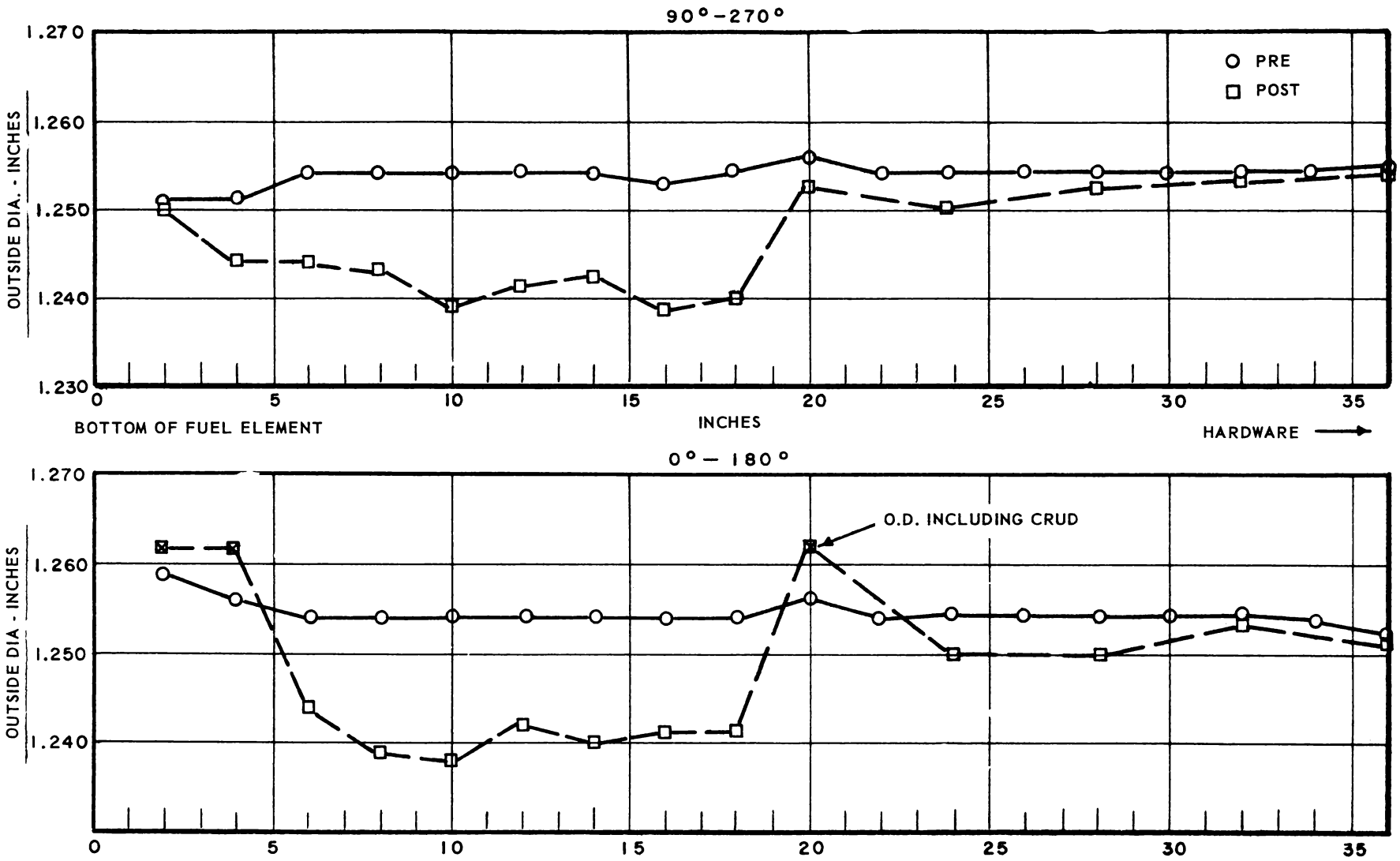

FIGURE 3.4
POST IRRADIATION MEASUREMENTS FOR SH-4 OUTSIDE DIAMETER

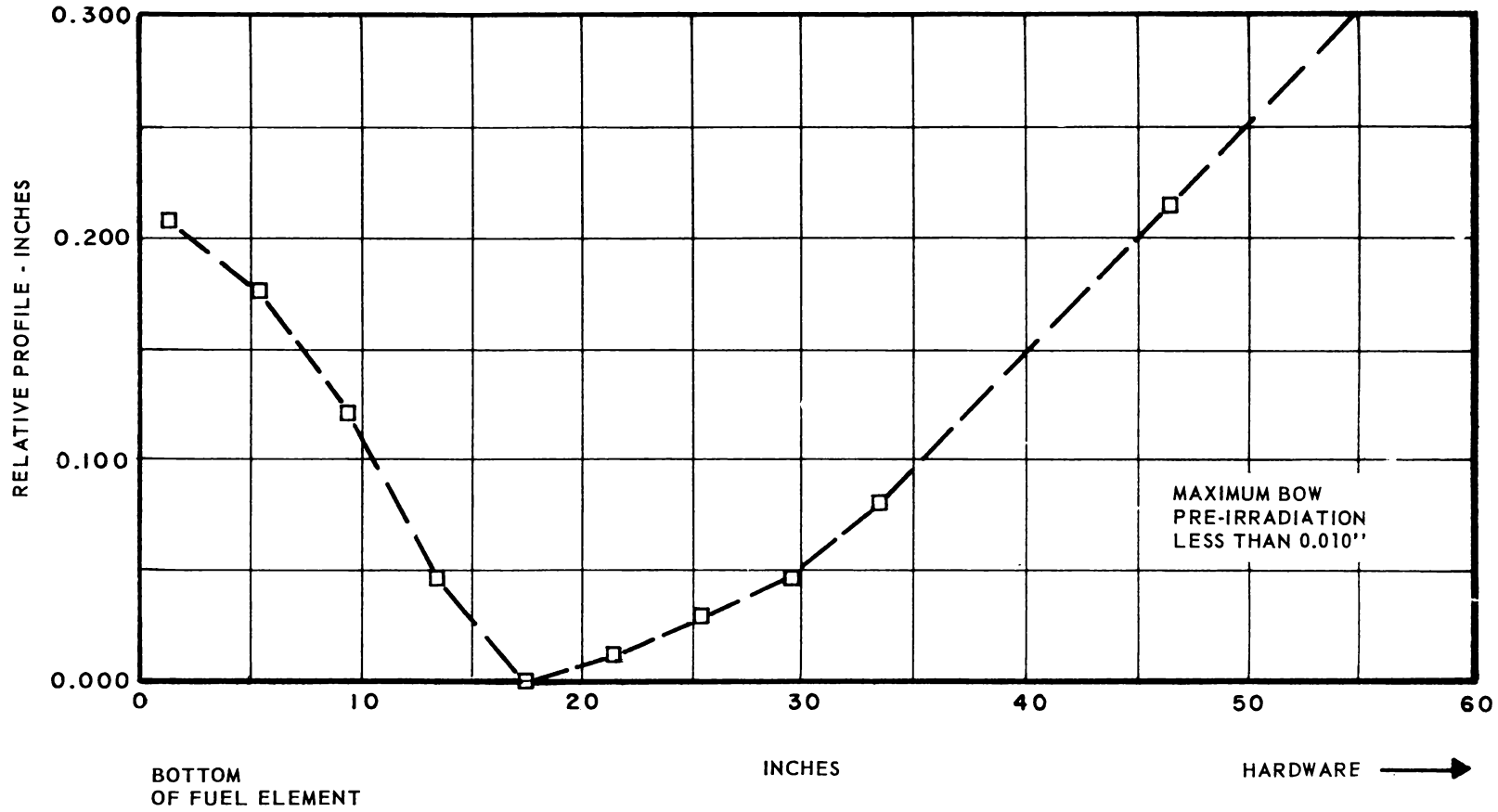

FIGURE 3.5
WARPAGE POST IRRADIATION MEASUREMENTS FOR SH-4
225° ORIENTATION

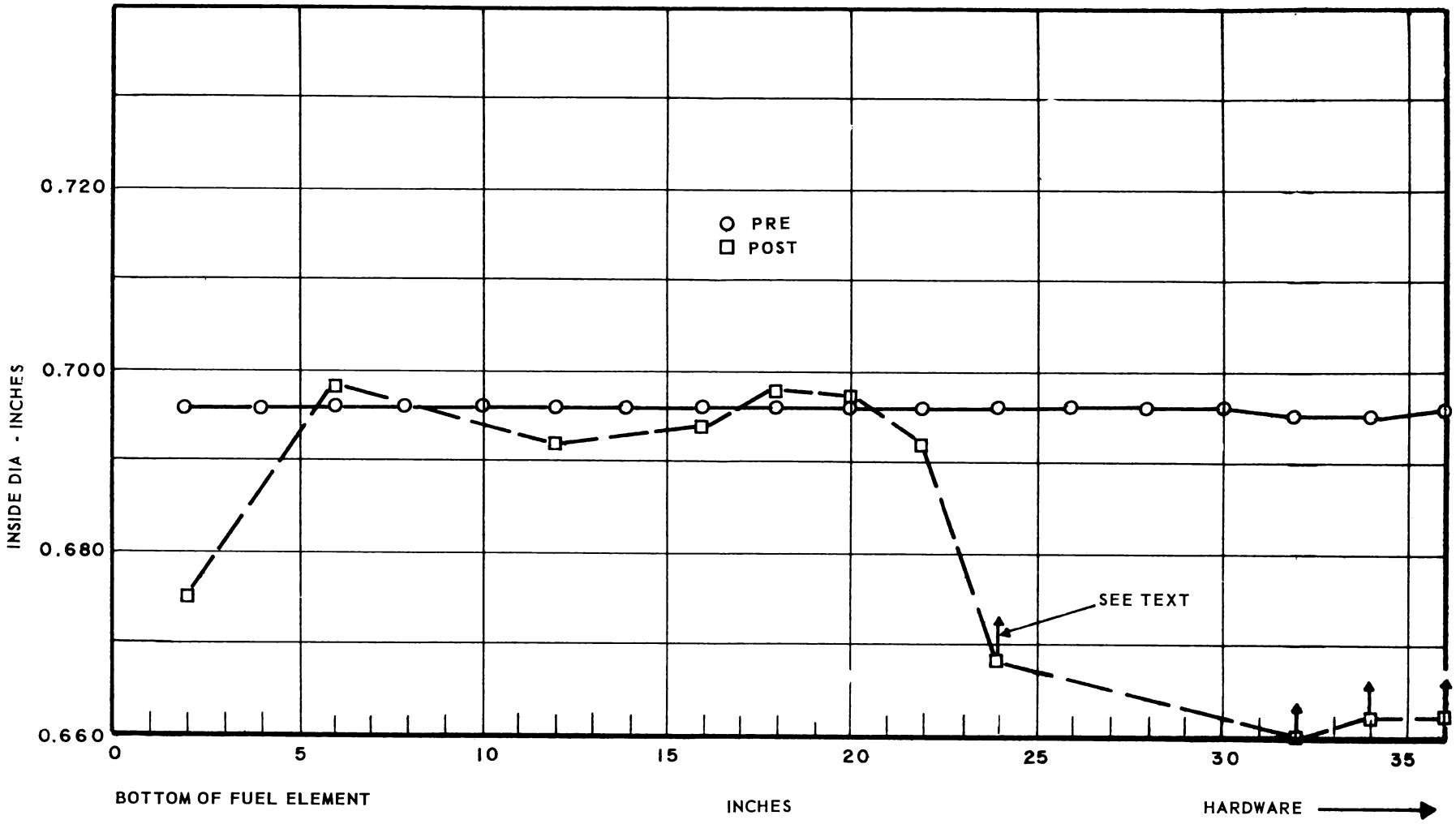

FIGURE 3.6
INSIDE DIAMETER POST IRRADIATION MEASUREMENTS

SH-4

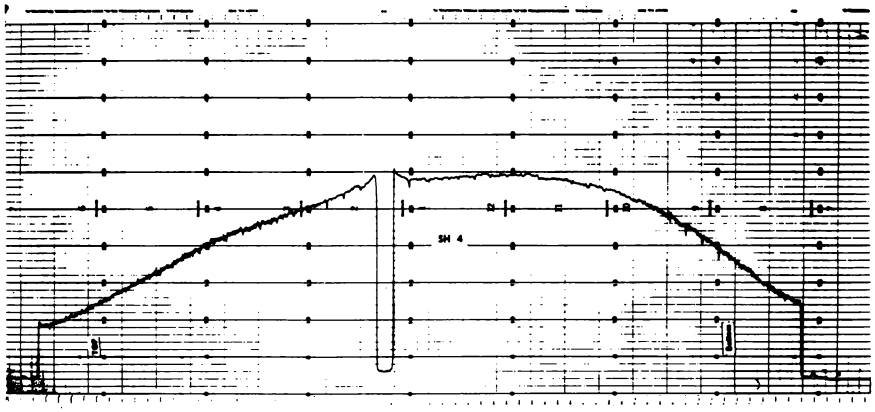

FIGURE 3.7
GAMMA TRAVERSE FOR SH-4. FLUX PEAKING NEAR ZrO_2 SPACER IS SHOWN

3.3 Fuel Fabrication

3.3.1 SH-4C - This 0.028" clad annular fuel element was completed. It was the last of a series of 3.5% enriched elements to be made and there was not sufficient fuel available to make all the pellets required. One of the unirradiated elements, SH-4A, was disassembled and the best pellets used to complete the fuel column of SH-4C. Internal diameters on the SH-4A pellets were considerably larger and thus increased the clad-pellet gap in the areas where they were used.

In assembling the fuel element, the pellets were first loaded on the internal cladding against the lower end plug which had been welded in place. The outer cladding tube was then placed over the pellet column from the same direction as the pellets had been loaded. The outer cladding passed only part way over the pellet column freely, from this point on it was necessary to force the cladding over the rest of the pellets. Loading the fuel in this manner resulted in the fuel column being held tightly in compression even before the plenum spring and upper end plug were inserted.

The assembled fuel element was outgassed by an improved method to insure a minimum internal pressure buildup during operation. This method is described later under fuel element outgassing.

This was the first fuel element to employ spiral wire type spacers welded to the end plugs. Considerable difficulty was encountered in holding the wire tight through the welding process. This resulted in a slight slackening in the wires on the finished fuel element.

3.3.2 SH-5A - This 0.016" clad annular fuel element was completed. Pellets were fabricated from 4% enriched powder and were ground to allow a

.005" diametral gap between I.D. cladding and pellets, and a .004" diametral gap between O.D. cladding and pellets. Pellets were first loaded into the O.D. cladding tube and then the I.D. cladding tube was easily inserted to its proper position. A double sleeve plenum support was used similar to that shown in Figure 3.7 of the Eighth Quarterly Progress Report. After the pellets, plenum support, and end plugs had been assembled in the two cladding tubes, the lower end plug welds were made and the O.D. cladding was welded to the upper end plug. The element was then swaged in nylon dies to reduce the O.D. diametral gap to less than .002 inches. The swaging operation resulted in a growth of .020" in the length of the O.D. cladding. Following the swaging operation, the I.D. cladding was welded to the upper end plug; this joint had been left free to accommodate O.D. cladding growth during the swaging operation. Outgassing of the fuel assembly was accomplished in the same manner as on SH-4C.

Spacing of SH-5A in the process tube was accomplished by a series of studs inside the process tube. The studs were welded in place and spaced every 18 inches to accommodate fuel element growth during reactor operation.

3.3.3 ESH-1 - Design of the fuel for the nine element assembly was completed. It includes both 0.016" and 0.028" thick O.D. cladding; all elements will have 0.028" thick I.D. cladding tubes. Spacing of the fuel elements in the process tubes will be accomplished by spiral wrapped wires and spiral fins chemically milled on the O.D. cladding.

Materials for the fuel elements are all available with the exception of the UO_2 required. Delivery on this material has been promised for early October. Fabrication of the 10% enriched fuel pellets was initiated with UO_2 borrowed from another AEC project.

3.3.4 Pellet Fabrication

In the manufacture of fuel pellets for ESH-1 an attempt is being made to establish a process which will allow the internal diameters to be sintered to the required size. The means which is being employed to accomplish this goal is a tight process control on the green density of the as-pressed pellets, the use of lubricated punches, and reduced binder content. Early indications appear to be very favorable with a marked improvement in size control; the specified internal diameter of .755 inches on ESH-1 pellets can be held in the sintering operation to within $\pm$ .0015 inches.

The improvement in pellet quality by the changes made to date has allowed recognition of several other problems in the pellet fabrication process. These include powder preparation, die fill, furnace stoking and furnace atmosphere. Work will be started in these areas as a second phase of the program and it is expected that it will result in even better size control, improved concentricity, and eliminate radial cracking during fabrication.

3.3.5 Fuel Element Outgassing

A vacuum outgassing process has been developed for UO_2 powder filled superheat fuel elements. Recent tests have shown that arc fused powders contain anywhere from 25 to 50 times the amount of gas that would be expected from conventional pellet fuel. The

outgassing cycle is shown in Figure 3.8. The assembled fuel element is heated to 400°C and then given a series of low pressure helium purges. Following the purges the element is cooled and filled to atmospheric pressure with dry helium. A plug is then welded in the upper end completing the fuel element closure.

3.3.6 Wire Spacer Attachment

A new method of wire spacer attachement has been adopted. Wires are cut to a set length and then welded at the ends to two stainless steel rings. The rings are made to fit on the end plugs and the wires are tightened by rotating the rings in opposite directions. Figure 3.9 shows a typical wire attachment on one end of an ESH-1 fuel element.

The following advantages are possible with this method:

1) Wire can be tightened uniformly to any desired stress level.
2) Wires can be made to form a tight envelope over the fuel body.
3) No special equipment is required for wire forming or attachment.

3.3.7 Chemically Milled Tubing

Experimental velocity booster tube and O.D. cladding have been received for the ESH-1 fuel elements. Figure 3.10 shows short sections of both sizes of tubing. The O.D. cladding was manufactured to the following specification:

Maximum fin dia.	1.390 inches
Outside tube dia.	1.250 ± .003
Wall thickness	0.028 ± .002
Number of fins	3
Fin pitch	36 inches

3.4 Fretting Corrosion - Spacer Development

The fuel element described on page 180 of the Eighth Quarterly Progress Report has been exposed for a total of 55 hours in dynamic superheated

FUEL ELEMENT OUTGASSING CYCLE

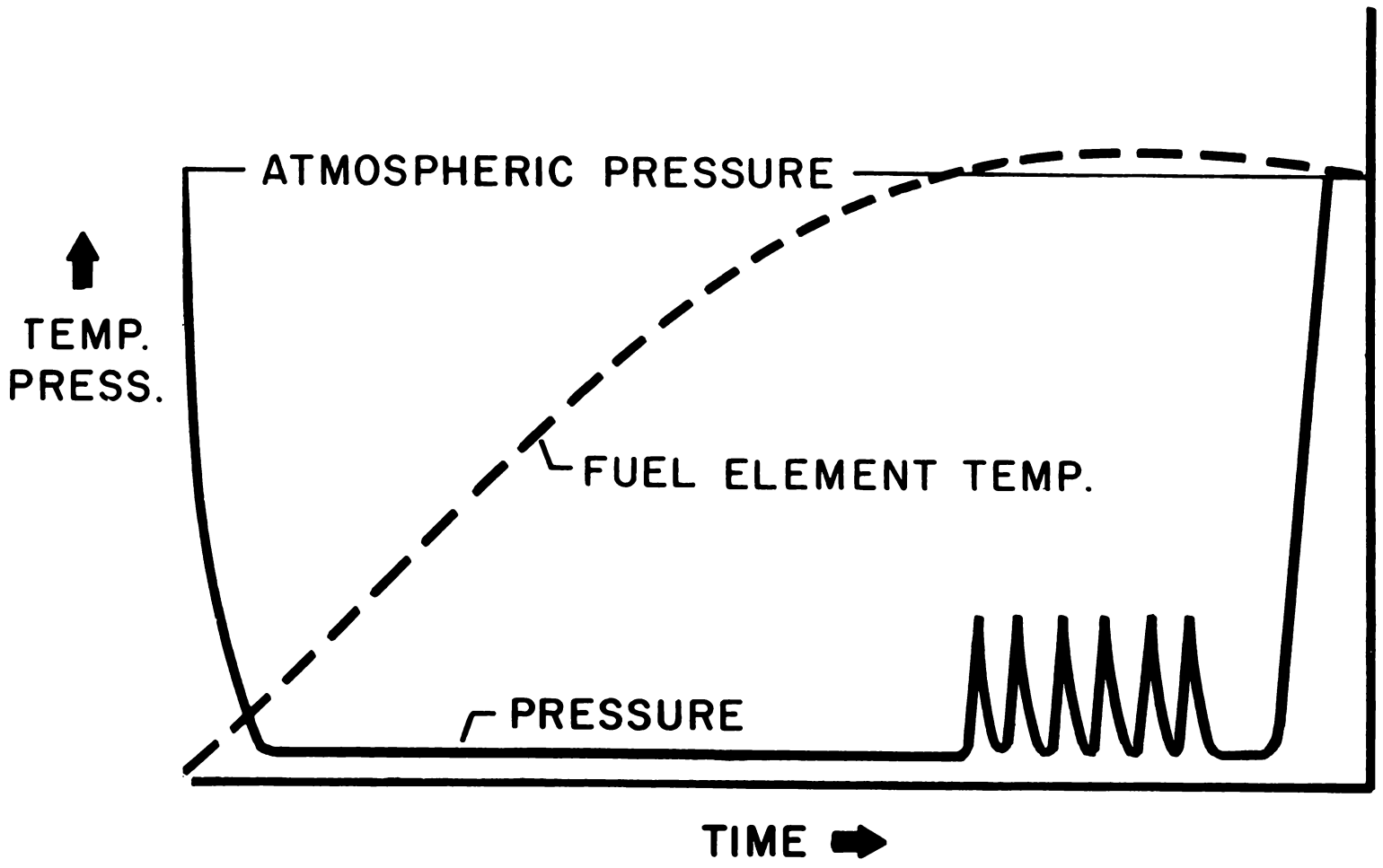

FIGURE 3.8

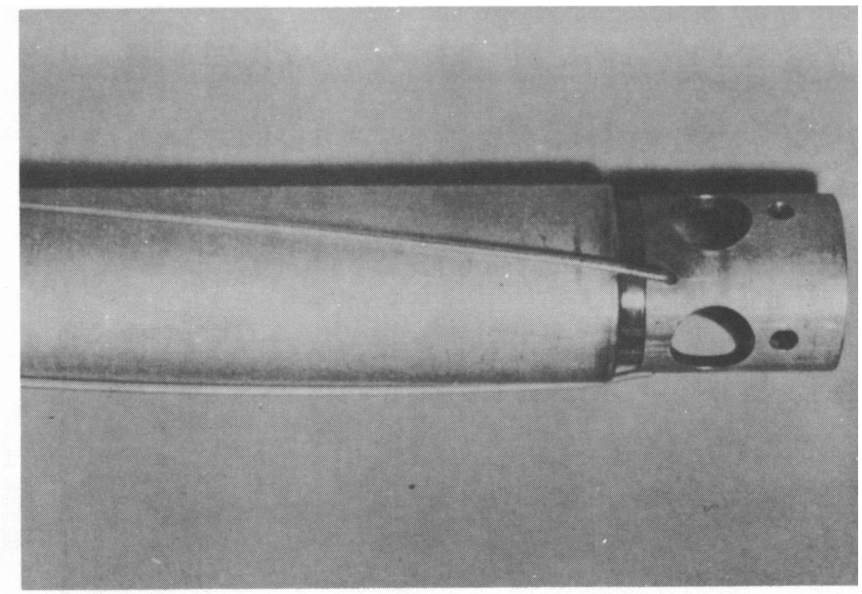

FIGURE 3.9
SPACE WIRE ATTACHMENT

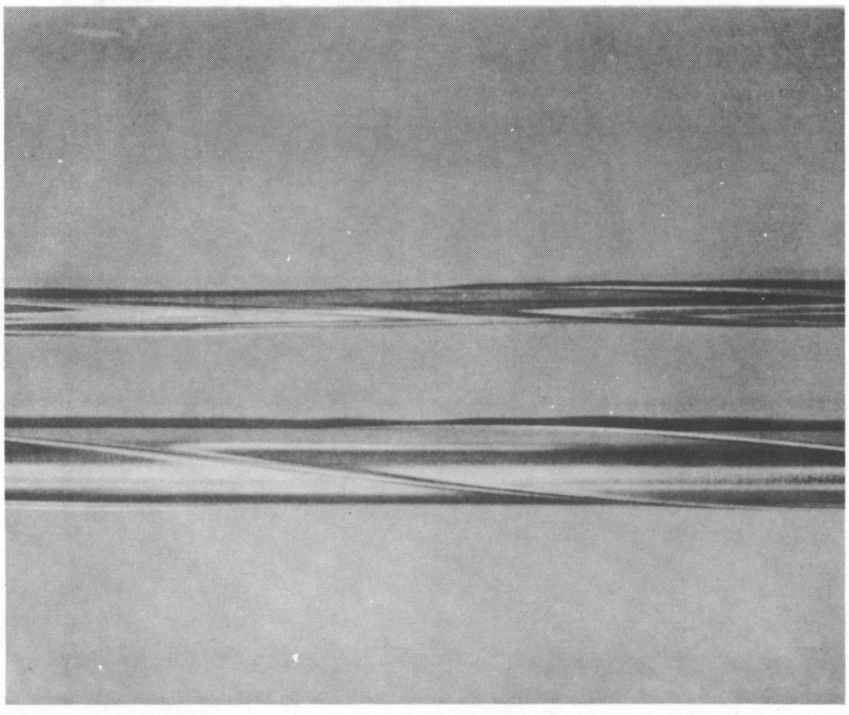

FIGURE 3.10
CHEMICALLY MILLED TUBING

steam. Loop operating conditions during this period were:

Pressure:	800-1200 lb/in^2
Temperature:	650-850^{o}F
Flow Rates:	750-1075 lb in/hr
Steam Velocities:	35-95 ft/sec

Maximum chloride content in the water (during loop startup) was 0.2 ppm. A complete chemical analysis of all startup water samples is being conducted.

4.0 TASK C - MATERIALS DEVELOPMENT

4.1 Tubing Quality Evaluation

Work has been initiated to ultrasonically test various sizes of 300 series stainless steel tubing in order to establish the quality of commercially available tubing. Tubing from at least three vendors will be tested to determine the number, size, and location of defects. This information will then be correlated with burst test data to establish a relationship between ultrasonically detectable defects and reduction in tube hoop strength. Details of the ultrasonic method calibration were given in the last quarterly report. The materials which will be tested are listed in Table 4.1.

TABLE 4.1

STAINLESS TUBING PURCHASED FOR NON-DESTRUCTIVE EVALUATION

Material	Condition	Geometry	Amount
316L	Annealed	0.625 x 0.028	30 ft.
316L	Annealed	0.750 x 0.028	40 ft.
316L	Annealed	0.750 x 0.016	40 ft.
347	Annealed	0.750 x 0.028	50 ft.
304L	Annealed	0.750 x 0.016	40 ft.
304L	Annealed	0.750 x 0.028	40 ft.
304L	Annealed	0.625 x 0.028	40 ft.
304	Annealed	1.250 x 0.028	50 ft.
304	Annealed	0.750 x 0.016	40 ft.
304	Annealed	1.250 x 0.016	20 ft.
304	Annealed	1.250 x 0.028	60 ft.
304	Annealed	0.750 x 0.010	60 ft.
304	Annealed	0.750 x 0.028	50 ft.
304	Annealed	0.625 x 0.028	50 ft.
304	Annealed	0.750 x 0.028	50 ft.

4.2 Strain Cycling Tests

4.2.1 Tensile Property Evaluation

The object of this task is the determination of the effect of fast neutron irradiation under nuclear superheat conditions on the post-irradiation elevated temperature tensile properties of austenitic

stainless steels. The tensile specimens used are cut from the walls of tubing obtained through normal vendor channels and representative of fuel cladding tubing used in prototype fuel elements. Specimens cut with their axes both parallel and transverse to the tube axis have been tested. Control tests have been completed on the following specimens, shown in Table 4.2.

TABLE 4.2

TENSILE PROPERTIES OF TUBING AT ROOM AND ELEVATED TEMPERATURES

Specimen	Test Temperature	Yield, kps	Ultimate kps	Elongation, %
304 Transverse	Room	49.7	91.0	56
304 Transverse	1250°F	26.0	45.6	27
304 Longitudinal	Room	56.1	100.2	54.5
304 Longitudinal	1250°F	29.6	48.9	28.3
316 Transverse	Room	61.0	89.5	41.2
316 Transverse	1250°F	31.6	51.8	18.3
316L Transverse	Room	60.2	86.8	55.5
316L Transverse	1250°F	26.9	48.0	12.6
347 Transverse	Room	51.8	88/3	51.5
347 Transverse	1250°F	27.9	45.7	15.6

Similar specimens accompanied by standard nickel-wire flux monitors are being irradiated in the instrument tube of the SH-4C fuel assembly.

4.2.2 Strain Cycle

This task has as its objective the determination of the effect of fast neutron radiation on the plastic deformation process in fuel cladding alloys. It is planned to investigate these effects by carrying out elevated temperature low-cycle strain fatigue tests (1) in the presence of fast neutron radiation, (2) after irradiation, and (3) In the absence of radiation. The original plan to use an apparatus capable of applying cyclic unaxial strain to tubular specimens has been abandoned because of procurement difficulties. The current apparatus is shown schematically in Figure 4.4. This apparatus is less

desirable from a strain analysis viewpoint because of the complicated strains applied but does apply deformations of the kind experienced by fuel cladding tubing. The tubing specimen is alternately collapsed and expanded between fixed mandrels by application of gas pressure. The strain range is controlled by the I.D. of the outer mandrel and the O.D. of the inner mandrel relative to the specimen thickness. Control specimens have been prepared with mandrels sized to give nominal positive and negative "hoop" strains of 6%, 3%, 2%, 1%, and 0.5%. In an initial control test with mandrels sized to give a nominal hoop strain of $\pm$ 6.8%, the specimen failed after 33 cycles at 1300°F. Post test examination disclosed that the specimen had wrinkled longitudinally and that failure was by longitudinal cracking. Since nitrogen rather than argon was used to deform the specimen, the possibility of surface nitride formation contributing to failure exists. The specimen is currently being examined by x-ray diffraction techniques for the presence of nitrides. Tests with other specimens, using argon as the driving gas, are in progress.

Irradiation schedule for this task in GETR is planned during January, which appears to be compatible with previous planning in the design of the in-reactor equipment.

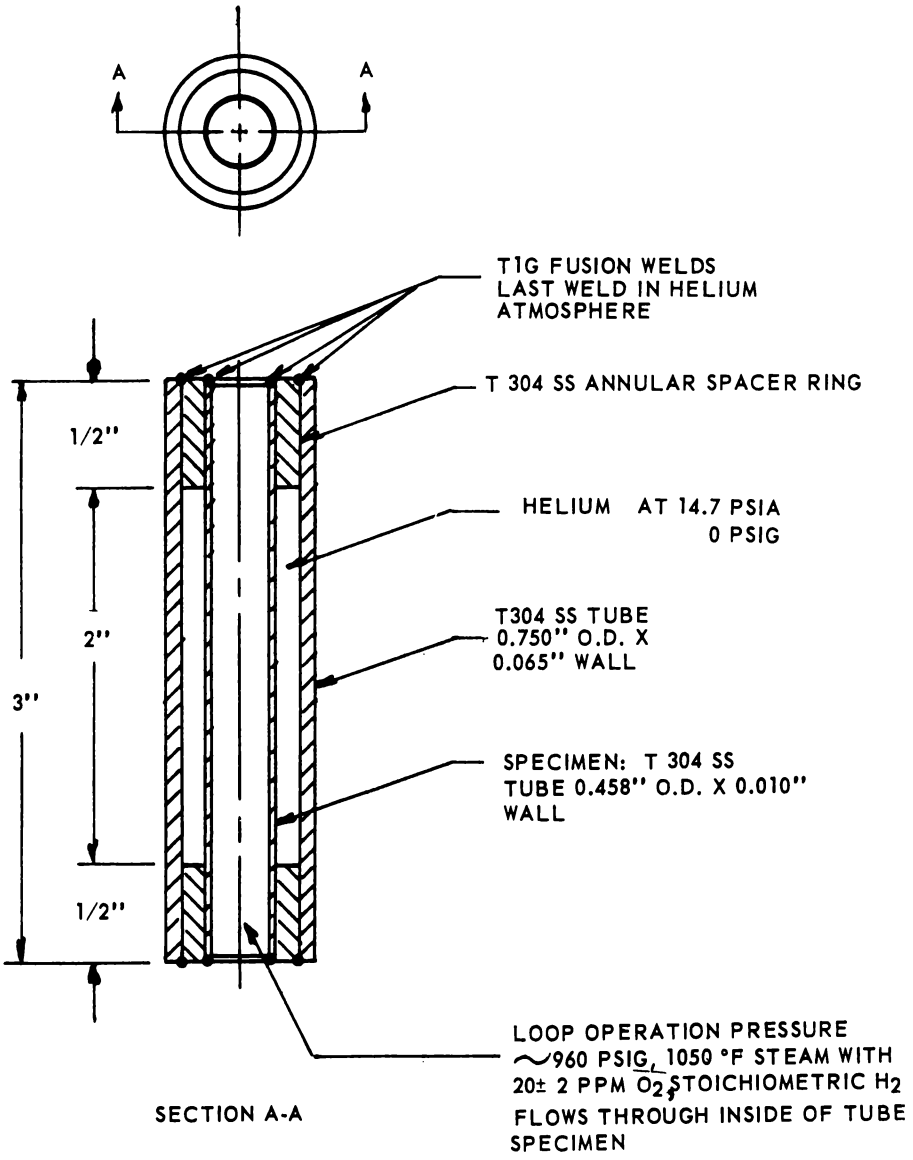

FIGURE 4.1
TUBING STRESS FIXTURE

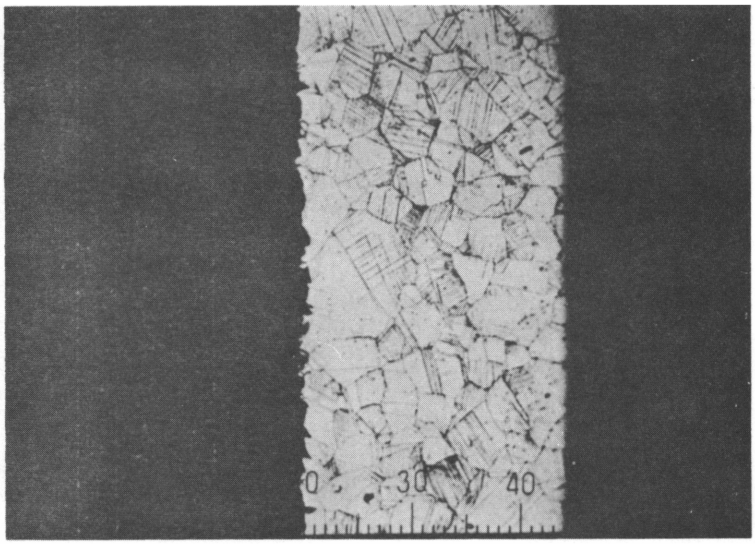

FIGURE 4.2
TRANSVERSE SECTION PARALLEL TO PRINCIPAL STRESS, 10% COLD WORKED TYPE 304 SS, EXPOSED TO 1050°F STEAM FOR 2000 HOURS, ELECTROLYTIC ETCH IN 10% OXALIC ACID, X-100

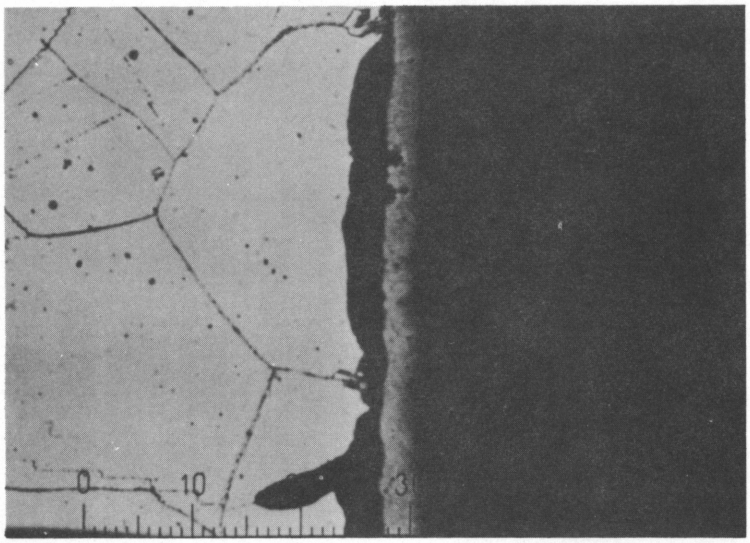

FIGURE 4.3
TRANSVERSE SECTION PARALLEL TO PRINCIPAL STRESS, ANNEALED TYPE 304 SS, EXPOSED TO 1050°F STEAM FOR 2000 HOURS, UNETCHED, X 400, 0.0001 INCH PER DIVISION

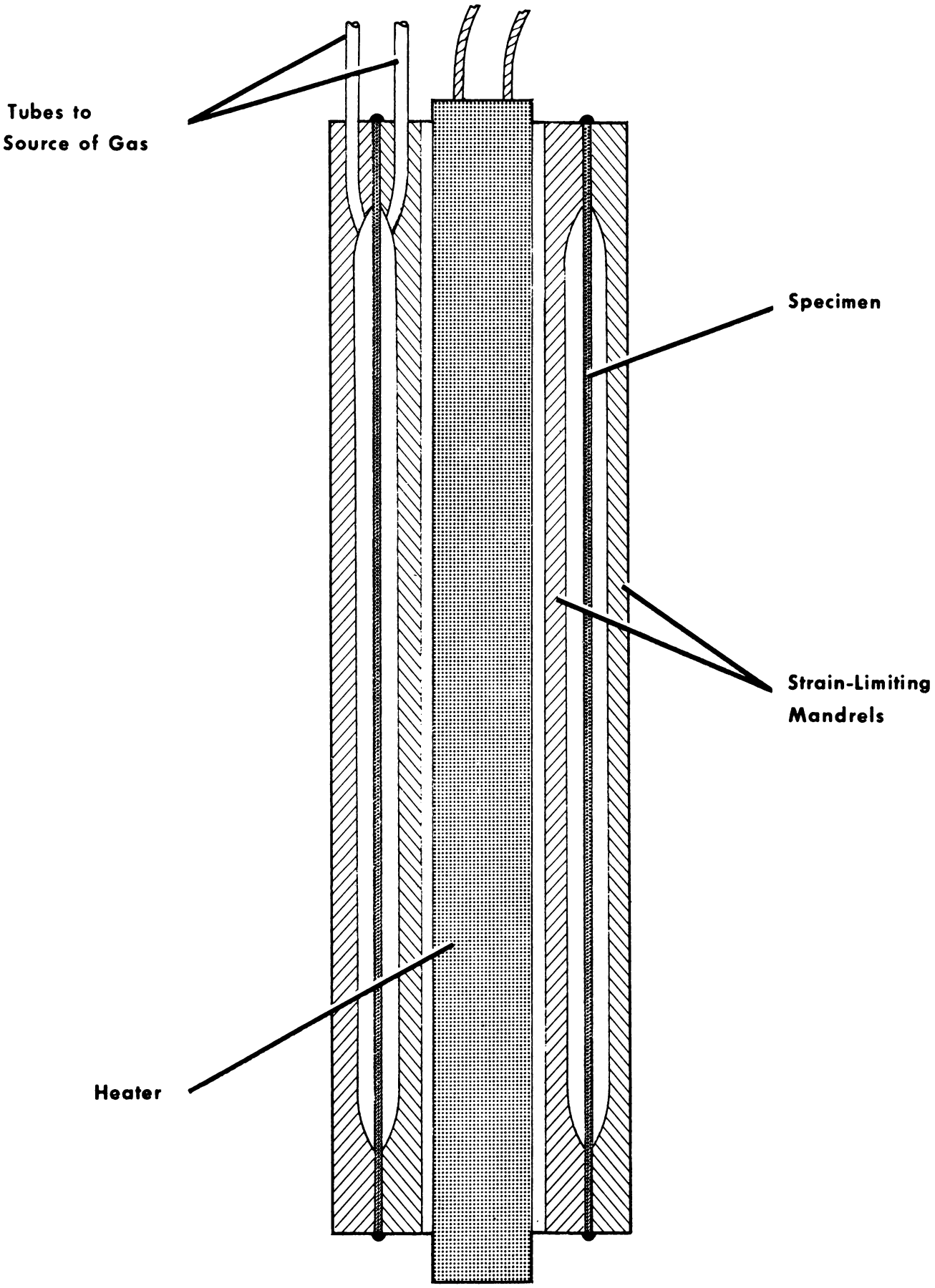

Figure 4.4 STRAIN-CYCLE CAPSULE - SCHEMATIC CONCEPT 2

5.0 TASK D - EXPERIMENTAL PHYSICS

5.1 AEC Superheat Critical Experiments

A topical report covering the experimental and analytic phases of the AEC Superheat Critical Program is being written.

5.2 ESADA-VESR Preliminary Critical Experiment Program

All of the experimental measurements for the ESADA-VESR Preliminary Critical Program are now complete, however, the experimental power distribution data are still in the process of reduction. As reported last quarter, the initial criticality was reached on June 28, 1961 with a core loading of 23-1/3 fuel bundles at 79°C. This critical size would indicate that the initial reactivity calculations were overestimating reactivity by about 2% $\Delta k/k$ in the unflooded condition. However, these original predictions have been revised for two reasons: a) a recent revision of the constant used with the current cross section libraries, accounting for 0.8% $\Delta k/k$, and b) the use of a more detailed regional description in the two-dimensional x-y analysis accounting for 1.2% $\Delta k/k$. These combined effects when taken into account result in reactivity agreement, for the unflooded cases, within 0.5% $\Delta k/k$. The reactivity discrepancy (calculated minus measured) for the flooded core is about 1.4% $\Delta k/k$.

The individual measurements are tabulated below for comparison to theory.

5.2.1 Uncontrolled "Just Critical" Measurements

5.2.1.1 Minimum Critical Size, Fully Reflected

The minimum critical size fully reflected was determined to be 23-1/3 bundles at 77.7°C. This is in good agreement with calculations which predicted a critical size of 23 bundles under these conditions (accounting for the two effects stated above).

5.2.1.2 Void Coefficient - 7 Aluminum Void Tubes per Bundle (6 centered in the moderator, 1 adjacent to the process tube) at approximately 80°C.

The observed void coefficient was (-2.2×10^{-4} $\Delta k/\%$ void) compared to a calculated value of (-1×10^{-4} $\Delta k/\%$ void) for a smeared void over the entire bundle. This is considered excellent agreement due to the very small magnitude of the coefficient in this core configuration.

5.2.1.3 Temperature Coefficient - Near 80°C

The observed temperature coefficient was ($+2.1 \times 10^{-4}$ $\Delta k/°C$) at 80°C compared to the calculated value of ($+1.9 \times 10^{-4}$ $\Delta k/°C$) at 80°C.

5.2.1.4 $(\partial\rho/\partial H)$ versus H (Pulsed Nuetron Source - Data Hand Analyzed)

The observed $(\partial\rho/\partial B^2)$ was (-6.85×10^3 $\$/\Delta B^2$) with a core buckling of 0.00258 cm^{-2} compared to a calculated value of about ($-.64 \pm 0.4 \times 10^3$ $\$/\Delta B^2$) at this buckling.

5.2.1.5 $(\partial\rho/\partial X)$ versus X (Pulsed Neutron Source - Data Hand Analyzed)

The observed data when extrapolated to the full core buckling indicate that the multiplication of the full core uncontrolled at 80°C is in the range of \$4 to \$5. This excess (as with the 23-1/3 bundle core) indicates that there is good agreement with the calculated reactivity (\$4.5) in this core configuration.

5.2.1.6 Reactivity as a Function of Temperature (80°, 60°, 40°, and 20°C)

The observed reactivity change indicated a loss in reactivity of \$2 in going from 80°C to 20°C which agrees exactly with the predicted value.

5.2.2 Full Core Measurements

5.2.2.1 Critical (Operating Type) Rod Position at 80°C

The observed critical rod position with the core fully reflected consisted of the inner four rods inserted halfway (24.38 inches above the bottom fuel plane) with the outer eight rods fully withdrawn. This rod insertion was calculated to be worth $4 indicating that the full core excess is about $4. This is consistent with the calculated full core excess reactivity of $4.5 for this core configuration.

5.2.2.2 Auxiliary Scram Rod Worth with the Rod Pattern Determined in (5.2.2.1)

The observed worth of the auxiliary scram rods was $1.6 which agrees excellently with the calculated value of $1.7 (1.2% $\Delta k/k$).

5.2.2.3 Void Coefficients at 80°C with the Rod Pattern Determined in (5.2.2.1) for Six Void Tubes Centered in the Moderator and also Adjacent to the Process Tubes

The observed void coefficients were:

a. Tubes centered in the moderator (.66% void) ($\Delta k/\Delta$ void) = + 1.9 x 10^{-4} k/% void.

b. Tubes adjacent to the process tubes (.66% void) ($\Delta k/\Delta$ void) = -12.7 x 10^{-4} Δk/% void.

These coefficients compare favorably with the calculated value of $\Delta k/\Delta$ void) = -2 x 10^{-4} Δk/% void for a uniformly distributed void in this condition.

5.2.2.4 Reactivity as a Function of Temperature for the Controls Distribution Determined in (5.2.2.1) and for All Rods Inserted for the Unflooded Core (80°, 60°, 40°, and 20°C)

The observed reactivity change indicated a loss in reactivity of $1.8 for the 5.2.2.1 controls distribution and about $1.1 for

the all rods in case in going from 80°C to 20°C. These are slightly less than the predicted temperature swings.

5.2.2.5 Reactivity Change Upon Flooding the Coolant Passage with the Controls Distribution Determined in (5.2.2.1)

The observed reactivity change was -$1.09 at 80°C. The calculated value for this controls distribution was, however, +$0.3, indicating a discrepancy of about $1.4 in predicting the cold floodirg effort for this controls distribution. This discrepancy was not initially uncovered since the measured value of -$1.09 was bracketed by calculated values of -$1.80 for the full core without controls and -$0.2 for the four inner rods fully inserted at 20°C. Recent two-dimensional analysis has shown that the flooding effect passes through a maximum when the central control bank is partially inserted.

5.2.2.6 Reactivity as a Function of Temperature for the Controls Distribution Determined in (5.2.2.1) and for All Rods Inserted for the Flooded Core (80°, 60°, 40°, and 20°C)

The observed reactivity change indicated a loss in reactivity of $2.5 for the controls distribution in (5.2.2.1) and about $1.8 for the all rods in case in going from 80°C to 20°C. These are slightly greater than the predicted temperature swings.

5.2.2.7 Worth of Individual Fuel Rods

With the outer eight control rods fully out and the inner four control rods inserted half way (24.38 inches from the bottom fuel plane) the worth of six individual fuel rods was determined at 80°C. The worths ranged from 70¢ to 2¢ and are shown in their respective positions on Figure 5.1.

E-VESR - OCTANT OF FULL CORE

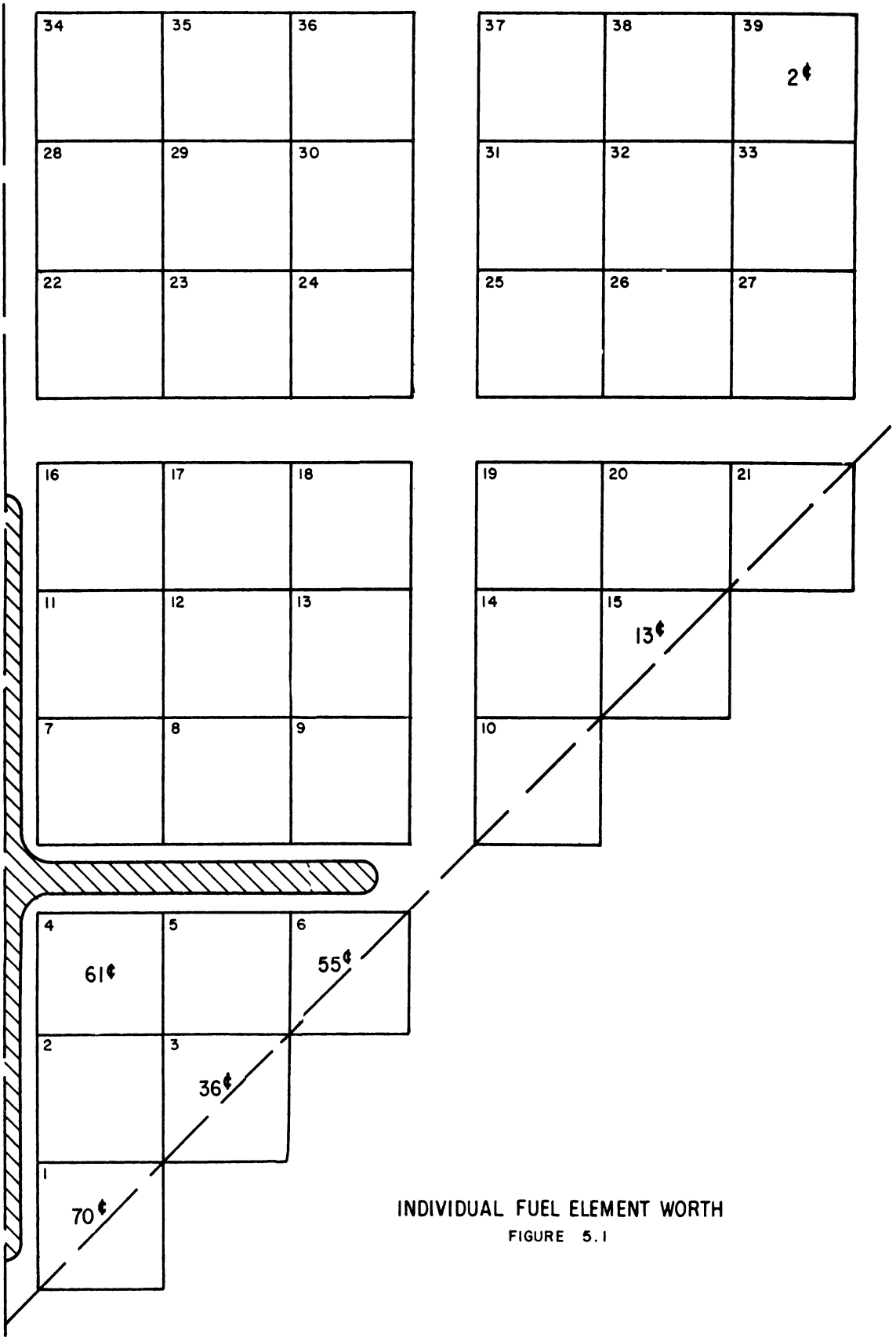

INDIVIDUAL FUEL ELEMENT WORTH

FIGURE 5.1

5.2.2.8 Position of Outer Eight Controls Inserted as a Bank for Just Critical at 80°C

The just critical position was determined to be 21.50 inches above the bottom fuel plane. This rod position was calculated to be worth about 3.2% Δk/k, which would indicate this excess for the full core uncontrolled at 80°C. This is consistent with previous measurements which have indicated that the excess is 3.1 ± 0.4% Δk/k at 80°C and indicate less than ± 0.5% Δk/k error in the post-measurement reactivity calculations.

5.2.2.9 Maximum Central Fuel Bundle Worth

The central fuel bundle worth was determined for the full core with the four central controls withdrawn and the outer eight controls fully inserted. The measured value was 5.3% Δk/k which is considerably higher than the pre-measurement prediction of 2.7% Δk/k. Since the measurement, however, it has been shown that if a more detailed geometric description is utilized, good agreement can be obtained between experiment and theory. Two alternate geometric descriptions bracketing the actual situation have now given the analytic fuel bundle worths of 4.1 and 6.1% Δk/k respectively. An exact geometric description was prohibited by the excessive mesh size and costly computer time required (about four hours of S-2000 time). However, if the exact geometry were used, an analytic fuel bundle worth of about 5% Δk/k would be expected.

5.2.2.10 Controls Worth Measurements (Corrected to 20°C)

a. Worth of Inner Four Control Rods Inserted as a Bank - The worth of the inner four rods was determined to be 7.6 ± 0.5% Δk/k compared to the pre-measurement prediction of 7.2% Δk/k.

b. Worth of Fourth Central Control Rod - The worth of the fourth central control rod with all eight outer control rods withdrawn was determined to be 1.7 ± 0.2% Δk/k. No analytic value is available for direct comparison.

c. Worth of Outer Eight Control Rods - The worth of the outer eight controls inserted in a bank was determined to be 5.9 ± 0.5% Δk/k compared to the pre-measurement prediction of 6.1% Δk/k.

d. Worth of All Twelve Control Rods as a Bank - The worth of all twelve controls inserted as a bank was determined to be 18 ± 2% Δk/k compared to the pre-measurement prediction of 14.8% Δk/k.

A topical report covering the experimental and analytic phases of the ESADA-VESR Preliminary Critical Program is being written.

6.0 TASK E - COOLANT CHEMISTRY

6.1 Out of Pile Evaluations

6.1.1 A description of the design and principles of operation of the C1-1 superheat facility developed to meet the many needs of out-of-pile superheat corrosion testing has been included in a topical report, GEAP 3778, "A Simulated Superheat Reactor Corrosion Facility".

6.1.2 Metallurgical Evaluations

The metallographic examination of a specimen exposed isothermally for 4500 hours in 1050°F superheated steam shows evidence of the start of blistering and porous areas in the scale, Figure 6.1. Although the metal-to-system losses have been minimal after 4500 hours exposure, the data indicate the possibility of the metal-to-system loss rate increasing with increased exposure. The possibility of flaking as a result of the blisters would result in a similar effect. An X-Ray Diffraction (XRD) analysis of the scale identified Fe_3O_4 adjacent to the metal surface with the balance of the scale being a mixture of Fe_2O_3 and Fe_3O_4.

No evidence of a structural change in the heat transfer specimens was noted other than the precipitation of the chrome carbides and the appearance of a high alloy layer at the metal surface in areas with metal temperatures of 1100°F and above. The layer shown in Figure 6.2 increased in depth with time of exposure up through the 2465 hours tested. For example, at a metal temperature of 1300°F the layer averages about 0.2 mil after 1000 hours exposure (Figure 6.2a)and about 0.5 mil after 2465 hours exposure (Figure 6.2b). An Electron Beam Microprobe analysis of the layer was performed by the Research Laboratory of the International Nickel Company. The

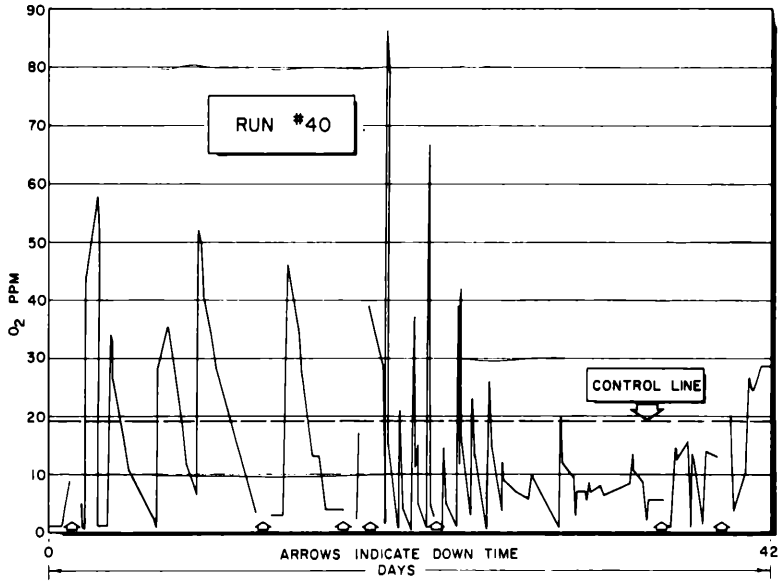

OXYGEN ANALYSIS PRIOR TO CONTROLLED OPERATION

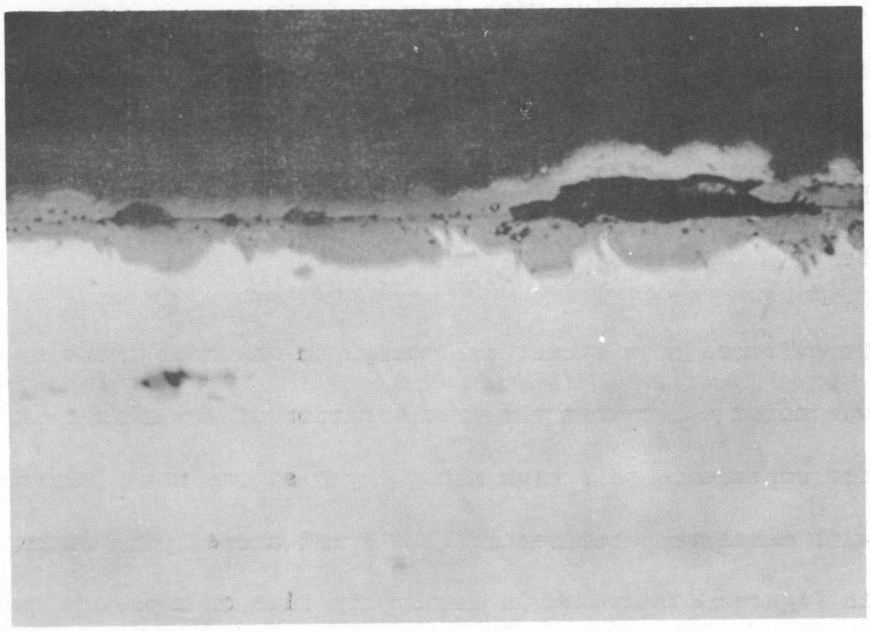

FIGURE 6.1 ISOTHERMAL EXPOSURE - TYPE 304 SS
1050° F SUPERHEATED STEAM
4500-HOURS EXPOSURE, NOT ETCHED

(500 X)

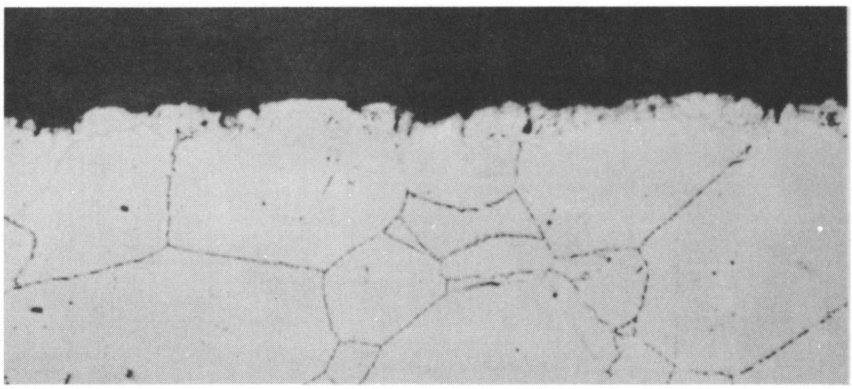

a. 1000-hr. exposure - descaled

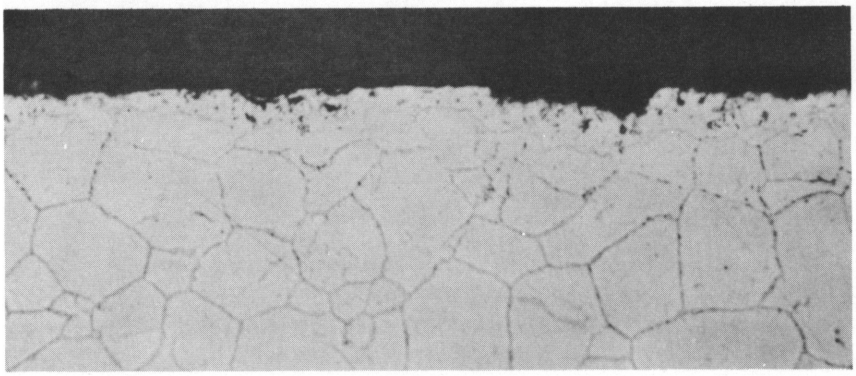

b. 2465 - hr. exposure - descaled

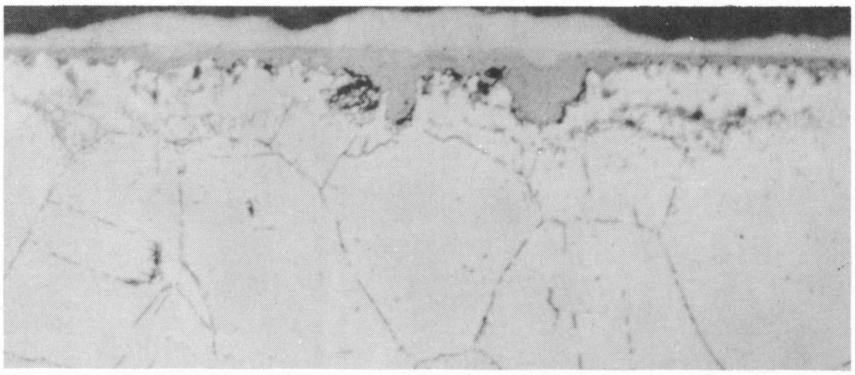

c. 2465 - hr. exposure - undescaled

FIGURE 6.2 HEAT TRANSFER EXPOSURE – TYPE 304 SS
CALCULATED METAL TEMPERATURE - 1300° F
GLYCEREGIA ETCH

(500 X)

results are charted in Figures 6.3, 6.4 and 6.5. No adverse effect on general corrosion occurred during the 2465 hours exposure. The layer was found to be highly magnetic.

6.1.3 Deposition

The deposition on the surface of the heater sheaths originates essentially from materials in the moisture carried with the steam from the steam drum. The boiling water to the steam drum was maintained at a resistivity of 2 megohm-cm., total solids of 1-2 ppm and chlorides at 0.03 ppm or below. With 1% moisture and 500 lbs. per hour of steam, a maximum of 75 mg. of chlorides and from 2.3 to 4.6 g. of solids could be carried over with the steam in 1000 hours of operation.

The insolubles appear to have deposited primarily over the first and second heater sheaths with a relatively heavy deposit of solubles at the entrance to the first heater. The amount of the deposit was variable from run to run although the color pattern remained essentially the same. The results of an X-Ray Fluorescence analysis of the deposits are listed in Table 6.1.

TABLE 6.1

X-RAY FLUORESCENCE ANALYSIS OF DEPOSITION PRODUCT

Element	%	Element	ppm
Cu	35	Mg	2000
Ni	29	Ba	1000
Cr	22	Mo	100
Fe	5	Al	50
Zr	5	Si	50
Ca	2	Mn	10
		Ag	5

Values are estimated, with no allowance made for the absorption of X-Ray by air or other matter.

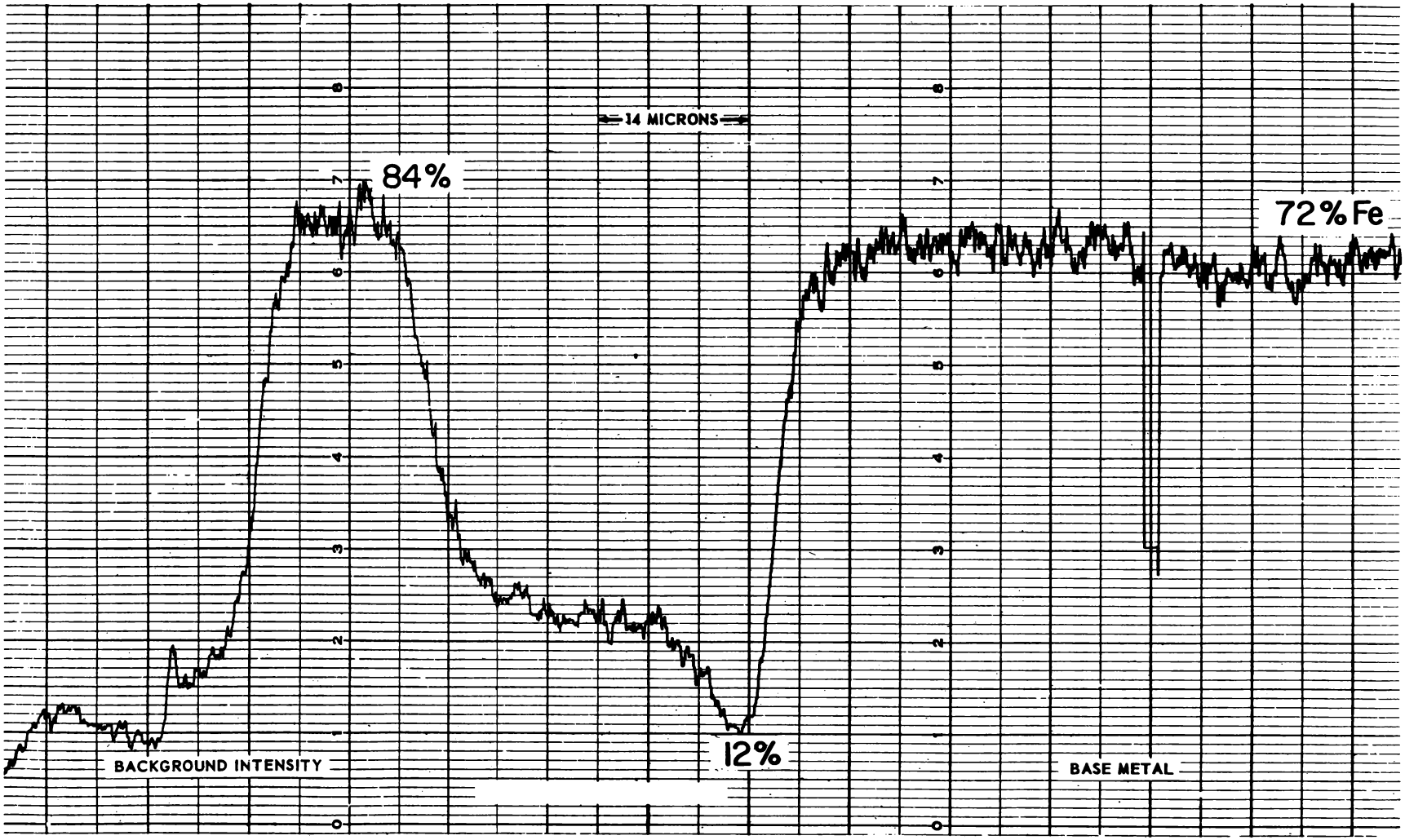

(COURTESY INTERNATIONAL NICKEL CO., RESEARCH LABORATORY, BAYONNE, N. J.)

FIGURE 6.3 ELECTRON PROBE MICROANALYSIS - IRON TYPE 304 SS, DESCALED HEAT TRANSFER SPECIMEN - 1300°F

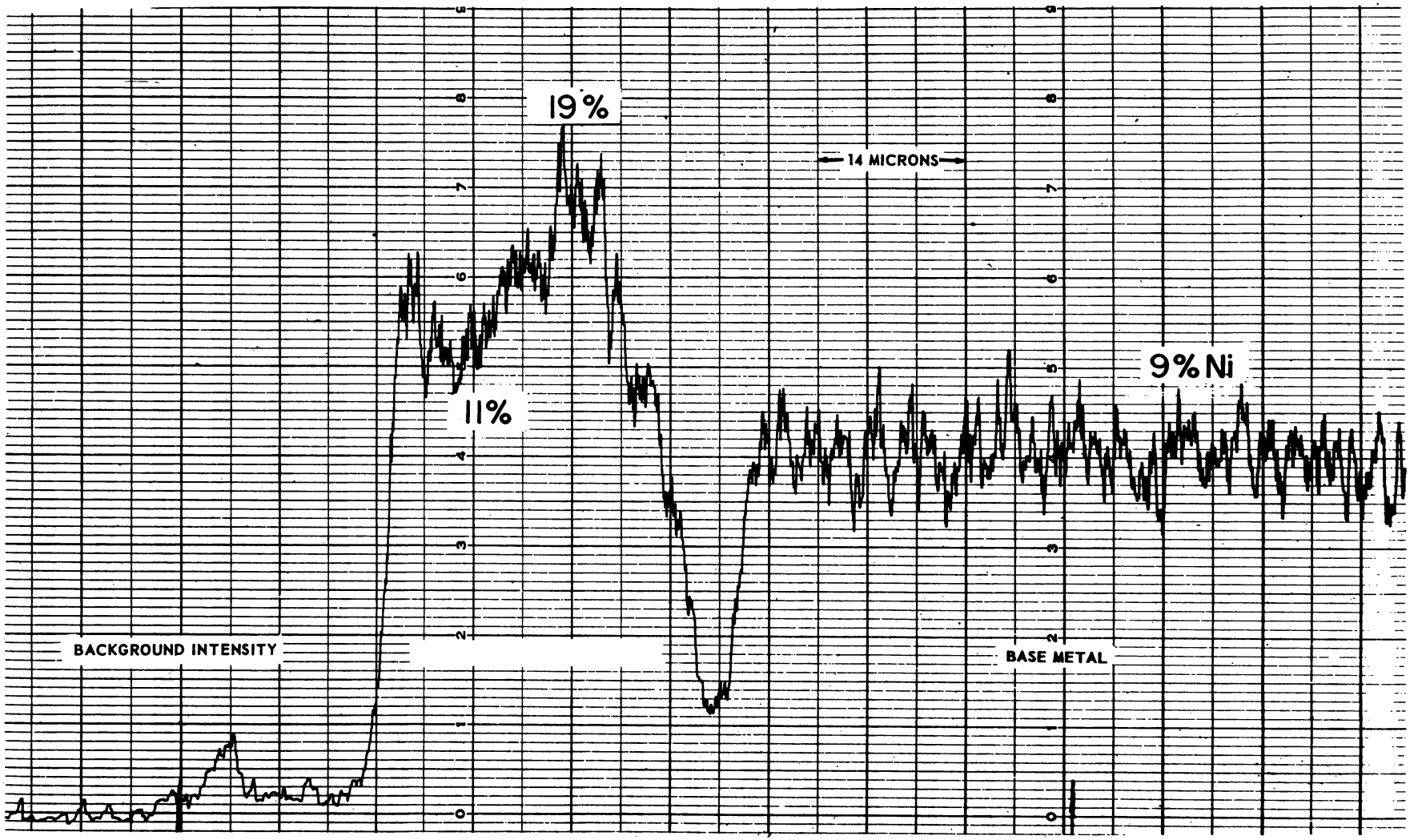

FIGURE 6.4 ELECTRON PROBE MICROANALYSIS - NICKEL
TYPE 304 SS, DESCALED HEAT TRANSFER SPECIMEN - 1300° F

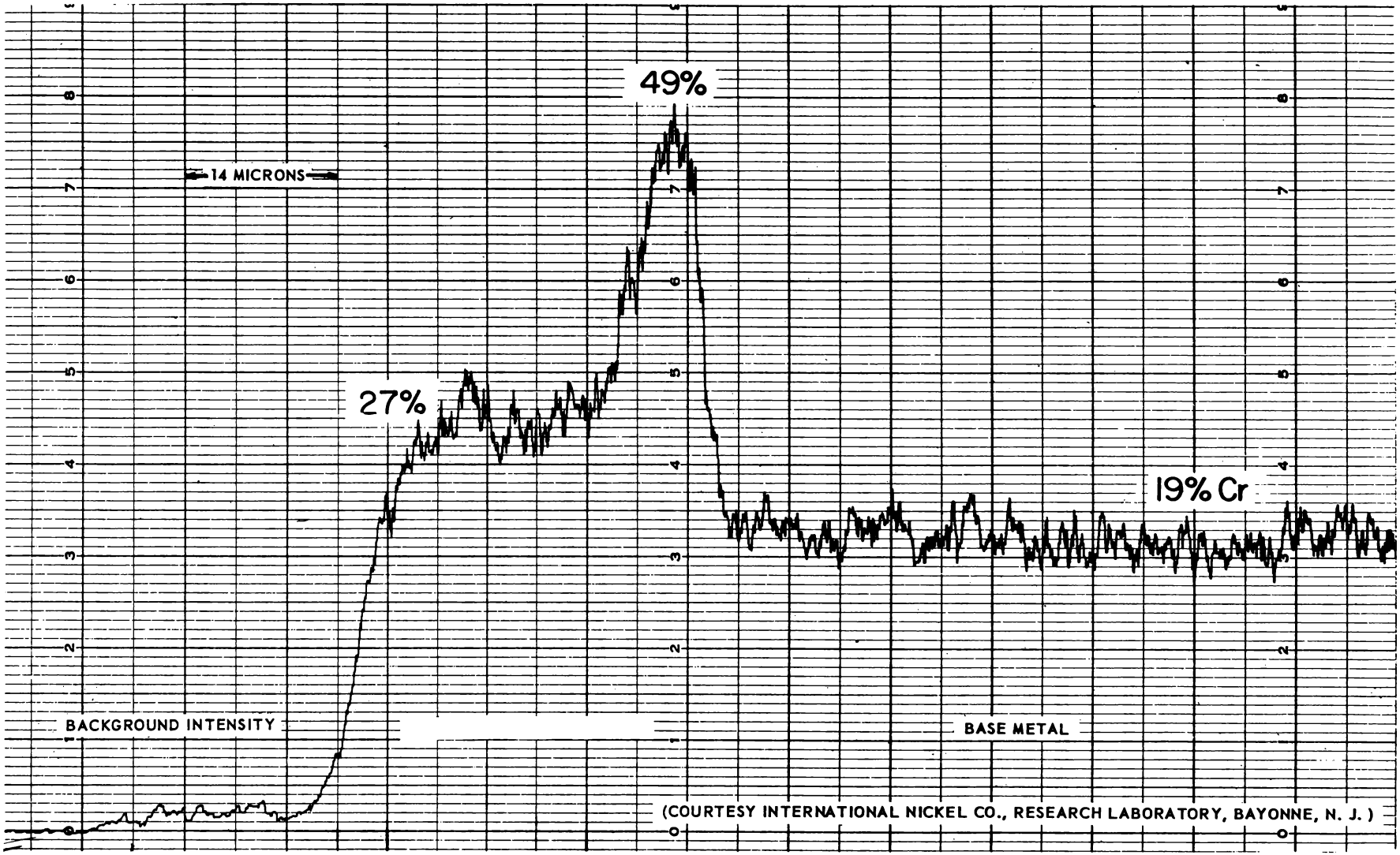

FIGURE 6.5 ECTRON PROBE MICROANALYSIS - CHROMIUM
TYPE 304 SS, DESCALED HEAT TRANSFER SPECIMEN - 1300 °F

A diffraction pattern contained many lines and was difficult to analyze. Attention was directed toward the chlorides and oxides of Cu, Cr, Ni and Fe because these metals were known to have been present. Lines in the diffraction pattern of the sample agreed well with the diffraction patterns of $CrCl_3$, $CuCl_2$, $FeCl_2$, $FeCl_3$ and $NiCl_2$. The lines of other chlorides of the same metals exhibited some agreement with the pattern of the sample.

The other two higher temperature heater sheaths had random areas of what appeared to be scale flaking and fluxing. A sheath exposed for 1000 hours was sectioned without descaling through several of these areas. Out of 6 separate areas examined two indicated an intergranular attack as shown in Figure 6.6. It is believed that such attack is caused by the deposit that resulted in the fluxing of the scale. The temperature in the area photographed was between 1050 and 1100°F. The metal temperature where the main body of the solubles deposit is between 800 and 850°F. Metallographic examination has indicated no intergranular attack in the lower temperature areas for the times exposed.

The following is indicated from these deposition studies:

1. Chlorides in the carryover water exist as several metallic chlorides. Rapidity and degree of attack may not be the same for each.
2. Areas of deposit of solids are probably a function of system geometry.
3. The prerequisites for chloride stress corrosion are present, i.e., oxygen, chlorides, stresses and moisture during startup and shutdown.

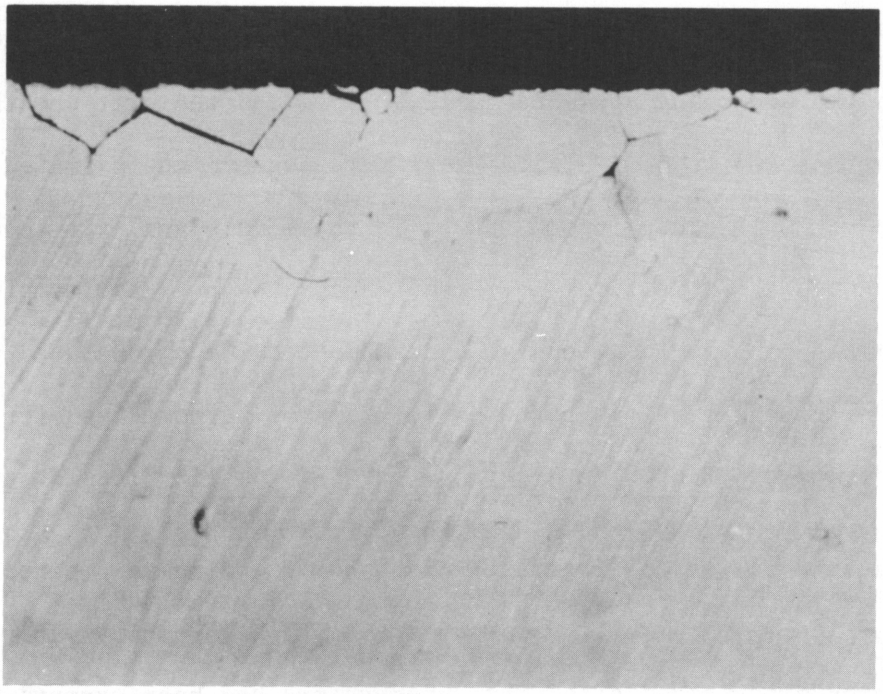

FIGURE 6.6 SECTION THRU FLUXED AREA HEAT TRANSFER EXPOSURE TYPE 304 S.S. CALCULATED METAL TEMPERATURE-1070°F NOT ETCHED

4. Intergranular attack was noted in an area associated with scale fluxing.

6.1.4 Chloride Stress Corrosion Tests

Chloride stress corrosion tests were started in the Cl-1 superheat facility September 1, 1961. The entrance and middle Type 304 SS sheaths are being stressed to 12,000 psi and the exit sheath (high temperature) to 6,000 psi. These stresses are approximated to produce 0.1% creep in 1000 hours in the middle and exit sheaths and one-half this level in the entrance sheath. Beam samples stressed over yield were placed in the steam, superheat and subcooled water coupon sections both for information purposes and for indications of problem areas in the Cl-1 facility itself.

The chloride in the recirculating water is being maintained at 1.5 $\pm$ 0.5 ppm. The facility was started with high purity water and the chloride added after the superheaters had been exposed to operating conditions for 100 hours.

The entrance and middle sheaths were examined after 400 hours exposure to the high chloride system. No visual evidence of damage was noted. The characteristic multicolored deposit was present at the entrance of the first superheater. The entrance heater and sheath assembly were replaced and the test will be continued in 400-hour units.

6.1.5 Coupon Testing

Corrosion testing of Type 304 stainless steel in a superheated steam environment (1050°F, 1000 psi, 20 ppm O_2) indicated that the oxidation rates of specimens under applied stresses are greater than those of

unstressed specimens. Corrosion scale formation on the stressed specimens after 1000 hours was about twice the thickness of the scale formed on unstressed material in the same length of time. After an additional 100 hour exposure for a total of 2000 hours, similar results were obtained. No stress corrosion cracking was observed in the specimens tested; however, due to the position of the coupon section in the testing facilities, the chloride contamination of the specimens was low. Tests indicate that corrosion Type 304 in 1050°F dry, but oxygen-containing steam will follow a parabolic pattern with a decreasing corrosion rate with time.*

The corrosion scale formed on the stressed specimens was found to be in two distinct layers. The outer layer has a metallic luster while the intermediate phase has a non-metallic, mottled, green-blue hue typical of the oxides of chrome and iron. The only observable difference in the scale between the 1000 and 2000 hour exposure times was an increase in thickness of both layers.

The thickness of the oxidation layers decreased with increasing cold work. For 1000 hours, the average oxide thickness was 0.6 mils for the annealed, 0.4 mils for the 10% cold worked and 0.2 mils for the 20% cold worked.

6.1.6 Discussion of Coupon Testing

Stressed tubing specimens of Type 304 stainless steel in the configuration shown in Figure 4.1 of the last (eighth) quarterly report, page 97, have been exposed in this environment for a total of 2000 hours with a complete microscopic inspection after the 1000 and 2000 hour exposure times. The test

* GEAP-3724, Nuclear Superheat Project - Seventh Quarterly Progress Report, January - March 1961, pp. 69-70.

configuration results in a stress of 21,000 psi tension during loop operation, which represents 100%, 90%, and 80% of the 1000 hour, 1% creep rate values for the annealed, 10%, and 20% cold worked specimens respectively.

6.1.6.1 Inspection Results After 1000 Hours of Exposure

These results were previously reported in GEAP-3785 but are included here in summary form, for an easy comparison with results obtained after 2000 hours of exposure to steam. A specimen from each tubing condition was sectioned and examined after 1000 hours exposure. No evidence of stress corrosion cracking was observed. The microstructures showed extensive carbide precipitation at the grain and twin boundaries as can be expected of normal 304 stainless heated above 900°F. However, as can be seen in Figure 4.5 in the last (eighth) quarterly report, page 101, the corrosive attack appears to be influenced more by the grain orientation than by the presence of precipitated carbides. The corrosive attack has produced a scale up to 1 mil in thickness on some of the grains as compared to a scale of about 0.2 mil formed on unstressed coupons exposed in previous runs of CL-1.

6.1.6.2 Inspection Results After 2000 Hours of Exposure

As in the case of the 1000 hour exposure specimens, no stress corrosion cracking was evident. The only noticeable change in the corrosion scale was an increased thickness to 1.5 mils as compared to 1.0 mils for the 1000 hour specimens. Some preferential oxidation occurred as

shown in Figure 4.3 of the eighth quarterly report, page 100. The corrosion "finger" appears to have followed a twin boundary into the grain. Specimens will be exposed for additional times and examined with particular attention being given to the possible growth and preferential location of these corrosion "fingers".

6.2 In-Pile Measurements

6.2.1 SADE Evaluations During SH-4 Irradiation

6.2.1.1 Chloride Levels

Chloride analyses of the VBWR primary water during the SH-4 irradiation period are listed in Table 6.2. These give a time average of 0.06 ppm and show a peak of 0.61 ppm. A source of chloride in the reactor was discovered on August 17 when a rise in the water conductivity was associated with operation of the VBWR multitube sampler. Cooling water drained to the sample sink and then to the reactor. This cooling water has since been rerouted to the sump. Days on which the multitube sampler was used are indicated in Table 6.2. Because of the carryover of reactor water to the VBWR steam separator, which drains to the hotwell, very rapid cleanup was achieved at a power level of 30 MWt. The cleanup half-life was about one hour, whereas, the half-life through the cleanup demineralizer is about four hours.

6.2.1.2 Radio Chemistry

Radiolytic gases - Previous attempts to measure the gas content of SADE steam by collection of the gas at low pressures (in order to reduce the gas content of the condensate)

have been unsuccessful because of non-uniformity of the samples. Presently, the gas content is being measured by collection of gas at atmospheric pressure so as to reduce the effect of non-uniformity by use of a much larger sample. Preliminary results indicate about 37 cc(STP)/kg of total gas in the entering steam (equivalent to 18 ppm O_2) and a five percent reduction in concentration or less during passage through the loop when the exit steam temperature is 820 to 890°F.

Fission gas - Measurements of fission gases in the steam entering the SADE loop and in that leaving the loop indicated no measurable release of fission products from SH-4 has occurred. Under the circumstances, with other leakers in the VBWR core, the detection limit for leakage from SADE was about 0.1 μc/sec of total fission gases with half lives greater than ten minutes. At a steady reactor power of 30 MWt, the fission gas passing through SADE (from VBWR steam) was approximately one μc/sec.

Condensate - The SADE condensate was sampled on August 9 and 10. The principal radioisotope present, other than 10-minute N-13, is F-18 which has a concentration of 1.1 x 10^3 μc/ml. Other nuclides identified by gamma ray spectroscopy were Ag-110m (10^{-5} μc/ml), Na-24 (10^{-5} μc/ml), and fission gases ($<10^{-4}$ μc/ml). Sodium is present in the VBWR hotwell and enters the SADE loop in the desuperheater water. Water from the recombiner was similar in composition to the condensate but contained less than ten percent

as much F-18. There was no water flow from the vent condenser.

TABLE 6.2

Date	Time	Cl^--ppm	Date	Time	Cl^--ppm
6-9	0852	Ca0.33	7-25	0900	<0.020
6-12	0940	0.151	7-26	0520	<0.020*
6-13	0700	0.070	7-27	0920	<0.020
6-14	0945	<0.020	7-28	0500	<0.020
6-23	1230	0.043	7-30	1945	<0.020
6-27	0955	0.066	8-1	0405	<0.020
6-28		0.026	8-3	1500	<0.020
6-30	1050	0.037	8-4	0610	0.026
7-3	1400	0.030	8-7	1100	0.179*
7-5	0558	0.047	8-8	0830	0.064
7-5	1100	<0.020	8-9	0910	0.021
7-7	0918	<0.020*	8-10	0910	0.025
7-9	0530	0.080	8-14	0910	0.032
7-10	0845	0.036	8-16	1430	0.036
7-11	0950	0.092	8-17	0925	0.054
7-12	0855	0.115	8-17	1430	0.611*
7-14		0.037	8-17	1500	0.465
7-18	1132	0.068*	8-17	1610	0.190
7-19	0915	0.034	8-17	1712	0.097
7-20	1030	<0.020*	8-17	1746	0.070
7-21	0958	0.030	8-17	1818	0.058
7-24	1000	0.030	8-18	0945	0.034

* Multitube sampler used on these days from about 0930 to 1130.

6.2.2 SADE Evaluations During SH-4C Irradiation

6.2.2.1 Chloride Levels

During the period this fuel element was installed in the reactor, the chloride concentration in the reactor water rose above 0.5 ppm on September 6 and on September 7 while the reactor was at full power. It was above 0.5 ppm for a total of 9 hours while the reactor was at 30 MW power. Subsequently, the chloride concentration in the reactor water was less than 0.1 ppm whenever the reactor power was greater than 2 MW until September 20, when it rose to 0.12 ppm and reached a maximum of 0.27 on September 21.

6.2.2.2 Activity Levels

Table 6.3 shows radiation survey readings during irradiation of SH-4C after activity level increases had been observed.

TABLE 6.3

RADIATION SURVEY READINGS OF SADE LOOP COMPONENTS DURING SH-4C IRRADIATION

Note: Upper readings taken 7 P.M. 9-24-61
Lower readings taken 10 P.M. 9-25-61

Location	mrad/hr	mr/hr	Background mr/hr
S-1106		300	15
		350	35
FE-1101	380	200	100
	1500	150	100
FCV-1112		150	100
		100	100
FCV-1103	2500	150	100
	1400	130	100
FCV-1101	10000	380	100
	3500	200	
Desup. Flange		120	100
		120	100
Desup. Line		100	100
		100	100
Desup. Line 10" upstream of TE-1109	230	300 230	100 40
FCV-1104		150	100
		100	35

TABLE 6.3 (continued)

Location	mrad/hr	mr/hr	Background mr/hr
West End		130	100
M. Condenser		100	25
Overall		180	100
M. Condenser		80	25
Overall		100	100
V. Condenser		40	30
Overall		100	Variable
Steam Line		100	Variable

7.0 TASK F - HEAT TRANSFER

7.1 Summary

Data from three shakedown runs, with Reynolds Numbers up to 880,000, have been reduced. These data, although approximate, provide reasonable agreement with extrapolation of ANL data obtained by Heineman as shown in Figure 7.1

Seven other runs have been made, with steam flow in a 0.370 in. x 10 ft. long tube, and data is expected to be reduced during the next reporting period.

Redesign of the annular and tubular flow assemblies has been completed. Redesign was necessary to avoid excessive bowing and electrical shorting that occurred in prior testing.

7.2 Design

The annular flow superheater has been redesigned to prevent electrical shorting of the inner heater tube. The assembly is shown in Figure 7.2. The inner superheater tube, part no. 9, has three short metal tube spacers, 0.089 in. in diameter, equally spaced on its outside diameter and spaced about 15 inches apart longitudinally. An outer tube, part no. 4, 0.006 in. thick forms the annulus enclosure. The inner heater and outer tube forming the annulus, are electrically connected in parallel. This design avoids the necessity of non-conducting spacers and eliminates electrical shorting problems.

The outer tube is made very thin such that its heat flux will be 17% of that of the inner heater tube, and thus have a small effect on the heat transfer coefficients which will be calculated using the inner tube wall temperatures.

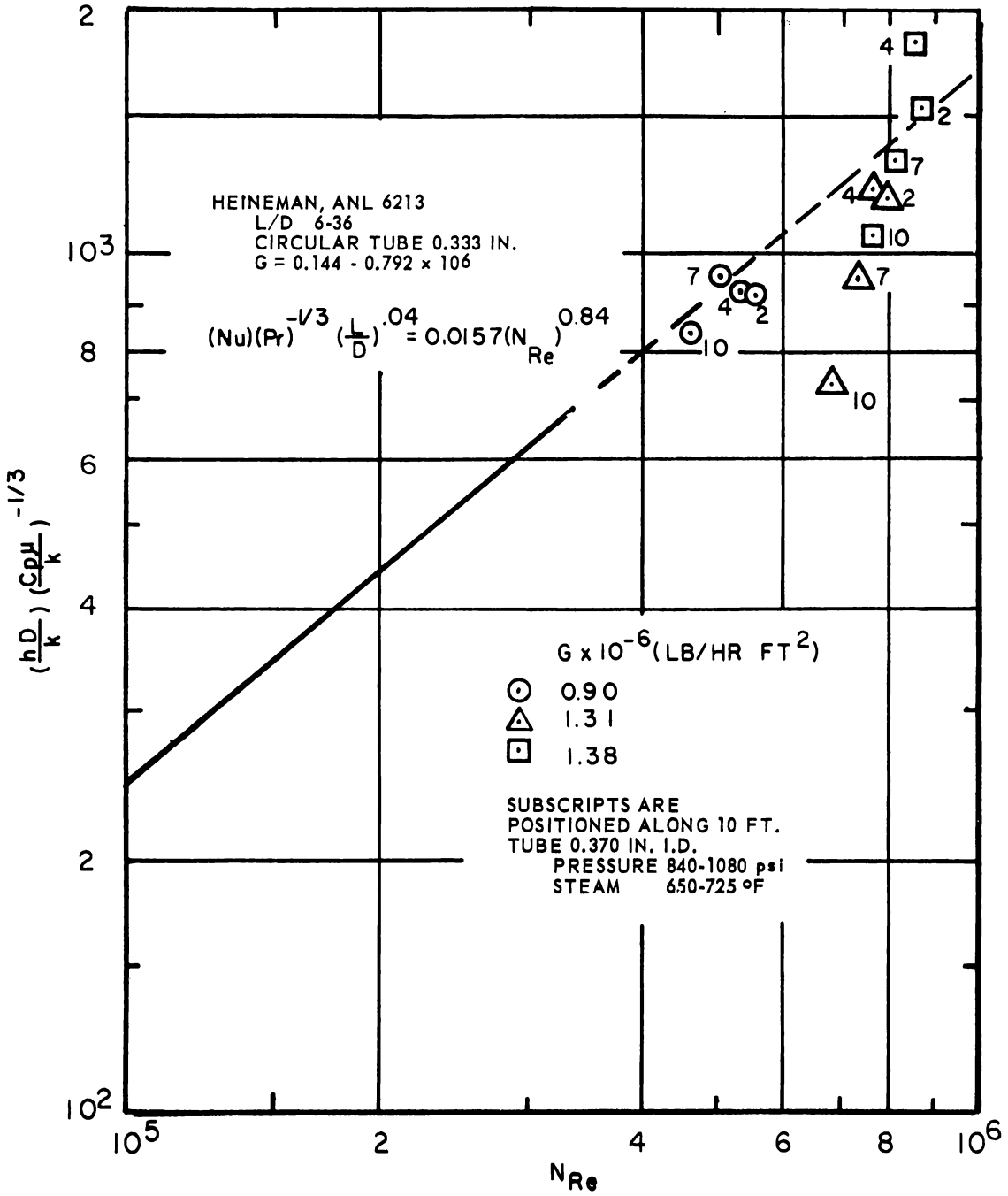

FIGURE 7.1
PRELIMINARY HEAT TRANSFER DATA
FOR SUPERHEATING STEAM

10		11	GENERAL ELECTRIC	141F900
UNLESS OTHERWISE SPECIFIED USE THE FOLLOWING:—			REV. NO. 0	TITLE ASM
APPLIED PRACTICES: 145A5481	SURFACES: 125√	TOLERANCES ON MACHINED DIMENSIONS: FRACTIONS ± 1/32, DECIMALS ± —, ANGLES ± —	141F900 DWG. NO.	HEATER ROD
			CONT. ON SHEET	FIRST MADE FOR SUPERHEAT F2

P.L. ISSUED

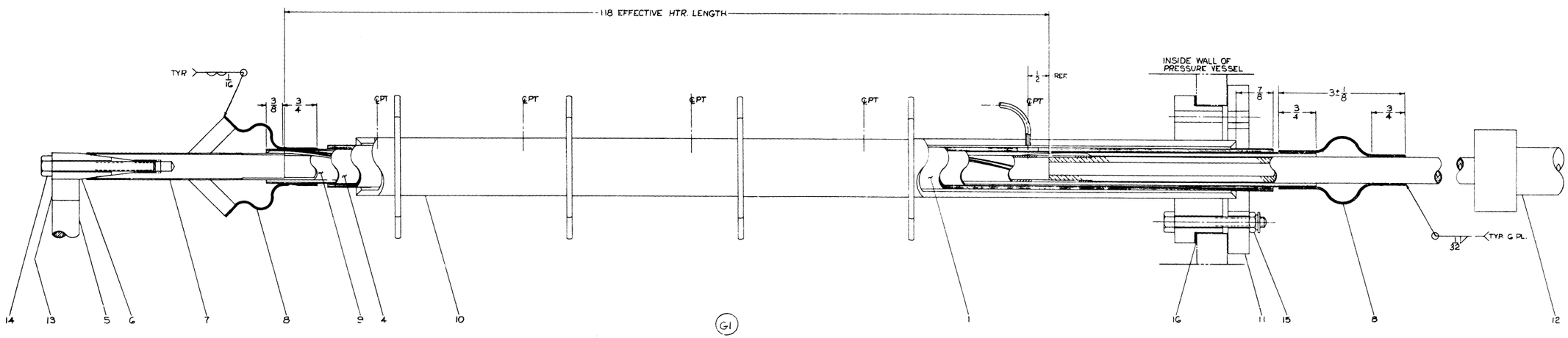

ANNULAR FLOW SUPERHEATER

Figure 7.2

Assembly of this annular arrangement will be made during the next series of experiments.

A new circular flow arrangement has also been designed as shown in Figure 7.3, in order to prevent bowing and resulting electrical shorting of the heater tube. The essential changes made are additional longitudinal spacers, with ceramic insulators, and a spring at the inlet end to counteract bowing moments.

Manufacture of parts for the circular assembly is expected to be complete the first week in November.

7.3 Operation

Operations during this quarter were restricted to steam flow in the 0.370" I.D. x 10 ft. long tube.

The first runs indicated too close a clearance between the ceramic spacers and the heater tubes. This resulted in cracking of the ceramics; some binding between ceramic and the heater tube; and eventually bowing and shortening of the tube.

The ceramic-tube clearances were increased, to allow freer expansion, and 7 runs were obtained with this assembly.

An assembly was tried with Durabla, used in lieu of ceramic spacers, but was found unsatisfactory in that bowing and shortening of the tube resulted. This was attributed to excessive expansion of the Durabla, which resulted in binding at the support positions, and eventually bowing of the tube and failure.

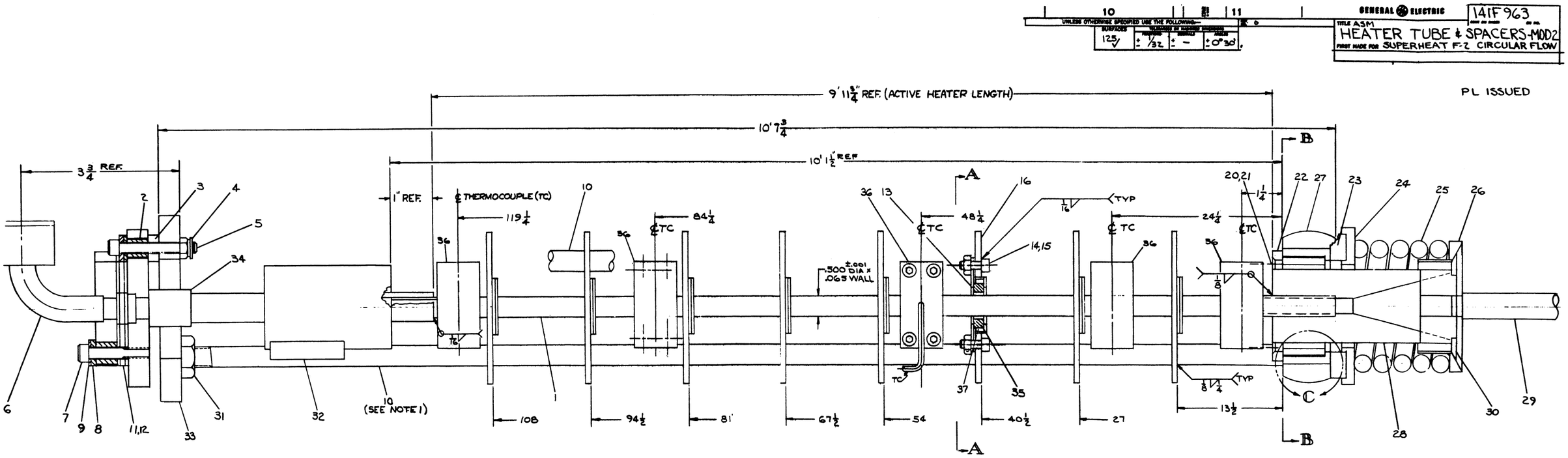

CIRCULAR SUPERHEAT ASSEMBLY

Figure 7.3

7.4 Data

Three runs, obtained in June, have been reduced and the results tabulated below.

TABLE 7.1

PRELIMINARY HEAT TRANSFER DATA FROM SHAKEDOWN RUNS*
CIRCULAR TUBE 0.370 IN. I.D. x 10 FT.
EFFECTIVE HEATING LENGTH

Run No.	Test Level (Ft. from inlet)	P* psi	G lb/hr-ft^2 x 10^{-6}	Q/A Btu/hr-ft^2 x 10^{-3}	Δt (^oF Wall-Bulk)	h Btu/hr-ft^2 ^oF	N_{Re} x10^{-3}	$\left(\frac{hD}{k}\right)R_r^{-1/3}$
2C	- 0.5	842	1.38					
	2			133	105	1790	880	1548
	4			137	97	2080	858	1840
	7			139	124	1490	818	1348
	10			147	163	1120	768	1100
3C	- 0.5	1079	1.31					
	2			143	97	1520	792	1223
	4			154	105	1510	774	1238
	7			154	134	1160	732	975
	10			154	137	900	686	731
4C	- 0.5	913	0.90					
	2			119	135	1100	557	938
	4			125	144	1070	538	945
	7			131	145	1120	509	984
	10			136	173	930	469	845

* Pressure control was poor, due to blockage of a condensate line and varied up to ± 20 psi during the runs.

The data tabulated above is plotted on Figure 7.1.

In addition to the data above, seven runs were made in September, but data is not yet reduced. Approximate conditions during these runs are tabulated below.

TABLE 7.2

UNREDUCED DATA FOR STEAM HEAT TRANSFER IN A 0.370 I.D. x 10 FT. TUBE

Run No.	Pressure psi	W lb/sec Steam Flow	t_s, °F Superheat	Temp., °F Steam at Exit
7C	800	0.21	300	822
8C	800	.21	270	786
9C	800	.23	428	939
6C	1000	.19	370	895
5C	1000	.28	335	865
11C	1100	.29	420	968
10C	1100	.31	290	841

8.0 TASK G - MECHANICAL DEVELOPMENT

8.1 Steam-Water Separation

8.1.1 Summary

During the report period efforts were entirely devoted to radial separator development. Results of tests in May and June (reported in the previous quarterly report GEAP-3785) were analyzed and a topical report of results issued (GEAP-3787). Further development of the radial separator was planned and a modified full circle separator model design.

8.1.2 Discussion

During May and June 1961, a pair of vanes and a full circle of vanes were tested as reported in the previous quarterly report, GEAP-3785. These results were analyzed and presented in a topical report, GEAP-3787, "Results of Air-Water and Steam-Water Tests on Radial Vane Steam Separator Models". It was concluded that these results were very encouraging but not sufficient to provide reliable information for use in establishing design parameters.

A modified full circle radial vane separator model has been designed as shown in Figure 8.1 and is being constructed for air-water and steam-water testing. The design is an extension of previous work and is expected to fill in gaps in the present knowledge of radial separator performance as well as avoid short comings of previous tests.

As shown in Figure 8.1, the full circle radial vane model consists of 18 active vanes and 18 inactive vanes mounted on a 10 inch diameter plenum. The vanes are 130° arcs of 4 inch radius.

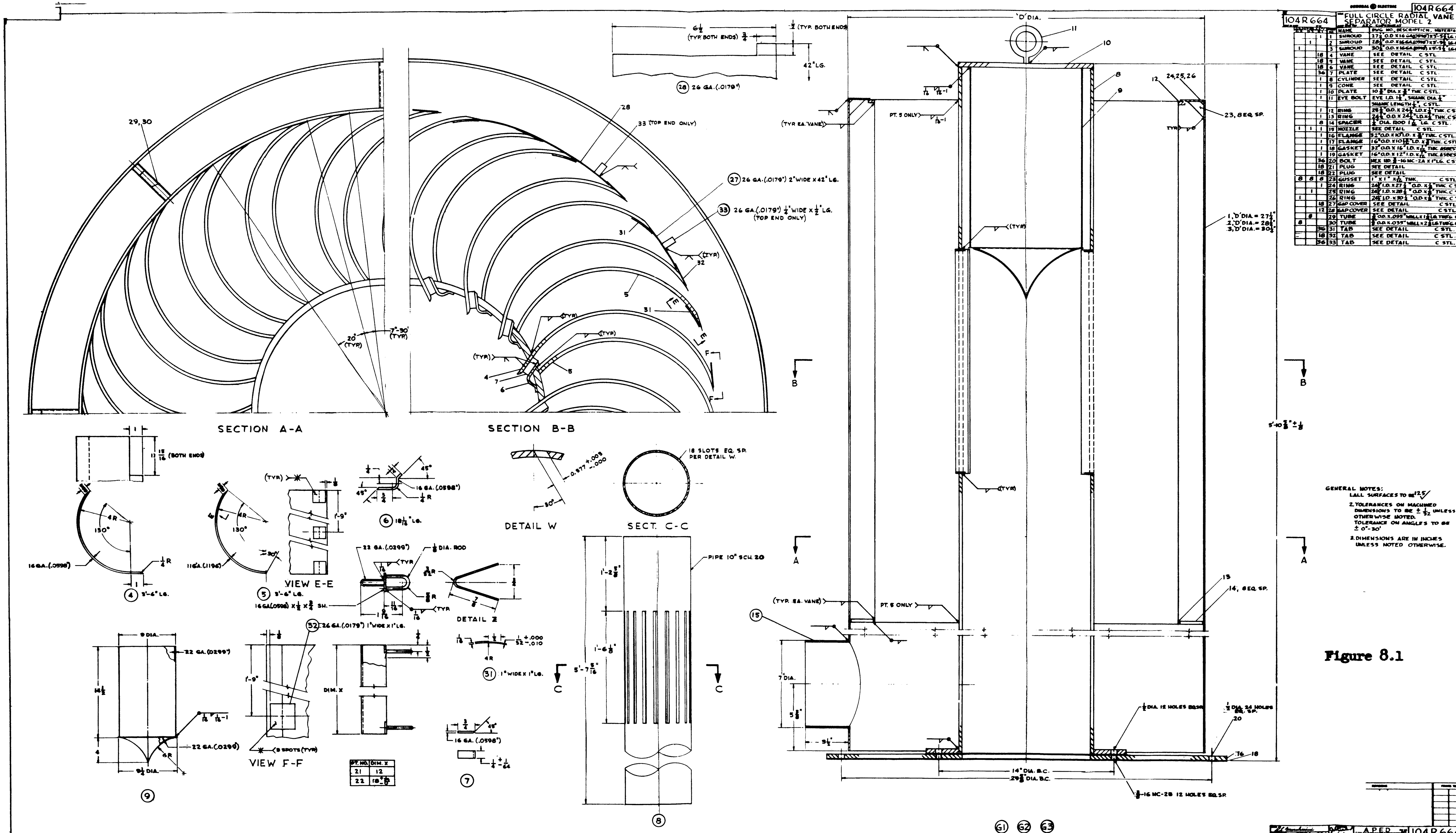
FULL CIRCLE RADIAL VANE SEPARATOR MODEL 2
104R664
SECTION A-A
SECTION B-B
DETAIL W
SECT. C-C
VIEW E-E
VIEW F-F
DETAIL Z
18 SLOTS EQ. SP. PER DETAIL W.
PIPE 10" SCH. 20
'D' DIA.
1,'D'DIA.= 27$\frac{3}{4}$"
2,'D'DIA.= 28$\frac{1}{4}$"
3,'D'DIA.= 30$\frac{1}{4}$"
APED
SAN JOSE

Figure 8.1

Nozzles ½" wide x 3/4" long x 18" high, supply mixture from the plenum to the vanes. The vanes extend 12 inches above and below the nozzle to prevent velocity and spread effects, which would cause overflow of mixture above the top of the vanes, and to maintain the same downcomer area well below the point of exit of water from the vanes.

The spread of the mixture on the vanes after leaving the nozzle is calculated to be about 4 inches. The analysis is based on the solution of the hydraulics problem of surface contours of an open channel stream after an abrupt expansion. The solution, as shown in Figure 34, page 560 of Hunter Rouse's "Engineering Hydraulics", was adopted by substituting centrifugal force for gravity force. Under these conditions the spread is independent of nozzle velocity.

8.1.3 Test Program

Two basic tests will be performed in steam-water mixtures

8.1.3.1 Carryunder Limitations

Carryunder tests will utilize 12-inch long plugs in the nozzles to limit nozzle height to 6 inches. With this arrangement velocities of the mixture from the nozzles and of water discharged into the downcomer will be in the range expected in a full scale separator operating in a nuclear reactor. Different diameter shrouds will be used to vary the downcomer area and hence the downcomer velocities. Prior to operation with steam-water mixtures, the model will be tested with air-water for both carry-under measurements and visual observations of flow configurations at various flow rates.

8.1.3.2 Carryover Limitations

Carryover measurements will utilize only 6 of the 18 nozzles, with the full 18 inch height of each nozzle being used during the test. This arrangement, with the downcomer full of discharge water, will result in velocities of the steam rising between the vanes being in the range of those expected for a full scale separator operating in a reactor.

The above arrangements are necessary in order to simulate full scale separator operation because of the flow capacity limitations in the test loops.

8.2 Seal Development

8.2.1 Summary

A seal has been successfully constructed using a vacuum filling method and a 0.093 inch diameter plug as a final closure. This seal was tested to determine its expansion as a function of temperature. The bulk expansion of the 50-50 solder caused a 0.045 inch increase in the diameter of the seal at 550°F. Based on the results of the expansion test, another seal is being made. The seal will be tested in the leak test fixture described in the April - June Quarterly Report. Tests to determine leakage flow rates will begin when the seal construction is complete. If the leakage flow rates are less than the specified maximums, the feasibility of the seal will be established.

A corrosion test program has been set up to evaluate the effect of the liquid solder on the stainless steel seal body at operating temperature. The test equipment and corrosion test samples are

being manufactured. The test samples will be sealed in tubes and subjected to the effects of liquid solder, stress and a temperature of 750°F for a period of two months.

8.2.2 Seal Fabrication

In the month of July an attempt was made to construct a seal by first casting the solder into the seal body in a vacuum and then making the sleeve welds. This method proved successful as far as the casting method was concerned, but difficulty was encountered in making the final sleeve weld. Examination of this weld showed that the solder was included in the weld bead. This is due to the large amount of heat required to make the weld. Because of these results, it was decided to alter the construction procedure so that the sleeve welds are made first, and then the seal is filled in a vacuum. The final closure weld will be a small (.093 in.) plug which will require a much smaller amount of heat.

During August and September a seal was successfully constructed by welding the sleeves first and casting the solder in a vacuum. A closure weld using the 0.093 inch diameter plug was achieved. Unfortunately the casting procedure was difficult to accomplish successfully. Work is being done to improve this procedure so that no shrinkage voids occur inside the seal as the solder cools after filling.

8.2.3 Seal Expansion Test

The seal mentioned previously was tested to determine its expansion as a function of temperature. The diameter of the seal increased from 1.790 in. at room temperature to approximately 1.845 in. at

550°F. Thermal expansion accounts for 0.010 inch and the bulk expansion of the solder accounts for 0.045 inch of the total 0.055 in. diameter increase.

8.2.4 Leak Test

Another seal will be made and tested in the leak test fixture based on the results of the expansion test. Tests to determine the leakage flow rates will be conducted when the seal construction is complete. If the leakage flow rates are less than the established maximums, the feasibility of the seal will be established.

8.2.5 Corrosion Test

A corrosion test program has been set up to evaluate the effect of the liquid solder on the stainless steel seal body at operating temperature. In particular, two mechanisms will be investigated: intergranular attack and stress corrosion cracking.

The test equipment has been designed and the equipment and test samples are being made. The samples will be sealed in tubes and subjected to the effects of liquid solder, stress (10,000 and 15,000 psi) and a temperature of 750°F. A test period of two months is planned.

8.2.6 Improved Solder

A high purity vacuum refined solder has been recently made available commercially. A sample order was placed, and the solder has been received. It is felt that this solder will improve seal performance and possibly eliminate the procedure of casting the seal in a vacuum.

9.0 TASK H - SADE AND E-SADE

9.1 SADE

9.1.1 SH-4 Irradiation

Irradiation of superheat fuel element SH-4 was performed in the SADE loop, between June 7 and August 20, 1961, at which time SH-4 was removed to permit installation of SH-4C. No abnormal activity levels were noted during this operation cycle. Superheated steam temperatures up to 900 F were achieved during steady operating conditions, with one transient period which reached 925 F. Power of the element was calculated to be 62 KW at 30 MW reactor power. Total exposure of the element was 54 MW hours or an average of 540 MWD/ton. Total steam flow past the element, during the irradiation period, has been estimated to be 1.1×10^6 lb.

The pre-irradiation examination of this element had been made in July, 1960, when manufacture of the element was completed. Post irradiation visual inspection plus non-destructive examination was completed after removal from the reactor. The fueled section of the element was badly warped in a manner similar to that noted on element SH-4B. Considerable corrosion and crud deposition were observed in the thermal liner cup, and on the fueled section exterior cladding. The hardware above the fueled section was free from crud plate-out. Corrosion on the fueled section exterior was blue-grey in color. Reddish brown deposits began about 8 inches below the top weld of the fueled section exterior. Relatively clean regions, free from deposit, were observed about 11 to 14 inches and 20 to 30 inches down from the top weld on the fuel cladding exterior.

Four corrosion and crud samples were taken for chloride ion analysis and one sample was taken for X-ray diffraction analysis from the exterior cladding. These samples are to be analyzed for chloride contamination and one sample will be checked to determine all constituents.

Post-irradiation measurements indicated that the outer cladding had collapsed rather uniformly upon the fuel, without forming longitudinal or circumferential wrinkles. There was severe bowing of the fuel element, however, and the deviation from straightness was measured as 450 mils compared with less than 10 mils pre-irradiation. Measurements indicated a necking down of the inner cladding of about 21 mils in diameter, near the bottom seal weld.

Several O.D. measurements were later spot-checked and found to be about 4 mils less than first post-irradiation measurements. Examination of the areas by Kollemorgen periscope showed that the first measurements included thickness of corrosion and crud plate-out, and the second measurements did not. Thus, the corrosion-crud film was about 1.5 to 2 mils in thickness.

An attempt to determine the location of the expansion monitor (gum-drop) of this element will be made with gamma scan plots. At present, no definite plans have been made regarding destructive examination of this element, which is necessary to examine this expansion monitor, unless the gamma scans can be interpreted.

Chloride levels in VBWR primary water during irradiation of SH-4 were measured as reported in detail in Section 6.2. The time average of chloride level was 0.06 ppm with a peak level of 0.61 ppm.

9.1.2 SH-4C Irradiation

Fuel element SH-4C was installed in the SADE loop on August 28. It remained in the loop until September 23, at which time the element was removed because condensate samples indicated that the element cladding had become defective.

Operation of the element during this period was as follows:

1. Total time on steam - 492 hr.
2. On steam - flow 1200 to 1500 #/hr. - 136 hr.
3. On steam - flow approximately 1000 #/hr. - 92 hr.
4. On steam - flow approximately 800 #/hr. - 220 hr.
5. Operation with exit steam temperature at 800 to 840 F - 212 hr.
6. Operation with exit steam temperature up to ≈775 F - 280 hr.
7. Maximum power (at 30 MW reactor power) - 63 KW.
8. Total output - 15.8 MW(t).
9. Average fuel exposure - 150 MWD/ton

The element was removed on September 25 after fission gases and iodines were detected in the effluent steam. Steam and condensate samples taken on September 21 contained more than normal amounts of fission products whereas samples of the 19th and earlier had given no indication of leakage. Measurements of the rate of fission gas release ranged from zero to 43 μc/sec. (six major isotopes) during a two-day period prior to shutdown of the reactor. Since measured iodine release also varied greatly, up to a maximum of 0.5 μc/sec. of I-11 and 0.1 μc/sec. of I-131, and the SADE radiation monitor showed a pronounced periodic variation, the observed variations in release rates are believed to have been real and to have indicated a "puffing" type of release. The relative microcuries of gaseous

isotopes was approximately constant on a fission yield basis. Coupons in the effluent steam line were contaminated principally with iodines. The amounts of radioactivity on particulate filters and charcoal absorbers exposed to VBWR stack gas indicate iodine and other fission products from the SADE element were present in the VBWR stack in concentrations far below the allowable discharge limits.

Design conditions for SH-4C are shown in Table 9.1

TABLE 9.1

DESIGN CONDITIONS FOR SH-4C

Power	73 KW
Fuel enrichment	3.5% U^{235}
Steam pressure	1000 psia
Active fuel length	36 3/32"
Outer clad, outside diameter	1.25"
Inner clad, outside diameter	0.75"
Clad thickness, outer and inner	0.028"
Clad material (weld-drawn tubing)	304 S.S.
Instrument tube, outside diameter	0.50"
Fuel (UO_2)% theoretical density	95%
Total fuel loading	3.98 Kg
Axial peaking factor	1.58
Contact conductivity, fuel to inner clad	500 Btu/hr-ft^2-^oF
Contact conductivity, fuel to outer clad	1000 Btu/hr-ft^2-^oF
UO_2 conductivity	1.1 Btu/hr-ft^2(^oF/ft.
Radial flux depression	1.12
Maximum clad temperature (STEADY)	1200^oF
Maximum superheat exit temperature (STEADY)	915^oF
Maximum heat flux (STEADY)	276,000 Btu/hr-ft^2
Minimum steam flow rate (STEADY)	795 lb/hr
Maximum fuel temperature (STEADY)	2700^oF
Maximum clad temperature (TRANSIENT)	1300^oF
Maximum superheat exit temperature (TRANSIENT)	980^oF
Maximum heat flux (TRANSIENT)	276,000 Btu/hr-ft^2
Minimum steam flow rate (TRANSIENT)	690 lbs/hr
Maximum fuel temperature (TRANSIENT)	2800^oF

SH-4C is similar to SH-4 element presently installed in loop except that inert spacers have been eliminated and spiral wire spacers are used to center the element in the process tube. A "gum-drop" experiment is incorporated in this element to determine relative movement

between fuel and cladding during operation, Figure 9.1 shows the design of this fuel element.

The actual measured power from SH-4C indicated that actual operating conditions for the element would be somewhat different from the original values listed in the design data package. The difference was the combined result of limiting maximum reactor power to 28 MW (whereas the design data package was based upon a predicted reactor power of 33 MW) and a slight discrepancy in predicted power from the fuel element itself. Revised design conditions for operation of this element are shown in Table 9.2.

TABLE 9.2

REVISED DESIGN CONDITIONS FOR SH-4C

VBWR power	28 MW
Fuel element power (SH-4C)	59 KW
Maximum clad temperature (STEADY)	1200 F
Maximum superheat exit temperature (STEADY)	930 F
Maximum heat flux (STEADY)	223,000 Btu/hr-ft^2-^{o}F
Minimum steam flow (STEADY)	627 lb/hr.
Maximum fuel temperature (STEADY)	2410 F
Maximum clad temperature (TRANSIENT)	1300 F
Maximum superheat exit temperature (TRANSIENT)	995 F
Maximum heat flux (TRANSIENT)	223,000 Btu/hr-ft^2-^{o}F
Minimum steam flow rate (TRANSIENT)	550 #/hr.
Maximum fuel temperature (TRANSIENT)	2490 F

Examination of the actual operating conditions for this element, during the period of irradiation up until the element was removed because of a suspected defect, showed that this element did not reach the design conditions at any time.

Some difficulty was encountered in removing SH-4C from the process tube. During installation, it had been noted that there was a tendency for the element to hang-up while being inserted, unless the element was rotated during insertion. For removal, the element was initially pulled directly upward in an attempt to remove it from the process

GENERAL ELECTRIC — 76D438 — CONT ON SHEET — DWG NO.

UNLESS OTHERWISE SPECIFIED USE THE FOLLOWING:— SURFACES 125 ▽ — TOLERANCES ON MACHINED DIMENSIONS: FRACTIONS ± 1/64, DECIMALS ± .005, ANGLES ± — REV NO. 0

TITLE: FUEL ELEMENT
FIRST MADE FOR SADE 4C FCF 221L140

GI	PART NO.	NAME	DRAWING NO., DESCRIPTION, MATERIAL, WEIGHT
1	1	END PLUG	ASTMA 269 OR 276. TYPE 304
1	2	COLLAR	ASTMA 269 OR 276 TYPE 304
1	3	END PLUG	ASTMA 269 OR 276 TYPE 304
1	4	FUEL FLANGE	985C340 G2
1	5	TUBE	ASTMA 269 TYPE 304 WD.
1	6	TUBE	ASTMA 269 TYPE 304 WD.
1	7	THERMAL LINER	114B5248G
3	8	WASHER	TYPE 304 STN. STL.
3	9	WIRE	TYPE 304 STN. STL
1	10	SPRING	149A4521P1
1	11	BAIL	114B5252G1
X	12	FUEL	PER ENG. INSTRUCTIONS.
1	13	PLUG	149A4542P1
2	14	SLIP RING	149A4543P1

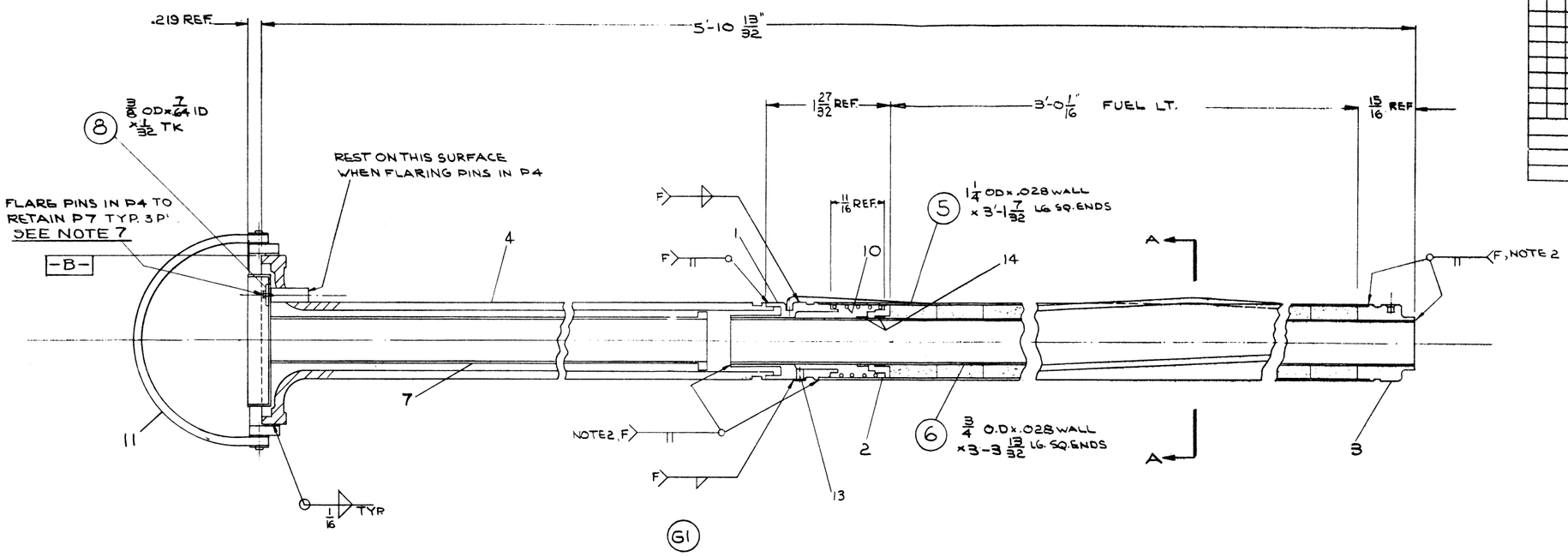

Figure 9.1

NOTES:

1. FOR INTERPRETATION OF GEOMETRIC TOLERANCING REFER TO DWG. 219B402.
2. THESE WELDS TO BE CHECKED FOR LEAKAGE WITH MASS SPECTROMETER EQUIP. MAX PERMISSIBLE LEAKAGE NOT TO EXCEED .005 MICRON CU. FT/HR.
3. ALL OTHER WELDS TO BE TESTED PER SEPARATE ENGINEERING INSTRUCTIONS.
4. HOLES IN END PLUGS TO BE IN LINE ± 1/16
5. FEGTAW FUSION WELD.
6. FOR WELD ROD USE E 308 WHERE REQUIRED.
7. ALIGN P7 ⊙B .006 BEFORE FLARING PINS TO HOLD P7 TIGHTLY.

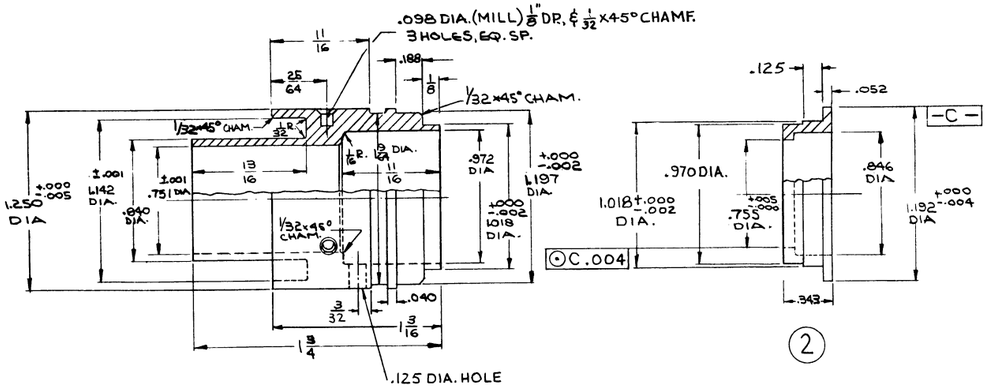

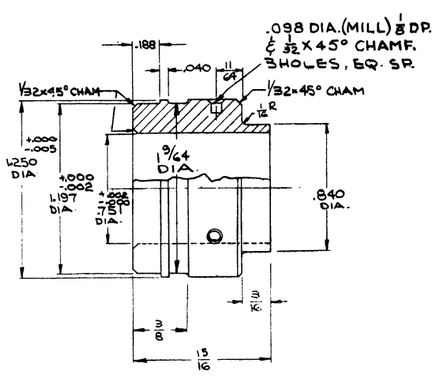

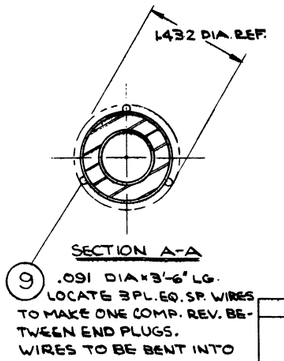

.091 DIA x 3'-6" LG. LOCATE 3 PL. EQ. SP. WIRES TO MAKE ONE COMP. REV. BETWEEN END PLUGS. WIRES TO BE BENT INTO HOLES IN END PLUGS AND WELDED IN POSITION.

AS BUILT

DESCRIPTION OF GROUPS	REVISIONS	PRINTS TO

MADE BY N.A. GRASSO 7-21-61 — CHECKED 1/24/61 — APED SAN JOSE

tube. The element came approximately half-way out before becoming tight in the process tube. It was then "screwed" while pulling in an attempt to "unscrew" the element if the spacer wires were acting as threads. The lifting bail failed during this procedure, before the element was further withdrawn from the process tube. A tool was then manufactured to hold the upper flange of the fuel element and this tool was employed to continue rotation and pulling of the element. This procedure proved ineffective so the fuel element-process tube couple was lifted by means of the tool and downward push applied to the process tube. This procedure removed the process tube, permitting transfer of the element to the spent fuel pit. Examination of the element seemed to show all spacer wires were broken or failed at the bottom welds.

Since the SADE loop had been operating for some period of time before it was determined conclusively that abnormal activity was being released by SH-4C, a survey of components of the loop was made to determine activity levels. Later review of the SADE loop radiation monitor chart showed that operations had continued for approximately 84 hours after the initial failure. Power during the period was nearly steady at 27 MW VBWR power and 57 KW from SH-4C. The reactor was shut down at 3:43 P.M. on September 23, 1961. Activity measurements made at the time are reported in Section 6.2. Chloride levels in the reactor were generally less than 0.1 ppm except for peaks of 0.5 ppm for about 9 hours and a gradual increase to 0.27 ppm immediately prior to removal.

Leakage of reactor water into the SADE test section through the lower tube bundle flange connection was measured on September 22

and found to be 7 lb/hr on the basis of sodium-24 concentration in the effluent steam condensate, neglecting plate-out on the fuel or piping. Carryover of entrained water in the entering steam was less than one-tenth this amount.

Detailed examination of the element is being conducted at the RML facilities. This examination has determined that the cladding failure occurred on the inside cladding, approximately 31.5 inches above the lower end of the fuel element. No cladding defects were visually evident in the outside cladding. The fuel element was bowed but in a pattern somewhat different from that of SH-4 and SH-4B. For this element, the bowing appeared to be concentrated near the upper end of the fueled section, whereas for the other elements, the bowing appeared nearer the middle of the fueled section. Examination of the wire spacers for this element showed that two spacers had failed adjacent to the lower end attachment welds, while the third had failed approximately six inches from the lower end.

9.1.3 SH-5A Design

Design and fabrication of SH-5A fuel element and associated hardware was undertaken during this period. This element employs .016 inch thick cladding of 304 stainless steel. The spacers for this design are small pins and are incorporated in the process tube itself, since the fuel clad is so thin that attachment of the spacers to it would be likely to cause damage which might later contribute to a clad failure. Fabrication of the process tube with spacer pins accurately spaced was difficult and the method employed - by setting the pins against a mandral - is limited as to accuracy obtained after welding of the pins.

Operating conditions for SH-5A were calculated and this information reviewed by the G.E. Safeguards Committee. Approval was given for installation of the .016 inch clad element in the SADE test loop. The exterior clad is not free-standing at operating conditions in this configuration, and relies upon the fuel for stability.

Initial design conditions for SH-5A are shown in Table 9.

TABLE 9.3

DESIGN CONDITIONS FOR SH-5A

Power	78 KW
Fuel enrichment	4.0% U^{235}
Steam pressure	1000 psia
Active fuel length	36"
Outer clad, outside diameter	1.25"
Inner clad, outside diameter	0.75"
Clad thickness, outer and inner	0.016"
Clad material (weld-drawn tubing)	304 S.S.
Instrument tube, outside diameter	0.50"
Fuel (UO_2)% theoretical density	95%
Axial peaking factor	1.58
Contact conductivity, fuel to inner clad	500 Btu/hr-ft^2/°F
Contact conductivity, fuel to outer clad	1000 Btu/hr-ft^2/°F
UO_2 conductivity	1.1 Btu/hr-ft^2/°F/ft.
Radial flux depression	1.14
Total fuel loading (calculated)	4.28 Kg
Maximum clad temperature (STEADY)	1200°F
Maximum superheat exit temperature (STEADY)	895°F
Maximum heat flux (STEADY)	283,000 Btu/hr-ft^2
Minimum steam flow rate (STEADY)	925 lb/hr
Maximum fuel temperature (STEADY)	2825°F
Maximum clad temperature (TRANSIENT)	1300°F
Maximum superheat exit temperature (TRANSIENT)	955°F
Maximum heat flux (TRANSIENT)	283,000 Btu/hr-ft^2
Minimum steam flow rate (TRANSIENT)	805 lb/hr
Maximum fuel temperature (TRANSIENT)	2915°F

Physics calculations predict the design fuel element power of 78 KW at a reactor power of 33 MW.

Prior to installation of the element, a revised calculation model for estimating the clad temperatures was settled upon as being somewhat more accurate, and more conservative than the previous code model. This calculation includes a correction, based upon the 0.5

power of the ratio of the bulk coolant temperature to the cladding surface temperature, which has now been included in the code for calculating these conditions. The following results show the difference in predicted conditions, based upon this change.

	Previous Code		New Code	
Inlet temp. - °F	545	545	545	545
Exit temp. - °F	895	883	838	903
Flow - lb/hr	925	1095	1095	925
Maximum clad temp. - °F	1200	1110	1200	1330
Element power - KW	78	78	78	78

Because of concern about leakage of the lower flange, with possible chloride contamination, wetting and drying of the initial fuel section, and damage to the fuel element which might result from wetting, it was decided to eliminate the thermal liner in the upper section of this element to provide a preheat for the inlet steam. This regenerative heat transfer would dry up to approximately 4% moisture from the inlet steam, or provide for 20 to 30 F superheat for dry saturated inlet steam.

With the thermal liner removed from the upper section of this fuel element, there will be an increase in the heat transfer from the superheated steam in the discharge section to the entering steam in the inlet section. The figures given in Table 9.4 are based upon no moisture in the entering steam. This is a conservative assumption since temperatures will all be correspondingly lower if moisture is present in the inlet steam.

TABLE 9.4

EFFECT OF REMOVING THERMAL LINER, SH-5A

	Steady	Transient
Inlet temperature - heater section °F	545	
Inlet temperature - fuel section °F	575	
Maximum steam temp. - fuel exit °F	857	910
Maximum steam temp. - heater exit	803	
Maximum clad temp. °F	1200	1300

TABLE 9.4 (Continued)

	Steady	Transient
Maximum heat flux - Btu/hr-ft^2	289,000	289,000
Maximum fuel temp. ^oF	2,770	2,860
Minimum steam flow rate lb/hr	1,180	1,030

Figure 9.2 presents the "as-built" drawing of this fuel element.

9.1.4 SH-4B Heat Transfer Performance Evaluation

9.1.4.1 Introduction

A study was made to compare measured steam temperatures with the predicted steam temperature gradient for element SH-4B. For this element, the steam was heated as it flowed down the first pass between the outside of the fuel element and the process tube. The second pass was upflow through the central hole of the fuel element between the instrument tube and the inside clad. The list presented below contains the important assumptions and bases that were used to analyze the performance of SH-4B.

9.1.4.2 Important Assumptions and Bases of Anlaytical Model

1. Linear radial flux depression across the fuel, 10%.
2. Axial peaking factor, 1.58.
3. One-dimensional (radial) heat transfer was assumed.
4. All steam properties are evaluated on a nodal, rather than a continuous, basis.
5. Eighteen axial nodes were used.
6. Heat loss to moderator water was accounted for.
7. System was in a steady state.
8. Constant thermal conductivities of 1.1 Btu/hr-ft^2 (^oF/ft) for UO_2 and 12.0 Btu/hr-ft^2 (^oF/ft) for stainless steel were used.

GENERAL ELECTRIC

UNLESS OTHERWISE SPECIFIED USE THE FOLLOWING:— SURFACES 63 V; TOLERANCES ON MACHINED DIMENSIONS: FRACTIONS ± 1/64, DECIMALS ±.005, ANGLES ± 1°; REV. 0

TITLE: FUEL ELEMENT 9H5A

FIRST MADE FOR GADE FCF 221L140

GROUP NO.	QUANTITY	GI	PART NO.	NAME	DRAWING NO., DESCRIPTION, MATERIAL, WEIGHT
		1	1	FUEL FLANGE	985C340 G1
		1	2	THERMAL LINER	114B5248G3
		3	3	WASHER	AISI TP 304
		1	4	BAIL	114B5252G1
		1	5	END PLUG	149A4522P1
		1	6	SPRING	149A4523P1
		1	7	SLEEVE	149A4524P1
		1	8	TUBE	ASTMA 269 TP 304
		1	9	TUBE	↓ ↓
		1	10	OUTER CLAD	↓ ↓ WD
		1	11	INNER CLAD	ASTMA269 TP304 WD
		X	12	FUEL	PER ENG. INSTR.
		1	13	END PLUG	149A4525P1
		T	14	CONE	149A4526P1

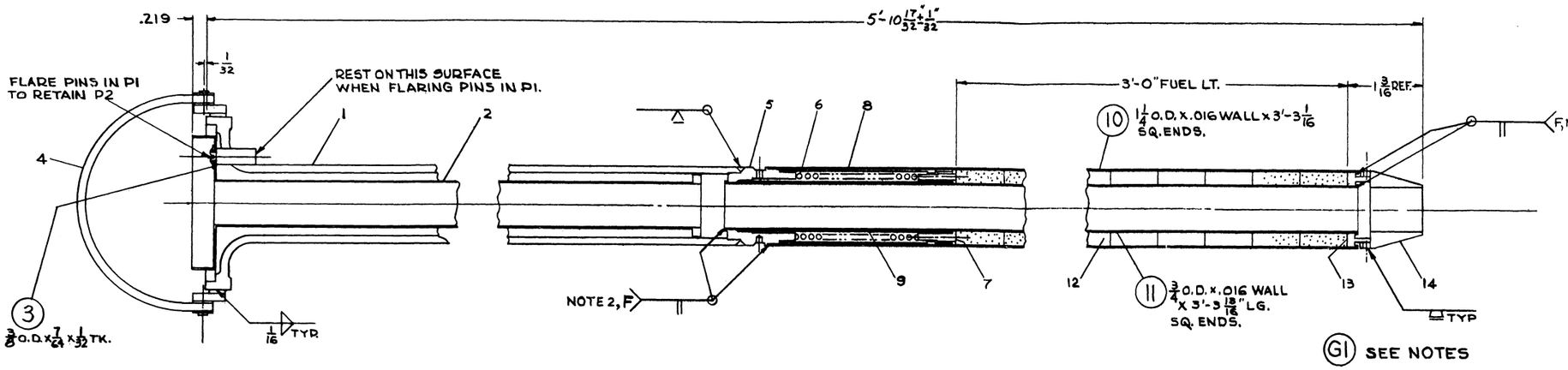

Figure 9.2

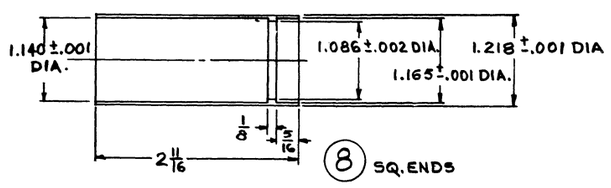

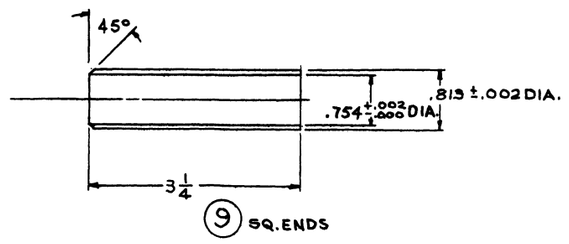

NOTES:
1. FOR INTERPRETATION OF GEOMETRIC TOLERANCING REFER TO DWG. 219B402.
2. THESE WELDS TO BE CHECKED FOR LEAKAGE WITH MASS SPECTROMETER EQUIP. MAXIMUM PERMISSIBLE LEAKAGE NOT TO EXCEED .005 MICRON CU. FT. / HR.
3. OTHER WELDS TO BE TESTED PER SEPARATE ENGINEERING INSTR.
4. F = AWGT FUSION WELD.
5. FOR WELD. ROD USE E308 WHERE REQ.

DESCRIPTION OF GROUPS	REVISIONS	PRINTS TO

APED — SAN JOSE

PRINTED IN U.S.A.

9. Outside fuel-to-clad contact coefficient was chosen as 1000 Btu/hr-ft^2 ^oF.

10. The effect of dimensional changes due to thermal expansion was neglected.

11. The heat transfer between the entrance and exit steam at the top of the fuel was neglected.

12. The effect of spacers was neglected.

13. The steam properties were evaluated at the bulk steam temperature for use in the steam film coefficient equation.

14. The effects of the type of entrance and the L/D ratio on the steam film coefficient were neglected.

15. The flux gradient across the fuel element was not accounted for.

9.1.4.3 Discussion and Results

The test results show that the first pass steam temperature rise was greater than expected and the second pass steam temperature rise was lower than expected. There are several assumptions in the analysis that could account for this discrepancy between predicted and observed temperature values. The most logical answer appears to be that the inside fuel-to-clad coefficient of 500 Btu/hr-ft^2 ^oF is too high.

Figure 9.3 shows the predicted steam temperatures as a function of length for inside fuel-to-clad contact coefficients of 75, 150, and 500 Btu/hr-ft^2 ^oF at 94 KW power, approximately 880^oF exit temperature and approximately

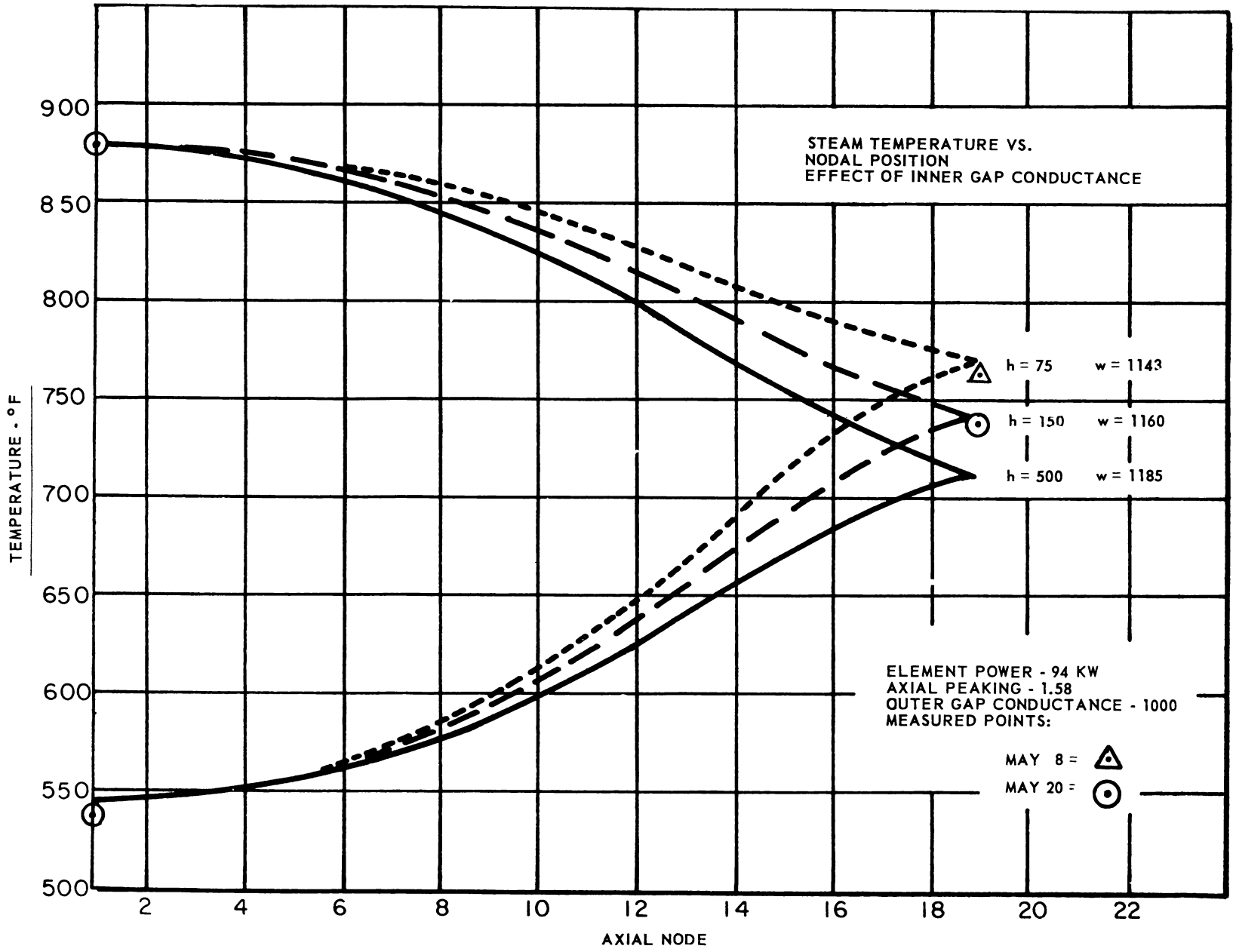

FIGURE 9.3
SH-4B ELEMENT

1160 lbs/hr steam flow. The differences in steam flow rate are due entirely to the change in heat loss to the moderator water.

Also shown on Figure 9.3 are the actual steam temperatures measured during two different days of operation. These two different sets of data were chosen because they are representative of high exit steam temperature operation. It should be noted that:

1. The entrance and exit temperatures of both sets of data are the same.
2. The interpass temperatures indicate that the inside contact coefficient varies between about 90 and 150 Btu/hr-ft^2 $^\circ$F, instead of the previous design value of 500 Btu/hr-ft^2 $^\circ$F.

The high gap resistance is due to the large diametrical clearance between the inside of the annular fuel pellets and the O.D. of the inner cladding. The measured cold diametrical gap ranged between 6 and 12 mils. When the fuel element is at power, the hot UO_2 expands away from the inner clad and increases the inside gaps by another 2 - 4 mils.

If the gap resistance of all fuel elements were consistently high, the fuel element design could be adjusted for a high inside gap resistance. The design average heat flux would only have to be reduced by a small amount (0 - 10%) to maintain the same maximum clad temperature.

If, however, the gap resistance is different for each fuel element due to limiting pellet manufacturing and tubing tolerance, or if the gap resistance changes with exposure, it would be necessary to derate the fuel element even more. This change in gap resistance changes the inside and outside heat fluxes and is particularly important to a single pass annular fuel element. In such an element, not only the heat flux changes but the steam temperature also changes. This single effect could reduce the allowable average heat flux by 25 - 40%.

9.1.5 NUSU Irradiation

9.1.5.1 Introduction

The NUSU fuel element is a combination boiling-superheat fuel element designed and fabricated by the Combustion Engineering Corporation. The fuel pellets were fabricated by the General Electric Company and installed in the fuel assembly by C.E. The irradiation of this assembly in the SADE loop is being performed at the request of the Atomic Energy Commission in place of irradiation of a combination boiling-superheat element fabricated by the General Electric Company in the fall of 1959. (See page 95 of GEAP-3290, "First Quarterly Progress Report.")

Figures 9.4 through 9.7 are design drawings of the NUSU fuel element based on drawings and information furnished by the General Nuclear Engineering Division of Combustion Engineering Corporation.

GENERAL ELECTRIC 1048654

SADE LIUSU TEST INSTALLATION

PL ISSUED

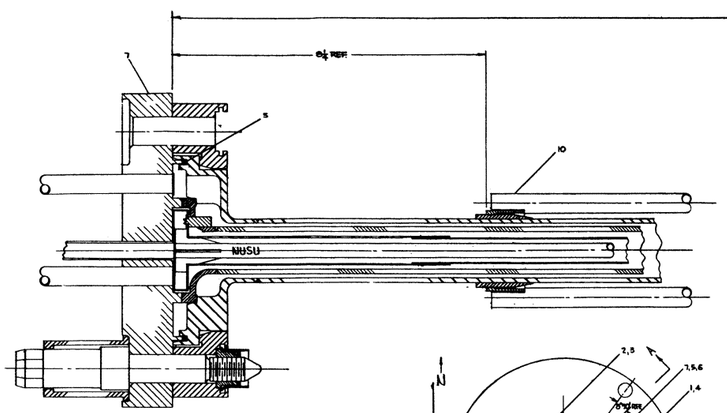

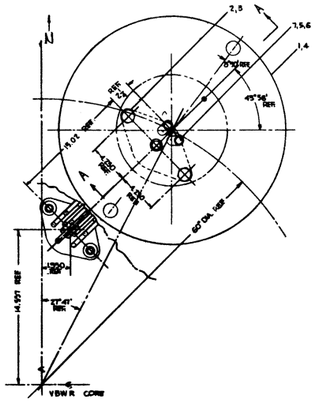

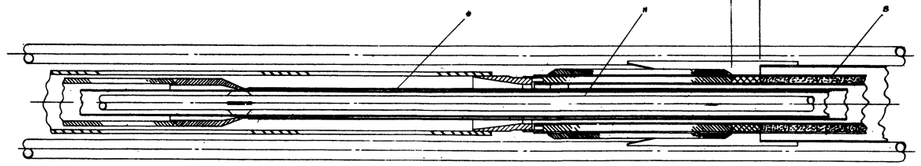

(61) FOR INSTALLATION IN VBWR. USE DWG 1978170 AS REF. FOR LOCATION & ASSEMBLY

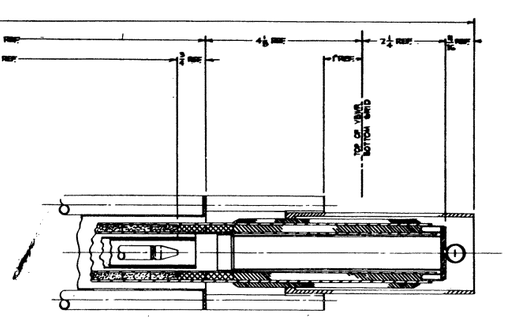

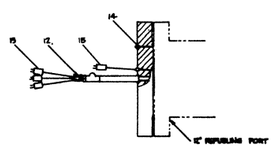

SECTION AA

Figure 9.4

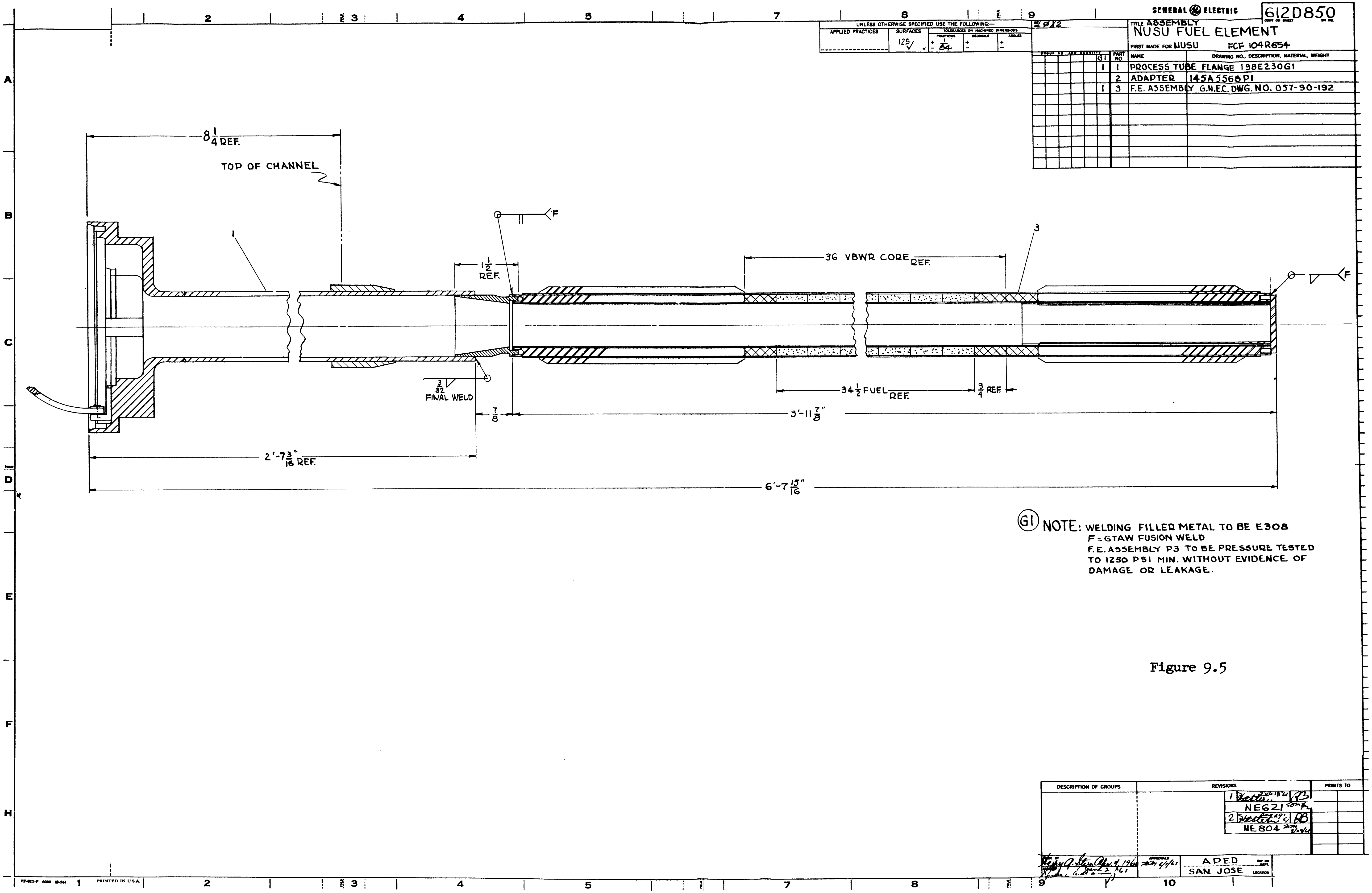

GENERAL ELECTRIC
612D850
TITLE ASSEMBLY
NUSU FUEL ELEMENT
FIRST MADE FOR NUSU FCF 104R654
UNLESS OTHERWISE SPECIFIED USE THE FOLLOWING:—
APPLIED PRACTICES
SURFACES
125
TOLERANCES ON MACHINED DIMENSIONS
FRACTIONS ± 1/64
DECIMALS ±
ANGLES ±
G1
PART NO.
NAME
DRAWING NO., DESCRIPTION, MATERIAL, WEIGHT
1 1 PROCESS TUBE FLANGE 198E230G1
2 ADAPTER 145A5568P1
1 3 F.E. ASSEMBLY G.N.E.C. DWG. NO. 057-90-192
8 1/4 REF.
TOP OF CHANNEL
1
F
1 1/2 REF.
36 VBWR CORE REF.
3
F
3/32 FINAL WELD
34 1/2 FUEL REF.
3/4 REF.
7/8
3'-11 7/8"
2'-7 3/16" REF.
6'-7 15/16"
G1 NOTE: WELDING FILLER METAL TO BE E308
F = GTAW FUSION WELD
F.E. ASSEMBLY P3 TO BE PRESSURE TESTED
TO 1250 PSI MIN. WITHOUT EVIDENCE OF
DAMAGE OR LEAKAGE.
DESCRIPTION OF GROUPS
REVISIONS
PRINTS TO
NE621
NE804
APED
SAN JOSE
PRINTED IN U.S.A.

Figure 9.5

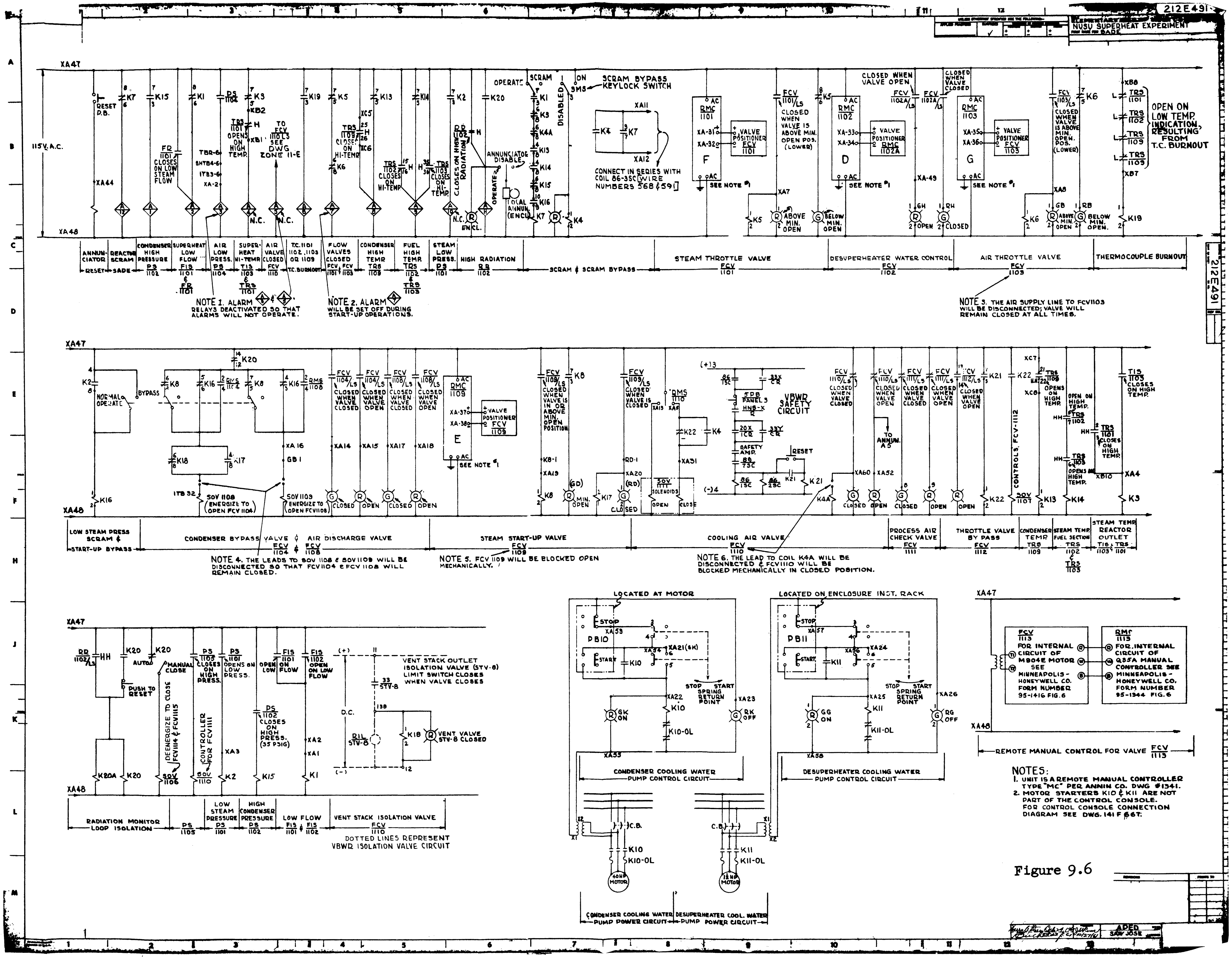

212E491
NUSU SUPERHEAT EXPERIMENT
115V. A.C.
SCRAM BYPASS KEYLOCK SWITCH
CONNECT IN SERIES WITH COIL 86-3SC (WIRE NUMBERS 568 & 591)
OPEN ON LOW TEMP. INDICATION, RESULTING FROM T.C. BURNOUT
ANNUN-CIATOR RESET
REACTOR SCRAM RESET
CONDENSER HIGH PRESSURE
SUPERHEAT LOW FLOW
AIR LOW PRESS.
SUPER-HEAT HI-TEMP.
AIR VALVE CLOSED
FLOW VALVES CLOSED
CONDENSER HIGH TEMP.
FUEL HIGH TEMP.
STEAM LOW PRESS.
HIGH RADIATION
SCRAM & SCRAM BYPASS
STEAM THROTTLE VALVE
DESUPERHEATER WATER CONTROL
AIR THROTTLE VALVE
THERMOCOUPLE BURNOUT
NOTE 1. ALARM RELAYS DEACTIVATED SO THAT ALARMS WILL NOT OPERATE.
NOTE 2. ALARM WILL BE SET OFF DURING START-UP OPERATIONS.
NOTE 3. THE AIR SUPPLY LINE TO FCV1103 WILL BE DISCONNECTED; VALVE WILL REMAIN CLOSED AT ALL TIMES.
VBWR SAFETY CIRCUIT
LOW STEAM PRESS SCRAM & START-UP BYPASS
CONDENSER BYPASS VALVE & AIR DISCHARGE VALVE
STEAM START-UP VALVE
COOLING AIR VALVE
PROCESS AIR CHECK VALVE
THROTTLE VALVE BY PASS
CONDENSER TEMP
STEAM TEMP FUEL SECTION
STEAM TEMP REACTOR OUTLET
NOTE 4. THE LEADS TO SOV 1108 & SOV1109 WILL BE DISCONNECTED SO THAT FCV1104 & FCV 1108 WILL REMAIN CLOSED.
NOTE 5. FCV 1109 WILL BE BLOCKED OPEN MECHANICALLY.
NOTE 6. THE LEAD TO COIL K4A WILL BE DISCONNECTED & FCV1110 WILL BE BLOCKED MECHANICALLY IN CLOSED POSITION.
VENT STACK OUTLET ISOLATION VALVE (STV-8) LIMIT SWITCH CLOSES WHEN VALVE CLOSES
RADIATION MONITOR LOOP ISOLATION
LOW STEAM PRESSURE
HIGH CONDENSER PRESSURE
LOW FLOW
VENT STACK ISOLATION VALVE
DOTTED LINES REPRESENT VBWR ISOLATION VALVE CIRCUIT
LOCATED AT MOTOR
LOCATED ON ENCLOSURE INST. RACK
CONDENSER COOLING WATER PUMP CONTROL CIRCUIT
DESUPERHEATER COOLING WATER PUMP CONTROL CIRCUIT
CONDENSER COOLING WATER PUMP POWER CIRCUIT
DESUPERHEATER COOL. WATER PUMP POWER CIRCUIT
REMOTE MANUAL CONTROL FOR VALVE FCV 1113
NOTES:
1. UNIT IS A REMOTE MANUAL CONTROLLER TYPE "MC" PER ANNIN CO. DWG #1341.
2. MOTOR STARTERS K10 & K11 ARE NOT PART OF THE CONTROL CONSOLE. FOR CONTROL CONSOLE CONNECTION DIAGRAM SEE DWG. 141 F 667.
APED SAN JOSE

Figure 9.6

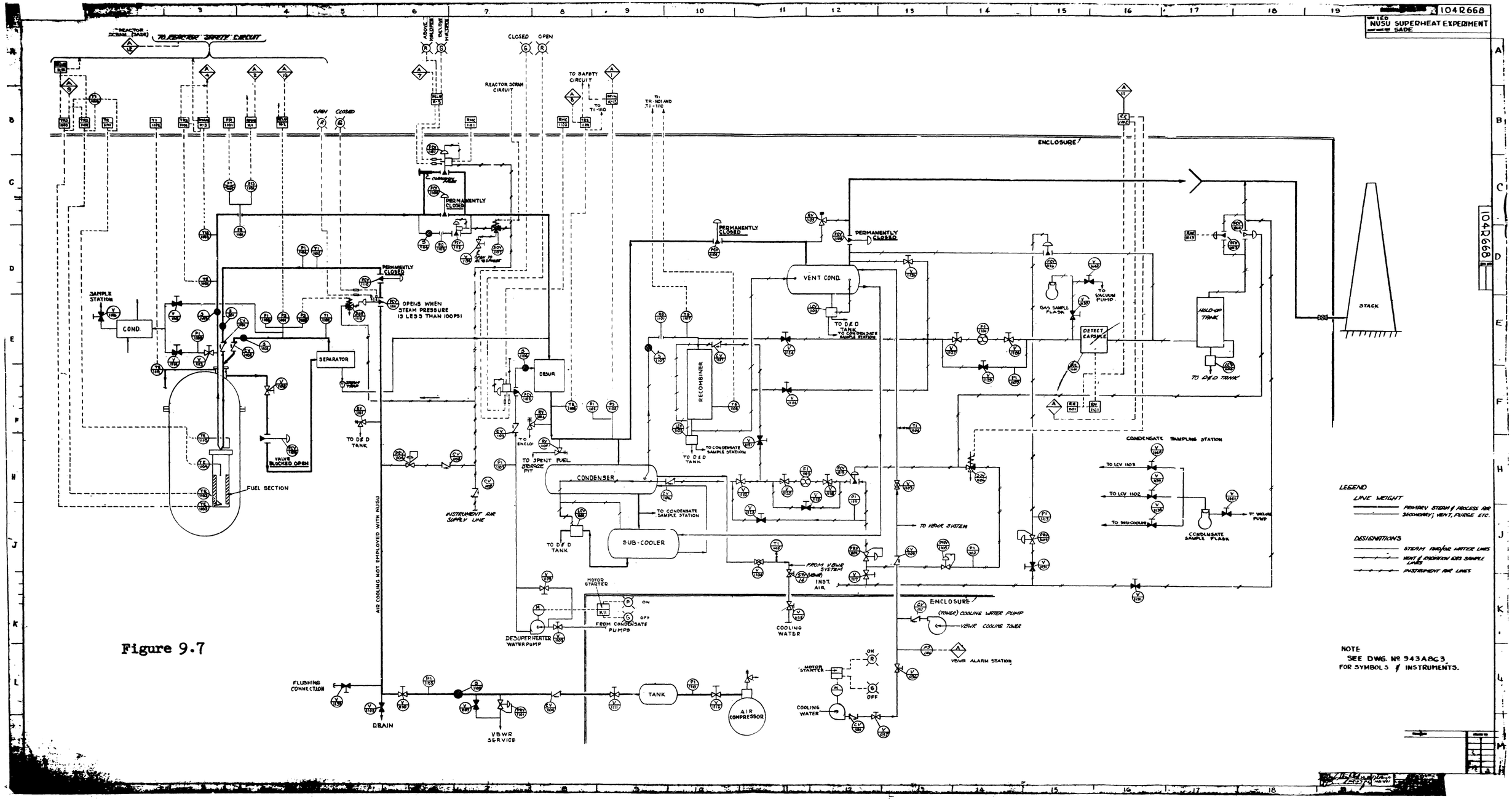
NUSU SUPERHEAT EXPERIMENT
SADE
104R668
TO REACTOR SAFETY CIRCUIT
REACTOR SCRAM CIRCUIT
TO SAFETY CIRCUIT
TO TR-101 AND TI-110
ENCLOSURE
PERMANENTLY CLOSED
OPENS WHEN STEAM PRESSURE IS LESS THAN 100PSI
SAMPLE STATION
COND.
SEPARATOR
VALVE BLOCKED OPEN
FUEL SECTION
TO D/E D TANK
INSTRUMENT AIR SUPPLY LINE
DESUP.
TO ENCLO.
TO SPENT FUEL STORAGE PIT
CONDENSER
TO CONDENSATE SAMPLE STATION
SUB-COOLER
RECOMBINER
VENT COND.
TO VBWR SYSTEM
FROM VBWR SYSTEM
INST. AIR
COOLING WATER
MOTOR STARTER
FROM CONDENSATE PUMPS
DESUPER HEATER WATER PUMP
AIR COOLING NOT EMPLOYED WITH NUSU
FLUSHING CONNECTION
DRAIN
VBWR SERVICE
TANK
AIR COMPRESSOR
GAS SAMPLE FLASK
TO VACUUM PUMP
DETECT CAPSULE
HALO-GEN TANK
STACK
CONDENSATE SAMPLING STATION
TO LCV 1103
TO LCV 1102
TO SEQ-COOLER
CONDENSATE SAMPLE FLASH
ENCLOSURE
(TOWER) COOLING WATER PUMP
VBWR COOLING TOWER
VBWR ALARM STATION
LEGEND
LINE WEIGHT
PRIMARY STEAM & PROCESS AIR
SECONDARY; VENT, PURGE ETC.
DESIGNATIONS
STEAM AND/OR WATER LINES
VENT & EVAPORATOR SAMPLE LINES
INSTRUMENT AIR LINES
NOTE
SEE DWG. Nº 943A8G3
FOR SYMBOLS & INSTRUMENTS.

Figure 9.7

A container for the NUSU fuel element has been designed and drawings released for comment. Because of the size of the upper flange on this fuel element, which was required to adapt the element to the SADE loop, it will be necessary to use the E-SADE fuel cask in case the can is required. Figure 9.8 shows this can.

9.1.5.2 NUSU Design Conditions

Additional information has been prepared covering installation of the NUSU element in the SADE test loop. This information has been based on a change in the expected maximum reactor power while this element is to be installed and on changes in some coefficients and factors. Operating conditions for NUSU are shown in Table 9.5.

TABLE 9.5

Design conditions for the NUSU element at 30 MW reactor power.

Fuel element power	102 KW_{235}
Fuel enrichment	3.5% U^{235}
Steam pressure	1000 psia
Active fuel length	34.5"
Outer clad, outside diameter	1.50"
Outer clad thickness	0.028"
Outer clad material	347 S.S.
Inner clad, outside diameter	1.072"
Inner clad thickness	0.025"
Inner clad material	Inconel X
Outer steam supply tube, outside diameter	0.814"
Water flow tube, outside diameter	2.00"
Water flow tube thickness	0.049"
Fuel (UO_2)% theoretical density	95%
Total fuel loading (UO_2)	4.25 kg
Inside clad-to-fuel contact coefficient	150 Btu/hr-ft^2-^oF
Outside clad-to-fuel contact coefficient	1000 Btu/hr-ft^2-^oF
VBWR power	30 MW
Axial peaking factor	1.58
Linear radial flux depression factor	1.10

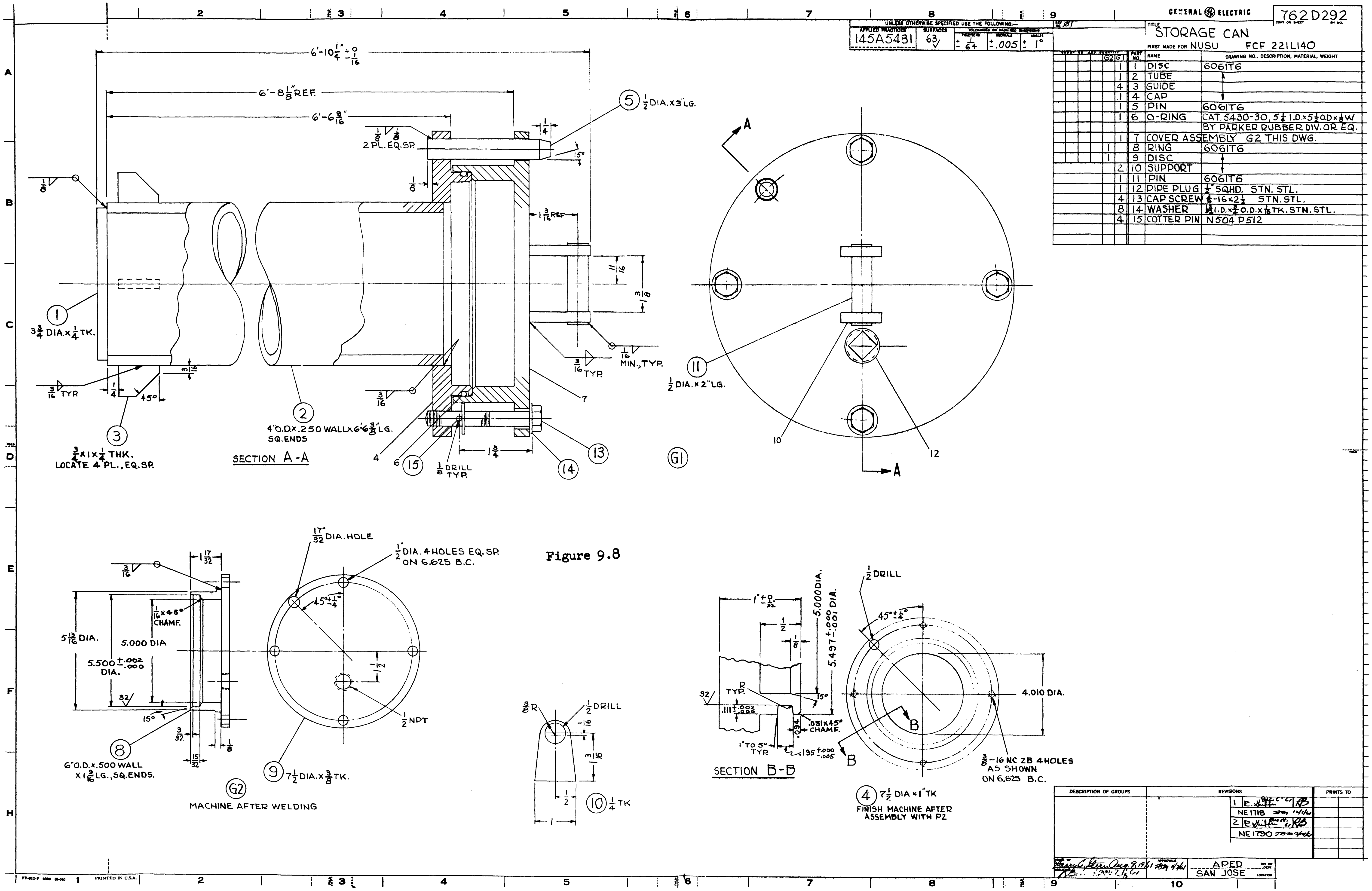

G2	G1	PART NO.	NAME	DRAWING NO., DESCRIPTION, MATERIAL, WEIGHT
	1	1	DISC	6061T6
	1	2	TUBE	
	4	3	GUIDE	
	1	4	CAP	
	1	5	PIN	6061T6
	1	6	O-RING	CAT. 5430-30, 5 1/4 I.D.x5 1/2 O.D.x 1/8 W BY PARKER RUBBER DIV. OR EQ.
	1	7	COVER ASSEMBLY	G2 THIS DWG.
1		8	RING	6061T6
1		9	DISC	
	2	10	SUPPORT	
	1	11	PIN	6061T6
	1	12	PIPE PLUG	1/2" SQ.HD. STN. STL.
	4	13	CAP SCREW	3/8-16x2 1/2 STN. STL.
	8	14	WASHER	13/32 I.D.x 3/4 O.D.x 1/16 TK. STN. STL.
	4	15	COTTER PIN	N504 P512

Figure 9.8

TABLE 9.5 (Continued)

Thermal conductivity (UO_2)	1.0 Btu/hr-ft^2-($^\circ$F/ft)
Maximum clad temperature[2] (STEADY)	1200°F
Maximum superheat exit temperature (STEADY)	761°F
Maximum steam side heat flux (STEADY)	201,000 Btu/hr-ft^2
Maximum water side heat flux (STEADY)	348,000 Btu/hr-ft^2
Minimum steam flow rate (STEADY)	570 lbs/hr
Minimum burnout ratio (STEADY)	2.87
Maximum fuel temperature (STEADY)	2915°F
Maximum clad temperature (TRANSIENT)	1300°F
Maximum superheat exit temperature (TRANSIENT)	807°F
Maximum steam side heat flux (TRANSIENT)	195,000 Btu/hr-ft^2
Maximum water side heat flux (TRANSIENT)	352,000 Btu/hr-ft^2
Minimum steam flow rate (TRANSIENT)	460 lbs/hr
Minimum burnout ratio (TRANSIENT)	2.84
Maximum fuel temperature (TRANSIENT)	2962°F

9.1.5.3 NUSU Start-up and Shutdown Information

The operation of the NUSU fuel element in the SADE loop will differ from previous operations mainly in that there will be no air cooling during start-up or shutdown. The NUSU fuel element does not have a process tube, and the probability of achieving full reactor pressure across the fuel element is much higher with air cooling than without. Furthermore, the air cooling feature isn't necessary since the NUSU element can cool itself sufficiently by convection heat transfer to the reactor water. The results of a conservative heat transfer analysis - to determine the maximum desirable reactor power before the start of steam flow - are listed below.

NUSU power (KW)	3.1	6.2	12.5
VBWR power (MW)	0.83	1.66	3.32
Maximum inside clad temperature ($^\circ$F)*	565	775	1205
Maximum outside clad temperature ($^\circ$F)*	430	505	660
Water temperature ($^\circ$F)*	400	445	545

* It should be noted that the water temperatures chosen are only representative of VBWR operation. However, for the 6.2 KW power case, the maximum clad temperature possible is 875°F, even if the water temperature is 545°F. The analysis is based upon the inside clad being completely insulated.

The maximum desirable reactor power before the start of steam flow is chosen as 1.5 MW. The main factor that dictated this choice was the possibility of thermal shock (water slug). The choice of a 300°F differential between peak clad temperature and reactor water temperature will minimize the shock, if one occurs.

9.1.6 SH-1 Defect Tests

Question about the adequacy of the SADE loop to test intentionally defected fuel elements had been raised. Since the defected element test has been planned for the purpose of measuring activity release rates and loop contamination, the operation of the system will be under carefully controlled and monitored conditions, and are not to be conducted on a routine basis. Additional information regarding the SADE loop and equipment, and the manner in which the defected elements would be tested was supplied to AEC for review. AEC license approval to conduct the test in the manner planned has now been received.

9.1.7 SADE Cladding Specimen Irradiation

Design and fabrication of an instrument tube incorporating specimens of cladding material was completed. This arrangement provides a means of irradiating specimens of material which might be suitable for superheat fuel element cladding, and exposing the specimens to a superheated steam environment without sacrifice of fuel element space.

The specimens are attached, by means of a flux measuring wire, to a retainer plate inserted in the lower portion of the instrument

tube. Samples of 304, 304L, 304E, 316, and 347 types of stainless steel were installed. A total of forty specimens were loaded into the assembly. Figure 9.9 shows the arrangement of this instrument tube.

9.2 E-SADE

9.2.1 External E-SADE System

Design and detailing of the external loop was completed during this period. The P. and I.D. for the system is given in Figure 9.10.

9.2.2 E-SADE Instrumentation

Design of the logic and instrumentation system has been approximately 90% completed. All basic instrumentation has been ordered and scheduled for acceptable delivery dates. The schematic diagram of the E-SADE control and safety system is given in Figures 9.11 and 9.12.

9.2.3 E-SADE Installation

Extensive planning was completed in preparation for the extended VBWR outage to permit installation of E-SADE equipment. This outage, scheduled for early in October, is planned for installation of the main condenser, start-up pump, and much of the other piping and valving located in the VBWR enclosure basement. Prefabrication of piping was used to minimize the reactor down-time required for the work. In addition, recent activity levels in the enclosure basement may prove to be a limitation upon the amount of time individual workers will be able to devote to installation in the basement. The enclosure patch, to provide additional enclosure

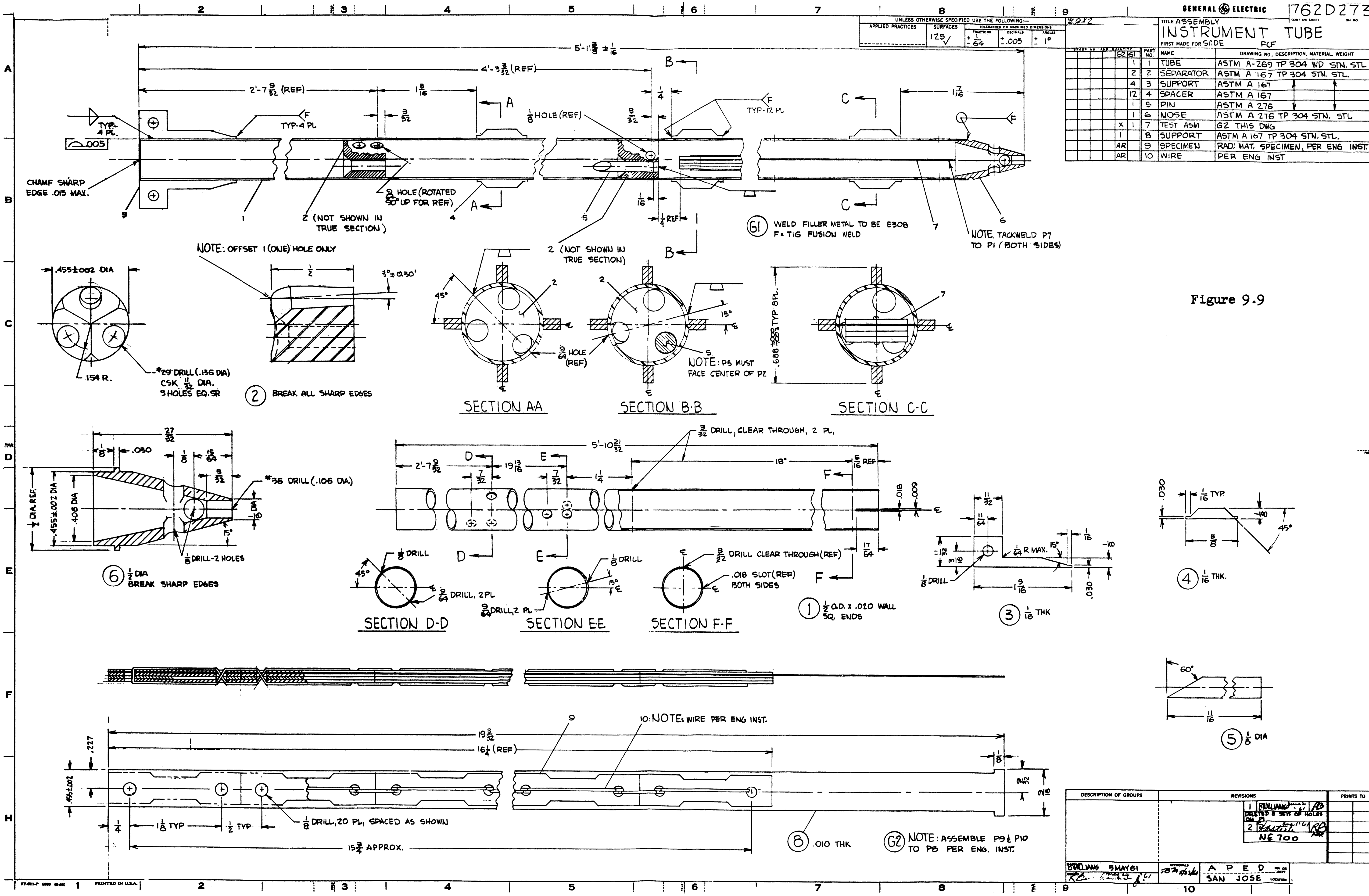
GENERAL ELECTRIC
762D273
TITLE ASSEMBLY
INSTRUMENT TUBE
FIRST MADE FOR SADE
UNLESS OTHERWISE SPECIFIED USE THE FOLLOWING:
APPLIED PRACTICES
SURFACES
125
TOLERANCES ON MACHINED DIMENSIONS
FRACTIONS ± 1/64
DECIMALS ± .005
ANGLES ± 1°
1 TUBE ASTM A-269 TP 304 WD STN. STL
2 SEPARATOR ASTM A 167 TP 304 STN. STL.
3 SUPPORT ASTM A 167
4 SPACER ASTM A 167
5 PIN ASTM A 276
6 NOSE ASTM A 276 TP 304 STN. STL
7 TEST ASM G2 THIS DWG
8 SUPPORT ASTM A 167 TP 304 STN. STL.
9 SPECIMEN RAD. MAT. SPECIMEN, PER ENG INST.
10 WIRE PER ENG INST
CHAMF SHARP EDGE .015 MAX.
2 (NOT SHOWN IN TRUE SECTION)
NOTE: TACKWELD P7 TO P1 (BOTH SIDES)
G1 WELD FILLER METAL TO BE E308 F: TIG FUSION WELD
NOTE: OFFSET 1 (ONE) HOLE ONLY
2 BREAK ALL SHARP EDGES
NOTE: P5 MUST FACE CENTER OF P2
SECTION A-A
SECTION B-B
SECTION C-C
6 1/2 DIA BREAK SHARP EDGES
SECTION D-D
SECTION E-E
SECTION F-F
1 1/2 O.D. X .020 WALL SQ. ENDS
3 1/16 THK
4 1/16 THK.
5 1/8 DIA
10: NOTE: WIRE PER ENG INST.
1/8 DRILL, 20 PL, SPACED AS SHOWN
8 .010 THK
G2 NOTE: ASSEMBLE P9 & P10 TO P8 PER ENG. INST.
A P E D
SAN JOSE

Figure 9.9

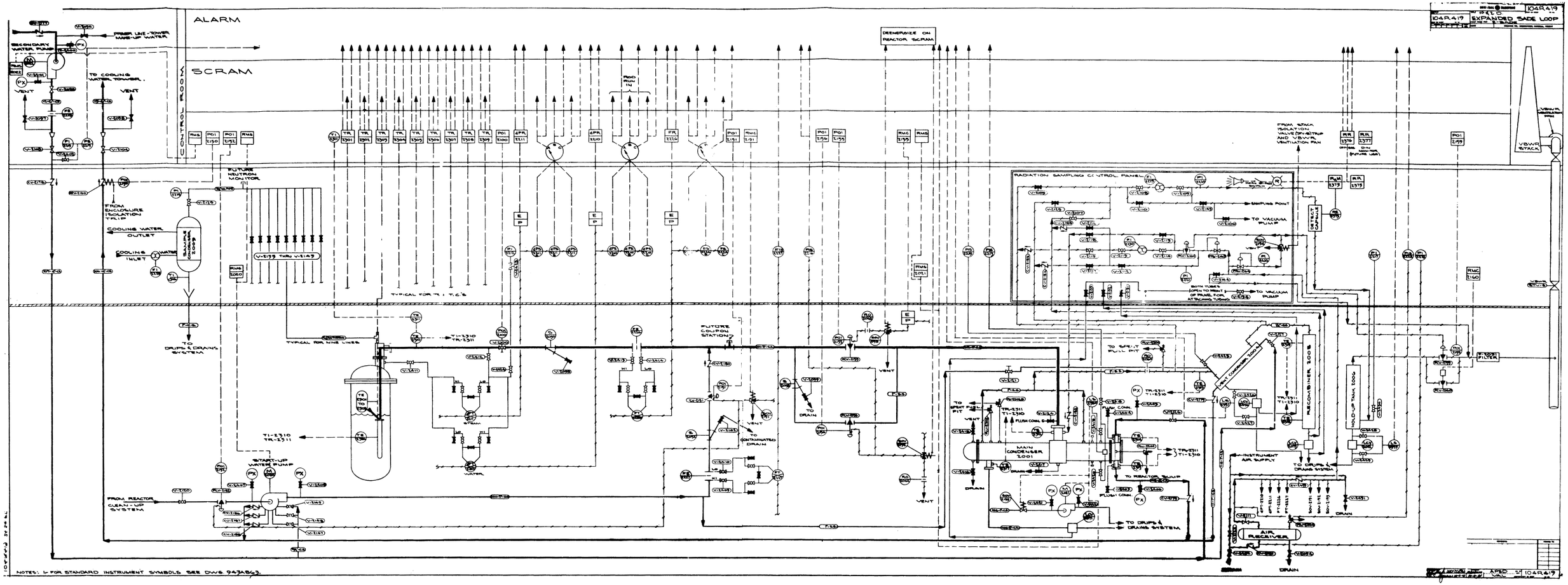
ALARM
SCRAM
DEENERGIZE ON REACTOR SCRAM
SECONDARY WATER PUMP
PRIMER LINE-TOWER MAKE-UP WATER
TO COOLING WATER TOWER
VENT
CONTROL ROOM
FROM ENCLOSURE ISOLATION TRIP
COOLING WATER OUTLET
COOLING INLET
SAMPLE COOLER 2019
FUTURE NEUTRON MONITOR
V-2193 THRU V-2149
TYPICAL FOR 7 T.C.'S
TYPICAL FOR NINE LINES
TO DRUM & DRAINS SYSTEM
FUTURE COUPON STATION
TI-2310 TR-2311
START-UP WATER PUMP
FROM REACTOR CLEAN-UP SYSTEM
TO CONTAMINATED DRAIN
RADIATION SAMPLING CONTROL PANEL
SAMPLING POINT
TO VACUUM PUMP
DETECT CAPSULE
FROM STACK ISOLATION VALVE (PV-A) TRIP AND V.B.V.M. VENTILATION FAN
V.B.V.M. STACK
TO SPENT FUEL PIT
MAIN CONDENSER 2001
AFTER CONDENSER 2002
RECOMBINER 2005
HOLD-UP TANK 2006
F-2001 FILTER
TR-2311 TI-2310
FLUSH CONN.
TO REACTOR SUMP
INSTRUMENT AIR SUPPLY
TO DRUM & DRAINS SYSTEM
AIR RECEIVER
DRAIN
VENT
NOTES: 1- FOR STANDARD INSTRUMENT SYMBOLS SEE DWG 943A862.

Figure 9.10

GENERAL ELECTRIC

TITLE ELEMENTARY DIAGRAM
9 ELEMENT SADE LOOP
FIRST PAGE FOR E-SADE

Figure 9.11

GENERAL ELECTRIC — 212E307

9 ELEMENT SADE LOOP

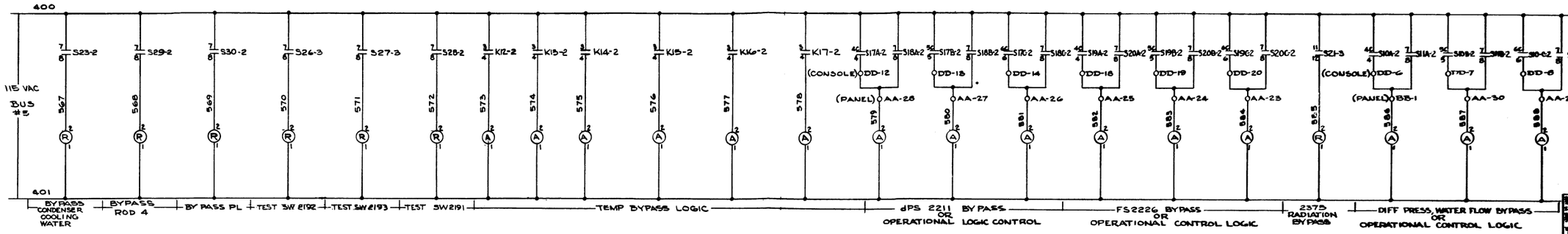

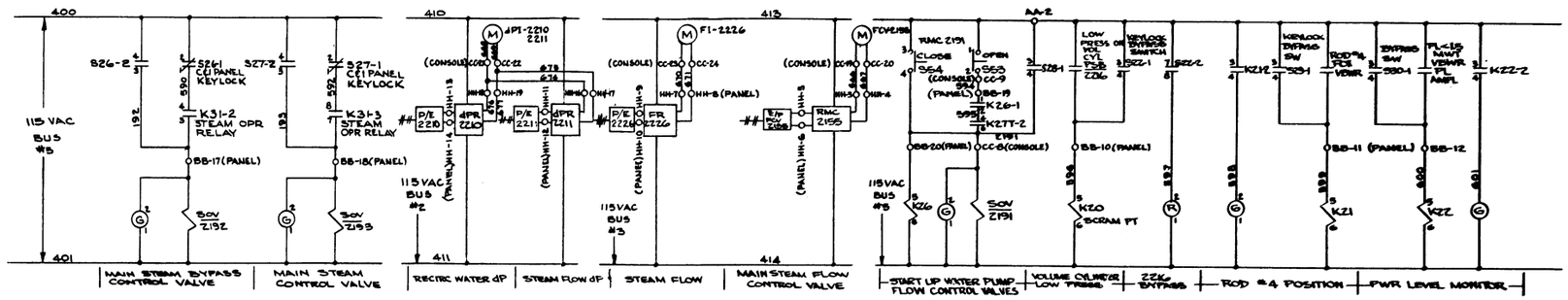

Figure 9.12

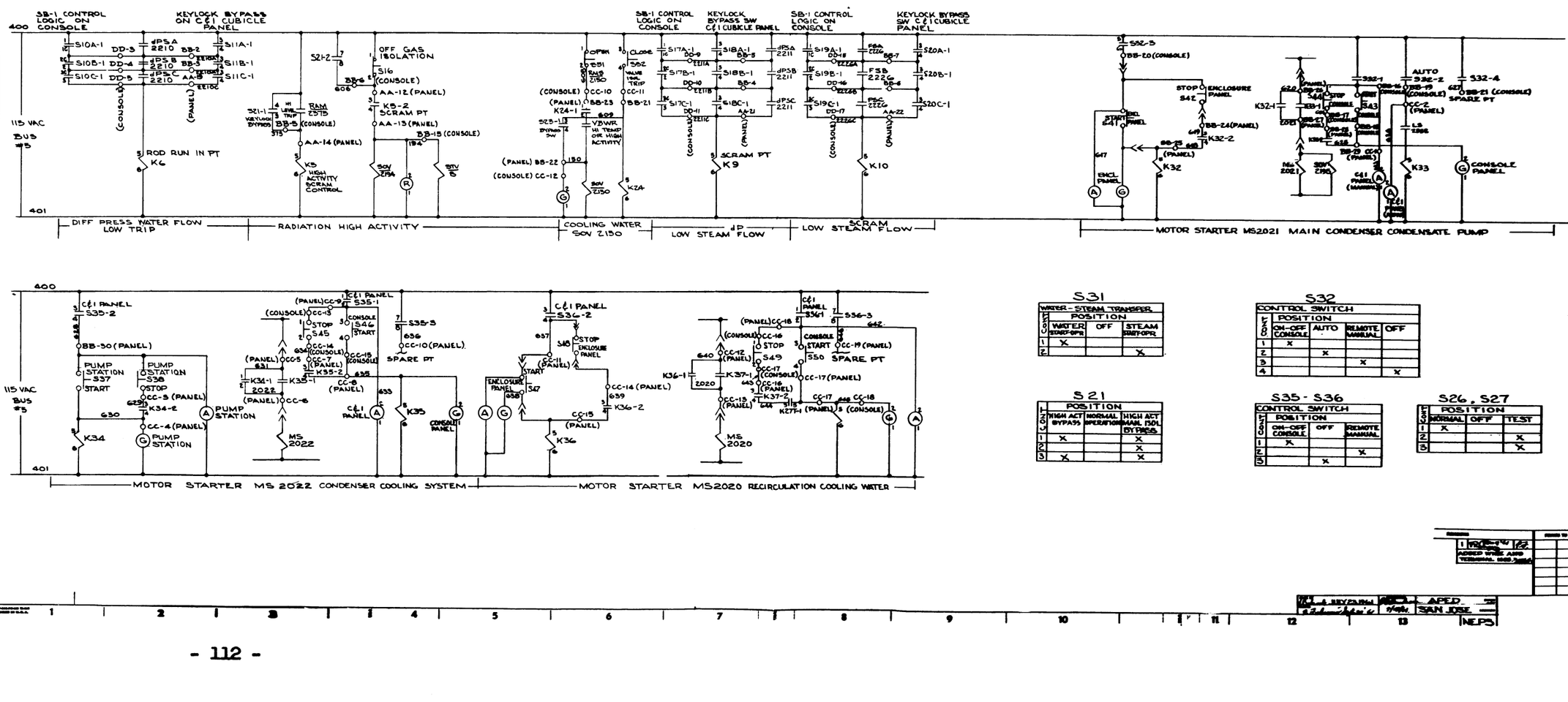

S31

CONT	WATER-STEAM TRANSFER POSITION		
	WATER START-OPR	OFF	STEAM START-OPR
1	X		
2			X

S32

CONT	CONTROL SWITCH POSITION			
	ON-OFF CONSOLE	AUTO	REMOTE MANUAL	OFF
1	X			
2		X		
3			X	
4				X

S21

CONT	POSITION		
	HIGH ACT BYPASS	NORMAL OPERATION	HIGH ACT MAN. ISOL BYPASS
1	X		
2			X
3	X		X

S35 - S36

CONT	CONTROL SWITCH POSITION		
	ON-OFF CONSOLE	OFF	REMOTE MANUAL
DN	X		
UP		X	X

S26, S27

CONT	POSITION		
	NORMAL	OFF	TEST
1	X		
2			X
3			X

penetrations for secondary water piping and instrumentation and control leads, has been fabricated and passed all preliminary inspections and has been delivered to the site awaiting installation during the reactor outage.

9.2.4 E-SH1 Design and Status

Fabrication of the special hardware items for E-SH1 has been in progress for some time and is continuing in the shop. Parts of the in-core assembly are about 75% complete, except for the final assembly of components which must be completed after the fuel elements are available for installation in the assembly.

The E-SH1 assembly is being reviewed to determine if changes from original estimates of fuel enrichment and operating conditions have occurred. This review showed that orificing of 8 of the 9 fuel elements of E-SH1 will be required in order to realize 1250°F clad temperature on all fuel elements. When the bundle is not orificed, it requires approximately 14000 lb/hr with VBWR operating at 35 MW. To maintain 1250°F clad temperature on all fuel elements by orificing 8 of the 9 elements requires a steam flow of approximately 10800 lb/hr when VBWR is operating at 35 MW.

The analysis to date results in the following ranges for the parameters listed, among the 9 fuel elements:

Flow rate - lb/hr 860 to 1450
Exit steam temp. - °F 830 to 870
Max. clad temp. - °F approximately 1250
Required orifice pressure drop - psi 7 to 35
Orifice diameter, d, inches $.45 \geq d \geq .20$

Further work to evaluate the effect of flux dip across the diameter of the various fuel elements is now being undertaken and will result in some changes to these values.

Figure 9.13 shoes the installation of the flow orifices in the individual elements for E-SH1.

Preliminary plans for E-SH2 have been for a single-pass configuration for the fuel elements, using a flow diverter tube to provide this arrangement. Cooling of the fuel elements after a shutdown is more difficult in this arrangement because the flow diverter tube functions essentially as an insulating liner when steam flow is stopped. A study to establish the cooling requirements for such an assembly was initiated. It appears that by limiting the maximum power per element to 58 KW and maintaining a nominal steam flow through the assembly for 2 to 3 hours, the element will be cooled adequately during reactor shutdown. Figure 9.14 shows the assembly of the equipment.

Because of the size, weight, and complexity of the E-SADE assembly, handing of the equipment within the reactor will be a major problem. A detailed plan for handling an irradiated assembly has been prepared on a preliminary basis and is now being reviewed to determine if it is adequate. When the plan is approved, it will be necessary to design some additional special equipment for handling of the assembly inside the reactor during transfer from the core to the handling cask.

9.2.5 E-SH2 Design and Status

9.2.5.1 Mechanical Design

The design of the E-SH2 annular fuel element is shown in Figure 9.15. The end fittings will be modified slightly from what is shown in this figure in order to incorporate

GENERAL ELECTRIC

UNLESS OTHERWISE SPECIFIED USE THE FOLLOWING:—

APPLIED PRACTICES	SURFACES	TOLERANCES ON MACHINED DIMENSIONS: FRACTIONS	DECIMALS	ANGLES
145A5481	63	± 1/64	± .005	± 1/4°

REV. NO. 0 — 985C642 — CONT ON SHEET — SH NO.

TITLE: ORIFICE ADAPTER — CONT ON SHEET — SH NO.

FIRST MADE FOR SHNEE

GROUP NO. AND QUANTITY G9	G8	G7	G6	G5	G4	G3	G2	G1	PART NO.	NAME	DRAWING NO., DESCRIPTION, MATERIAL, WEIGHT
1	1	1	1	1	1	1	1	1	1	THERMAL TUBE	985C247G-1
1	1	1	1	1	1	1	1	1	2	CONE	ASTM 276 TYPE 304.
								1	3	ORIFICE	115A8774 P-1
3	3	3	3	3	3	3	3	3	4	SET SCREW	8-32-UNC-2A x 1/4 LG. FL.PT. HEX. SOC. HD. STN. STL.
							1		5	ORIFICE	115A8774 P-2
						1			6	ORIFICE	P-3
					1				7	ORIFICE	P-4
				1					8	ORIFICE	P-5
			1						9	ORIFICE	P-6
		1							10	ORIFICE	P-7
	1								11	ORIFICE	P-8
1									12	ORIFICE	115A8774 P-9

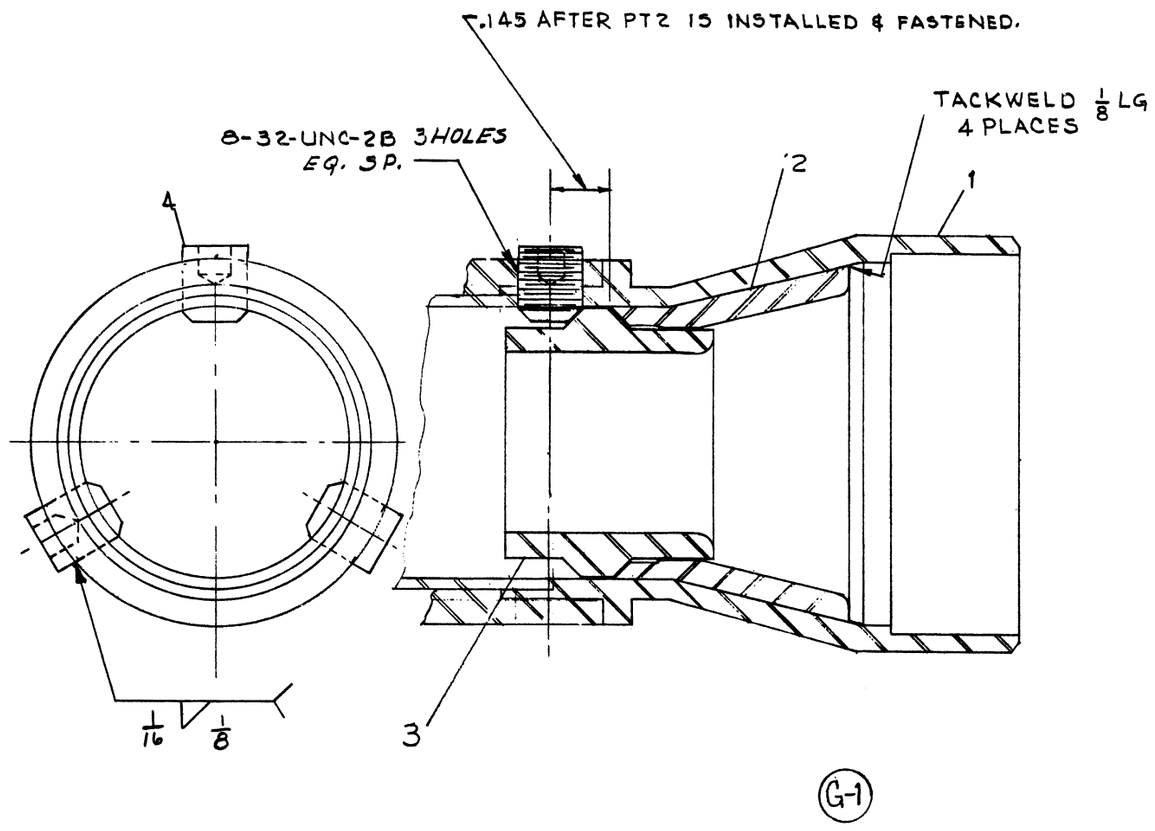

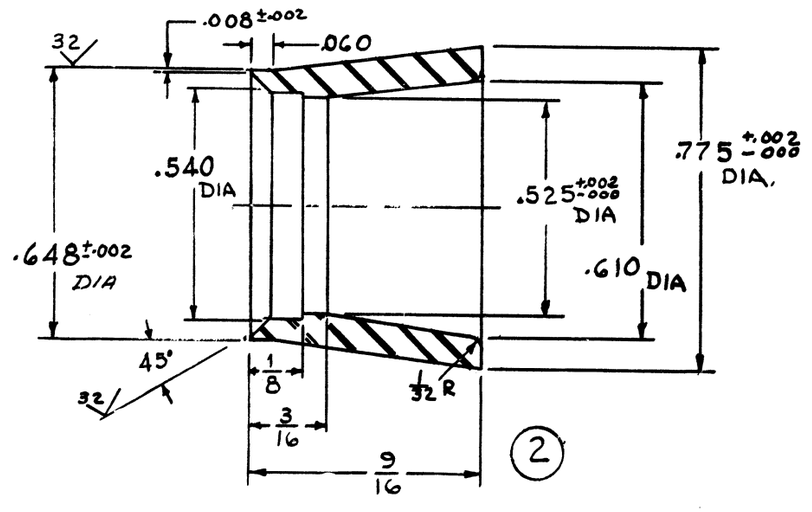

Figure 9.13

DESCRIPTION OF GROUPS	REVISIONS	PRINTS TO

MADE BY K Glover 10-2-61 — APPROVALS S.F.H. — APED SAN JOSE — DIV. OR DEPT. LOCATION — 985C642 CONT ON SHEET SH NO.

FF-806-P 7M (7-56) PRINTED IN U.S.A.

NINE ELEMENT FUEL ASM
(SINGLE PASS)
SHNEE III F.F. 717 & 719

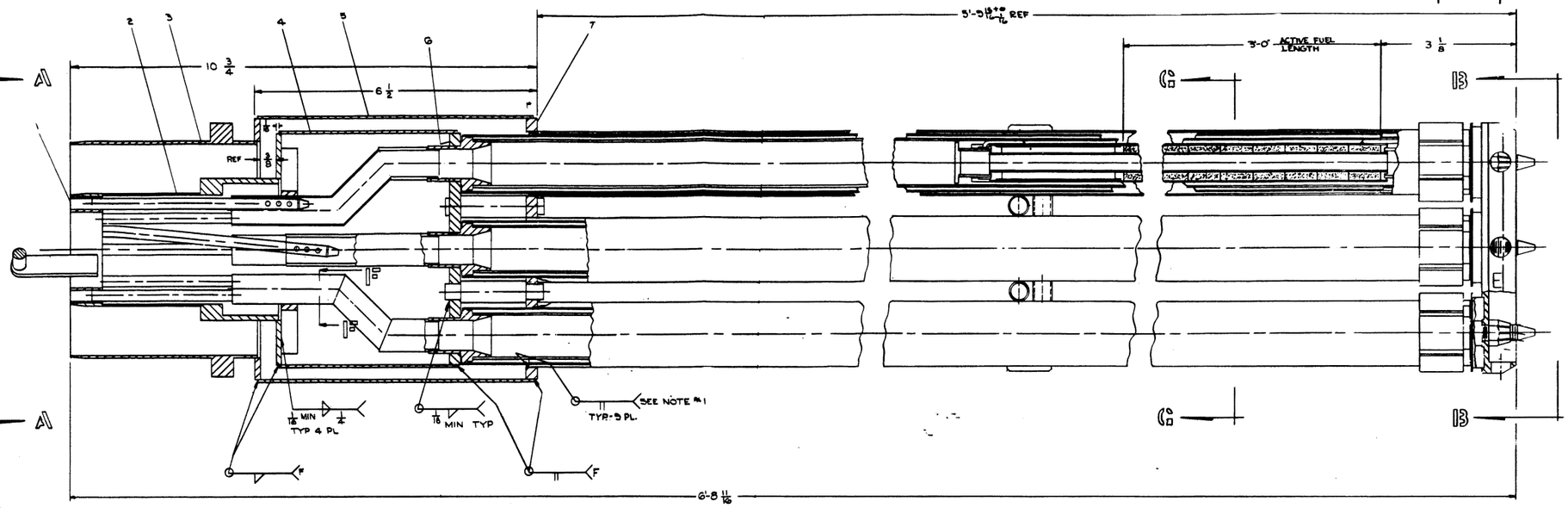

SECTION C-C

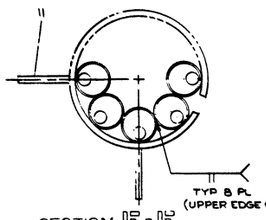

SECTION B-B

NOTE: DO NOT WELD P11 TO P8 OR P7

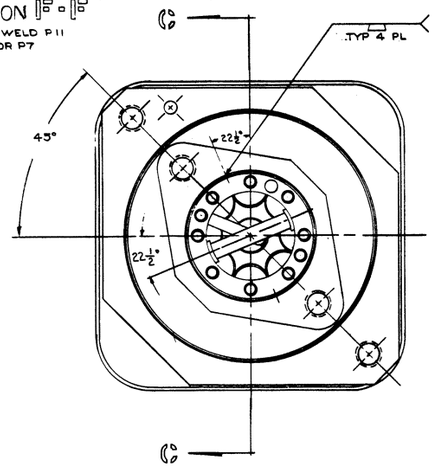

VIEW A-A

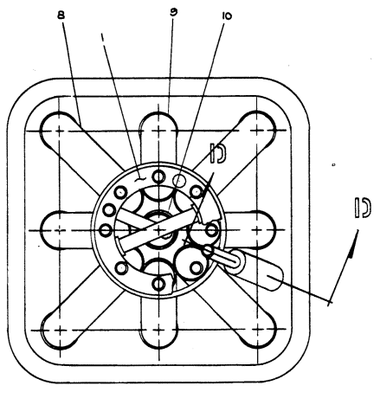

VIEW A-A
P2 THRU P5 REMOVED

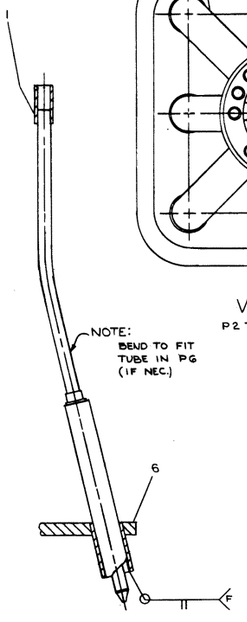

SECTION D-D

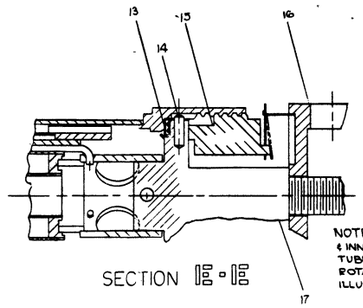

SECTION B-B

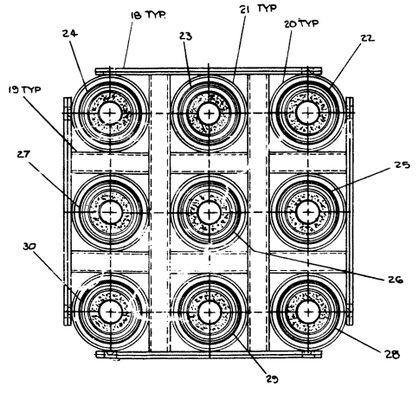

SECTION C-C

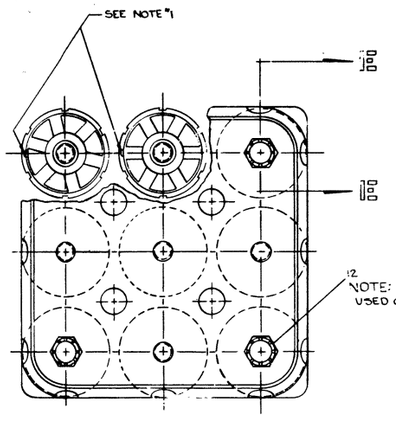

VIEW B-B

NOTES:
1. ALL INNER SLOTS OF PROCESS TUBE PART 20 & 21 MUST FACE IN ONE DIRECTION AS SHOWN. LETTER "E" ON ELEMENT SPACER PART 16 MUST FACE SAME DIRECTION AS SLOTS IN PART 20 & 21.
2. ALL WELDING FILLER METAL TO BE E308
3. F = GTAW FUSION WELD

Figure 9.14

APED SAN JOSE 212E449

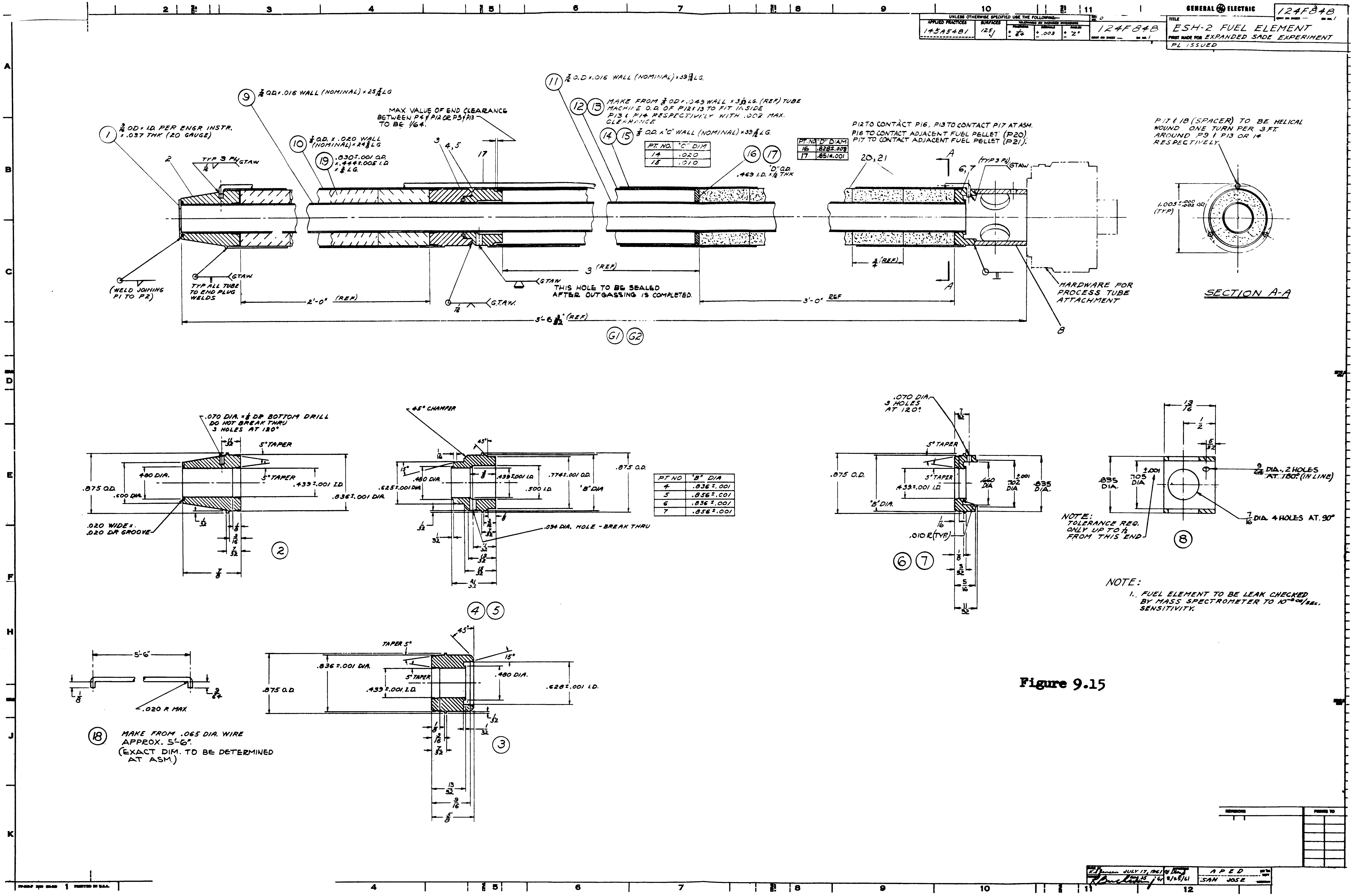
GENERAL ELECTRIC
124F848
ESH-2 FUEL ELEMENT
FIRST MADE FOR EXPANDED SADE EXPERIMENT
PL ISSUED
UNLESS OTHERWISE SPECIFIED USE THE FOLLOWING
145A5481
MAX VALUE OF END CLEARANCE BETWEEN P4 & P12 OR P5 & P13 TO BE 1/64.
P12 TO CONTACT P16, P13 TO CONTACT P17 AT ASM.
P16 TO CONTACT ADJACENT FUEL PELLET (P20)
P17 TO CONTACT ADJACENT FUEL PELLET (P21).
P17 & 18 (SPACER) TO BE HELICAL WOUND ONE TURN PER 3 FT. AROUND P9 & P13 OR 14 RESPECTIVELY.
THIS HOLE TO BE SEALED AFTER OUTGASSING IS COMPLETED.
HARDWARE FOR PROCESS TUBE ATTACHMENT
SECTION A-A
(WELD JOINING P1 TO P2)
TYP ALL TUBE TO END PLUG WELDS
NOTE: TOLERANCE REQ. ONLY UP TO 1/2 FROM THIS END
NOTE:
1. FUEL ELEMENT TO BE LEAK CHECKED BY MASS SPECTROMETER TO 10⁻⁸ cc/sec. SENSITIVITY.
MAKE FROM .065 DIA. WIRE APPROX. 5'-6". (EXACT DIM. TO BE DETERMINED AT ASM.)
PT. NO. "C" DIM
14 .020
15 .010
PT. NO. "D" DIAM.
16 .828±.001
17 .851±.001
PT NO "B" DIA
4 .836±.001
5 .856±.001
6 .836±.001
7 .856±.001
APED
SAN JOSE

Figure 9.15

the wire spacer attachment technique being developed in the fabrication of the E-SH1 fuel elements. Table 9.6 shows the enrichment and clad thicknesses for the various fuel elements.

The E-SH2 fuel elements will be of the once-through, or single-pass coolant flow. Inner and outer clad temperatures will be balanced by orificing to control the fraction of coolant steam flowing through the inner and outer flow passages. Initial calculations indicated that power output could be 65 to 70 KW per element, but this has been reduced to 58 KW because of emergency cooling considerations. All fuel elements will have a three-foot active fuel length and will be identical except for outer clad thickness. Five elements will have outer clad of 7/8" O.D. x 0.020" wall tubing, and four elements will have outer clad of 7/8" O.D. x 0.010" wall tubing. The outer cladding will be swaged in all cases. Inner clad of all elements will be 7/16" O.D. x 0.016" wall tubing. Cladding material will be type 304 stainless steel.

In spacing the E-SH2 fuel elements, three 0.065" diameter wire spacers will be used for each element, and each wire will make one complete spiral in three feet of element length. The wires will be fastened only at the end plugs. On the top of each fuel element there will be a dummy segment nearly identical to the active fuel region, except that stainless steel pellets will be used rather than fuel pellets. The dummy segment is separated from the

active fuel region by end plugs, and brings the total element fuel length to more than 5 feet. The purpose for including the dummy segment is to test wire spacers on long fuel elements.

TABLE 9.6

E-SH2 ANNULAR FUEL ELEMENT ENRICHMENT AND CLAD THICKNESS

Element	UO_2 Enrichment (%)	Outer Clad Thickness (Mils)
A	6%	20
B	10%	10
C	10%	10
D	6%	20
E	10%	10
F	10%	10
G	4.5%	20
H	6%	20
I	6%	20

9.2.5.2 Heat Transfer Considerations

The computer code SPAM was used in determining the required flow rates, flow gaps, and flow split to inner and outer flow passages for the E-SH2 annular fuel. Balancing the inner and outer clad maximum temperatures was one of the main considerations in the thermal analysis. This balance depends on the values of clad-to-fuel contact conductance and on the flow split between the inner and outer flow passages. For example, a flow split of 63% to the outer pass and 37% to the inner pass

(1000 lb/hr total) resulted in a matching of inner and outer clad maximum temperatures to within 50 ^{o}F (outer clad hotter) at a power level of 60 KW and outer clad-to-fuel conductance of 300 Btu/hr-ft^{2}-^{o}F. Reducing the outer conductance to 1000 and the inner conductance to 225 gave essentially the same result. On paper there is no problem in matching the clad temperatures more closely (changing the inner conductance from 225 to 265 brings inner and outer clad temperatures to within 5^{o}F), but the clad-to-fuel conductances are not known precisely enough to make a closer temperature balance worthwhile. Data obtained from SH-4B and SH-4C irradiation show the inner conductance to be somewhat smaller than that used in E-SH2, but it must be noted that E-SH2 is a one-pass fuel element and results from a bayonet type, two-pass element may not be applicable.

Other analytical work completed for E-SH2 includes the effect of plastic strain cyling on cladding life, and permissible unsupported length of outer cladding. The claculations show that plastic strain cycling should not cause failure during the anticipated irradiation time for E-SH2, and that maximum permissible unsupported length of the 0.010" outer clad may be as small as 0.050". The combined effect of manufacturing tolerances and length increase during swaging may result in a greater axial gap than 0.050", so the plenum support will be changed slightly to include a spring loaded support plug similar to that used in SH-5A (Figure 3.7, Eight Quarterly Progress Report).

9.2.6 Back-up Rod Type Fuel Element Design

Work is underway on two rod fuel geometries as possible replacements for one or two of the nine fuel elements. Design of a single rod assembly is complete except for final drawings. This rod has cladding of 1/2" O.D. x 0.016" wall 304 stainless, and utilizes 0.058" diameter wire spacers. This rod would replace annular element E-SH-2C and would have a power level near 19 KW with 5.2% enriched UO_2 fuel. The single rod design requires its own flow tube, and so will not permit rod and annular fuel elements to be interchanged. The single rod can be replaced with another similar rod, however.

The second rod geometry consists of a cluster of rods having an O.D. of 0.280" and tube wall of 0.020" - corresponding to the rod dimensions for the 300 MW(e) Mixed Spectrum Superheat Reactor. The cluster will be composed of six rod fuel elements surrounding a central non-fueled rod. Hot spot problems are decreased, and shutdown cooling is made easier by leaving the center tube empty. This rod cluster would replace the annular element E-SH-2G and would have an enrichment of 6.9. Design power would be 60 to 65 KW for the cluster. It is planned to use Hastelloy X as the clad material for three of the rod fuel elements and Incoloy as the cladding of the other three. As in the other designs for E-SH2, spiral wires spacers will be used. To be conservative in this initial E-SADE rod cluster, it is planned to use three 0.040" diameter wires on each of the rods rather than two wires or the single wire reported in the literature for some gas cooled reactor rod clusters. The decision to use three wires is based partly on the

bowing which occurred in the SADE SH-4 series of elements. By increasing the number of wires, the number of support points is increased proportionately for a given number of turns of each wire, and bowing and proper spacing can thus be better controlled. In order to avoid interference between the wires on a given fuel rod and the wires on the adjacent rods, and to promote mixing of the coolant steam, half of the fuel rods will have left hand wrapped wires and half will have right hand wrap. The right hand and left hand rods will alternate and the center tube will not have wires. To facilitate identification, the Incoloy cladding will utilize left hand wrap, and Hastelloy clad will utilize right hand wrap. In each case, the wire will be of the same material as the cladding.

There are several design problems associated with the rod cluster that are not present in the annular design and vice versa. One consideration already mentioned is the hot spot problem in the rod cluster. Other considerations are end fittings for keeping the rod cluster in one piece during transfer, and for maintaining in-core position. A satisfactory end fitting has been designed for the steam outlet end of the rod cluster. This fitting permits free axial expansion to account for differential expansion due to flux gradients and different cladding materials. An end fitting for the steam inlet end of the cluster has been designed, but the restricted space and re-entrant steam flow of the E-SH2 design will probably require modification of this fitting to permit better steam flow in the entrance region. For a given maximum clad temperature and heat flux, the rod cluster design does not permit as high steam exit temperature as the annular fuel does, if

a circular flow tube is used with the cluster. However, if a scalloped flow tube is used, or other means are provided to reduce the wasted flow area between any two of the 6 fueled rods and the liner, the rod cluster can be made to produce steam of as high or higher temperature than the annular design. For the E-SH2 rod cluster, the simple expedient of partially blocking the wasted flow area with six rods of 7/64" diameter was taken. Calculations indicate that for a given steam flow and exit temperature the presence of the velocity booster rods decreases the maximum clad temperature about 100°F.

A preliminary design drawing of the rod cluster has been made, and further design work will be supplemented by fabrication of mockups of several of the rod cluster parts.

10.0 TASK H - MIXED SPECTRUM SUPERHEATER DESIGN STUDY

10.1 Prototype Reactor Design

10.1.1 Introduction

During this period, the thermal hydraulic parametric studies initiated in the last quarter were completed. The ground rules and criteria for the study are discussed in the Eighth Quarterly Report. Briefly, the primary requirements are that the characteristics of the core during flooding and unflooding of the superheater, the Doppler effect in the fast core, and the control and coupling between the superheating and boiling sections of the core are to be representative of the 300 MWe reference design. The thermal hydraulic requirements are:

Outlet temperature	950°F
Central fuel temperature	4500°F
Maximum surface temperature	1250°F
Maximum flow velocity	250 ft/sec

The present parametric study covers a power range of 10 MWt to 40 MWt for a two-pass superheat core and 25 MWt to 65 MWt for a single-pass core. These ranges represent power produced in the superheating section only. The conditions used for the study are given in Table 10.1. The influence of the following parameters are considered:

Pitch-to-diameter ratio	Coolant flow velocity
Fuel rod diameter	Fuel surface heat flux
Fast core power output	Fuel surface film temperature drop
Coolant flow cross-sectional area	First-to-second pass volume ratio

10.1.2 General Results for a Single-pass Superheater

Previous studies for this concept involving its physics and thermal hydraulics have indicated that a fast core of

TABLE 10.1

CONDITIONS USED FOR PARAMETRIC STUDY

Operating pressure	1000 psia
Saturated steam inlet	545°F
Superheated steam outlet	950°F
Core length	30 inches
Core diameter (excluding fast buffer)*	30 inches
Maximum fuel rod surface temperature	1250°F
Maximum fuel center temperature	4500°F
UO_2 conductivity	1 Btu ft/hr °F ft^2
Cladding conductivity	13 Btu ft/hr °F ft^2
Fuel-to-cladding gap heat-transfer coefficient	1000 Btu/hr ft^2 °F
Flow Factors:	
By-Pass leakage	5%
Mechanical allowance	4%
Orifice error allowance	5%
Circumferential variation in film coefficient	± 20%
Physics Factors:	
Radial peak to Avg.	1.46
Axial peak to Avg.	1.3
Local peaking	1.08
Overpower (1.1) (1.136)	1.25
Total peak to Avg.	2.56
Core blockage by structural elements	10%

* This dimension does not include fast buffer, but it should be noted that the total superheater power shown on the curves in Figures 10.1 through 10.9 includes the power generated in the fast buffer as well as that in the fast core proper.

approximately a 30-inch cube would permit reasonable simulation of the 300 MWe reference design. It has been shown that the major limitation in the prototype design would be a tendency toward high clad temperatures at low power levels. The reason for this is that the quantity of steam available to cool the fast core is proportional to the reactor power. Since the saturation temperature and the superheated exit steam temperature are fixed, the fast core power must be adjusted to the steam flow to obtain the required exit temperature. Thus the total power is determined by the power produced by the boiler. Since the cross-sectional area of the fast core remains constant, an increase in reactor power causes an increase in steam mass flow through the superheating section. This results in better heat transfer.

To maintain a given fuel control temperature, the fuel rod diameter must be reduced as the power is raised. This increases the total heat transfer area in the fast core. The net effect of the increase in surface area and the improvement in heat transfer mentioned above is to more than compensate for the increase in power. Thus, going to lower powers will result in higher film drops and surface temperatures. These factors will, in effect, set a lower limit on the power that can be produced by the prototype reactor.

To illustrate these points, the parameters for the single-pass fast core study are shown in Figures 10.1 and 10.2. It can be seen from Figure 10.1 that to satisfy the thermal

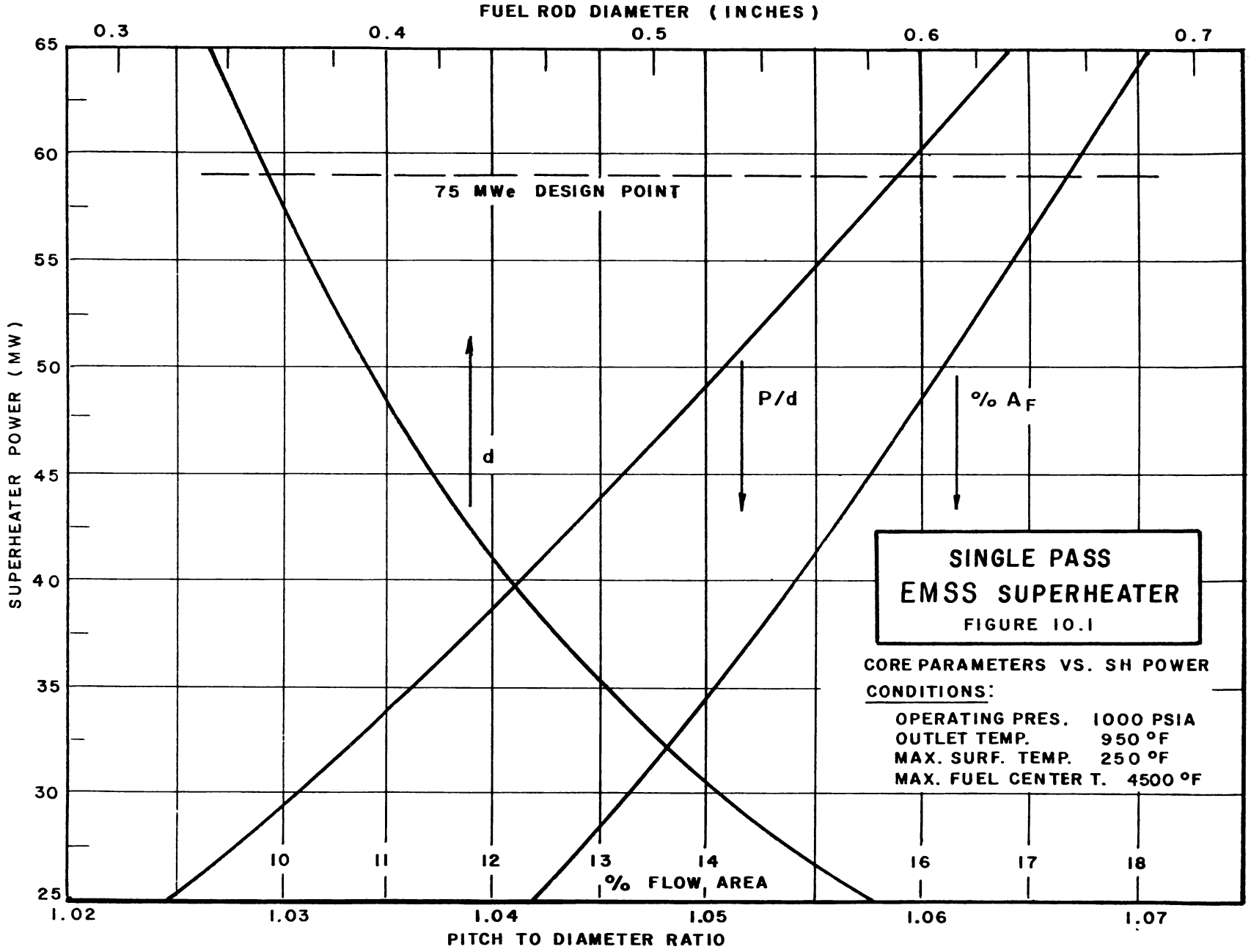
FUEL ROD DIAMETER (INCHES)
0.3
0.4
0.5
0.6
0.7
65
60
55
50
45
40
35
30
25
SUPERHEATER POWER (MW)
75 MWe DESIGN POINT
d
P/d
% A_F
10
11
12
13
14
16
17
18
% FLOW AREA
1.02
1.03
1.04
1.05
1.06
1.07
PITCH TO DIAMETER RATIO
SINGLE PASS
EMSS SUPERHEATER
FIGURE 10.1
CORE PARAMETERS VS. SH POWER
CONDITIONS:
OPERATING PRES. 1000 PSIA
OUTLET TEMP. 950 °F
MAX. SURF. TEMP. 250 °F
MAX. FUEL CENTER T. 4500 °F

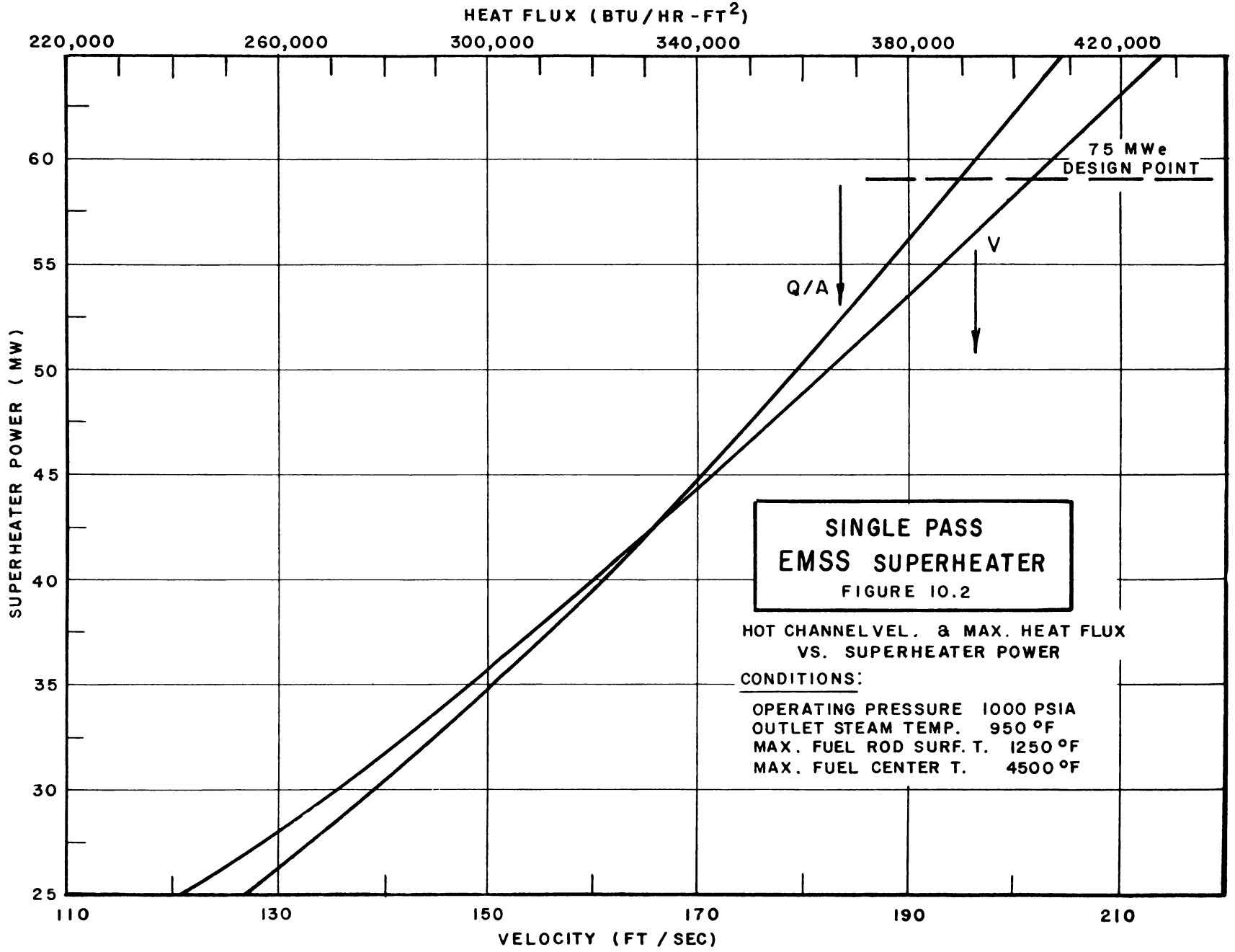
HEAT FLUX (BTU/HR-FT^2)
220,000
260,000
300,000
340,000
380,000
420,000
60
55
50
45
40
35
30
25
SUPERHEATER POWER (MW)
75 MWe
DESIGN POINT
Q/A
V
SINGLE PASS
EMSS SUPERHEATER
FIGURE 10.2
HOT CHANNEL VEL. & MAX. HEAT FLUX
VS. SUPERHEATER POWER
CONDITIONS:
OPERATING PRESSURE 1000 PSIA
OUTLET STEAM TEMP. 950 °F
MAX. FUEL ROD SURF. T. 1250 °F
MAX. FUEL CENTER T. 4500 °F
110
130
150
170
190
210
VELOCITY (FT / SEC)

hydraulic requirements, the pitch-to-diameter ratio of the fuel rods must go down as the fast core power is reduced. Thus a lower limit is imposed on the fast core power by the uncertainty in peripheral variation in fuel rod temperature which becomes more pronounced as the rods become more closely packed. At the higher values of fast core power, the rod spacing can be increased, but the coolant velocity is also increased. As mentioned previously, the reason for this is that the steam flow rate increases directly as the power, but the core equivalent diameter is kept constant. The increase in rod spacing acts to keep the velocity from increasing as fast as the power, but the net effect is to raise the velocity as shown in Figure 10.2. If the core size is kept constant, as it is for this study, the power output will be limited by the maximum allowable steam velocity. If higher powers are desired, larger core sizes should be considered. For a given core size, the final design will represent a compromise among the desired power, rod spacing, and maximum allowable steam velocities.

It should be pointed out that the primary reason for the relatively high velocities determined in this study, as compared to the 300 MWe reference design, is due to the difference in coolant pressures. In the reference design, the coolant pressure is 1500 psia, while in the present study the pressure is 1000 psia. The question of the optimum pressure for the Mixed Spectrum Superheater remains to be resolved. The tentative choice of 1000 psi for the prototype was made in order to utilize B.W.R. experience at 1000 psi.

Figures 10.1 and 10.2 also show how the fuel rod diameter, coolant flow cross-sectional area, and the surface heat flux varies with fast core power for the thermal hydraulic conditions stated above.

10.1.3 75 MWe Prototype Design

During this reporting period, work was initiated on the design of a 75 MWe prototype plant. This plant is intended not only to serve as a developmental tool, but also is expected to generate useful power. Power plant economics will therefore influence the conceptual design of the plant. Some preliminary thermal hydraulic considerations for the 75 MWe plant are discussed below.

The design point for this plant is shown in Figures 10.1 and 10.2. Based on a plant efficiency of 38.5 percent, the power produced in the fast core is 59 MWt for the 75 MWe total plant output. The pertinent reactor parameters corresponding to this power level are listed in column 2 of Table 10.2. These values are not necessarily optimum and are given for reference only.

Since the parametric curves show only trends for the given conditions, corresponding values were calculated at 59 MWt superheater power to determine the influence of possible uncertainties in several other parameters. The parameters considered and the values used are: (1) fuel conductivity of 1.5 Btu/hr ft^2 (^oF/ft); (2) 30% improvement in film coefficient due to the wire wrap; and (3) superheated steam

outlet temperature reduced to 900°F. The results of these calculations are shown in Table 10.2 along with the "design point" values which are given in column 2.

The reference 300 MWe design uses a conductivity of 1 for UO_2 and a central temperature limitation of 4500°F (in accordance with the ground rules of the AEC study for which the design was prepared). Recent work however, has indicated that UO_2 has a higher effective conductivity and that the MSS design will profit from this. From the point of view of a prototype designed to match conditions of a larger reactor the use of higher conductivity will require a lower pitch to diameter ratio. Column 3, Table 10.2 shows the effect of higher UO_2 conductivity on coolant velocity and pitch-to-diameter ratio. The velocity is increased and the rod spacing is decreased to accommodate the higher linear heat generation rate. This points out the need for thermal and hydraulic data at low P/D ratios and indicates that a problem may exist in designing an experimental reactor to match the reference design, if a higher conductivity were used without changing the maximum fuel center temperature.

Experimental work with wire-wrapped rods (IDO-28549 Army Gas-Cooled Reactor Systems Program - Semi-Annual Progress Report - February 1960) indicates that a film coefficient improvement of about 30% over the calculated one considering no wire wrap may be obtained. It is difficult to say just how much the wire wrap helps for the present design without doing some experimental work representative of conditions considered for

TABLE 10.2

PARAMETERS FOR 75 MWe PROTOTYPE FOR VARIOUS CONDITIONS

Parameter	Based on Table 10.1 Conditions	Table 10.1 Conditions with k = 1.5 Btu/hr-ft ^{o}F	With 30% Increase in h Due to Wire Wrap	900^{o}F Exit Temp. (355^{o}F Superheat)	24 inch Fast Core Equivalent Diameter
Pitch-to-diameter ratio	1.059	1.035	1.095	1.090	1.085
% flow area (void fraction)	17.4	13.9	22.0	21.4	20.8
Fuel rod diameter, inches	0.354	0.440	0.344	0.345	0.271
Hot channel velocity, ft/sec	204	253	160	176	264
Maximum heat flux, Btu/hr-ft^2	390,000	461,000	402,000	401,000	487,000

EMSS. Since it is felt that some improvement will result, an optimistic 30% film coefficient improvement was considered (column 4, Table 10.2) to determine its effect. The results indicate a more desirable P/D and velocity as can be seen by comparing the figures in column 4 with those in column 2.

The pitch-to-diameter ratio is determined by the velocity necessary to keep the surface temperature below some maximum limit (in this case 1250°F). Since the surface temperature is directly related to the bulk coolant temperature in the region of the maximum heat flux, an appreciable improvement in the pitch-to-diameter can result from lowering the bulk temperature. As shown in Table 10.2, if the outlet steam temperature were lowered 50°F the pitch-to-diameter ratio could be raised from less than 1.06 to 1.09 which would reduce the velocity from 204 fps to 176 fps.

For a thermal output of 59 MW in the fast core, the power density is relatively low (155 KW/liter). If physics requirements (Doppler and flooding effects) could still be met, it might be possible to go to a smaller; high-power-density core. To show the effect of a smaller core size on the thermal hydraulic parameters, a brief study was made on a fast core with the equivalent diameter reduced from 30 to 24 inches. As shown in column 6 of Table 10.2, the pitch-to-diameter ratio increases and the rod diameter decreases. The net flow area decreases, however, due to the reduced core diameter. This results in approximately 30 percent increase in hog channel velocity from 204 to 264 ft/sec. Thus an important factor in determining the minimum core size may be the maximum allowable coolant velocity in addition to the physics.

10.1.4 Results for a Two-Pass Superheater

Since the pitch-to-diameter ratio limits the single-pass superheater to relatively high powers, a two-pass flow arrangement was considered to extend the superheater range down to 10 MWt. Two-pass flow is beneficial because it helps to keep the surface temperature low by increasing the steam velocity since flow area is reduced in each pass. The pressure drop, however, is increased significantly, since both velocity and the length of the flow path are increased.

For this study, the core parameters are considered for first-to-second-pass core volume ratios of 1.36, 1.83, and 2.53. This range covers the cases where the pitch-to-diameter ratio is lowest in the second pass to that where the pitch-to-diameter ratio is lowest in the first pass. The results of these calculations for maximum pitch-to-diameter ratios limited by rod surface temperature are shown in Figures 10.3 through 10.8.

It can be seen on Figure 10.3 that the hot channel velocity is much greater in the second pass than in the first pass. This is easily understood, since the bulk coolant temperature and the heat flux are both higher in the second pass than in the first pass.

The maximum heat flux (Figure 10.4) in the second pass is about 15% higher than in the first pass. This is due to the higher neutron flux and power density in the second pass which is in the center region of the core. The fluxes are higher even though the rod diameter is smaller, and there is more heat transfer surface per unit volume in the second pass. The maximum heat

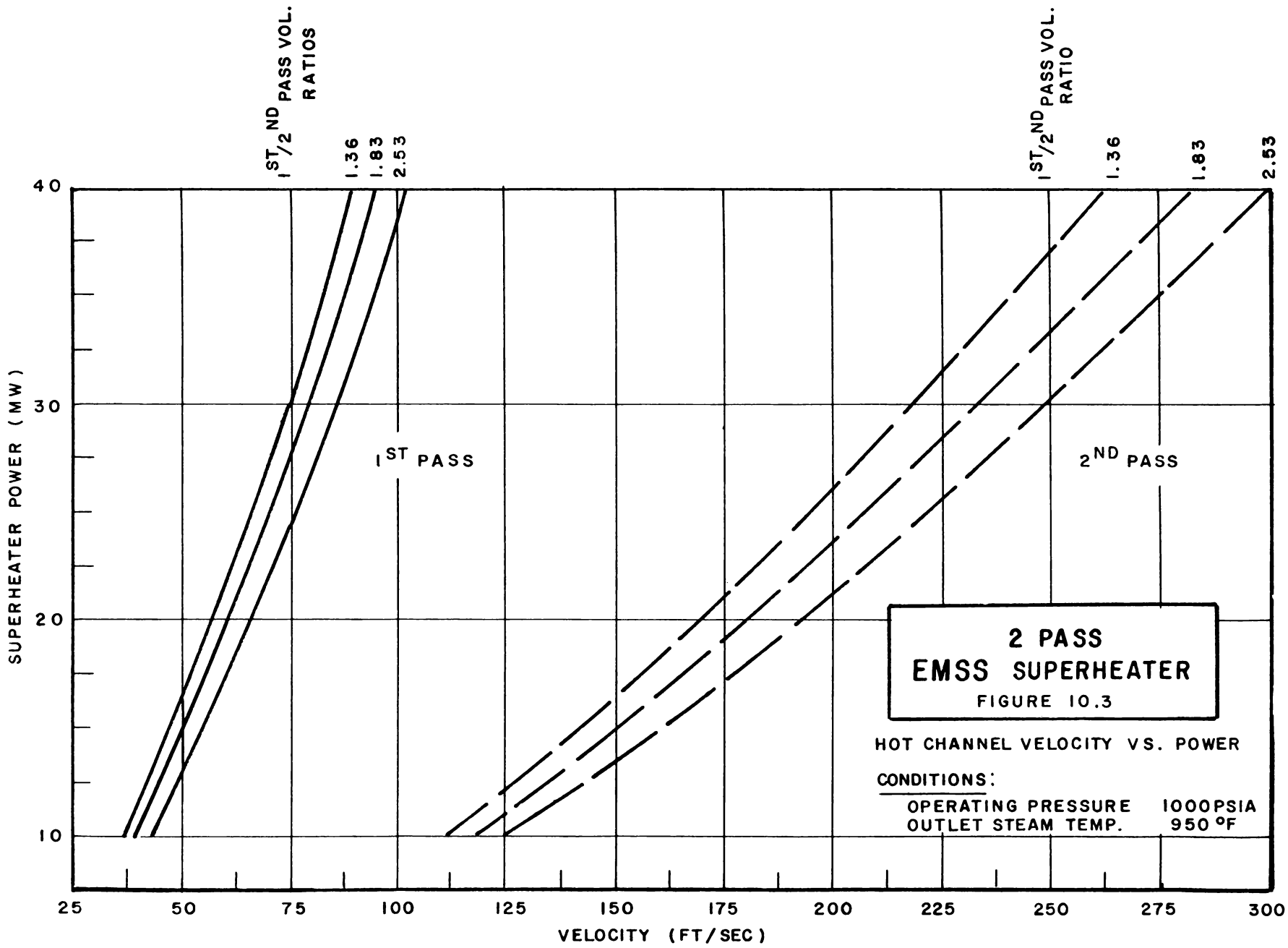
1ST/2ND PASS VOL. RATIOS
1.36
1.83
2.53
1ST/2ND PASS VOL. RATIO
1.36
1.83
2.53
SUPERHEATER POWER (MW)
40
30
20
10
1ST PASS
2ND PASS
25
50
75
100
125
150
175
200
225
250
275
300
VELOCITY (FT/SEC)
2 PASS
EMSS SUPERHEATER
FIGURE 10.3
HOT CHANNEL VELOCITY VS. POWER
CONDITIONS:
OPERATING PRESSURE 1000PSIA
OUTLET STEAM TEMP. 950 °F

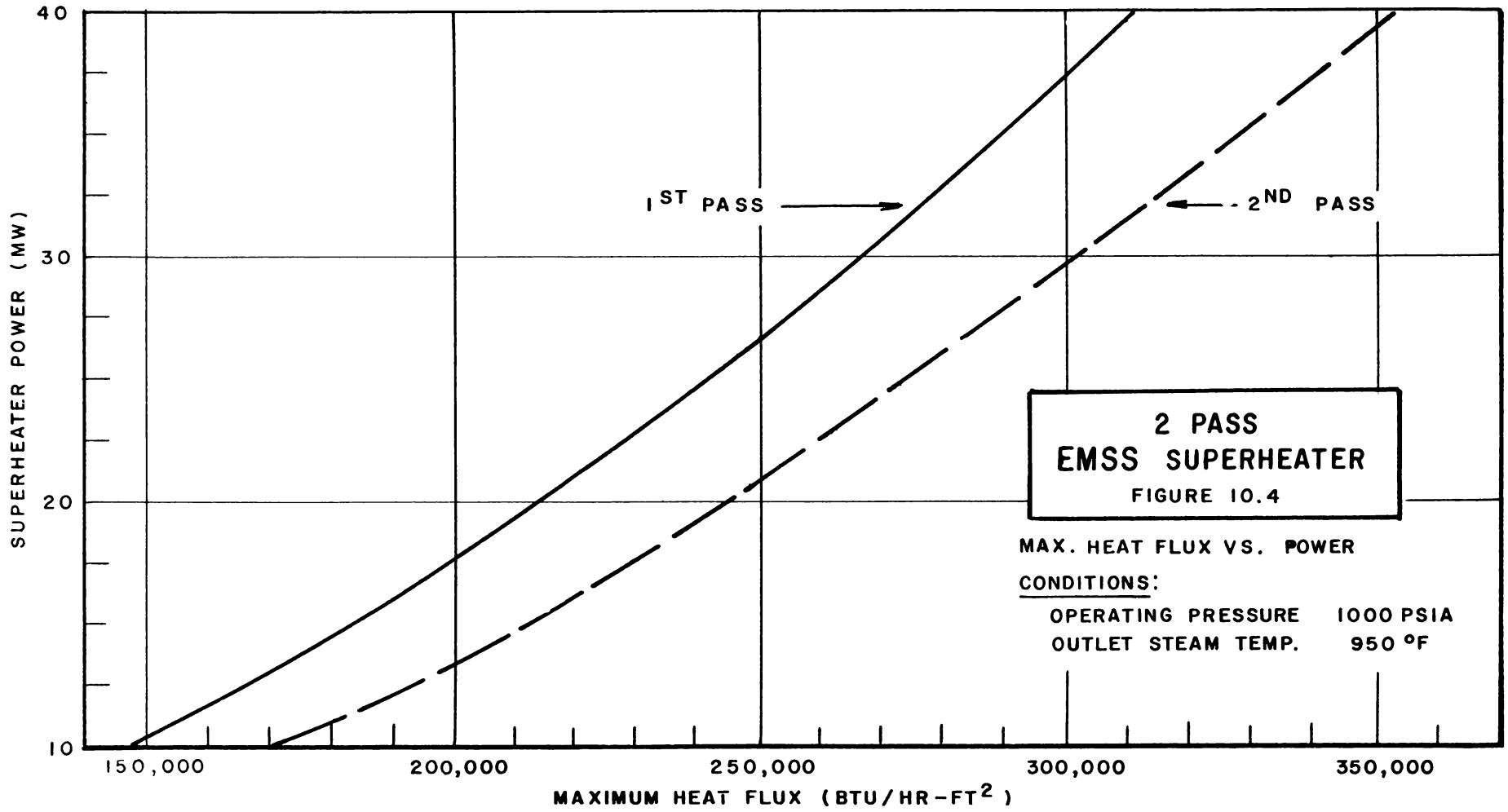
40
30
20
10
SUPERHEATER POWER (MW)
1ST PASS
2ND PASS
150,000
200,000
250,000
300,000
350,000
MAXIMUM HEAT FLUX (BTU/HR-FT2)
2 PASS
EMSS SUPERHEATER
FIGURE 10.4
MAX. HEAT FLUX VS. POWER
CONDITIONS:
OPERATING PRESSURE 1000 PSIA
OUTLET STEAM TEMP. 950 °F

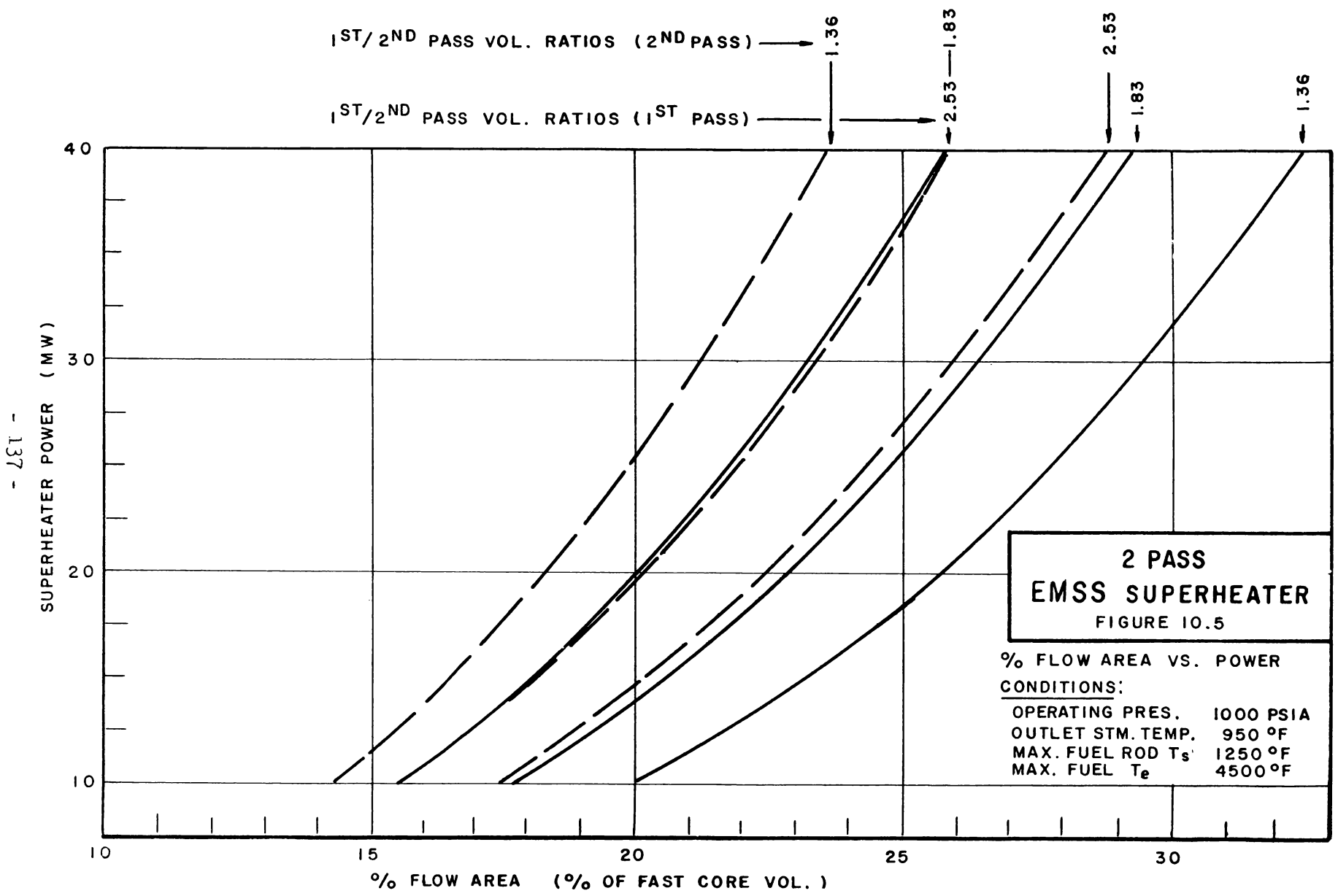
1ST/2ND PASS VOL. RATIOS (2ND PASS)
1ST/2ND PASS VOL. RATIOS (1ST PASS)
1.36
1.83
2.53
2.53
1.83
1.36
40
30
20
10
SUPERHEATER POWER (MW)
10
15
20
25
30
% FLOW AREA (% OF FAST CORE VOL.)
2 PASS
EMSS SUPERHEATER
FIGURE 10.5
% FLOW AREA VS. POWER
CONDITIONS:
OPERATING PRES. 1000 PSIA
OUTLET STM. TEMP. 950 °F
MAX. FUEL ROD Ts 1250 °F
MAX. FUEL Te 4500 °F

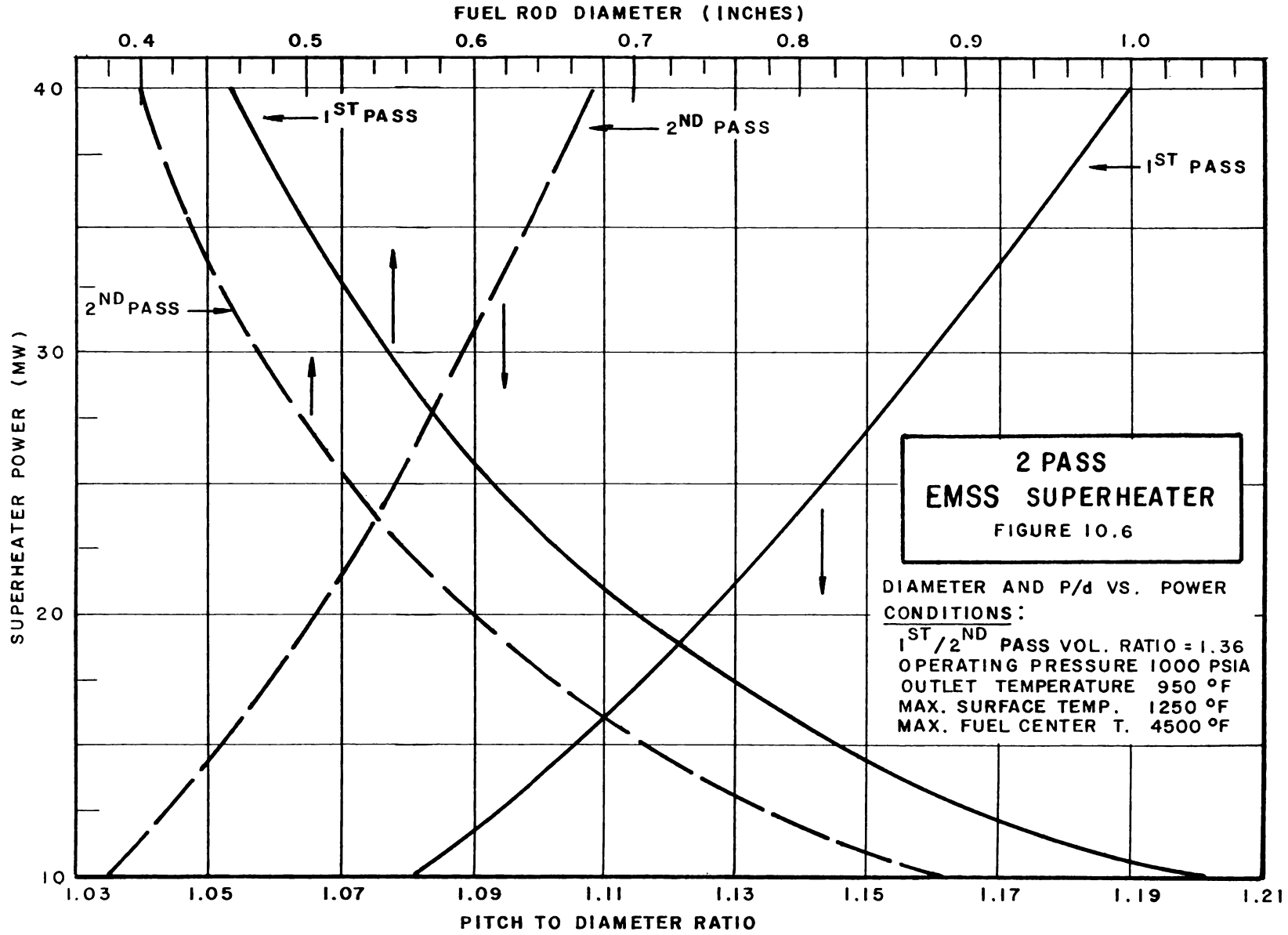
FUEL ROD DIAMETER (INCHES)
0.4
0.5
0.6
0.7
0.8
0.9
1.0
40
30
20
10
SUPERHEATER POWER (MW)
1ST PASS
2ND PASS
2ND PASS
1ST PASS
2 PASS
EMSS SUPERHEATER
FIGURE 10.6
DIAMETER AND P/d VS. POWER
CONDITIONS:
1ST/2ND PASS VOL. RATIO = 1.36
OPERATING PRESSURE 1000 PSIA
OUTLET TEMPERATURE 950 °F
MAX. SURFACE TEMP. 1250 °F
MAX. FUEL CENTER T. 4500 °F
1.03
1.05
1.07
1.09
1.11
1.13
1.15
1.17
1.19
1.21
PITCH TO DIAMETER RATIO

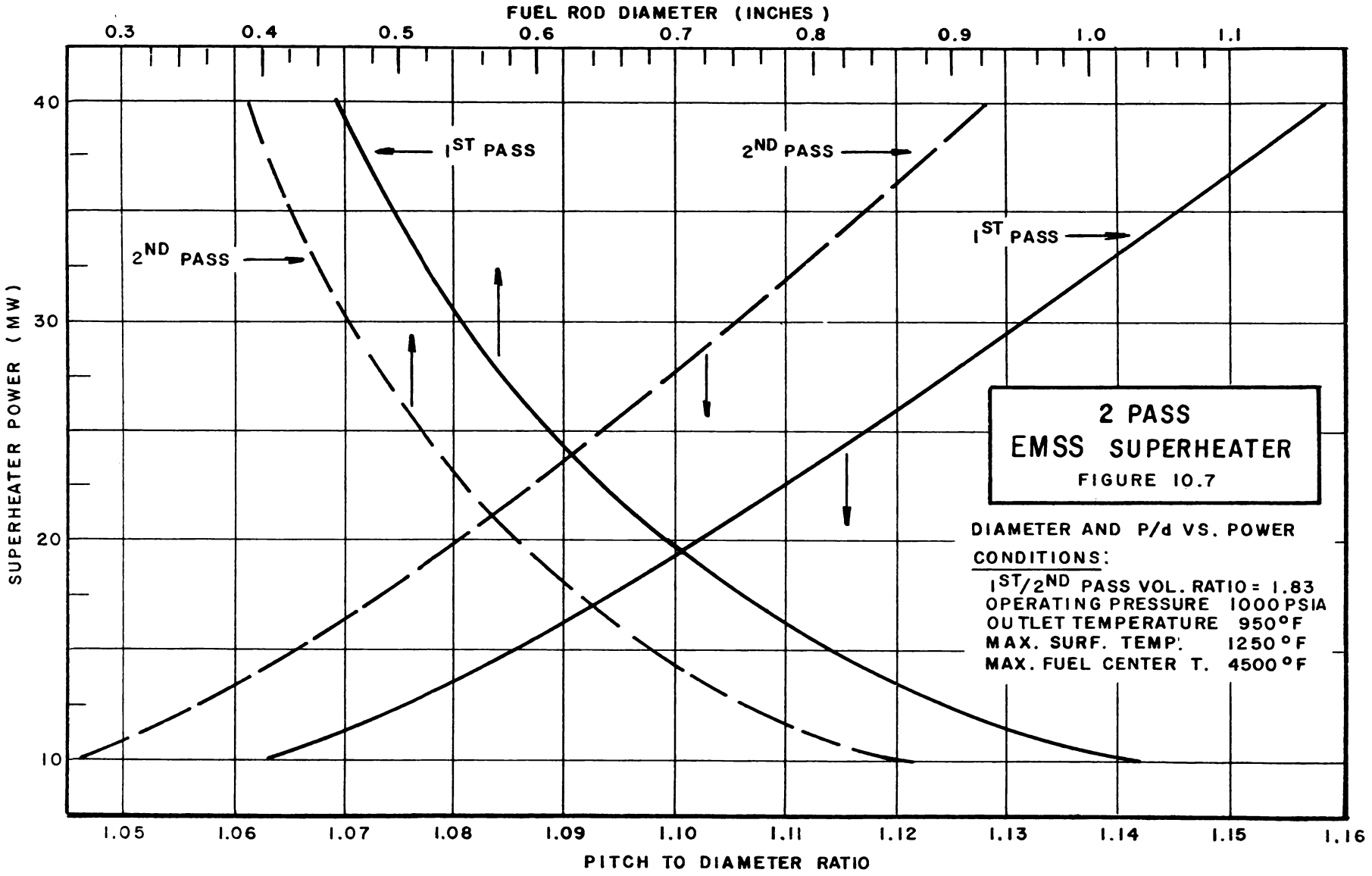
FUEL ROD DIAMETER (INCHES)
0.3
0.4
0.5
0.6
0.7
0.8
0.9
1.0
1.1
SUPERHEATER POWER (MW)
40
30
20
10
1ST PASS
2ND PASS
2ND PASS
1ST PASS
1.05
1.06
1.07
1.08
1.09
1.10
1.11
1.12
1.13
1.14
1.15
1.16
PITCH TO DIAMETER RATIO
2 PASS
EMSS SUPERHEATER
FIGURE 10.7
DIAMETER AND P/d VS. POWER
CONDITIONS:
1ST/2ND PASS VOL. RATIO = 1.83
OPERATING PRESSURE 1000 PSIA
OUTLET TEMPERATURE 950°F
MAX. SURF. TEMP. 1250°F
MAX. FUEL CENTER T. 4500°F

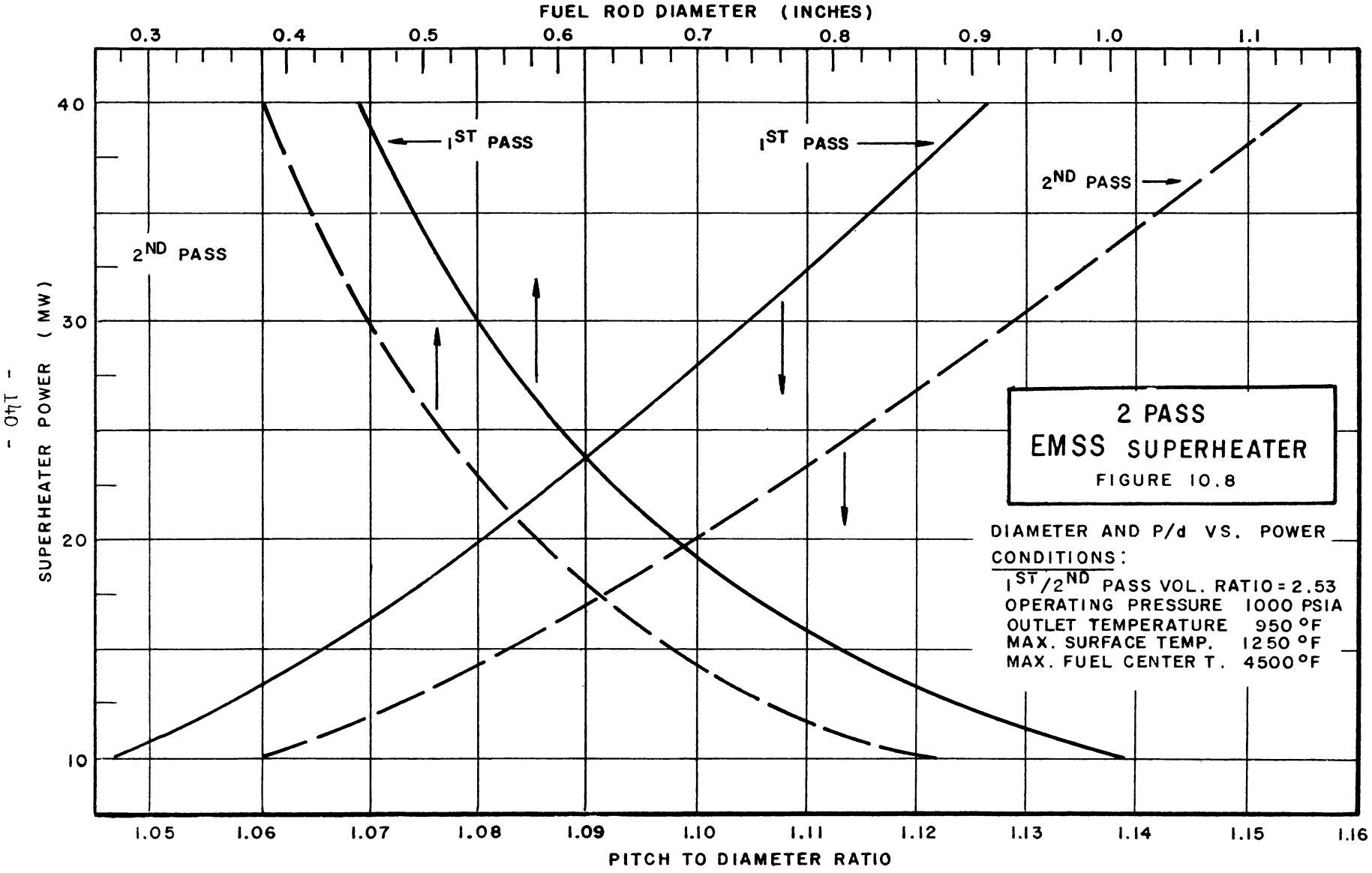
FUEL ROD DIAMETER (INCHES)
0.3
0.4
0.5
0.6
0.7
0.8
0.9
1.0
1.1
40
30
20
10
SUPERHEATER POWER (MW)
1ST PASS
1ST PASS
2ND PASS
2ND PASS
2 PASS
EMSS SUPERHEATER
FIGURE 10.8
DIAMETER AND P/d VS. POWER
CONDITIONS:
1ST/2ND PASS VOL. RATIO = 2.53
OPERATING PRESSURE 1000 PSIA
OUTLET TEMPERATURE 950 °F
MAX. SURFACE TEMP. 1250 °F
MAX. FUEL CENTER T. 4500 °F
1.05
1.06
1.07
1.08
1.09
1.10
1.11
1.12
1.13
1.14
1.15
1.16
PITCH TO DIAMETER RATIO

flux for each pass did not vary appreciably for the volume ratios considered, so only one curve is shown for each pass.

The rod diameters and the pitch-to-diameter ratios are shown on Figures 10.6, 10.7 and 10.8 for the first-to-second pass volume ratios of 1.36, 1.83, and 2.53 respectively. In comparing the pitch-to-diameter ratio curves on Figures 10.7 and 10.8, it can be seen that at some intermediate volume ratio, the pitch-to-diameter ratios for each pass would be equal. This is shown on Figure 10.9 which is a plot of volume ratio vs. pitch-to-diameter ratio for the 30 MW superheater power case. If curves for other superheater powers were plotted, they would be similar in shape intersecting at about the same volume ratio (2.18). The curves would intersect at higher or lower pitch-to-diameter ratios depending upon the power (higher P/D for higher power, lower P/D for lower power). This volume ratio is the optimum one considering only pitch-to-diameter ratio, i.e., the minimum P/D ratio is as large as possible on both passes while meeting the design criterion. Above this point a smaller pitch-to-diameter ratio is required in the first pass. Below this point, i.e., relatively larger second pass, a smaller pitch-to-diameter ratio is required in the second pass.

Although the volume ratio considered above is an "optimum" one considering only pitch-to-diameter ratio, the first pass film drop is very high at this point. This is due to the fact that the same limiting surface temperature was considered in each pass, and the bulk coolant is about 200^{o}F less at the core midplane in the first pass. Since the film drop is very high at

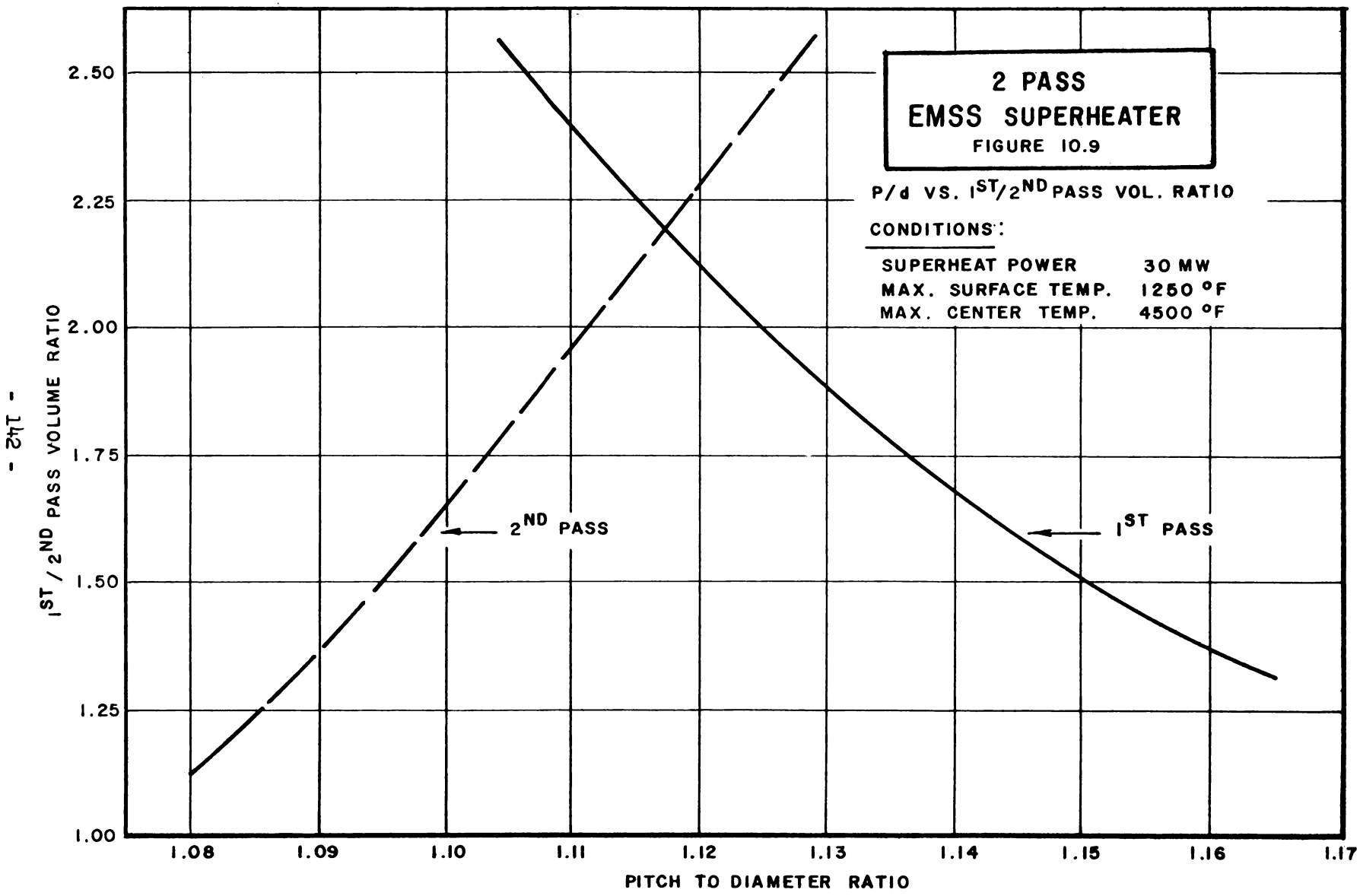
2 PASS
EMSS SUPERHEATER
FIGURE 10.9
P/d VS. 1ST/2ND PASS VOL. RATIO
CONDITIONS:
SUPERHEAT POWER 30 MW
MAX. SURFACE TEMP. 1250 °F
MAX. CENTER TEMP. 4500 °F
2ND PASS
1ST PASS
1ST / 2ND PASS VOLUME RATIO
PITCH TO DIAMETER RATIO
2.50
2.25
2.00
1.75
1.50
1.25
1.00
1.08
1.09
1.10
1.11
1.12
1.13
1.14
1.15
1.16
1.17

this "optimum" volume ratio, an actual design should be a compromise. A lower first-to-second-pass volume ratio with a somewhat lower second-pass pitch-to-diameter ratio can be selected. Using the same pitch-to-diameter ratio for both passes results in lower fuel surface temperatures and film drops in the first pass since heat transfer is improved there. To illustrate this, the film drops are plotted in Figure 10.10. From this and Figure 10.9, it can be seen that for a volume ratio of 1.0, the film drop in the first pass is about equal to that in the second pass. The pitch-to-diameter ratio has decreased from about 1.117 to about 1.075.

In interpreting the results of this study, it is felt that the trends shown by the curves of Figures 10.1 through 10.10 are reasonably accurate. The actual values may be somewhat in error because of uncertainties in the heat-transfer coefficients due to the presence of the wire wrapping. There is evidence to show that the heat transfer coefficients can be significantly improved (at the expense of pressure drop) by the wire-wrap spacers. The curves presented in Figures 10.1 through 10.10 are pessimistic in that no allowance is made for this improvement. An estimate of this effect can be obtained by comparing the values shown in columns 2 and 4 of Table 10.2. The values in column 4 assume a 30 percent increase in the heat transfer coefficient over that used in the results of column 2.

10.2 Safety Studies

10.2.1 Introduction

In the last reporting period it was shown that an extreme case of

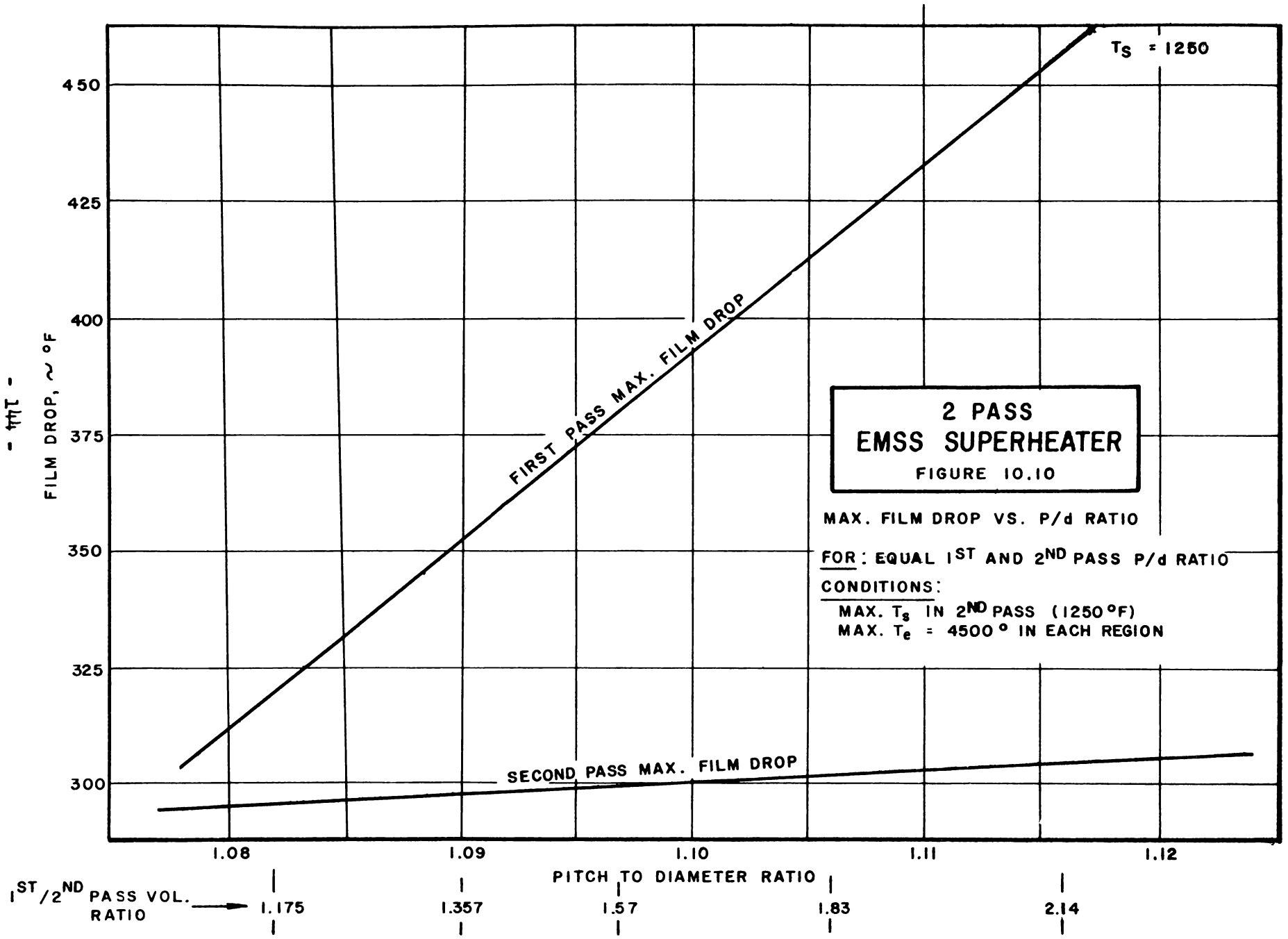
T_S = 1250
FIRST PASS MAX. FILM DROP
SECOND PASS MAX. FILM DROP
FILM DROP, ~ °F
450
425
400
375
350
325
300
1.08
1.09
1.10
1.11
1.12
PITCH TO DIAMETER RATIO
1ST/2ND PASS VOL. RATIO
1.175
1.357
1.57
1.83
2.14
2 PASS
EMSS SUPERHEATER
FIGURE 10.10
MAX. FILM DROP VS. P/d RATIO
FOR: EQUAL 1ST AND 2ND PASS P/d RATIO
CONDITIONS:
MAX. T_s IN 2ND PASS (1250°F)
MAX. T_e = 4500° IN EACH REGION

melting in the fast core could result in a reactivity addition of approximately 9% for the prototype. This calculation assumed that the superheater section melted and slumped so that all the steam volume was instantaneously removed from the core. It is clear that such a condition is hypothetical and would be impossible to achieve in practice. The heat generated by the critical mass will tend to disperse the fissionable material and inhibit, if not stop, the nuclear reaction well before complete compaction could occur.

To obtain a more realistic estimate for the orders of magnitude of reactivity inputs due to core meltdown, a computer program was initiated to calculate the rate at which the fast core could become molten during a loss-of-coolant accident. The program is set up to provide information regarding the spatial distribution of the molten material (fuel and cladding). This will permit calculation both of reactivity changes in the original core configuration as melting progresses and rates of reactivity addition as the molten fuel slumps into a new critical mass. These reactivity calculations are now in progress.

10.2.2 Approach to the Problem

The procedural steps to be followed in the analysis are as follows:

1. Evaluate the temperature and melting history of single fuel rods under loss-of-coolant conditions. The initial conditions of the rods will represent various radial positions in the fast core at normal full power operation.
2. Determine the reactivity, hence the power level, for the fast core for various stages of meltdown. The various stages of meltdown are illustrated in Figure 10.11.

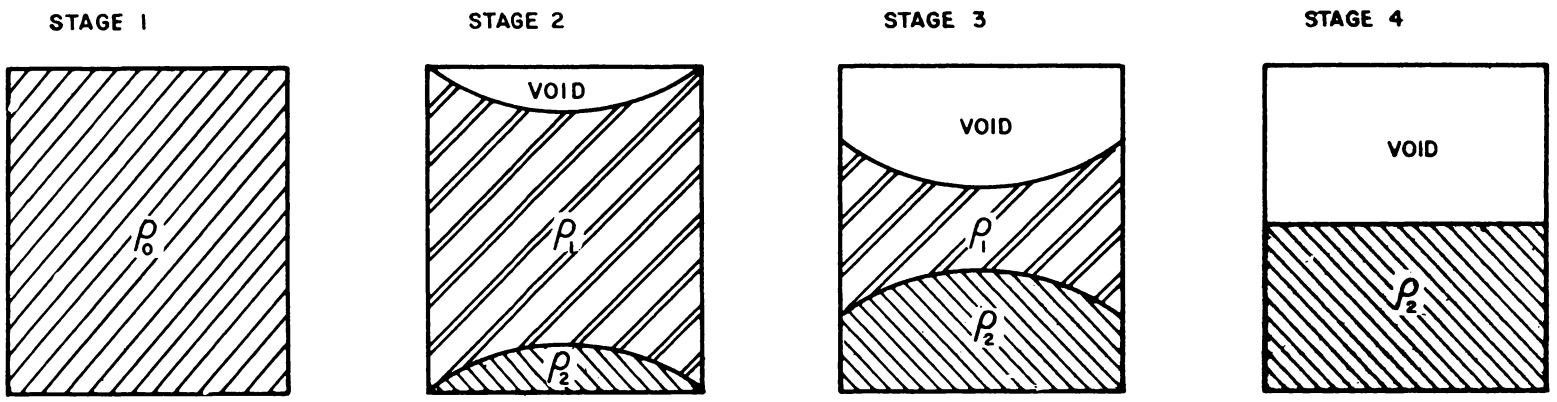

ρ_0 = INITIAL DENSITY

ρ_1 = DENSITY OF MEAT WITHOUT CLAD

ρ_2 = DENSITY OF FUEL PLUS MOLTEN CLAD

MELTDOWN STAGES FOR REACTIVITY CALCULATIONS

FIGURE 10.11

3. On the basis of steps 1 and 2, determine the time intervals between the various stages and from this the rate of change of power throughout the configuration.
4. From the power levels determined in step 3, evaluate the changes in temperature and state at various locations in the configuration.
5. Evaluate the effects of inertia and change of state on the redistribution of the core materials.

The first four steps outlined above will provide some insight into the sequence of events (e.g., whether fuel or cladding melts first) and also the time intervals at which various events occur. This information will be useful in formulating mathematical models to represent the subsequent course of events. For example, whether it is reasonable to assume that the molten core material freezes and plugs the lower blanket region and what form of analysis should be made to account for the effects of inertia and change of state will become more clear. The results should indicate what basic assumptions concerning a meltdown are reasonable and point out areas where more refined calculational methods are advantageous.

10.2.3 Calculations

10.2.3.1 Objective

The objective of these calculations is to obtain the melting and temperature history of the fuel rods described below for the case of constant power and no coolant flow for the five different initial temperature and power conditions also described below. These conditions correspond to five radial core locations at normal full power operation.

10.2.3.2 Basic Assumptions

1. No heat flow to surrounding medium.
2. Heat generation rate remains constant for each position throughout the problem.
3. Each fuel rod is divided into 10 equal-volume axial modes.
4. Upon melting, a clad node is removed from the heat-transfer problem, while a meat node is maintained at its melting temperature.

10.2.3.3 Configuration

Rod length	42 in.
Meat OD	0.240 in.
Clad thickness	0.020 in.

10.2.3.4 Initial Conditions

1. Axial power distribution (Btu/in^3 sec)

Axial Node No.	Tube Number 1	2	3	4	5
1	7.64	6.99	5.97	4.60	3.12
2	10.88	9.96	8.52	6.55	4.52
3	13.66	12.53	10.71	8.24	5.71
4	15.69	14.35	12.28	9.44	6.54
5	16.73	15.30	13.09	10.07	6.98
6	16.73	15.30	13.09	10.07	6.98
7	15.69	14.35	12.28	9.44	6.54
8	13.66	12.53	10.71	8.24	5.71
9	10.88	9.96	8.52	6.55	4.52
10	7.64	6.99	5.97	4.60	3.12

2. Clad node temperature, ^{o}F

Axial Node No.	Tube Number 1	2	3	4	5
1	847	828	798	757	713
2	978	951	908	850	789
3	1096	1063	1008	935	860
4	1191	1152	1090	1005	919
5	1251	1216	1149	1059	967
6	1287	1246	1179	1089	947
7	1296	1257	1195	1110	1024
8	1271	1238	1183	1110	1035
9	1218	1191	1148	1040	1029
10	1177	1158	1128	1087	1043

3. The meat node temperatures are shown graphically in Figures 10.12 through 10.16.

4. Material constants:

Clad: $k = 12.58$ Btu/hr-ft$^{\circ}$F

$= 490$ lbs/ft^3

$C_p = 0.12$ Btu/lb$^{\circ}$F

$T_m = 2575^{\circ}$F (melting temp.)

Meat: $k = 1.0$ Btu/hr-ft$^{\circ}$F

$= 650$ lbs/ft^3

$C_p = 0.08$ Btu/lb$^{\circ}$F

$T_m = 4800^{\circ}$F (melting temp.)

Fuel-clad gap coefficient $h_g = 500$ Btu/hr-ft^2 $^{\circ}$F

10.2.4 Preliminary Results

Calculations describing the melting history of five radial regions in the fast core were made under the assumptions described above. These melting calculation results are shown graphically in Figures 10.17 and 10.18 at time-dependent clad and meat melting zones respectively. Only a half-section of the fast core is shown since the temperature conditions are symmetrical under the assumptions of this problem.

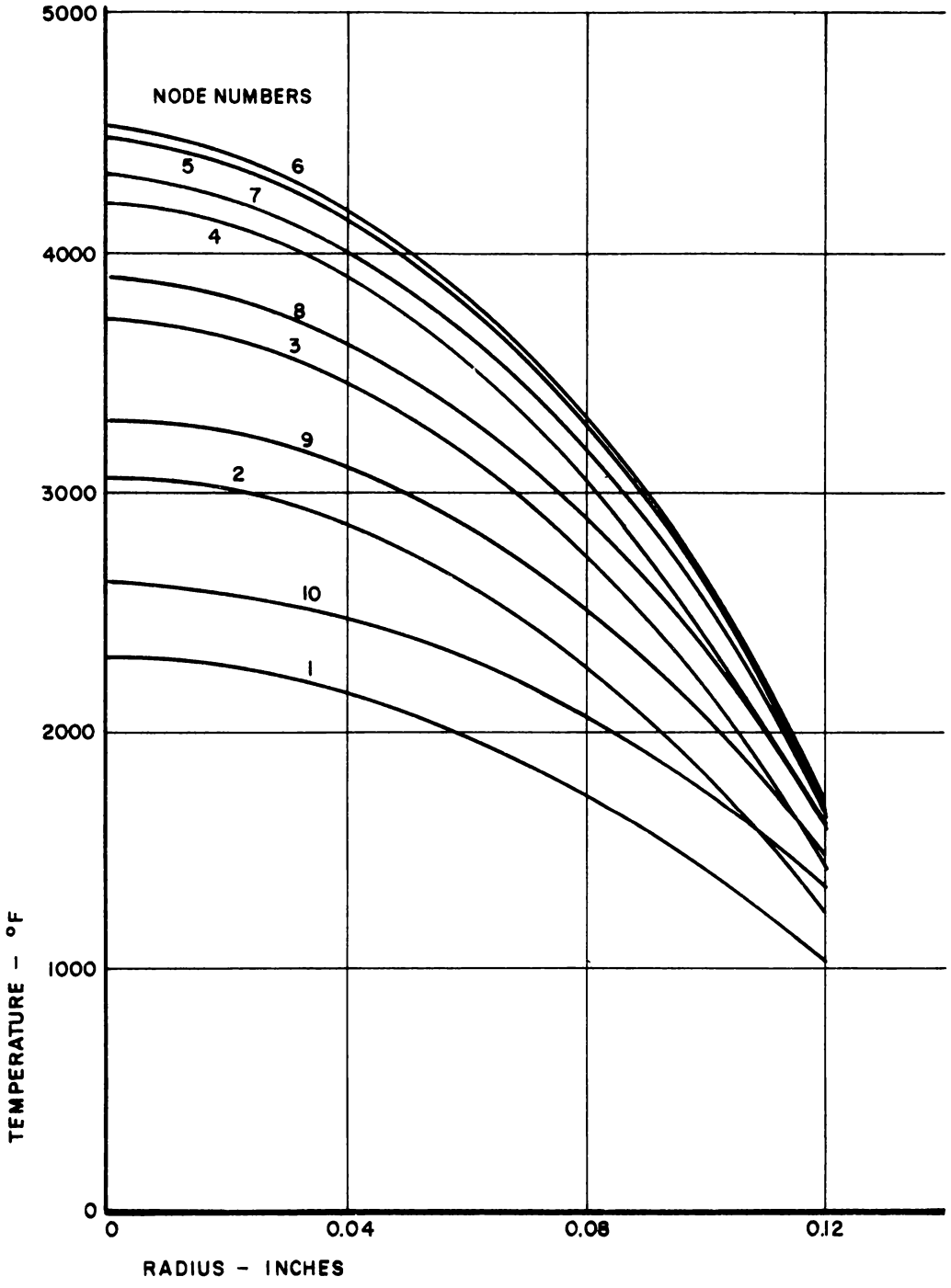

TUBE MELT TUBE NO. 1
MEAT STEADY STATE TEMPERATURES

FIGURE 10.12

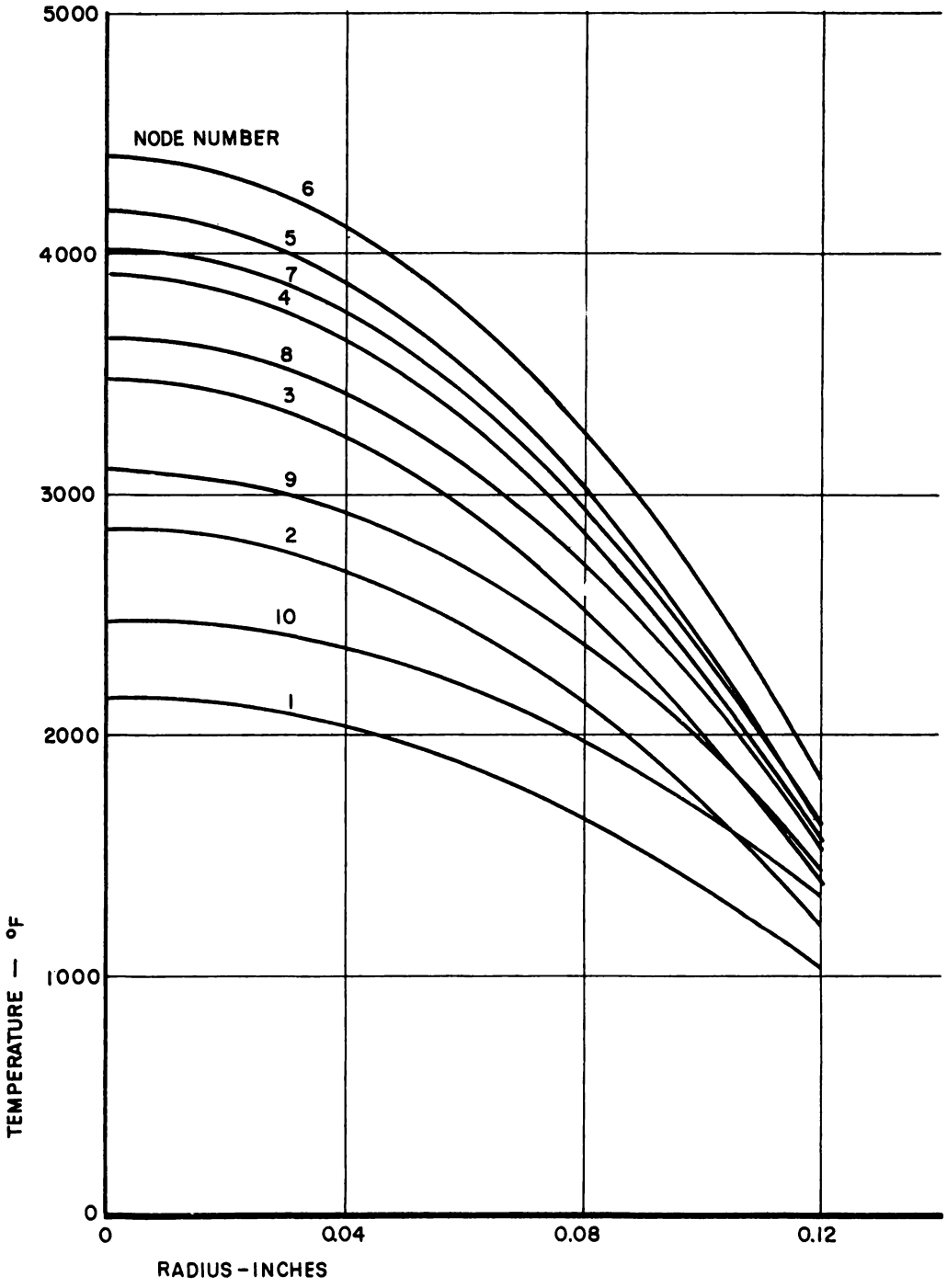

TUBE MELT TUBE NO. 2
MEAT STEADY STATE TEMPERATURES

FIGURE 10.13

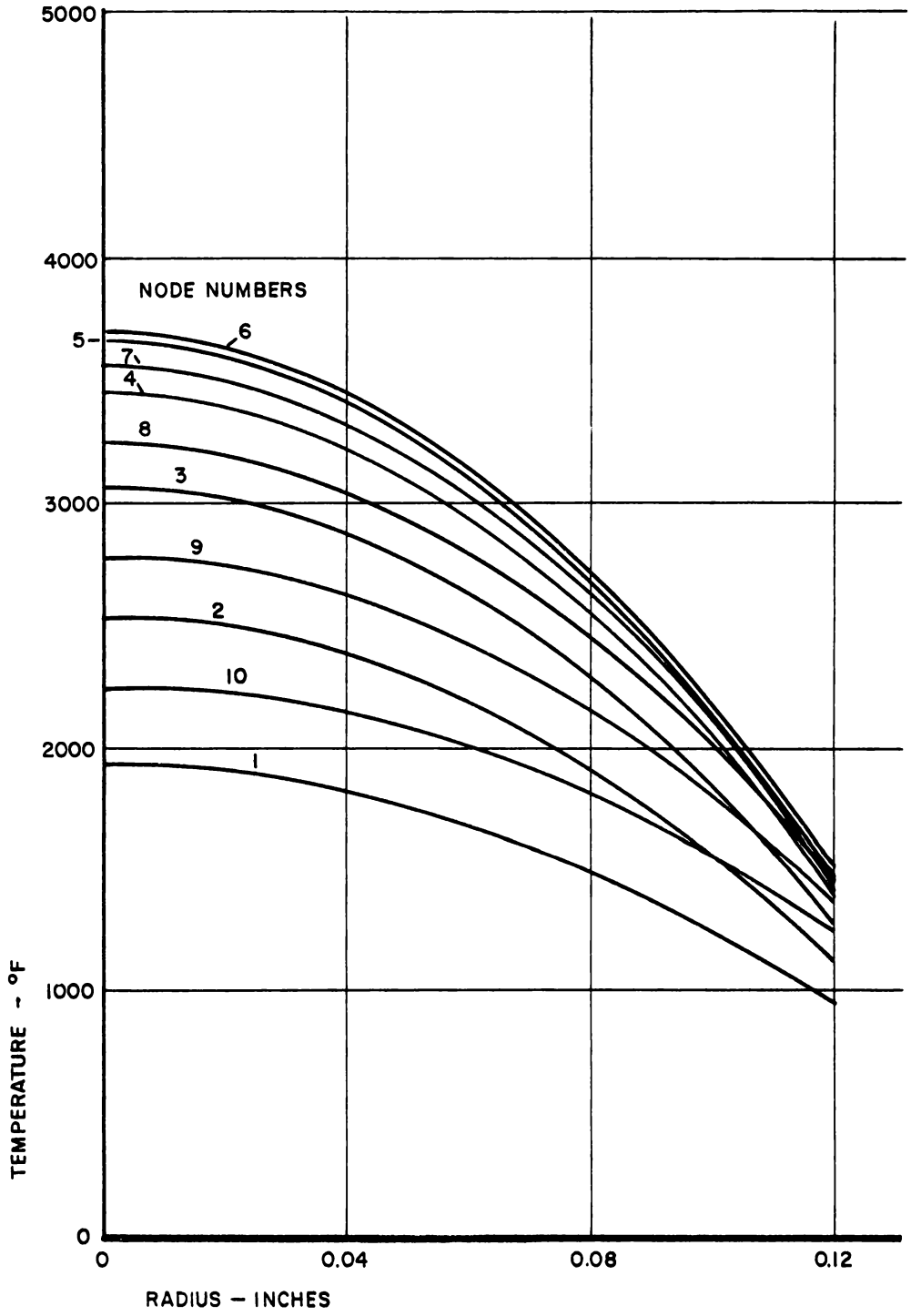

TUBE MELT TUBE NO. 3
MEAT STEADY STATE TEMPERATURES

FIGURE 10.14

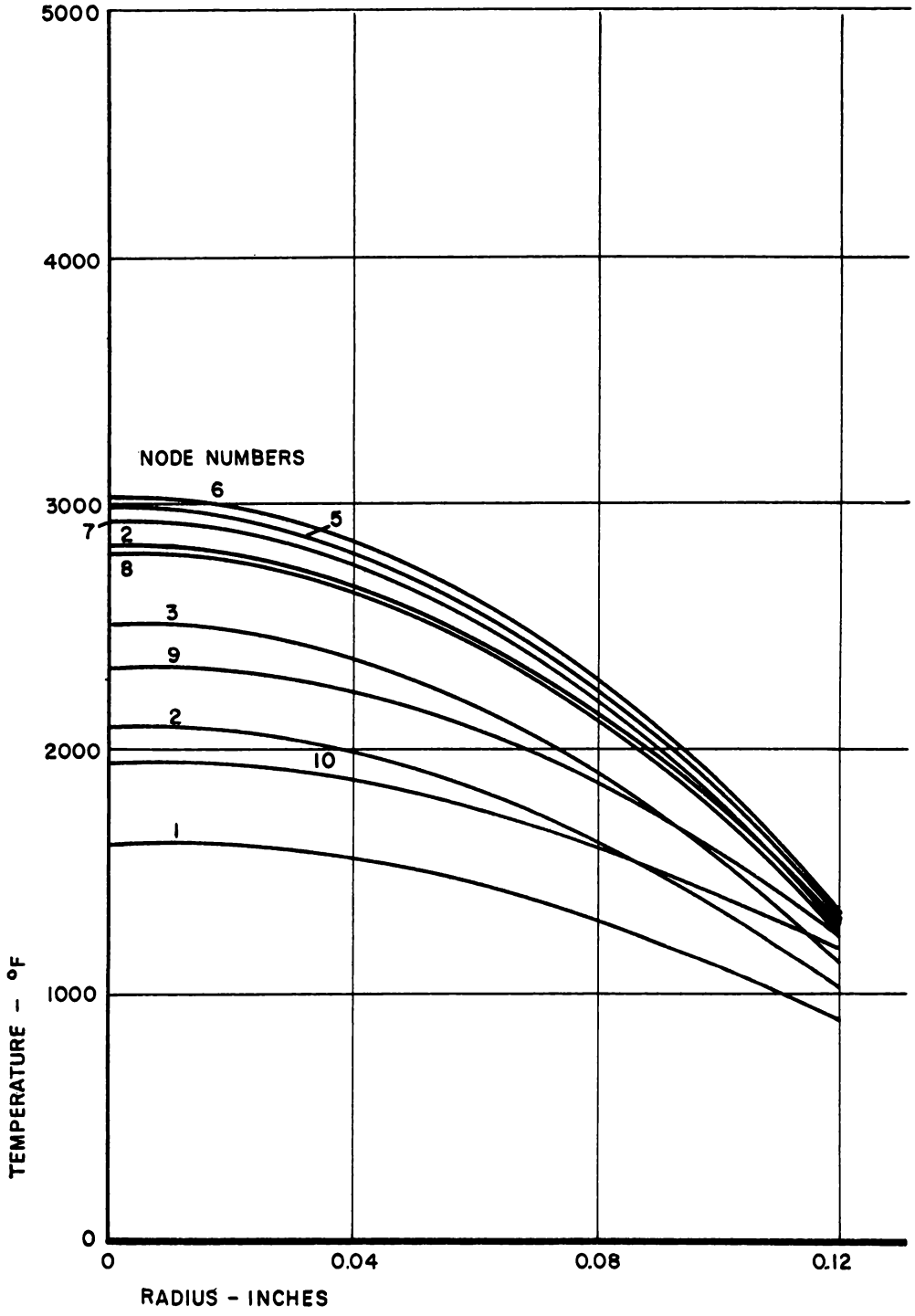

TUBE MELT TUBE NO. 4
MEAT STEADY STATE TEMPERATURES

FIGURE 10.15

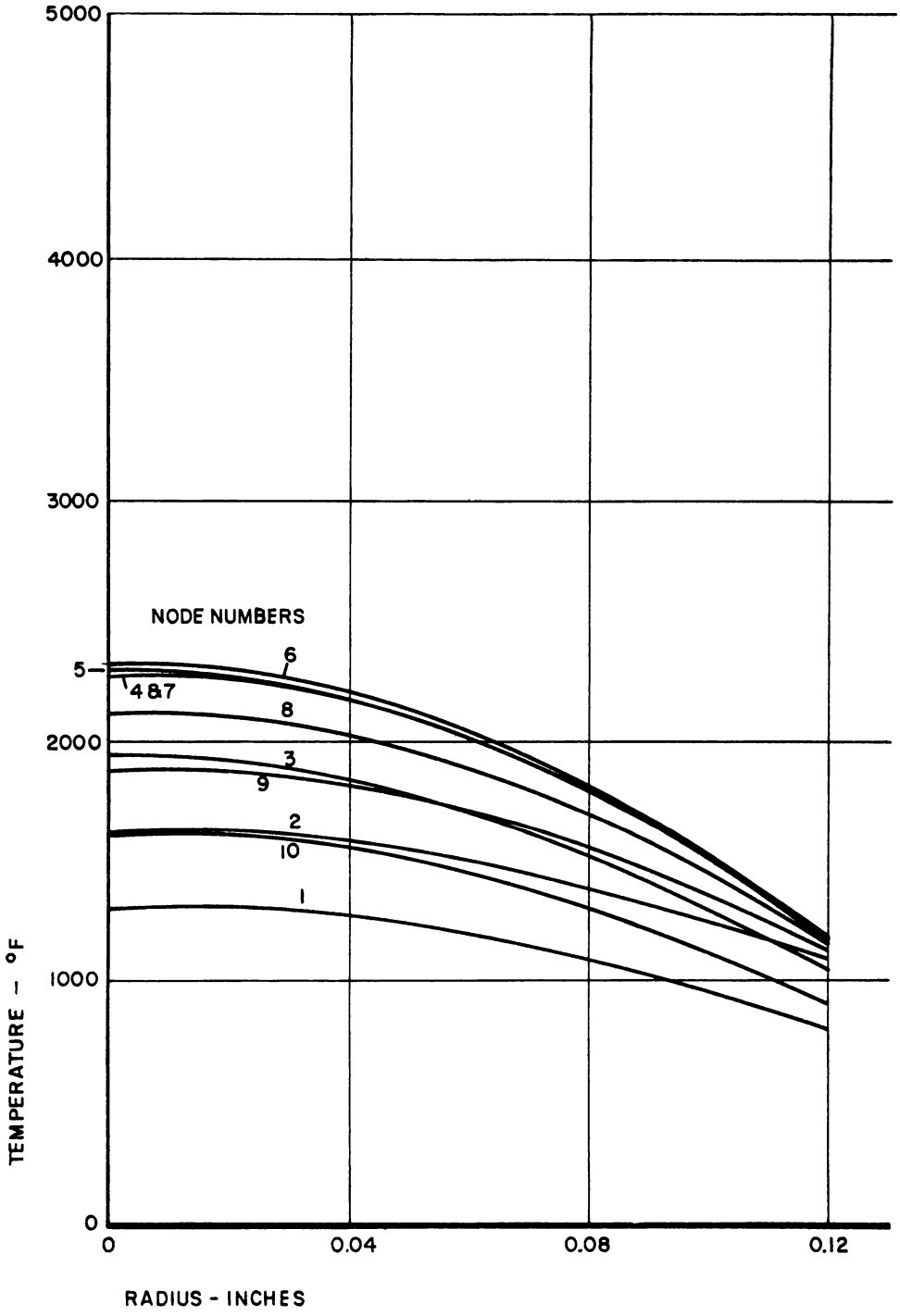

TUBE MELT TUBE NO. 5
MEAT STEADY STATE TEMPERATURES

FIGURE 10.16

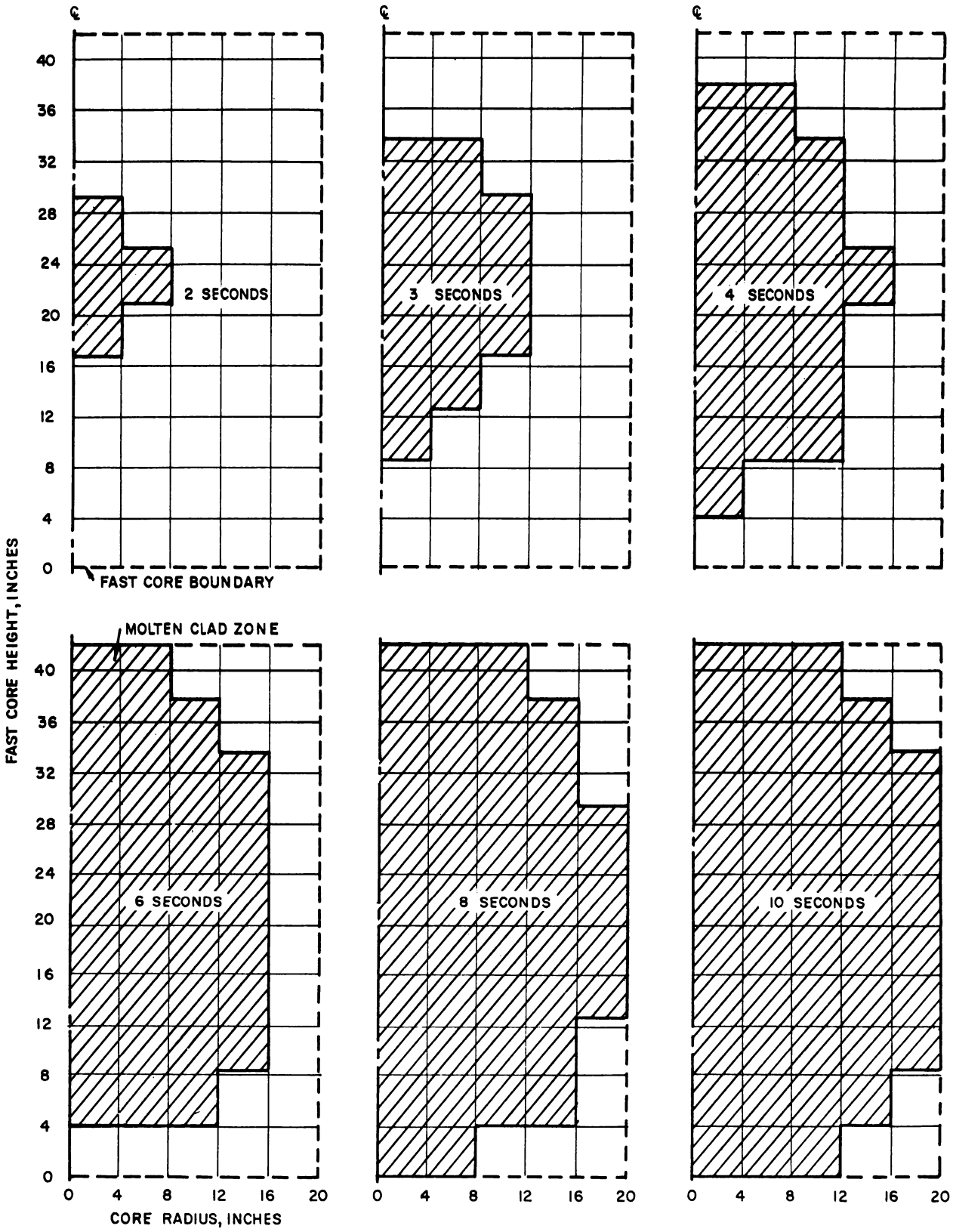

GRAPHICAL REPRESENTATION OF PROGRESSION OF CLAD MELTING IN MSSR FOR A LOSS-OF-COOLANT CASE

FIGURE 10.17

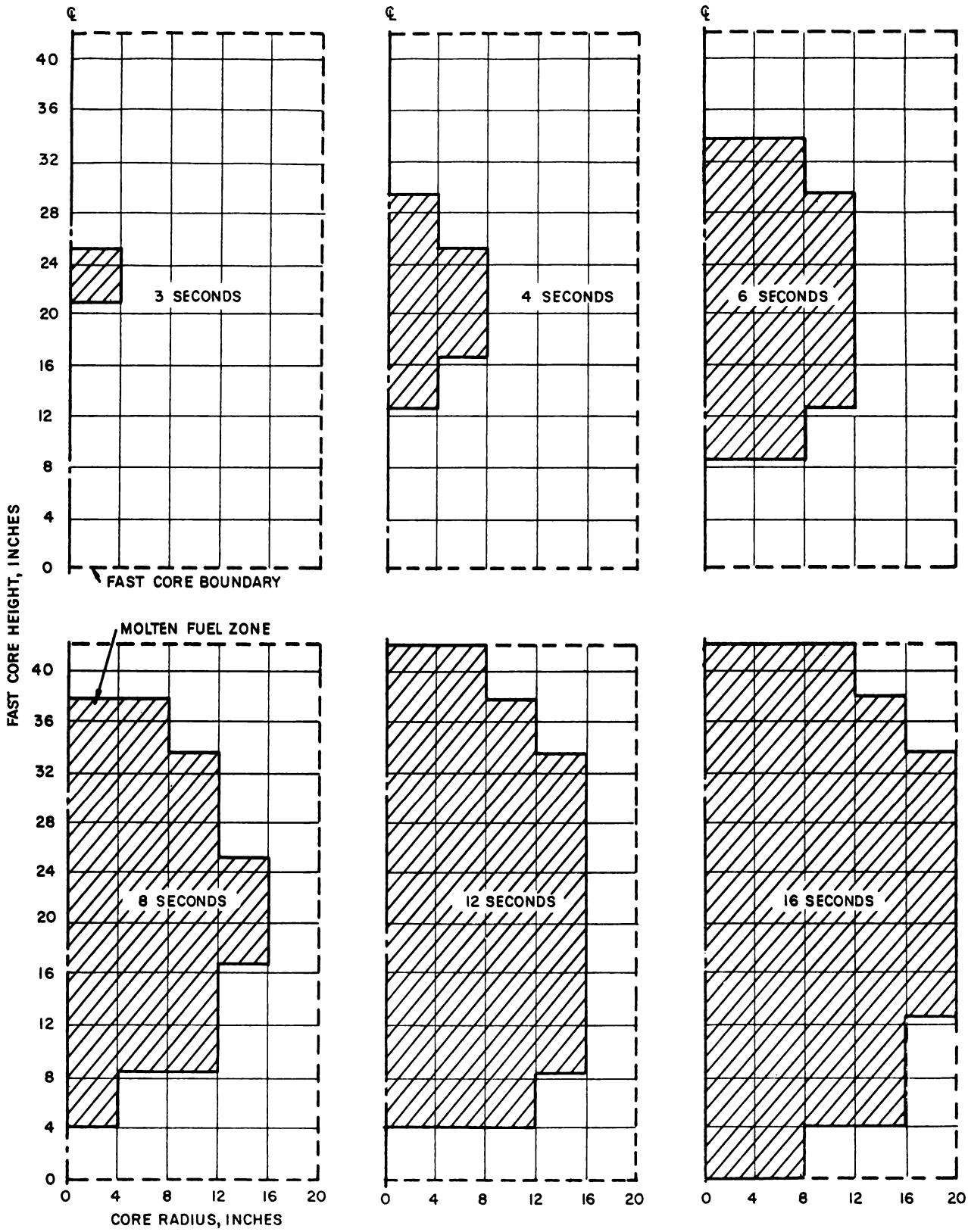

GRAPHICAL REPRESENTATION OF PROGRESSION OF FUEL MELTING IN MSSR FOR A LOSS-OF-COOLANT CASE

FIGURE 10.18

It is noted that under the assumptions of this hypothetical accident (i.e., loss of coolant without a scram at full power) the meat does not start to melt until approximately three seconds after loss of coolant. At this time, approximately 15% of the clad in the fast core has exceed its melting temperature. About 48% of the clad in the fast core has melted at six seconds. At the end of 12 seconds, 49% of the meat in the fast core has melted.

These preliminary melting time results are to be used for the determination of initial rates of material redistribution (i.e., rates of change of reactivity) and for "available time scales" for corrective action (e.g., spray cooling, control rod actuation, etc.)

10.3 In-Pile Experiments - E-SADE Loop

Design work has been initiated to study the possibility of irradiating prototype MSSR fuel elements in the E-SADE loop. A cluster of seven rods has been analyzed from the standpoint of heat transfer and fluid flow to establish the dimensions of the fuel bundle. The following criteria were used:

Steam inlet temperature	550°F
Steam outlet temperature	950°F
Maximum surface temperature	1250°F
Pressure (nominal)	1000 psia

The power produced in the element will be in the neighborhood of 65 KW. Physics calculations are now in progress to establish the required fuel enrichment.

The thermal hydraulic calculations show that the desired temperature conditions can be attained for fuel rods 0.280 inch in diameter spaced at a pitch-to-diameter ratio of 1.14. These dimensions are representative of the 300 MWe MSSR reference design reported in GEAP 3590.

10.4 MSS Reactor Physics

10.4.1 Methods Development

Further work on methods development has led to the formulation of 4-group cross-sections which give excellent agreement with the 20-group set previously used. The 4-group and 20-group calculations agree well in predicting power distribution as well as with respect to reactivity. The availability of the 4-group constants is important in that it will permit rapid and inexpensive survey calculations, and it will permit use of two-dimensional computer codes which are limited to a maximum of 4 groups.

10.4.1.1 Twenty-Group Cross Sections

The cross sections above 9 kev (i.e., the top 13 groups) recently reported by Yiftah, et al.* have been incorporated into a 20-group cross section set for MSS design calculations. Below 9 kev the self-shielded cross sections previously developed for the fast superheater of the MSS were used. A different set of cross sections below 9 kev appropriate for a boiling water reactor spectrum was used in the boiler regions.

* S. Yiftah, D. Okrent, and P.A. Moldaver, Fast Reactor Cross Sections, Pergammon Press, New York (1960).

A 300 MWe design problem was run using both the new 20-group cross sections and the 18-group cross sections used in all prior MSS work, and these results are compared in Table 10.3. The higher criticality factor for the 20-group set will result in slightly lower fuel inventories. The harder spectrum for the 20-group set will decrease the negative Doppler coefficient.

10.4.1.2 Four-Group Cross Sections

A 4-group cross section set was generated by condensation of the 20-group set for the spectrum of a small prototype MSS design. Incentives for the use of a 4-group calculation include:

1. Direct comparison of one-dimensional calculations and two-dimensional PDQ calculations is possible.
2. Analysis of results is easier, less tedious, and more illuminating with fewer groups.
3. Computer time is shorter. A 4-group calculation requires about one-third the time required for a 20-group calculation.

Agreement was first obtained between the 4- and 20-group calculations for the specific design from which the 4-group cross sections were generated. The 4- and 20-group results for this design are given in Tables 10.4 and 10.5. The power distributions for the two calculations are shown in Figure 10.19. A comparison was then made for a second design with a quite different thermal buffer (i.e., with a much higher power density than

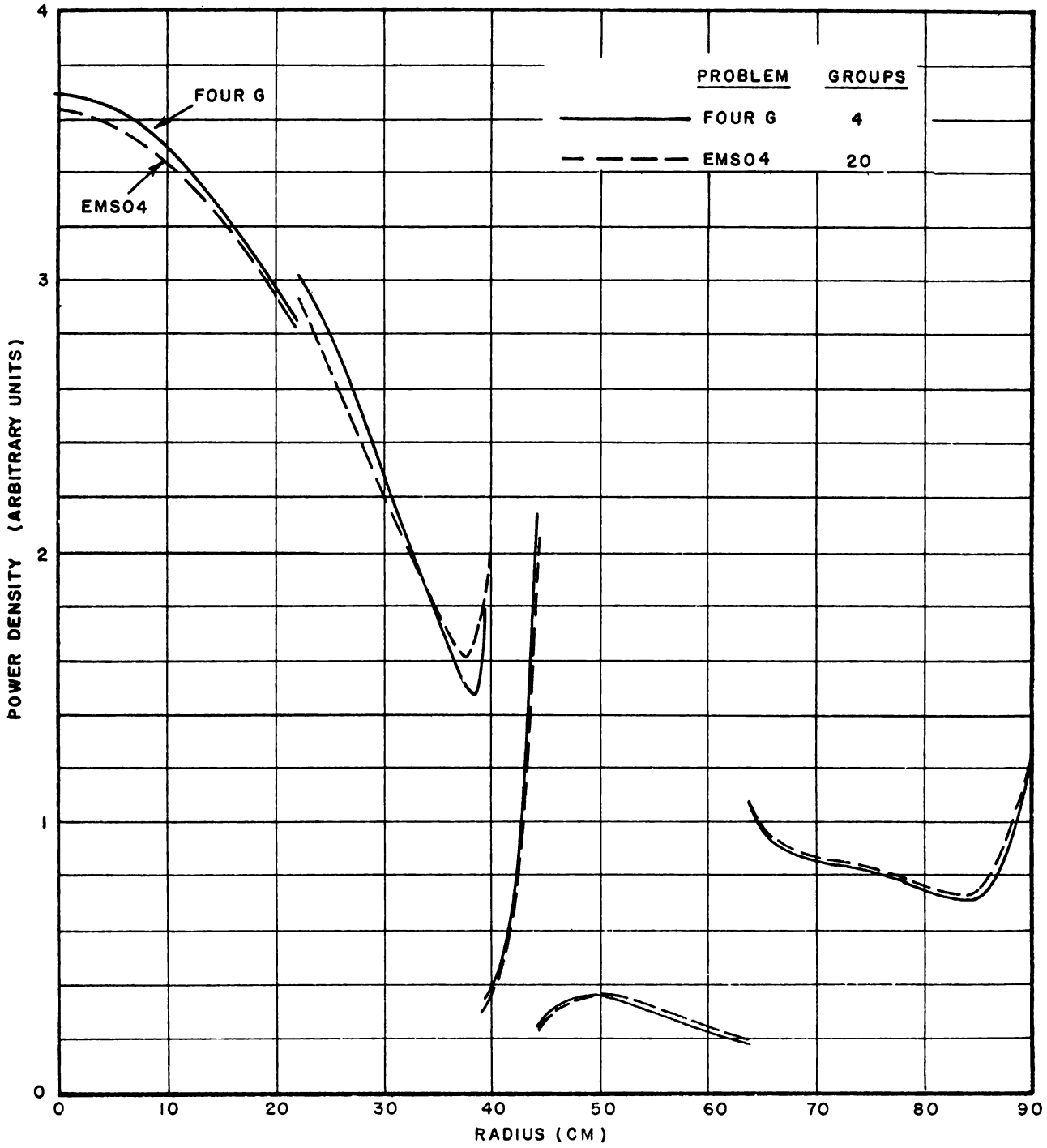

POWER DISTRIBUTIONS FOR FIRST DESIGN

FIGURE 10.19

before), still using the same cross sections generated from the first design. These results are given in Tables 10.6 and 10.7 and the power distributions are shown in Figure 10.20.

The agreement between the 4- and 20-group calculations is excellent for both designs. Four-group calculations will be used for all design and parameter studies except for an occasional check with a 20-group calculation, for final design, and for studies requiring great detail in the energy spectrum such as the calculation of Doppler and flooding coefficients. If departure from the present design is sufficiently severe as indicated by disagreement with 20-group check calculations, a new 4-group set will be generated.

TABLE 10.3

COMPARISON OF 20-GROUP AND 18-GROUP CROSS SECTION CALCULATIONS

	20-Group	18-Group
Problem Number	EMS04	B0081
Criticality Factor	1.004	0.989
Power Distribution		
Fraction Power in Superheater	0.332	0.349
Fraction Power in Boiler	0.668	0.651
Fission Spectrum in Fast Core		
Median Fission Energy	0.33 Mev	0.25 Mev
Fraction Fissions Below 9 kev	0.072	0.129

TABLE 10.4

CRITICALITY FACTOR AND POWER DISTRIBUTION, FIRST DESIGN
COMPARISON OF 4-GROUP AND 20-GROUP CALCULATION

Problem Number	4-Group FOURJ	20-Group EMSO4
Criticality Factor	1.0077	1.0038
Power Distribution (Fraction Power in Each Region)		
Superheater	0.516	0.512
Boiler	0.484	0.488
Fast Core (2nd pass)	0.196	0.195
Fast Core (1st pass)	0.276	0.276
Fast Buffer	0.044	0.041
Thermal Buffer	0.073	0.075
Blew Core	0.411	0.413

TABLE 10.5

FISSION SPECTRUM, FIRST DESIGN
COMPARISON OF 4-GROUP AND 20-GROUP CALCULATIONS

		Fraction Fissions by Group		Integrated Fission Spectrum	
Region	Group	4-Group	20-Group	4-Group	20-Group
Fast Core (2nd pass)	1	0.5272	0.5264	0.5272	0.5264
	2	0.4002	0.4012	0.9274	0.9276
	3	0.0725	0.0723	0.9999	0.0000
	4	0.0001	0.0001	1.0000	1.0000
Flow Core	1	0.0425	0.0432	0.0425	0.0432
	2	0.0066	0.0065	0.0491	0.0497
	3	0.1224	0.1225	0.1715	0.1711
	4	0.8285	0.8289	1.000	1.0000

TABLE 10.6

CRITICALITY FACTOR AND POWER DISTRIBUTION, SECOND DESIGN
COMPARISON OF 4-GROUP AND 20-GROUP CALCULATIONS

Problem Number	4-Group BUFQR	20-Group BUF20
Criticality Factor	1.0174	1.0158
Power Distribution (Fraction Power in Each Region)		
Superheater	0.545	0.538
Boiler	0.455	0.462
Fast Core (2nd pass)	0.202	0.199
Fast Core (1st pass)	0.294	0.252
Fast Buffer	0.049	0.047
Thermal Buffer	0.223	0.226
Slow Core	0.232	0.236

TABLE 10.7

FISSION SPECTRUM SECOND DESIGN
COMPARISON OF 4-GROUP AND 20-GROUP CALCULATIONS

		Fraction Fission by Group		Integrated Fission Spec.	
	Group	4-Group	20-Group	4-Group	20-Group
Fast Core (2nd pass)	1	.5257	.5238	.5257	.5238
	2	.4013	.4031	.9270	.9269
	3	.0729	.0730	.9999	.9999
	4	.0001	.0001	1	1
Fast Buffer	1	.2204	.2388	.2204	.2388
	2	.0294	.0307	.2498	.2695
	3	.0880	.0890	.3378	.3585
	4	.6622	.6415	1	1
Thermal Buffer	1	.0511	.0587	.0511	.0587
	2	.0066	.0063	.0577	.0650
	3	.1194	.1166	.1771	.1816
	4	.8229	.8184	1	1
Slow Core	1	.0433	.0446	.0433	.0446
	2	.0079	.0078	.0512	.0524
	3	.1445	.1443	.1957	.1967
	4	.8043	.8033	1	1

10.4.2 Thermal Buffer Optimization

It has long been recognized that the thermal buffers of the 300 MWe reference design (GEAP-3590) and the early prototype MSS design (GEAP-3785) were far from optimum designs. The thermal buffer in each of these designs had several shortcomings; in particular, the power density was too low and the conversion ratio was too high.

In the present design of the prototype MSS, three changes were made in the thermal buffer to overcome these deficiencies.

1. The U-235 enrichment was increased from that of depleted uranium to 1.2% in order to increase the power density.
2. The water-to-fuel volume ratio was increased from 1.2 to 2.4 for two reasons. An increase in coolant volume fraction was necessary to remove the extra heat resulting from the increased

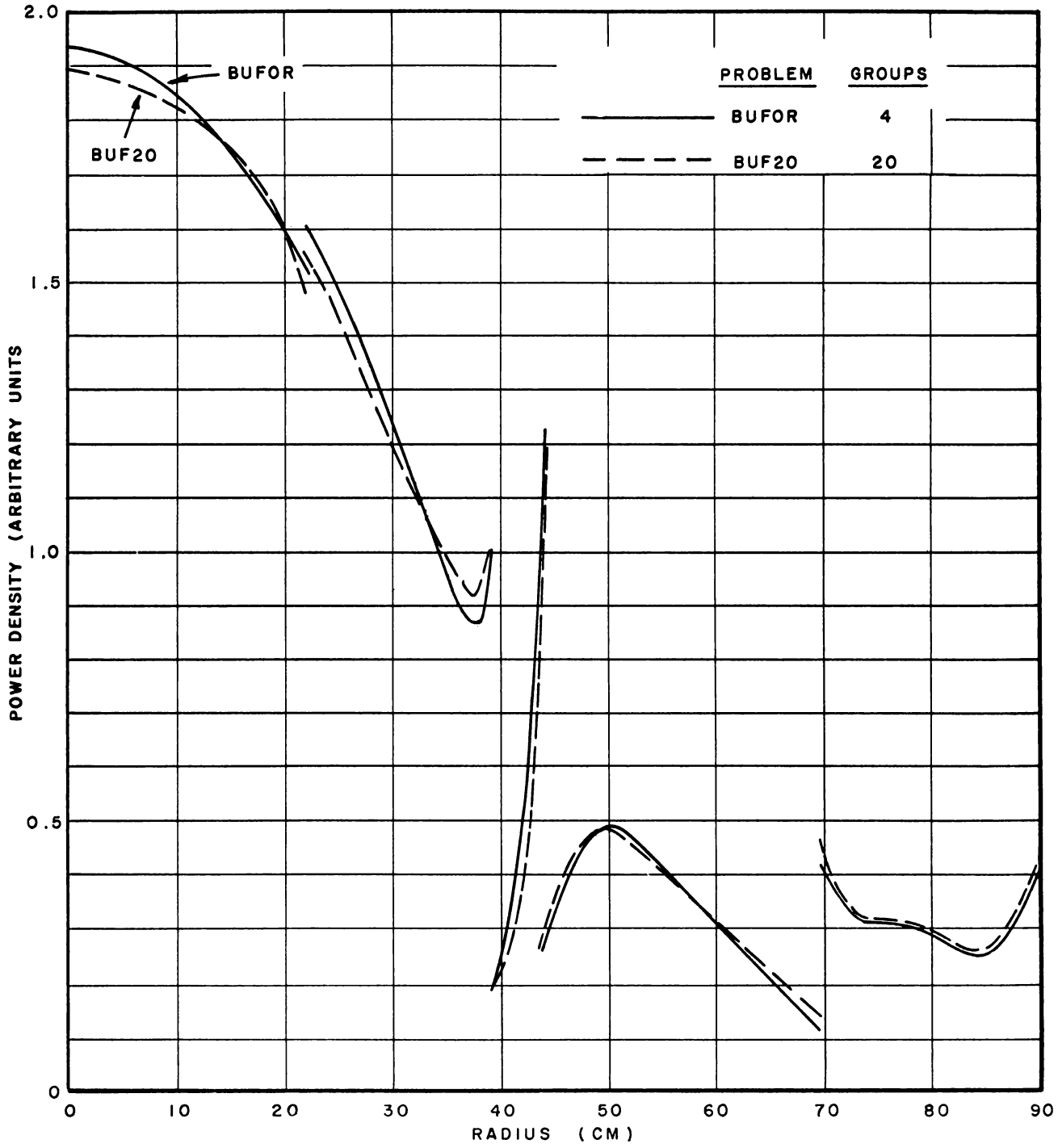

POWER DISTRIBUTIONS FOR SECOND DESIGN

FIGURE 10.20

power density. The increased moderating power caused a reduction in the conversion ratio to about unity so that the power would not increase with burnup.

3. The high power density in the 7.7 in. thermal buffer would cause a power spike at the inner edge of the slow core. To prevent this spike, the thickness of the thermal buffer was increased to 10 in. and the inner 1.5 in. of the slow core was highly poisoned.

The effects of these modifications are summarized in Table 10.8 in which the earlier and modified designs are compared. It is noted that the desired power density and conversion ratio in the thermal buffer were achieved. From Figure 10.20 it can be seen that the power spike at the inner edge of the slow core was reduced to the peak power in the thermal buffer.

	Earlier Design	Modified Design
U^{235} enrichment in thermal buffer	0.3%	1.2%
Water to fuel ratio in thermal buffer	1.2	2.4
Fuel volume fraction in thermal buffer	.4	.25
Width of thermal buffer	7.7 in	10 in
Pu enrichment in superheater	12.6%	12.1%
Criticality factor	1.008	0.999
Fraction power in superheater	.32	.37
Fraction power in thermal buffer	.09	.29
$\frac{\text{Avg. power density in thermal buffer}}{\text{Avg. power density in slow core}}$	.29	.97
$\frac{Pu^{239} \text{ production rate in thermal buffer}}{U^{235} \text{ absorption rate in thermal buffer}}$	3.68	1.07

10.4.3 500 MWe MSS Burnup Studies

Preliminary fuel cycle calculations were made for a 500 MWe MSS. Calculations were made for both plutonium and U-235 fueled cores, and for burnup of 50,000 and 100,000 MWD/T. Results are presented in Tables 10.9 and 10.12. There is considerable uncertainty in the results shown for the fast and thermal buffers since the burnup calculations considered them as single homogenized regions and kept the spectrum constant for the full burnup cycle. Actually there will be considerable spatial and time variations in these regions. A new computer program is now in the check out stage which will permit burnup calculations which account for both spectral and spatial changes during the fuel cycle. It is hoped to have results for the next quarterly report.

TABLE 10.9

FAST CORE BURNUP, 500 MWe MSS

INITIAL FUEL	DISCHARGE EXPOSURE MWD/T	ISOTOPE	ENRICHMENT (%) INITIAL	DISCHARGE
Uranium-235	50,000	U-235	18.83	12.58
		Pu-239	0	2.44
		Pu-240	0	0.10
		Pu-241	0	0
Uranium-235	100,000	U-235	20.39	8.78
		Pu-239	0	4.04
		Pu-240	0	0.34
		Pu-241	0	0.02
Plutonium	50,000	Pu-239	12.20	10.44
		Pu-240	5.80	5.93
		Pu-241	0	0.81
Plutonium	100,000	Pu-239	12.68	9.16
		Pu-240	5.74	5.90
		Pu-241	0	1.63

TABLE 10.10

FAST REFLECTOR BURNUP, 500 MWe MSS

Fast Core Burnup (MWD/T)	ENRICHMENT (%) 0	50,000	100,000
U-235	0.30	0.26	0.23
Pu-239	0	0.82	1.63

TABLE 10.11

FAST BUFFER BURNUP, 500 MWe MSS

Burnup	ENRICHMENT (%) 0	50,000	100,000
U-235	5.00	1.44	0.41
Pu-239	0	1.51	1.49
Pu-240	0	0.73	1.17
Pu-241	0	0.16	0.35

TABLE 10.12

THERMAL BUFFER BURNUP, 500 MWe MSS

Burnup	ENRICHMENT (%) 0	15,000	30,000
U-235	1.20	0.23	0.04
Pu-239	0	0.97	1.16

10.5 65 MWt Prototype

The mechanical design and physics work reported in the last quarterly report were completed. An investigation was made as to the suitability of the VESR facility for housing the prototype. It was concluded that the VESR facility could be utilized and successful operation of the prototype would permit confident extrapolation to large size reactors. The work is described in a topical report which is appended here.

A PRELIMINARY STUDY OF A 65MWt MIXED SPECTRUM SUPERHEATER PROTOTYPE WHICH UTILIZES THE VESR FACILITY

I. SUMMARY AND CONCLUSIONS

A study was made to determine if the VESR facility would be suitable for testing a prototype of the Mixed Spectrum Superheater. A reactor is described which fits the VESR vessel and facility. This prototype differs considerably in specific detail from the large 300 MWe reference design. However, the basic features of the concept are present, and successful operation of the prototype would permit confident extrapolation to large size reactors.

The mechanical design presented has been discussed with the VESR Design Group, and no major incompatibilities with the VESR facility were discovered. However, there are potential trouble spots, in particular, the control element requirements, and the need for further detailed design work is clearly indicated.

Table I is a summary of the major characteristics of the 65 MWt prototype and the 300 MWe reference design.

Table II outlines the information to be obtained from the prototype, and some of the difficulties.

II. INTRODUCTION

As part of the continuing program to develop the Mixed Spectrum Superheater as an economical power producer, it is desirable to build a prototype as a developmental tool. One possibility is to utilize the VESR facility when the VESR development program has been completed. An alternative is, of course, to design a new facility specifically as a test of the MSS concept.

The work discussed in this report is concerned only with the first alternative. It presents the results of the brief study undertaken to determine the feasibility of fitting the EMSS into the VESR facility. The conceptual design presented here has not been optimized. It is intended only to establish the approximate power levels and to serve as the framework for identifying the problems that may arise if the project should be undertaken.

It should be noted that the present study is not complete in itself and should be considered to be one part of a more general study on the prototype design of the Mixed Spectrum Superheater. Parametric studies to establish a conceptual design not restricted to a pressure vessel the size and shape of VESR are being carried out. The results of that work will be reported in the near future. A more detailed explanation of the criteria for the prototype as well as physics and some preliminary safeguard studies will also be discussed at that time.

III. GROUND RULES

This study is aimed at the design of a Mixed Spectrum prototype reactor which simulates as closely as possible the important characteristics of a large power producing MSSR. To this end the following requirements were placed on the design:

A. Approximately 25% of the total reactor power is to be generated in the fast core.

B. The neutron spectrum, Doppler effect, flooding effect, neutron lifetime, and coupling between thermal and fast cores should be representative of a large power reactor. Preliminary work indicated that this would require a fast core section of approximately 30" or greater. For this study, therefore, the fast core dimensions were set at 30" cube.

TABLE I

Design Parameters for Prototype and Reference Designs

Parameter	65 MWt Prototype				300 MWe Reference Design	
	Fast Core 1st pass	Fast Core 2nd pass	Slow Buffer	Boiler	Fast Core	Boiler
Fuel rod O.D., inches	0.685	0.685	-	-	0.280	0.444
Clad thickness, inches	0.040	0.040	-	-	0.020	0.026
Pitch-to-diameter ratio	1.04	1.10	-	-	1.14	-
Max. surf. temp., ^{o}F	1050	1220	-	-	1250	628
Max. fuel temp., ^{o}F	4300	4000	-	4500	4500	4500
Max. heat flux, Btu/hrft^2	210,000	210,000	-	-	610,000	362,000
Avg. heat flux, Btu/hrft^2	96,000	96,000	-	-	224,000	99,000
Pressure, psia	1,000	1,000	1,000	1,000	1,500	1,500
Coolant exit temp., ^{o}F	790	950	545	545	950	600
Thermal power, MW	12.6	7.4	-	45	245	570
Coolant mass flow, lbs/hr	241,000	241,000	-	2.41×10^6	2.8×10^6	30×10^6
Max. velocity, ft/sec	115	135	-	8	183	10
Power density, Kw/liter	41.6	62.8	18.3	18.8	217	35.7
Peak/Avg. power ratios:						
Radial	1.63	1.12	1.44	1.37	1.5	1.2
Axial	1.3	1.3	1.5	1.5	1.3	1.5
Other	1.34	1.34	2.03	2.03	1.34	2.03
Overall	2.84	1.95	4.38	4.17	2.62	3.65

(Continuation of) TABLE I

Design Parameters for Prototype and Reference Designs

Parameter	65 MWt Prototype				300 MWe Reference Design	
	Fast Core 1st pass	Fast Core 2nd pass	Slow Buffer	Boiler	Fast Core	Boiler
Volume, liters	328.4	117.9	1168	1254	1127	15,940
Volume fractions:						
Fuel	0.585	0.563	0.250	0.267	0.455	0.267
Steam	0.164	0.248	0.120	0.113	0.237	0.113
Water	-	-	0.480	0.527	-	0.527
Steel or Zr	0.251	0.189	0.150	0.093	0.308	0.093
Vol.coolant/Vol.fuel	-	-	2.4	2.4	-	2.4
Fuel enrichment, %						
U-235 loading	17.0	17.0	1.20	3.64	-	2.3
Pu-239 loading	-	-	-	-	13.0	-
Fuel loading, Kg						
U-235	217	103	32	112	-	905
Pu-239	-	-	-	-	832	-
Neutron lifetime, μsec	8.0				2.4	
% fissions below 10 Kev	10.0				24.0	
Eu content for zero flooding effect, % by volume	0.6				0.2	

TABLE II

Phenomenon	Comment
Startup and Shutdown	During startup and shutdown, fast core will operate at as low a level as possible, while power is generated in periphery of boiling core. Requirements are more difficult to meet in protoype because of small size of boiling core. Design must insure that fast core will not overheat. Problem requires analysis for prototype. Successful demonstration in prototype would prove feasibility for large reactor.
Control	Ability to control power split and power shape would be demonstrated in prototype. It will be more difficult to achieve good power shapes in boiling section of prototype due to its small size. Extrapolation to large reactor would require analytical work to take into account differences in relative size of boiling and superheating sections. (Note: mechanical problems of supplying necessary control elements are discussed in body of report).
Emergency Cooling	Two pass-flow arrangement of prototype calls for more complex valving and flow sequencing. Single-pass reference design permits simpler cooling arrangement. Unknown factor for each is effectiveness of spray cooling for closely spaced rods. Large reference design has larger pitch-to-diameter ratio, so prototype will provide more severe test.
Flooding and Unflooding	The principle of utilizing epithermal poisons to control flooding effect can be demonstrated in prototype. Smaller prototype core will require higher concentration of epithermal poison than larger reference design.
Reactor Dynamics	Operation of the prototype will provide basic test and will permit check of analytical methods. Extrapolation to large size involves some problems as extrapolation of results from small BWR to large BWR.
Water Carryover Steam Carryover Erosion and Corrosion Radioactivity Carryover Operating Malfunctions Fuel Cycle Management Operating Experience Unexpected Problems	Useful and meaningful information will be obtained in these areas since important relevant conditions in prototype are the same as in large reference design.
Mechanical Design	Major features of large MSS can be checked in prototype although two-pass configuration complicates the situation.

TABLE II (Contd.)

Phenomenon	Comment
Fuel Technology	Fuel surface conditions and internal meat temperatures duplicate conditions in large reactor. Specific power is lower and larger-radius rods are used. Almost all important questions can be answered. In first core, it is presently planned to utilize U-235 O_2 - U-238 O_2. Later cores or individual elements can be tested with Pu-239 O_2 - U-238 O_2.

C. The thermal hydraulic conditions are:

1. Maximum fuel center temperature, 4500°F

2. Maximum fuel surface temperature, 1250°F

3. Superheater steam outlet temperature, 950°F

4. Coolant pressure, 1000 psia.

IV. THERMAL HYDRAULICS

The reference MSS design (GEAP-3590) has the steam from the boiler section pass down through the superheater section and out through the vessel bottom. The VESR vessel and piping do not appear suited for this arrangement so that a two-pass superheater core was considered. The superheated steam leaves the vessel through a port in the top head of the VESR; the port is part of the original VESR design. (The use of two-pass flow in the superheater is also advantageous from the point of view of reducing the power requirements of the prototype while satisfying the thermal-hydraulics requirements. See Figure 1 and the 9th Quarterly Report of Superheat Project.)

The results of the thermal-hydraulic calculations are shown in Figure 2. These curves show the variation in the maximum surface temperatures in the first and second passes as a function of the ratio of bulk coolant temperature rise in the first pass to bulk coolant temperature rise in the second. For these curves, it is assumed that the power density is uniform over the fast core. The ratio of bulk coolant rise is varied by changing the relative volumes of the two passes. the pitch-to-diameter ratios in Figure 2 are 1.04 and 1.10 for the first and second passes, respectively. In order to meet surface temperature limitations, it is desirable to have as small a pitch-to-diameter ratio as possible before the effects of peripheral heat transfer variations become dominant. The value of 1.10 was chosen for the second pass since it is representative of the reference design (P/d = 1.13); the value of 1.04 was chosen in an attempt to minimize power requirements.

From Figure 2, it can be seen that with 20 MWt in the superheater section and a ratio of first-to-second pass bulk coolant temperature rises of 1.6, the maximum surface temperature in the second pass is 1220°F. This is close to the 1250°F limit of the reference design. The corresponding maximum surface temperature of the first pass is 1050°F. Thus, there is margin in the event that peripheral temperature variations in the first pass are more than expected. (There are meager experimental data in this region of small pitch-to-diameter ratios.) One could use this margin to increase the pitch-to-diameter ratio of the first pass. This will result in a higher first-pass surface temperature and an increased film drop which is desirable since temperatures become sensitive to slight flow variations. There is room for further work optimizing the thermal hydraulics and a need for experimental data at low pitch-to-diameter ratios. However, it is believed that a power level of 20 MWt, a pitch-to-diameter ratio of 1.10 in the second pass, and 1.04 in the first pass, and a ratio of coolant temperature rises of first to second pass of 1.6 lead to a core which can accommodate further maneuvering.

The remaining parameters defining the prototype design are listed in Table I.

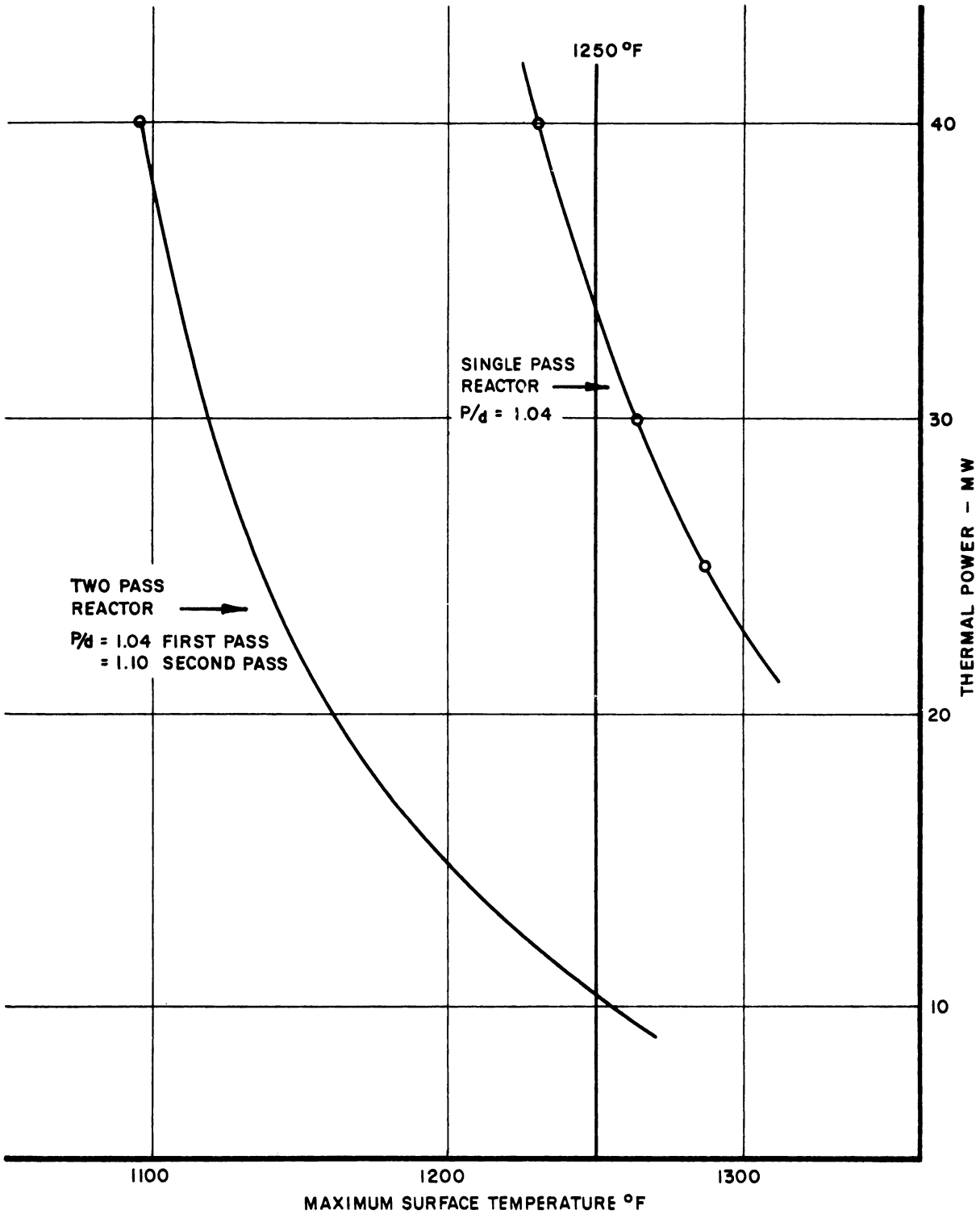

POWER VS SURFACE TEMPERATURE MIXED SPECTRUM FAST CORE
4500° CENTER TEMPERATURE

FIGURE 10.21

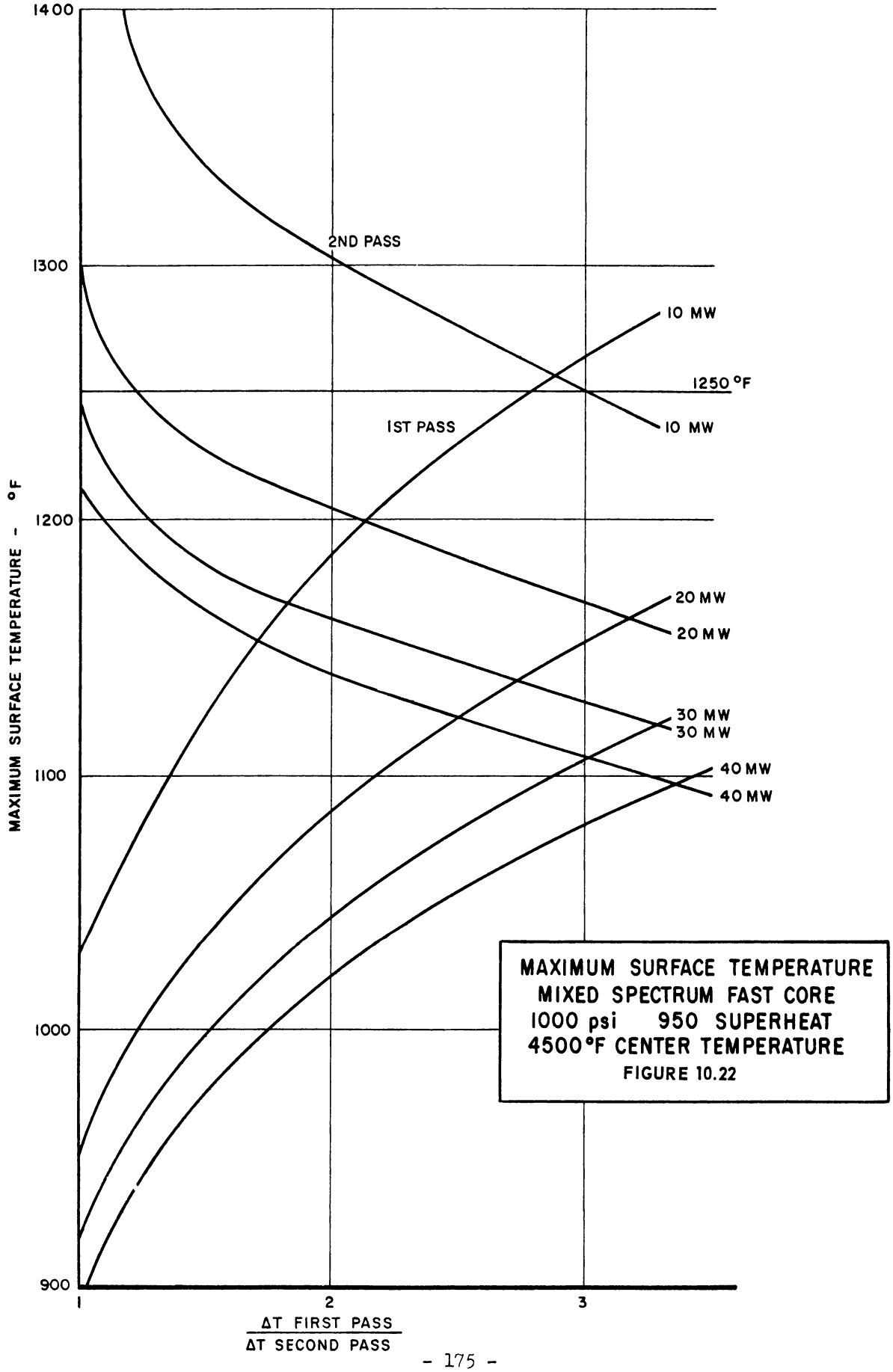

MAXIMUM SURFACE TEMPERATURE
MIXED SPECTRUM FAST CORE
1000 psi 950 SUPERHEAT
4500°F CENTER TEMPERATURE
FIGURE 10.22

V. MECHANICAL DESIGN

A. General

A conceptual design of the EMSS combines a two-pass fast-spectrum superheating section with a thermal boiler resulting in a three-pass system. The core of this reactor consists of five annular regions which, in going from outside to inside, are: Thermal boiler, thermal buffer, fast buffer, fast superheater first pass, and fast superheater second pass. The coolant flow is upward through the thermal boiler and thermal buffer. The steam-water mixture formed in the boiler is separated at the surface of the mixture. The separated water passes down outside the boiling core shroud and is recirculated through the boiling core. The steam passes upward through the steam dryer and down through the outer region of the offset duct from which it enters the first pass of the superheater. The steam, which at this point has about 250°F superheat, passes through the turning section below the core, up through the second pass of the superheater, through the center region of the offset duct and out of the vessel through the venturi in the vessel top cap.

Control for the fast core is provided by three 1/2 element fuel bundles in the first pass, which can be lowered below the fast core. Poison blades for control of the boiling core and isolation of the fast core from the boiling core are driven from below through nozzles in the vessel bottom head.

B. Core Force Analysis and Support

A preliminary force analysis was made for the core area to determine the magnitude of forces which must be supported at the various regions. This was accomplished by assuming a 10 psi pressure drop in the boiling core and calculating pressure drops in the steam separator, saturated steam downcomer, fast core first and second passes, and the superheated steam riser. This information is shown in the following table and the estimated component weights and net forces are shown in Figures 3 and 4. The support method, as described below, is shown in Figure 5 (Drawing 212E418).

Table III

Pressure Drops Used in Force Analysis

Region	Pressure Drop (psi)
Thermal Core	10 (assumed)
Steam Separator	3
Steam Downcomer	3
Fast Core First Pass	22
Fast Core Second Pass	15
Superheated Steam Riser	2
Total from Thermal Core Inlet to Reactor Outlet	55

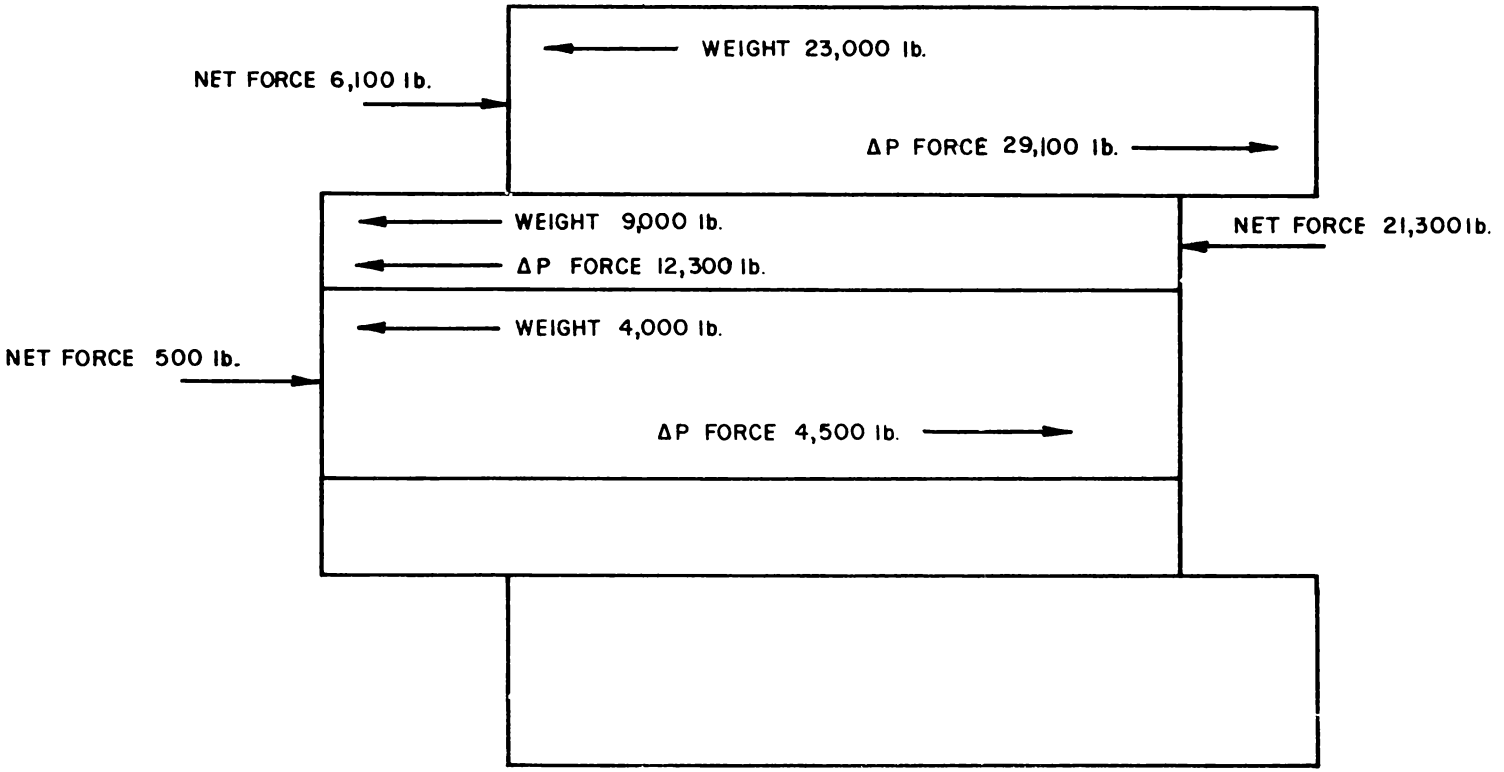

65 MWt EMSS CORE FORCES

FIGURE 10.23

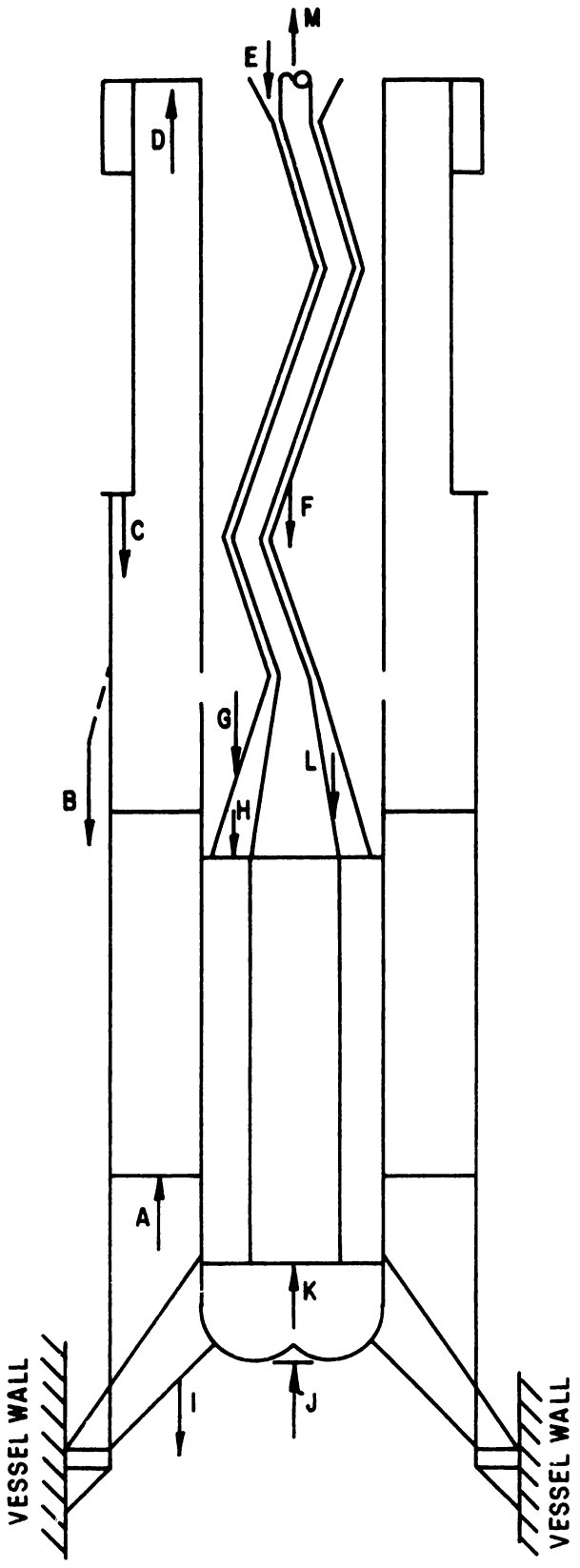

THERMAL CORE SUPPORT
NET FORCE 2,000 lb. UPWARD

FAST CORE SUPPORT
NET FORCE 3,500 lb. DOWNWARD

LOCATION	DESCRIPTION	FORCE LBS.
A	THERMAL CORE NET FORCE	6,100
B	THERMAL CORE SUPPORT & OUTER SHROUD WT.	6,500
C	STEAM SEPARATOR WEIGHT	6,000
D	STEAM SEPARATOR ΔP FORCE	8,400
E	STEAM DOWNCOMER ΔP FORCE	200
F	OFFSET DUCT WT.	3,700
G	DOWNCOMER TRANSITION ΔP FORCE	4,000
H	FAST CORE 1ST PASS NET FORCE	21,300
I	FAST CORE SUPPORT WT.	2,000
J	FAST CORE TURNING SECTION P FORCE	32,000
K	FAST CORE 2ND PASS NET FORCE	500
L	STEAM RISER TRANSITION ΔP FORCE	5,000
M	STEAM RISER ΔP FORCE	200

EMSS CORE FORCES

FIGURE 10.24

GENERAL ELECTRIC 212E418

CORE ARRANGEMENT
FOR THE NUCLEAR SUPERHEAT PROJECT
F.C.F. ON 212E413

FIGURE 25

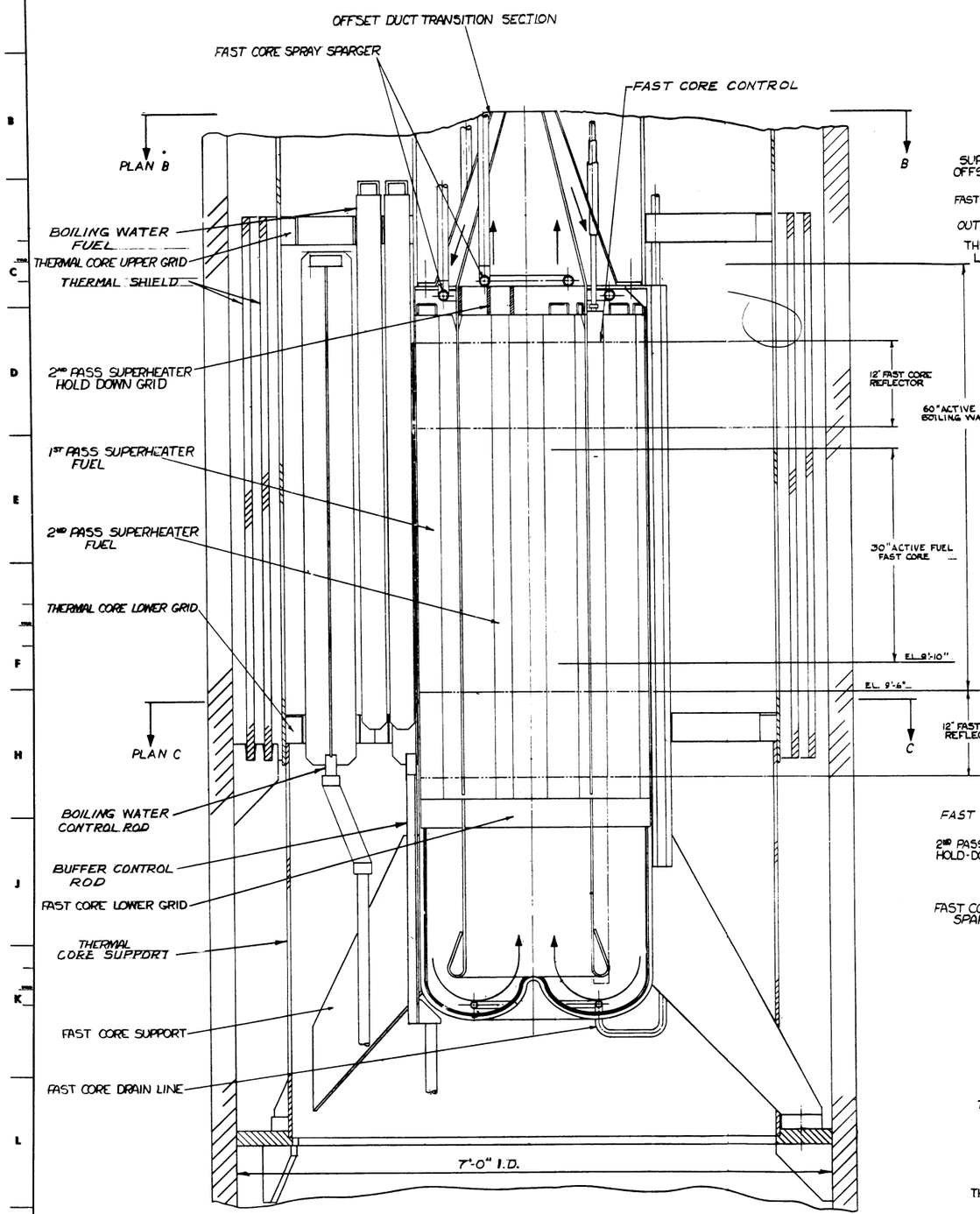

ELEV. A-A

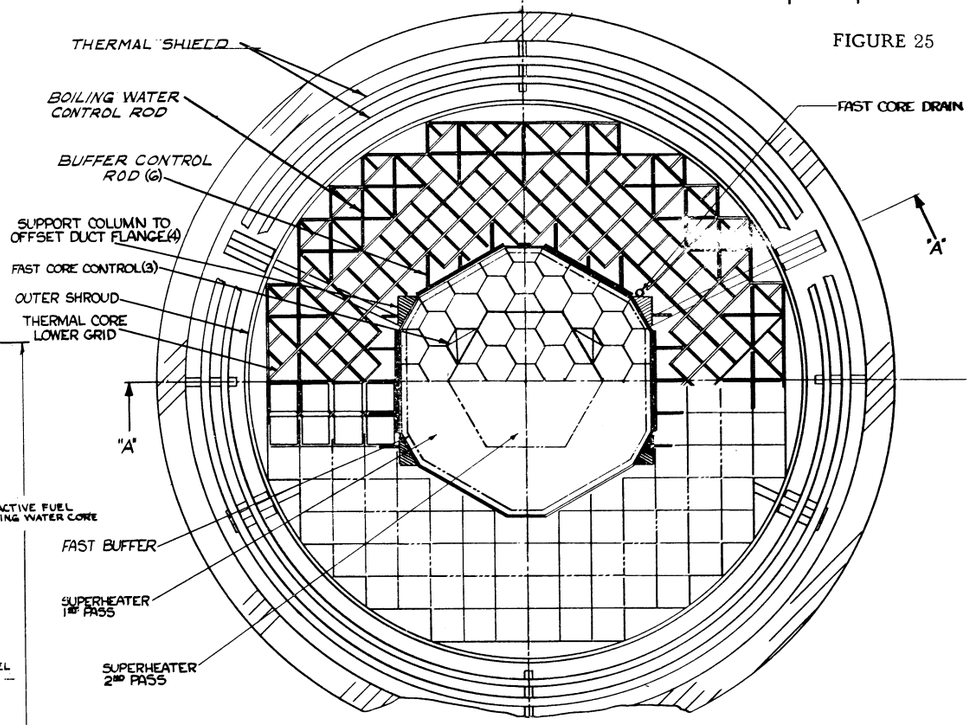

PLAN C-C

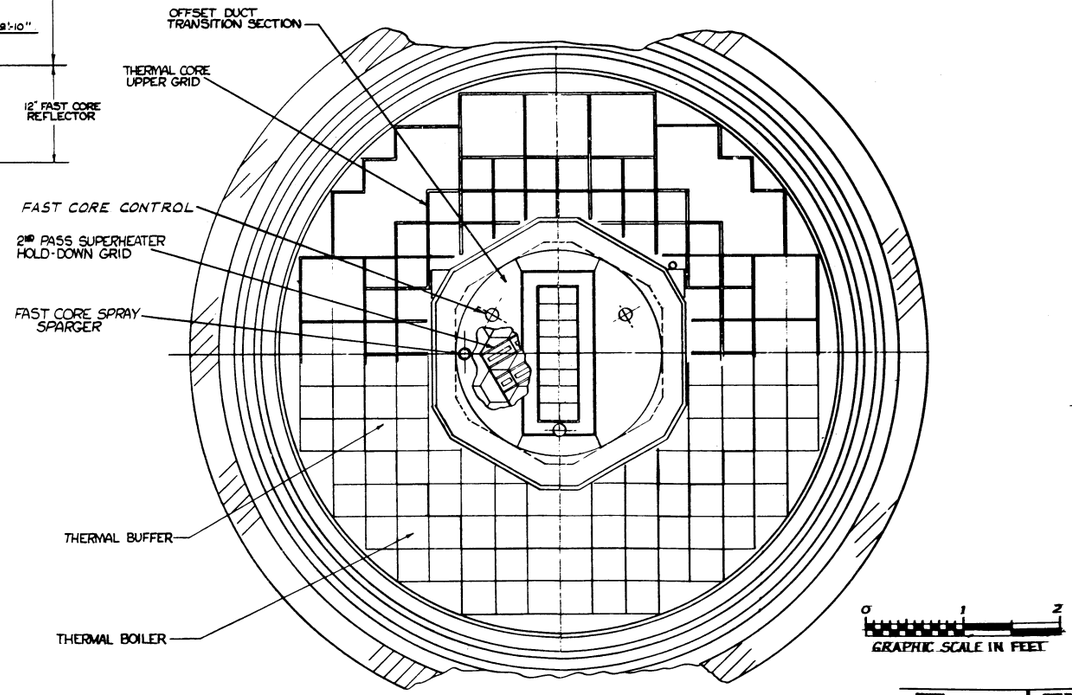

PLAN B-B

The thermal core fuel is supported by the lower grid which is attached to the outer shroud. This outer shroud and the fast core support plates are bolted to a support ledge welded to the vessel wall. Based on a boiling core pressure drop of 10 psi while the reactor is operating, there will be a net upward force of about 3 tons which is retained by a spring loaded hold-down device attached to the upper grid which, in turn, is attached to the outer shroud.

The fast core support comes from the ledge on the vessel wall by means of 4 vertical support plates which are attached to the lower grid and flow guide assembly of the fast core. Smaller extensions of these supports extend up outside the fast core container to support the offset duct on a flange above the fast core. Since flow is downward in the first pass of the fast core, the only support necessary is the lower grid. However, in the second pass, both lower and upper grids are necessary since there is a net force upward of about 750 pounds due to the pressure loss in the core while the reactor is at full power. The upper support comes from a hold down grid which is a part of the offset duct assembly.

There is no upper guide grid for the fast core fuel bundles since they must be held tightly in place while the reactor is operating and it must be possible to move the outermost elements in toward the center while refueling, in order to clear the offset duct flange. These fuel bundles will be held together by the higher pressure coolant in the thermal core acting against the relatively thin fast core container walls.

The estimated forces caused by the pressure drops and component weights result in a net upward force of approximately 2000 lbs. on the thermal core support, and a downward force of about 3500 lbs. on the fast core support. These forces are transmitted to the pressure vessel through the system of supports shown sketched in Figure 5. The magnitudes of the net forces and the various force components listed in Figures 3 and 4 are sufficiently low so that stresses will not be excessive. In fact, the present safety margins are so large that the forces can be increased considerably before the support stresses will become limiting.

In carrying out this analysis of forces, the weights of the steam separators have been included, although it is now felt that separators are not necessary. Omitting the separators will result in larger net upward forces, but the large safety margins provided will absorb the increase in stresses. The analysis was, therefore, not repeated with the separators omitted. It is concluded that although additional detailed design will be required, the provision of the internal core support system should not raise unusually difficult problems.

C. Offset Duct

A double-wall offset duct is used as a downcomer for the saturated steam (the outer flow area of the duct) and as a riser for the superheated steam (center region of the duct). This arrangement provides a saturated steam insulating layer between the water and the superheated steam. The water surrounding the offset duct reduces radiation streaming to the vessel head.

A hexagonal-shaped extension of the offset duct extends to the lower support grid of the fast core and forms a flow guide between the first and second passes. This extension was used to eliminate the problem of providing an inaccessible seal between first pass inlet and second pass outlet above the fast core, where an approximate 37 psi pressure difference exists.

A continuous grid will be used in the center region of the offset duct to prevent it from collapsing due to the differential pressure existing between it and the outer region. The outer duct will be strengthened by external ribs. This will enable relative movement of inner and outer ducts to accommodate the greater thermal expansion of the center duct. The control shaft passage through the offset duct assembly will be made up of a continuous guide pipe passing through larger pipe sections which are welded to the offset duct. This arrangement prevents leakage between flow regions and provides a guide for the center duct inside the outer one.

The two ducts will be connected at the transition and flange region by ribs which will also take the place of the external strengthening ribs used on the upper portion of the duct. The weight of the offset duct along with the downward forces due to differential pressures acting on the transition section will be supported by the flange above the fast core. The upper region of this offset duct will be laterally supported by guides attached to the pressure vessel wall.

D. Steam Separation and Drying

The boiler region of the prototype will be cooled by natural circulation. As the initially sub-cooled water flows upward through the thermal core, it increases in steam quality. Chimneys are provided at the upper end of the core to furnish the natural circulation driving head. The steam-water mixture flows out of the chimneys and is separated by gravity separation at the surface of the mixture. For the low power densities considered here, the exit steam velocity is of the order of 0.8 ft/sec, which is sufficiently low for free-surface separation. The superficial velocity of the steam entering the steam dryer mounted in the vessel top head is in the order of 1 to 1.5 fps. which, based on experimental work covered in "Interim Report on Steam Dryer Development", GEAP 3563, appears to be conservative.

Based on steam dryer tests referred to above, the moisture content entering the offset duct should be 0.1%. Considering 0.1% moisture in the steam and the heat transferred from the offset duct center region (superheated steam riser) to the outer region (steam downcomer) the steam should enter the first pass of the superheater with about 9°F superheat. This may be an advantage from a corrosion standpoint. The corresponding temperature drop in the superheated steam riser would be approximately 22°F. It should be pointed out, however, that predictions of heat transfer at these high-quality steam conditions is still uncertain.

E. Control Rod Drives

A definite disadvantage of adapting the EMSS to the VESR pressure vessel is the limited number and location of the control drive penetrations in the vessel bottom head. Since it is difficult to line up the control element positions in the EMSS core with the existing nozzles, some ingenuity is required to provide adequate controls. In some locations, it is necessary to gang as much as three control rods together since only one nozzle is available.

Another contributing factor is that in VESR, the control rods are bunched together near the center of the vessel, while in the EMSS, control rods are required closer to the vessel periphery. This necessitates offsets on the control rod drives of as much as 10.2 inches so that the control drive shafts are subjected to an eccentric axial loading. Although the maximum axial loading is considerably less than the critical buckling loads, it does not appear to be desirable to load the drive shafts eccentrically since alignment problems, particularly during scram, will be accentuated. Also, ganging the control rods may make it difficult to satisfy the "stuck-rod" criterion, which has not yet been considered for this concept. Alternate control systems should be considered.

One possibility is to use top-mounted control drives. Since steam separators are not required for this system, space is available at the top of the reactor. It will be necessary to modify or replace the present VESR head, but this should be relatively inexpensive. Another alternative could be to use internal control drives, but experience in this area is lacking.

It is evident that additional work is required to develop an acceptable control system. The problems do not appear to be insurmountable, however, and one of the above mentioned alternatives should prove to be adequate.

F. Pressure Vessel Shielding

The water shielding above and below the reactor core is at least equivalent to that provided in the 300 MWe reference design, but the vessel wall shielding in the core area is somewhat less. Preliminary calculations by Nuclear Systems Engineering indicate a ten-year vessel life based on 100% use. This should be adequate if one considers a realistic use factor for an experimental reactor. It should be remembered, however, that if the VESR vessel is used, part of the vessel's useful life will already be gone because of VESR experiments.

Based on the preliminary calculations mentioned above, a thermal shield thickness of 2 inches appears adequate to protect the vessel wall from excessive gamma heating. In the EMSS design layout, this is shown as two one-inch-thick shields.

VI. REACTOR PHYSICS

A. Introduction

The physics of the small MSS prototype is intended to simulate the physics of a large power producing MSS. The analysis discussed below indicates considerable differences in the details of the physics of a large MSS and the small prototype. However, the general features of the large reactor are present, and it is believed that the prototype will permit verification of the fundamental physics behind the Mixed Spectrum concept.

B. Power Distribution

The power distribution for one case calculated is shown in Figure 6. The fraction of power produced in the various regions is shown in Table IV. The power distribution in the small core simulates the major characteristics

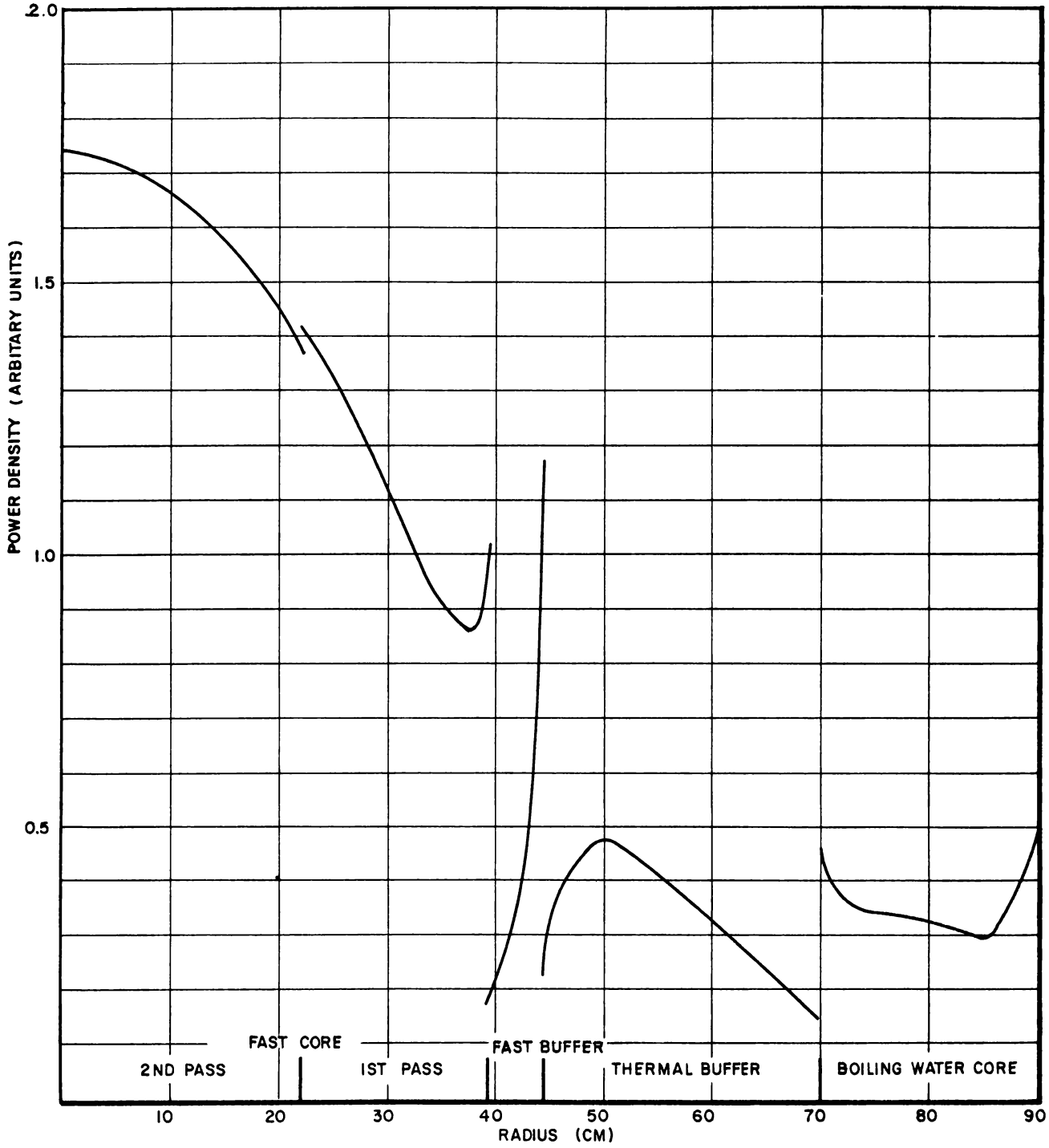

POWER AS A FUNCTION OF RADIUS

FIGURE 10.26

Table IV Power Distribution

Region	Fraction of Power
Superheater	
Fast Core	0.34
Fast Buffer	0.03
Total	0.37
Boiler	
Slow Core	0.34
Thermal Buffer	0.29
Total	0.63

Table V Radial Peak-to-Average Power Factor

Region	Peak/Avg. Power
Superheater (including fast buffer)	1.64
Superheater (excluding fast buffer)	1.42
Boiler (including thermal buffer)	1.42
Thermal Buffer	1.44
Thermal Core	1.37

Table VI Conversion Ratios

Region	U-238 Capture/Pu-239 or U-235 Absorption
Fast Core	0.646
Fast Core and Axial Reflectors	0.888
Fast Buffer	1.207
Thermal Buffer	1.070
Thermal Core	0.397

of that of a large MSS core with one important exception, i.e., the power shape in the boiling section is not well simulated because the boiling core is small relative to the fast core. However, the fast core power distribution, and the distribution in the buffer regions, are representative of a large core. In addition, calculations indicate that considerable information will be obtained on the ability to alter the power split between fast and slow core although here, the small size of the boiling core will limit the tests. In the calculation illustrated, the fraction of power produced in the superheater is higher than desirable, but other work shows that the power split can be altered by use of the fast core control elements.

The radial peak-to-average power factors for each region are given in Table V. Four group flux distributions are shown in Figure 7.

C. Design of the Buffer Region

The buffer regions for the small MSS serve the same functions as the buffers in the 300 MWe reference design described in GEAP 3590. However, the detailed buffer designs for the small MSS differ in several respects from the 300 MWe reference design of GEAP 3590. The thickness of the fast buffer was increased and the fast buffer enrichment was decreased in order to decrease the power gradient and, hence, the stresses across the fuel rods. Considerably better use is being made of the thermal buffer region in the present design than was made in the 300 MWe design. The power density in the thermal buffer is now nearly equal to that in the boiling core and the radial peak-to-average power for the thermal buffer, the slow core, and the combined buffer and core are all nearly identical (see Table V). The initial conversion ratio is nearly unity. These improvements over the 300 MWe thermal buffer design were made by increasing the water-to-fuel volume ratio from 1.2 to 2.4 and by increasing the U-235 enrichment from that of depleted uranium of 1.2%. These changes would be made in the large reactor too so that in this respect, the buffer designs of the small MSS would be representative of that in a large power reactor.

D. Conversion Ratio

The conversion ratio of the clean hot core is given for each region in Table VI. An initial conversion ratio close to unity in the buffer regions is necessary to prevent the peak power densities in these regions from increasing with burnup. The internal conversion ratio in the fast core is close to that of the 300 MWe reference design since the enrichments in the two cases are nearly identical.

E. Fission Spectrum and Neutron Flux

The spectrum of fission events for each region is given in Table VII. In Table VIII, the eleven-group fission spectrum of the fast core in both the small MSS design and the 300 MWe reference design are compared. The spectrum in the small MSS is harder than that in the 300 MWe design; however, it is significant that in both cases there is a large contribution from fission events below 25 Kev. It should be noted that these are spectra averaged over each entire region, whereas the spectrum near the edge of the superheater is significantly softer due to the slow neutrons returning from the boiler. The four-group neutron fluxes are plotted in Figure 7, and the rise of the group-three flux near the edge of the superheater shows the origin of the softer spectrum here.

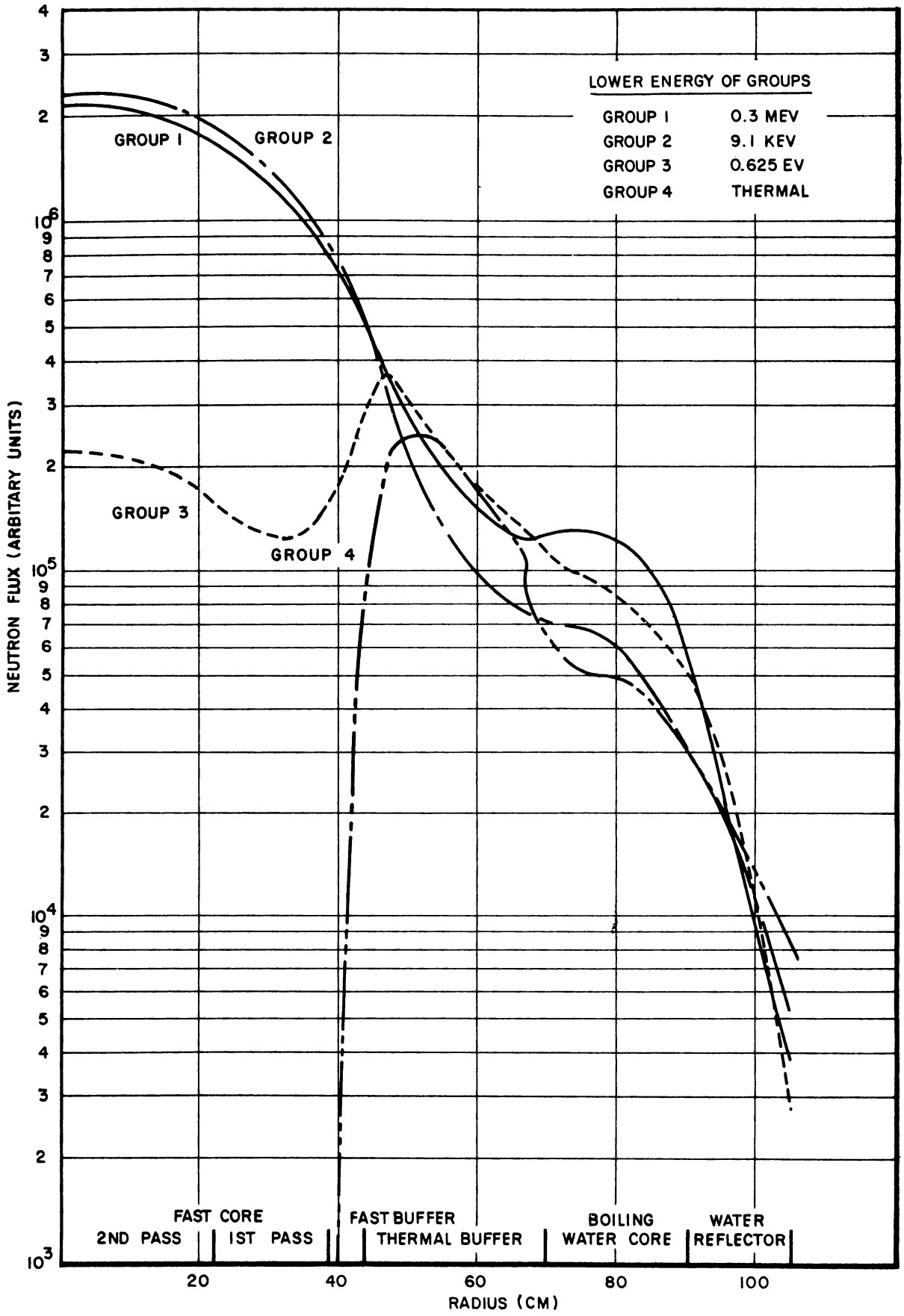

FOUR GROUP NEUTRON FLUXES AS A FUNCTION OF RADIUS

FIGURE 10.27

Table VII

Fission Spectrum (4 Groups)

Region	Description	Group	E_{lower}	Fraction Fissions in Group	Integrated Spectrum
1	Fast Core	1	0.3 Mev	.5116	.5116
		2	9.1 Kev	.3956	.9072
		3	0.625 ev	.0880	.9952
		4	Thermal	.0048	1
2	Fast Buffer	1	0.3 Mev	.2578	.2178
		2	9.1 Kev	.0290	.2468
		3	0.625 ev	.0881	.3349
		4	Thermal	.6651	1
3	Thermal Buffer	1	0.3 Mev	.0513	.0513
		2	9.1 Kev	.0066	.0579
		3	0.625 ev	.1191	.1770
		4	Thermal	.8230	1
4	Slow Core	1	0.3 Mev	.0439	.0439
		2	9.1 Kev	.0081	.0520
		3	0.625 ev	.1493	.2013
		4	Thermal	.7987	1

Table VIII

Fast Core Fission Spectrum (11 Group)

Group	Lower Energy Limit	Fraction Fissions per Group		Integrated Fission Spectrum	
		Small MSS	300 MWe MSS	Small MSS	300 MWe MSS
1	225 Mev	0.135	0.096	0.135	0.096
2	1.35	0.119	0.106	0.254	0.202
3	0.825	0.070	0.054	0.324	0.256
4	0.5	0.092	0.083	0.416	0.339
5	300 Kev	0.091	0.064	0.507	0.403
6	180	0.095	0.079	0.602	0.482
7	110	0.078	0.068	0.680	0.550
8	67	0.060	0.059	0.740	0.609
9	25	0.096	0.086	0.836	0.695
10	9.1	0.064	0.068	0.900	0.763
11	Thermal	0.100	0.237	1.000	1.000

F. Reactor Safety

The roles of the Doppler coefficient and void coefficient in the boiler on the boiler kinetics and safety are essentially unchanged from their roles in a standard BWR. In the fast core, the Doppler coefficient provides the necessary prompt shutdown mechanism. More slowly acting reactivity effects in the fast core are fuel and clad expansion coefficients, steam coefficient, and void coefficient due to void perturbations in the coupled boiler. Information relating to fast core safety which has been obtained thus far is presented below.

1. Flooding

The potential flooding accident, in which the operating fast core is flooded was briefly analyzed using methods reported in GEAP-3737 and GEAP-3785. Flooding the superheater to which no epithermal poison has been added introduces +12% reactivity into the fast core. By adding 0.6% by volume europium oxide to the superheater, no change in reactivity occurs on flooding. This zero reactivity change also applies for the unflooding accident. Previous calculations showed that, for a near zero reactivity change between the unflooded and completely flooded conditions, a large decrease in reactivity occurred when the large size superheater (approx. 3.5 ft on a side) was half-flooded and a small increase in reactivity occurred when a small superheater (approx. 1.5 ft on a side) was half-flooded (GEAP-3737). The superheater size under consideration here, which is 2.5 ft on a side, is intermediate between the two sizes referred to above, but the results obtained in GEAP-3737 are not exactly applicable here since the coolant and fuel volume fractions differ from the present case. Qualitatively, one would expect the variation during flooding to be negative and less for the present superheater than for the 300 MWe design. It appears that the general feasibility of using epithermal poisons to limit the reactivity effect of flooding can be demonstrated. Loss of pressure in the superheater would introduce 0.5% reactivity, about the same as in a large MSS.

2. Superheater Doppler Coefficient

The Doppler coefficient in the superheater has not been calculated explicitly. However, work on the Fast Oxide Reactor has involved detailed calculations of Doppler effects for fast reactors of the type in the superheating section of the Mixed Spectrum Reactor. A comparison of the spectra for the two cases and the relative enrichments indicates that the Mixed Spectrum prototype will have a Doppler coefficient in the range of $-5^{-10} \times 10^{-6}$ $\Delta k/^{o}C$. A comparison between the spectrum of the small prototype and the large reference design MSS indicates a substantially softer spectrum for the large MSS in the important region below 25 kv. The significance, if any, of this softer spectrum will require more detailed analysis.